DYNAMIC FRACTURE CHARACTERISTICS OF SELECTED ROCKS

by

Umesh Prasad, B.Tech., M.Eng., P.Eng.

Department of Mining and Metallurgical Engineering

McGill University

Montreal

A Thesis submitted to the Faculty of Graduate Studies and Research

In partial fulfilment of requirements for the

degree of Doctor of Philosophy

May 2000

ABSTRACT

Fragmentation by blasting is distinct from other method of rock breakage due mainly to the short time scale involved in the application of stresses. The resulting fractures and the factors which control it are much less understood in rock than in similarly rate-sensitive fracture process in metals and composites. Various attempts, using strength of material, comminution principles, fracture mechanics, and micro-structural damage mechanics, have been made to describe the process of fragmentation albeit with only limited success. This is largely due to a general paucity of actual experimental data, and selective treatment of the fracture process by individual workers. In the present work, the dynamic rock properties, applicable to non-static fragmentation process have been measured and compared with measured values of other fracture related properties. Further, these are examined to establish correlation with respect to their physical, mineralogical and micro-structural characteristics. The rock types selected for the present work ranged from nearly homogenous isotropic rock to an-isotropic rocks. The nearly isotropic rock were represented by three different types of granites. The an-isotropic rocks consisted of gneissic granite, gneiss, marbles, limestone, and quartz.

The dynamic compressive strength at a strain rate of 10^3 /sec was determined using a Split Hopkinson Pressure bar apparatus. The work index at an intermediate strain rate was determined by standard Bond rod mill for aggregate particle size of less than 12.5 mm. The fracture toughness was measured using three point bending method as suggested by ISRM. The compressive and tensile strengths were measured using standard rock

mechanics test methods. The microstructural characteristics were measured by petrographic analysis using micro-photographs.

The dynamic compressive strength, measured under a strain rate of 10^3 /sec, has been found to be about 2.5-4.6 times the compressive strength measured under static conditions (strain rate of 10^{-6} /sec) for similar dimensions of rock samples in a wide variety of rock types. It has also been found that this ratio is higher for low strength rocks, and lower for high strength rocks. However, care should be taken when comparing the dynamic strength to the static strength when measured in different diameters, especially, in coarse grained specimens. It has been shown that the microstructural properties affect the compressive strength significantly when the minimum dimension of the specimen is less than about 10 times the largest grain or crack size in the test samples.

The particle size distribution resulting from high velocity impact breakage is much smaller than in the static case. The degree of fineness (50% passing) generated under dynamic breakage is well correlated with the dynamic compressive strength; however, there appears to be no correlation between static compressive strength and the corresponding fragment size distribution.

Except for static compressive strength, the dynamic strength was found to have no significant correlation with the measured values of fracture toughness, tensile strength, or comminution work index. Among the microstructural properties, the crack density parameter was found to have the strongest correlation with the dynamic strength. This was not so with the average or the largest grain size or crack size.

The fracture toughness value is found to be controlled by the largest crack or grain size and to some extent, by porosity. The effect of crack density appeared to be non-linear; the fracture toughness initially decreases with increase in crack density, but further increase in the latter results an increase in toughness. This suggests the behaviour of rocks in dynamic compressive breakage is different than that due to static single crack growth.

The work index (WI), which represents a fracture process at an intermediate strain rate correlates better with the Brazilian tensile strength than the static and high strain rate compressive strengths. The WI was also found to have very good correlation with compressibility of the test sample. This is to be expected due to the load characteristics typical to the rod mill employed in the study. Furthermore, the WI was shown to have excellent correlation with the average grain size, but poor correlation with the largest grain size or crack density. This is according to expectation, as these would be largely absent in the small-scale particles employed in the comminution studies.

The structural characteristics are shown to be key parameters in all the fracture processes. However, their role is different for different rock breakage processes. In fragmentation process involving relatively small size fragments, such as blasting, both micro- and macro-fractures play a dominant role. In crushing and grinding involving fragmentation in the scale of grain size or smaller the micro-structure would be represented better by specific grain size distribution than micro-fracture or crack density. However, in all non-static fracture process, such as blasting or comminution, the use of static strength values in predicting fragment size distribution can lead to significant errors.

RÉSUMÉ

La fragmentation des roches par sautage diffère des autres méthodes de fracturation principalement par la courte durée de l'application des charges. Les fractures qui en résultent et les facteurs qui les contrôlent sont nettement moins bien compris pour la roche que pour les processus sensibles aux taux de fracturation similaires chez les métaux ou les composites. Cela est attribuable à la rareté des données expérimentales actuelles et du traitement du processus de fracturation par les différents chercheurs. Dans le présent travail, les propriétés dynamiques des roches telles qu'elles s'appliquent au processus non-static de la fragmentation ont été mesurées et comparées avec des valeurs mesurées d'autres propriétées associées à ces fractures. De plus, elles sont examinées pour établir des corrélations avec les caractéristiques physiques, minéralogiques et microstructurales. Les types de roches choisies dans la présente étude varient entre des propriétés presque purement isotropiques ou totalement anisotropiques. Les roches practiquement isotropiques sont représentées par trois différents types de granite. Les roches plutôt anisotropiques consistent en un granite à gneiss, en un gneiss, un marbre, un calcite, et un quartz.

La résistance dynamique de compression au taux de déformation de 10^3 /sec a été déterminée en utilisant un appareil Split Hopkinson Pressure Bar. L'indice de Travail à un taux intermédiaire de déformation a été obtenu par un broyeur à tige Bond pour des aggréggats aux particules de 12.5 mm et moindres. La rugosité des fractures a été mesurée par trois points d'inflexion tel que suggéré par l'ISRM. Les résistances en compression et en tension sont obtenues par les méthodes d'essais standard en mécanique des roches. Quant aux caractéristiques microstructurales, elles ont fait l'objet d'analyses pétrographiques à l'aide de micro-photographies.

La résistance en compression dynamique mesurée au taux de 10^3 /sec a montrée des valeurs de 2.5 à 4.6 fois supérieures à la résistance mesurée en conditions de taux de déformation statique (10^{-6} /sec) pour des échantillons de roches aux dimensions comparables et pour différents types de roches. En regard des résistances statiques, il est

montré que ces rapports mesurés sont supérieurs pour les roches de faibles résistances et plus faibles pour les roches plus résistantes. Cependant, une certaine vigileance doit être apportée lorsque l'on compare les résistances dynamiques aux résistances statiques selon différents diamètres, spécialement pour le cas des échantillons aux grains grossiers. Il est montré que les propriétés microstructurales affectent significativement la résistance en compression quand les dimensions minimales du spécimen est moindre que dix fois la dimension du plus gros des grains ou d'une fracture de l'échantillon testé.

La granulométrie des particules issuent d'un cassage par impact à haute vitesse est nettement plus fine que pour le cas d'un cassage en condition statique. Le degré de finesse (50% passant) obtenu en condition de cassage dynamique est bien ellée avec la résistance en compression dynamique; néanmoins, la correspondance entre la résistance statique et la granulométrie des fragments associés ne montre pas de corrélation.

Sauf pour la résistance en compression statique, la résistance dynamique n'a pas permi de trouver une dépendance significative avec les valeurs de rugosité des fractures mesurées, la résitance en tension, ou l'indice de travail en communition. Parmi les propriétés microstructurales, la densité des fissures a été le paramètre le plus significatif en regards de l'incidence sur la résistance dynamique. L'extension à la moyenne ou à la plus grande des dimensions des grains ou des fissures n'a pas montré de dépendance.

Il a été trouvé que la valeur de la rigidité d'une fracture est contrôllée par la plus grande des fissures ou de la grande dimension du plus gros grain, et dans une certaine mesure, par la porosité. L'effet de la densité des fissures apparaît comme non-linéaire; la rigidité de la fracture diminue initialement avec l'augmentation de la densité des fissures, mais augmente subséquemment avec une densité de fissures plus importante. Cela suggère que le comportement de la rupture en compression dynamique diffère de celui imputable à la progression d'une fissure en condition statique.

L'indice de travail (WI- Work Index), lequel représente le processus de fracturation à un taux de déformation intermédiaire montre une meilleur corrélation avec l'essai brésilien de résistance en tension qu'avec la résistance en compression a haut taux

de déformation. Le WI a aussi montré une bonne dépendance avec la compressibilité des échantillons. Cela pouvait être présagé compte tenu des caractéristiques de chargement typiques du broyeur à tiges employé dans cette étude. De plus, le WI à montré une forte dépendance avec la dimension moyenne des grains, mais une certaine indépendance vis-à-vis la plus grande dimension des plus gros grains ou de la densité des fissures. Cela est en accord avec nos previsions puisque ces derniers sont absent des échantillons à grains fins utilises donc les ëtudes de broyage.

Les caractéristiques structurales ont montrées qu'elles étaient les paramètres clés dans tous le processus de fracturation. Cependant, leur rôle diffère selon les processus de rupture utilisés. Dans les moyens de fragmentation engendrant des fragments de faible grosseur comme durant le sautage, les micro et macro-fractures jouent tes un rôle important. Pour le broyage et l'alésage qui induisent une fragmentation à l'échelle du grain ou plus petite, la micro-structure est davantage mieux représentée par une distribution granulométrique que par la densité des micro-fractures ou des fissures. Il ressort que pour tous les processus de fracturation non-statique, l'utilisation de la résistance statique pour prédir la distribution granulométrique n'est pas valable.

ACKNOWLEDGEMENTS

This research could not have been completed without the help and contribution from many persons and organisations. I am specially indebted to my supervisor, Prof. B. Mohanty, for his most helpful criticism, keen interest, continued guidance and many useful discussions and suggestions throughout this investigation. I am also grateful to Prof. F. P. Hassani for his invaluable support and encouragement during the course of this research.

I wish to express my sincere and deep gratitude to Prof. J. A. Nemes of the Department of Mechanical Engineering for sharing with me his knowledge on dynamic strength measurement by Split Hopkinson Pressure Bar. My sincere gratitude also goes to Prof. H. S. Mitri, for allowing me to use his computer laboratory as and when needed.

I would like thank G. Panangiotidis and Dr. E. M. Sakoma of the Department of Earth and Planetary Science for making thin sections of the rock types, and helping me with the petrographic studies for the test rocks, respectively. The help extended by the R. Sheppard of the Department of Civil Engineering is highly appreciated for allowing me to conduct some of the tests in his laboratory.

The help and encouragement provided by the staff and colleagues of the Department of Mining and Metallurgical Engineering, especially, Dr. M. Momayazzadeh, S. Servant, J. Marwan, P. Gueveremont, P. Mujumdar and Norma Procyshtn are also gratefully acknowledged.

Partial financial support received through research funding by Orica Canada Inc. during the course of this study is also gratefully acknowledged.

Finally, the author expresses his deepest appreciation to his wife, Seema and her daughter, Yashi, without whose love, constant encouragement and support, this thesis would never have been completed.

TABLE OF CONTENTS

LIST OF FIGURES

Figure **Page**

LIST OF TABLES

LIST OF SYMBOLS

σ	Stress
σ_c	Unconfined compressive strength
σ_t	Tensile strength
ϵ	Strain
ϵ_I	Incident strain
ϵ_R	Reflected strain
ϵ_T	Transmitted strain
E	Young's modulus
μ	Shear modulus
K	Bulk modulus
ν	Poisson's ratio
ρ	Density
τ	Shear strength
V_p	Longitudinal or primary (P) wave
V_s	Shear or secondary (S) wave
C	Rod velocity
u_1	Displacement at the left end of the specimen in SHPB test
u_2	Displacement at the right end of the specimen
F_1	Force at the left end of the specimen
F_2	Force at the right end of the specimen
D	Diameter of the specimen in fracture toughness test
θ	Angle of the chevron notch at the apex
a_0	Depth of the chevron notch from surface
t	Thickness of the chevron notch
S	Span of the support roller in three point bending
F_{max}	Maximum load at which failure occurs
X_u	Net displacement at zero load
X_f	Net displacement at maximum load
P	Non-linearity factor
K_Q	Fracture toughness determined at level I according to ISRM
K_{IC}	Modified fracture toughness determined at level II according to ISRM
F_{50}	Feed size of rock aggregates at which 50 % of the fragments passes
F_{80}	Feed size of rock aggregates at which 50 % of the fragments passes
P_{50}	Feed size of rock aggregates at which 50 % of the fragments passes
P_{80}	Feed size of rock aggregates at which 50 % of the fragments passes
W_i	Work Index

CHAPTER 1

INTRODUCTION

1.1 Introduction to rock breakage

Rock is one of the most common building materials used in surface and subsurface structures. Large amount of rocks are also excavated for extracting ore and minerals, and creating openings. The subject of dynamics of fracture in rock is, therefore, a matter of significant concern to professionals in geological, mining and civil engineering disciplines. Fracture of rock can be achieved by heat, high pressure water jets, mechanical means, or by action of explosives. Fragmentation by heat or hydraulic means is normally employed in very specialized applications. Mechanical means are employed for comminution processes such as crushing and grinding, and tunnel boring operations. These can not be generally applied to fracturing of rock mass in large scale. Fragmentation by explosives, on the other hand, can be applied in all scales, and is

considered the most cost effective means of reducing size, from very large blocks of rocks to millimeter scales. The annual consumption of industrial explosives in north American market alone is about 3 million tons. The great advantage of explosives over other fragmentation techniques is the amount of energy available and the rapidity with which the later can be transferred to rock. The total energy produced in unit time even in a small diameter borehole can reach 2.5×10^4 MW, exceeding the generating power of the great majority of large power stations in the world today.

Explosives can be in solid or liquid form or any combination thereof. Through proper initiation, a small portion of the explosives can be converted in a fraction of milliseconds into gaseous products with release of very high heat and pressure. An explosive charge in a borehole is usually initiated by a detonator or detonating cord or any combination of these. The resulting chemical reaction rate, commonly known as the velocity of detonation, can vary 2500 to 6500 m/s in commercial explosives. The corresponding energy release can easily exceed 5 MJ per kg of explosives. The detonation process is characterized by very high pressure (often exceeding 10 GPa) and temperature (3000°C). The resultant release of shock and gas energy leads to fragmentation of rock.

A large number of factors influences the blasting process. These can be grouped under three categories, e.g. explosives characteristics, rock characteristics, and the blasting parameters (such as blast geometry and timing). The fracture behaviour of rock, especially, under dynamic loading condition, is a key parameter in understanding the rock fragmentation process in blasting. Much work on dynamic fracture mechanics has been

done for metals, composites and ceramics. Only a very limited amount of work has been done on the fundamentals of the breakage process in rocks under dynamic loading conditions.

1.2 Objective of the study

Compared to our knowledge base on detonation properties of commercial explosives, the properties of rock which control the fracture process are poorly known. The exact mechanism of fracture and the factors which control it are much less understood in rock than in similarly rate-sensitive fracture process in metals and composites. Various attempts have been made to explain the dynamic process through different conceptual approaches. These include strength of material, comminution principles, fracture mechanics, and microstructural damage mechanics, but they have had only limited success in investigating the phenomenon. The present work aims to fill some of these gaps in our knowledge by considering the fragmentation process with a broader perspective, Figure 1.1. The commonly designated rock properties applicable to these processes are measured in the laboratory and compared with the dynamic rock properties. Additionally, the fracture related properties of rocks are examined for any possible correlation with respect to their physical, mineralogical and micro-structural characteristics. More specifically the present study aims to,

a) analyze the process of fragmentation as a function of strain rates,

b) analyze the fracture process in rock on the basis of comminution properties,

Figure 1.1: Rock properties and rock fragmentation

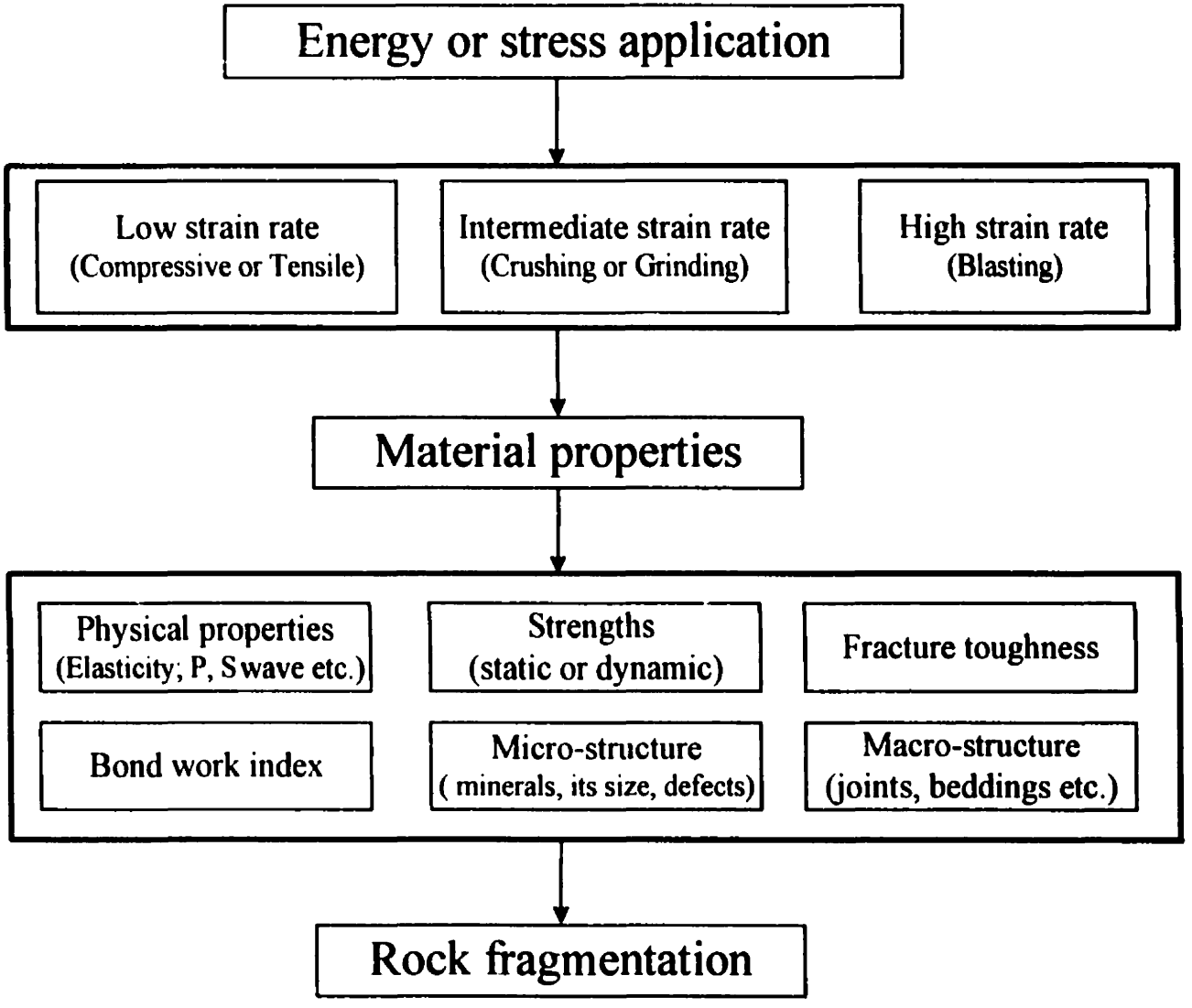

c) measure physical, and mechanical properties such as seismic wave velocity, elastic properties, density, porosity, compressive and tensile strengths,

d) measure dynamic compressive strengths at strain rates comparable to blasting using Split Hopkinson Pressure Bar apparatus in laboratory-scale samples,

e) measure fracture toughness of rocks in the laboratory-scale samples,

f) measure microscopic structural properties (grain sizes, and grain characteristics, crack sizes, and crack density) in rock and its influence on fracture related properties,

g) demonstrate the underlying principles which control rock fragmentation through synthesis of these data.

1.3 Thesis Organization

This research explores in detail the dynamics of rock fragmentation and comminution in rocks. The fragmentation system is viewed essentially as a strain-rate related process. The designated material properties underlying different fracture processes are measured and analyzed. Further, the physical, mineralogical, and micro-structural properties are measured to explore if these control the fracture related material properties. The thesis is organized in 9 chapters.

Chapter 1 presents a general view of the rock fragmentation system. The importance of dynamic fragmentation is outlined and the need for the present work is justified. The objective, the outline of the research work, and the statement of originality

are also described.

Chapter 2 describes the dynamic rock fragmentation system in blasting. The properties of explosives, the time frame of fragmentation, and the process of rock fragmentation are explained in detail.

Chapter 3 details the characteristics of rock with reference to rock fragmentation.

Chapter 4 reviews the theoretical basis of rock fragmentation process. Fragmentation under different stress and strain rate conditions are described. The process of fragmentation using various approaches are discussed and compared.

Chapter 5 is devoted to the materials selected and methods adopted for their study in the present work. The various sub-sections describe the background of the materials and methods, and the measurement of physical, mechanical, and seismic properties of rocks. The measurement of dynamic compressive strength, and the fracture toughness in the laboratory are also elaborated.

Chapter 6 presents the measurement of comminution properties (Bond work index) representing fracture property at an intermediate strain rate.

Chapter 7 describes the details of the micro-structural measurements. The minerals identified, the crack and grain sizes measured and the method of measuring the crack density are also explained.

Chapter 8 analyses and discusses the various results obtained in previous chapters. The fracture related properties of rocks are compared and further, the influence of micro-structure on them are discussed in detail.

Chapter 9 presents the overall conclusions and recommendations for future work.

1.4 Statement of originality

The original contributions described in this thesis consist of:

a) Measurement of dynamic compressive strengths of rocks under high strain rates (10^3/sec) and comparison with static compressive strengths (strain rate of 10^{-6}/sec) in the same rocks with samples of identical dimensions.

b) Measurement of fragment size distribution of rocks after dynamic and static compressive breakage.

c) Measurement of microstructure (i.e. crack density and grain characteristics) for various rock types from micro-photographs, and study of their effect on dynamic strength, fracture toughness, and work index.

d) Assembly of an apparatus for the measurement of fracture toughness of rocks according to International Society of Rock Mechanics standards with the help of existing equipment setup. This include design and development of a loading and alignment assembly for securing rock specimen under stable condition and achieving the proper alignment of chevron notch during the fracture toughness test.

e) The dynamic compressive strength has been shown to range between 2.5 to 4.6 times the corresponding static strength for similar dimension of rock samples. The resulting particle size distribution under dynamic fracture process has been demonstrated to be much smaller than that of the static case, and correlated well, unlike the latter, with the dynamic compressive strength.

f) It has also been shown that the selection of the sample diameter for the unconfined compressive strength test is very critical, especially, in coarse grained rocks. It has been confirmed that the unconfined compressive strength is representative only when the sample diameter is an order of magnitude larger than the largest grain size. The present work gives an experimental justification for the previously established rule of thumb.

g) It has been shown that the dynamic compressive strength cannot be inferred either from Brazilian tensile strength or the fracture toughness.

h) The extent of cracking or the crack density has been found to affect greatly the dynamic compressive strength, whereas the largest crack or grain size affects the tensile strength and the fracture toughness. Overall, the dynamic properties are significantly different from their static counterparts, and therefore, the latter's use in predicting fragmentation behavior of rock in blasting would lead to erroneous conclusions.

CHAPTER 2

ROCK FRAGMENTATION BY EXPLOSIVES

Rock fragmentation by explosives is the key issue taken in the present work. The processes involved in it are complex. The strain rate involved in this process vary from very high (shock effect) to low (gas energy). The fragmentation mechanism varies from simple crushing to high impact loading. The following section describes very briefly the characteristics of explosives relevant to the process of blasting.

2.1 Constituents of Explosives

The bulk of the explosives used today consists of a mixture or compound of suitable oxidisers and fuels. When suitably initiated, these compositions decompose at supersonic rates. The rate of reaction is known as the velocity of detonation, VOD. For commercial explosives VOD should depend not only on the compositions but also on its geometry such as diameter and density. The basic compositions of most explosives consist of carbon, hydrogen, nitrogen and oxygen compounds (C, H, N, O). Explosive compounds such as tri-nitro-toluene (TNT), nitroglycerine (NG) and penta-erythritol-tetra

nitrate (PETN) are self explosives and do not need additional oxygen or fuels. However, most commercial explosives contain very small amount or no self explosives, but rely on mechanical means of sensitisation. Glass micro balloons or gas micro-bubbles are employed as non-explosive sensitizer in commercial explosives. Examples of various types of oxidisers, fuels and sensitizer in common use today are shown in Table 2.1. The most common commercial explosives in use today is called ANFO, which is a mixture of porous ammonium nitrate prills and fuel oil at a ratio of 94 to 6.

Table 2.1: Examples of various types of ingredients in explosives of common use.

Oxidisers	Combustibles or fuels	Sensitizer
Nitrates of NH_4, Na, K or Ca; Oxygen.	Fuel oil, aluminium powder, Paraffin, or silicon.	TNT, PETN, amine nitrates, gas micro-bubbles, glass micro balloons.

The reaction in an explosive, once initiated, is self-sustaining in nature. This results in a steady reaction rate or velocity of detonation (VOD). Detonation of an explosive in a borehole results in transformation of explosive compounds into gaseous products and the release of energy at an extremely rapid rate. The gaseous products mainly contains nitrogen, oxides of nitrogen and carbon, oxygen, water vapour etc.. The constituents of explosives may also include some chemical compounds dictated by the environmental conditions. For example, antacid promotes stability in storage, low freezing point components prevent the explosive from freezing at low temperatures, flame depressants and coolants reduces the size, duration and temperature of flame during the explosion,

especially, in underground coal mining operations.

2.2 Types of Explosives

In mining and construction, the explosives used can be broadly classified into two categories, a) detonator sensitive explosives, and b) booster sensitive explosives. Detonator sensitive explosives are initiated by detonators and are more sensitive. These are characterised by low critical diameters and are used in small diameter boreholes. Booster sensitive explosives are less sensitive and needs high explosives for initiation. The critical diameter is correspondingly higher and hence these are used in larger diameter boreholes.

The modern trend in commercial explosives is to dispense with the use of self-explosives entirely on account of safety and cost. However, NG based explosives, commonly known as dynamites, are still manufactured for some specific applications. These are all detonator sensitive products such as GEOGEL, POWERFRAC. Examples of non-NG sensitised explosives in this category of small diameter slurry and emulsion explosives are TOVEX, MAGNAFRAC, MAGNUM etc.. These are used in the diameter range of 25 mm to 100mm and come in the form of paper or plastic wrapped cartridges. The booster sensitive explosives are initiated by a suitable booster (such as Pentolite). Bulk ANFO, slurries, emulsion, and Heavy ANFO are examples in this category. The hole diameters are in the range of 90 mm to 400 mm for these products. These are largely bulk loaded into the borehole. ANFO can also be pneumatically loaded into boreholes. The loading pressure is about 500 kPa. Under these conditions, ANFO is pulverised in the

borehole. This renders it detonator sensitive and thus used widely in underground workings. Table 2.2 shows typical explosives types, their constituents, typical particle size of the oxidiser and their velocity of detonations

2.3 Explosives Characteristics

The relevant properties of commercial explosives are, density, velocity of detonation, detonation and borehole pressure, and strength or energy.

Table 2.2: Common explosives with their constituents and characteristics.

Explosive	Oxidiser	Fuel	Sensitizer	Particle or droplet size	VOD (m/s)
ANFO	Solid	Liquid	-	2.0 mm	3000-4500
Slurry	Solid or liquid	Solid or liquid	Solid, liquid, or m-b	0.2 mm	3000-5000
Emulsion	Solid or liquid	Solid or liquid	Solid, liquid, or m-b	0.002 mm	3000-6000
Heavy ANFO	Solid or liquid	Liquid	Liquid or m-b	2.0 mm	3500-4500
Dynamites	Solid	Solid	liquid	0.2-2.0 mm	2500-6000

Note: m-b stands for micro-bubbles, VOD range attributed to varying borehole diameters.

2.3.1 Density:

This is the weight of the explosive per unit volume. It is also sometimes referred to as loading density, as the density of an explosive column in a deep borehole can be larger than that of the explosives sample. The density controls detonation properties as well as the amount of explosives which can be loaded in a borehole.

2.3.2 Velocity of Detonation (VOD)

VOD is the rate of chemical reaction when suitably initiated, or the velocity of

detonation wave which travels through the explosive column. The VOD in a commercial explosives depends on the density and the diameter of the explosives as well as its composition. The degree of coupling with the blast hole and the size of the booster may also affect the VOD. There is a minimum diameter at which explosives can detonate, and it is called the critical diameter. The critical diameter of NG-based explosives could be as low as 10 mm, whereas, for poured ANFO it is 75 mm. The VOD in commercial explosives increases with diameter, indicating more ideal detonation reaction. For most booster sensitive explosives, ideal reaction applies to only in extremely large borehole diameters. The VOD of the commercial explosives range from 1900 m/s (for some permitted explosives, used in underground coal mines) to 7600 m/s for booster explosives. Higher VOD explosives are preferable for hard and intact rocks due to higher detonation pressures. However, low VOD explosives release gas for longer period of time, thus are more suitable for jointed and fractured rock which needs mostly displacements.

2.3.3 Detonation pressure:

On detonation of an explosive, a dynamic pressure is generated in the reaction zone behind the reaction front. The value of detonation pressure depends on the density and VOD of explosives (see also Table 2.3). According to hydrodynamic theory it is calculated by:

$$P_d \approx \frac{1}{4} \rho VOD^2 \qquad (2.1)$$

where, ρ, is the density of explosive (g/cc) and VOD is the velocity of detonation (km/s),

P_d, the detonation pressure in GPa. The latter may exceed 10 GPa for some commercial explosives.

2.3.4 Borehole pressure:

It is a hypothetical pressure that would be generated following completion of detonation reaction in a borehole, at a constant volume without heat loss to the surrounding rocks. The detonation pressure decays quickly followed by a more stable pressure called borehole pressure. In most explosives this is taken approximately to be half of the detonation pressure. It should be noted that the detonation pressure is dependent on the squared power of VOD. If the explosives reacts with one half of the ideal rate of detonation, the detonation pressure is one quarter of the maximum theoretical pressure. The borehole pressure depends mainly on the chemical compositions of the explosives, density and the degree of completion of the reaction.

2.3.5 Strength and Energy:

The energy, strength or power of an explosives in the explosives industry is used to rate the commercial explosives. The explosives energy is associated with the total release of energy and the efficiency with which it is transmitted to the rock. All these factors pose difficulties in defining energy of an explosives with a single parameter. Moreover, most commercial explosives exhibit non-ideal detonation behaviour. The ideal reaction in commercial explosives is approached only in extremely large diameters. By simply varying the charge diameter, the explosive may behave in a very different manner, despite having the same chemical composition. The effect of this non-ideal reaction is

most readily evident in the change of velocity of detonation, VOD as a function of charge diameter. Factors affecting explosives strength and the explosives rating on ideal and non-ideal detonation have been reviewed thoroughly by Mohanty (1988). The explosives energy is currently calculated by the thermodynamics of explosion. It is described by: a) Absolute Weight Strength, AWS; b) Absolute Bulk Strength, ABS; c) Relative Weight Strength, RWS; and d) Relative Bulk Strength, RBS. The AWS or ABS are the absolute amount of available energy (Joules) in each kilogram or in each cubic metre of explosives, respectively. The ratio of the AWS and ABS of an explosive to AWS and ABS of some standard explosive, such as ANFO, is called the Relative Weight Strength and Relative Bulk Strength (RWS, and RBS), respectively.

2.4 Fragmentation process

The fragmentation process in blasting is initiated by detonation of explosive in the borehole. The energy in the explosives is liberated over a very short period of time, in the form of shock and gas under high temperature (3000^0C) and pressure (~ 10 GPa). During and after completion of reaction in the explosives, the borehole wall is subjected to very high pressures by shock and gas. When the explosive-rock interface is reached by the detonation front, a high intensity shock wave is propagated into the rock. The transfer of energy to the rock is a function of both characteristics of the explosive and the rock. The wave propagates in the rock in a spherical or cylindrical front depending upon the shape of the explosive and the mode of initiation of the explosive column. The shock waves (in the form of radial and tangential stresses) are transmitted into the rock. In the vicinity of the

borehole wall, a significant amount of energy is used up in crushing the rock. This might extend to about 2-4 times the radius of the borehole so long as the shock amplitude exceeds the dynamic compressive strength of the rock. This compressive crushing may be due to the radial as well as the tensile stress pulses, as the later is also compressive in nature in the immediate vicinity of the borehole (Mohanty, 1982). Radial cracks are propagated from the centre of the hole by the tangential component of the stress wave both in the horizontal and vertical directions (perpendicular to the radial direction from the borehole). Radial cracking all along periphery as well as along the depth of the borehole, occurs when tensile stress associated with these waves are more than the dynamic tensile strength of the rock. Mohanty (1982) has shown the existence of a third set of cracks concentric to the axis of the borehole. This is because of a presence of a tensile phase in the radial stress, especially, at some distance away from the borehole wall. At larger distances the magnitude of tensile stress in both radial as well as tangential stresses are the same, which results in a three dimensional network of cracks and fragments. The shock wave dies out rapidly depending upon the distance from the borehole and the type of rock. When the compressive wave reaches a free face or a discontinuity, some part of the energy is reflected back into the media and some is transferred across the discontinuity depending upon the relative impedance of the two media. If the impedance is same, the wave propagates across the boundary without reflection. In case of a free face (e.g. air being the second medium), most of the compressive stresses will be reflected back as tensile stress. This tensile wave gives rise to spalling at free face so long as its stress amplitude is larger

amplitude is larger than the dynamic tensile strength of rock. The reflected wave may also extend or create new or existing cracks. In most explosives, the radial shock wave energy away from the vicinity of the borehole is only 5-15 % of the total energy of the explosive (Langefors and Kihlstrom, 1978). The third phase of fragmentation is relatively slow and is due to high temperature, high pressure explosion gases still resident in the borehole before being released to the atmosphere. Although the borehole pressure is significantly less than the detonation pressure, it is still sufficiently higher than the strength of the rock mass. The gas penetration in the vicinity of the crushed annulus zone extend the pre-existing cracks or the previously generated crack due to the shock waves. The fragmentation in this time frame is relatively slow but is most effective as the crack get more time to propagate in this time frame. The energy in the explosion gases is also largely responsible for the displacement of the entire rock mass. Additional cracking may take place due to the relative movement of the different rock layers. Some further breakage may occur by release of load in full column of the rock, flexure of the rock mass in the form of a beam, in-flight collisions among the rock fragments and their impact with ground. The overall useful energy for the fragmentation of rock to suitable size, and displacement of this volume to a certain distance normally consumes significantly less than the total explosive energy available in the borehole. The balance of energy is used up in producing some of the undesirable effects such as fly rocks, over-breaks, vibration and air blast, ejection of stemming and consequent release of explosive energy into air. The breakdown of energies in different group is shown in Table 2.3.

Table 2.3: Breakdown of energy components in blasting

<table>
<tr><th colspan="4">Explosive energy</th></tr>
<tr><th colspan="3">Shock energy</th><th>Gas energy</th></tr>
<tr><td>Radial</td><td>Tangential</td><td>Circumferencial</td><td>Crack opening</td></tr>
<tr><td colspan="3">Crushing of hole, crack opening or extension</td><td>Crack growth or fragmentation</td></tr>
<tr><td colspan="3">Spall energy and kinetic energy</td><td>Mass movement</td></tr>
<tr><td colspan="3">Seismic energy</td><td>Kinetic energy</td></tr>
<tr><td colspan="3">Acoustic energy</td><td>Collision or impact</td></tr>
</table>

2.5 Fragmentation time frame

The whole blasting process can be divided into four time frames. These time frames may overlap and are functions of following parameters: detonation characteristics of the explosives, elastic and strength properties of rock, wave velocity, blast geometry and initiation timings. The first time frame starts from detonation of explosives in the scale of tens of microseconds to a few milliseconds. The velocity of detonation of commercial explosives in rocks has been shown in Table 2.2. The maximum pressure felt by rock at the borehole wall is dependent on the explosive density, VOD, and coupling of explosives to rock. The second time frame starts at the instant of shock wave formation at the borehole wall and its propagation away from the immediate vicinity of the borehole. The most important waves (longitudinal, tangential and Rayleigh waves) travel at different speed which depends on the type of rock, density, depth of explosion, confinement, moisture and water content of the medium. The velocity of these waves in rocks ranges

waves in rocks ranges from about 3-6 km/sec, 2-3 km/sec, and about 1.5-2.7 km/sec, respectively. The velocity of crack growth on the other hand is much lower than these waves, and it might approach about 80-90 % of the velocity of Raleigh wave. The time duration for the wave propagation starts from about 0.1 ms to about 2 milliseconds. The third time frame consists of gas pressure expansion and starts at about 0.1 ms and lasts from 10 to 100 milliseconds. The final pressure before venting of explosion gases through ejection of stemming or cracks in the rock, is considered to be 100 MPa. The work expended in the gas expansion to this pressure is considered the effective energy of the explosive. The fourth and last time frame consists of rock mass movement due the velocity of the rock mass obtained from gas expansion. This time starts at about one millisecond and can last up to one second for a single blasthole. In actual blasting, upto one thousand holes may be initiated in a specific sequence resulting in fragmentation of a million tons or more of rock, but in the rock mass surrounding each hole, the fragmentation is very similar.

The strain level for dynamic breakage of rock is about 0.1 to 2 % and the time frame of blasting ranges from few microseconds to a second. The former corresponds to the completion of reaction in the explosives column and dynamic stress applications, whereas the latter corresponds to the completion of full blasting process. This leads to a strain rate of the order of 10^{4}/sec to 10^{-2}/sec in the blasting process.

2.6 Conclusions

Fragmentation by blasting is different from other methods of rock breakage due to

the short time frame involved. Since the explosive energy is released in a fraction of a second or less, the power available for rock fragmentation is extremely large. Also, since the energy applied is in the time frame of a few milliseconds, the resulting fracture do not have sufficient time to propagate in a stable manner. This leads to creation of a large network of small cracks to dissipate the available energy. This is in sharp contrast to the relatively few and long cracks generated in rock by means of less powerful processes such as hydraulic and mechanical fracturing.

The strain level for dynamic breakage under brittle conditions is about 0.1 to 2 %, and the time frame of blasting processes is typically in the range of few microseconds to a second. This results in a strain rate of the order of 10^{4}/sec to 10^{-2}/sec. The measured properties in laboratory under static conditions cannot always be applied for such high strain rate phenomenon. The energy or strength, velocity of detonation and density are the three important parameters which must be considered in the selection of an explosive. The high strain rate fragmentation processes, as in blasting, incorporate a whole of fragmentation processes such as, crushing, high velocity cracking, coalescence of propagating cracks, and the relatively lower velocity of cracking of the rock mass due to explosion gas pressures, somewhat analogous to hydraulic fracturing.

CHAPTER 3

CHARACTERISTICS OF ROCK

The response of rock to stress is dependent upon many factors such as, rock type, its mineralogy, microscopic and macroscopic structures, deformational and strength characteristics, and the time duration of loading. These parameters are described briefly in the following pages.

3.1 Rock types

Although rocks are usually classified as igneous, metamorphic and sedimentary types, they have generally little relevance to the fragmentation process, except through their physical properties. In igneous rocks, the rate of cooling in original magma largely determines the grain size. Slow cooling results in coarse grained, intrusive rocks (e.g. gabbro, granite, etc.). Rapid cooling leads to fine grained rocks (e.g. basalt, rhyolite, etc.).

All rock types are subject to weathering. Transport, accumulation and subsequent compaction of these weathered particles give rise to sedimentary rocks (e.g. sandstone, limestone, etc.). These may be massive or characterized by extensive bedding and jointing. The thickness of the beds, the quality and quantity of the filling material between these joints, as well as their orientation and width, determine the strength of the rock mass. Both igneous and sedimentary rocks type can be subjected to subsequent heat and pressure. This may result in re-melting and re-crystallization of the rock, which upon cooling gives rise to metamorphic rocks (e.g. schist, gneiss, etc.). Metamorphism is usually associated with extensive deformation, fracture and pulverization, prior to re-crystallization. In general igneous rocks are characterized by high strength and the sedimentary ones by low strength.

3.2 Mineralogy and grain size

Rock is composed of one or more minerals in granular form. All these grains are in intact position due to grain interlocking and cementing materials consisting of other minerals, cohesive granular aggregates, and moisture present therein. The structure of a grain network, unlike that of the crystal lattice in a single grain, is rarely homogenous and periodic. The strength of rock is dependent on the strength of the constituting minerals as well as the cementing materials. At the microscopic level the strength of rock is dependent on the presence of cracks, voids and inter-granular features.

Although there exist more than 2000 kinds of minerals, only about seven of them represent the most common constituents of rocks. These include quartz, feldspars, mica,

hornblende, calcite, kaoline, and dolomite. The quartz as a cementing material makes a rock strong, on the other hand clay as a cementing material causes a rock to be weak. Mica, which is fissile and weak is also a very common mineral. It may be found alone, weathered with clay inclusion or in combination with other minerals and contributes to the strength, anisotropy and porosity of the rocks.

3.3 Macroscopic and microscopic structures

3.3.1 Macroscopic structures

The macroscopic structures consist of joints, partings, faults, bedding planes, etc.. These discontinuities are generally regular. Any crack growth originating from random microstructures is limited by the regular macro-structures. Depending on the extent of macro-structures present, a rock mass may behave as an assemblage of blocks. On the other hand the same may behave as a massive or intact rock in the absence of macro-structures (e.g. a laboratory specimen). These structures can best be described by: a) those that relate to the brokenness of the rock mass i.e. block size, volumetric joint count, and b) those that relate to the characteristics of individual joints and joints sets (i.e. orientation, spacing, roughness and the filling material between the joints). These parameters control the insitu strength, deformability and support requirements of the rock mass. These parameters are described briefly in the following sections.

Block size in rock mass is measured by the distance between two successive joint planes, at the surface or underground or in a core obtained from core drilling. The block size can vary from a few centimetres to several metres. Consequently, the strength of a

rock mass may vary from being very weak to very strong. The behaviour of strength with respect to block size is shown in Figure 3.1, Franklin and Dussault (1989).

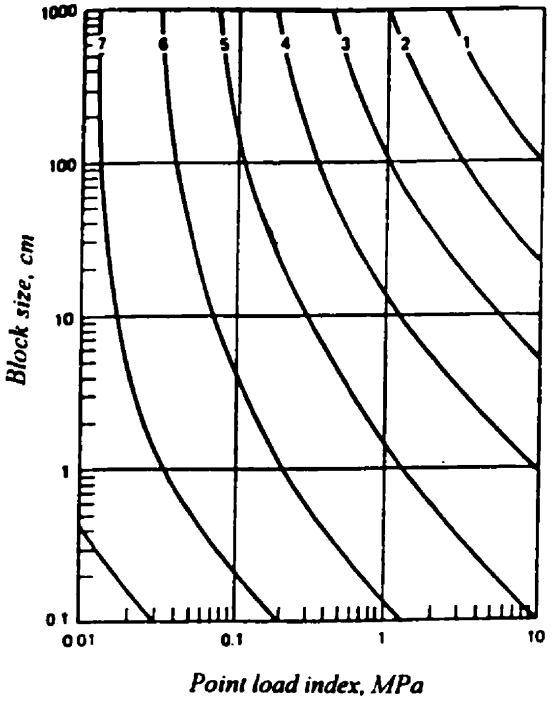

Figure 3.1: Block size vs. strength characteristics of a rock mass differentiating weak rocks (>7) from strong rocks (<2), after Franklin and Dusseault (1989).

It shows the rock mass block size and their point load strength (load at failure determined by Schmidt hammer test, for example). The diagram differentiates between a weak rock which can be excavated by mechanical ripping (lower left hand corner in Fig. 3.1), from a strong rock mass. The later is hard and must be blasted, but requiring almost no support (upper right hand corner). The number 1, 2, 3, etc. signifies the extent of

support required and it increases with increasing number. For example the number 1 signifies no support requirements for the rock mass which is hard and larger block size. However, the number 8 signifies great extent of support in underground operations for weak and smaller block sized rock mass. The block size can be measured on the basis of spatial or volumetric joint density. The latter can vary from less than 1 to 60 or more joints/m^3, in very large blocks to crushed rocks, respectively. Lithological factors, in terms of macroscopic features, may play a significant role in bedded deposit. The information can be helpful in minimising the explosive by deck-charging in an open-pit or designing the necessary support in underground. Borehole logging, sometimes regular face or high-wall mapping helps in getting the detailed information of lithological diversity.

3.3.2 Microscopic structures

The term microscopic structure refers to the arrangement of crystals, grains, particles and any microscopic cracks contained in the rock. The strength of a crystal depends on its lattice structure, in the absence of any void or microcrack. A group of crystals of one or more minerals forms grains. Grains are in intact position due to the cementing materials which consist of cohesive granular aggregates, other minerals and moisture. The strength of a grain, therefore, may depend on the minerals, as well as on the nature of microstructures and cementing materials. The strength of rock in turn thus depends on the grain networks, cracks or voids, minerals and the cementing material present in it. The role of microstructures is the key to understanding the fracture behaviour of rock in all small and medium scale size reduction processes, such as

blasting, crushing and grinding. The appearance of these microstructure in the rock matrix affects not only the physical properties such as, density, porosity, permeability and moisture content capacity of rock, but greatly affects its strength unlike the macro-structures. The measurement of microstructures and their role are discussed in greater details in the materials and methods section.

3.4 Porosity and density

A rock mass may contain solid, liquid and gaseous components. The combined liquid and gas volumes comprise of pores and voids. The volume percent of pores is denoted as the porosity, the mass per unit volume is denoted as density. The density is sometimes classified under different name such as the bulk density, the dry density and the grain density depending upon the consideration of the weight of the water content, the weight of the solid content, and the volume of solid content, respectively. These can be expressed in equations 3.1, 3.2 and 3.3.

$$\rho_{bulk} = \frac{M_s + M_w}{V_s + V_w + V_a} \tag{3.1}$$

$$\rho_{dry} = \frac{M_s}{V_s + V_w + V_a} \tag{3.2}$$

$$\rho_{grain} = \frac{M_s}{V_s} \tag{3.3}$$

where, M and V represent the mass and volume; the subscripts a, w, and s, denote mass or volume for air, water and solid content, respectively. The strength of a rock is usually

higher for higher grain packing density (i.e. inverse of porosity). The decrease of strength as function of porosity in a vesicular lava is shown in Figure 3.2. The decrease of strength with porosity is seen to be exponential. Although most rocks are characterised by much lower porosity (e.g. 0.1-1.0 %), Figure 3.2 does clearly illustrate the role of porosity on strength.

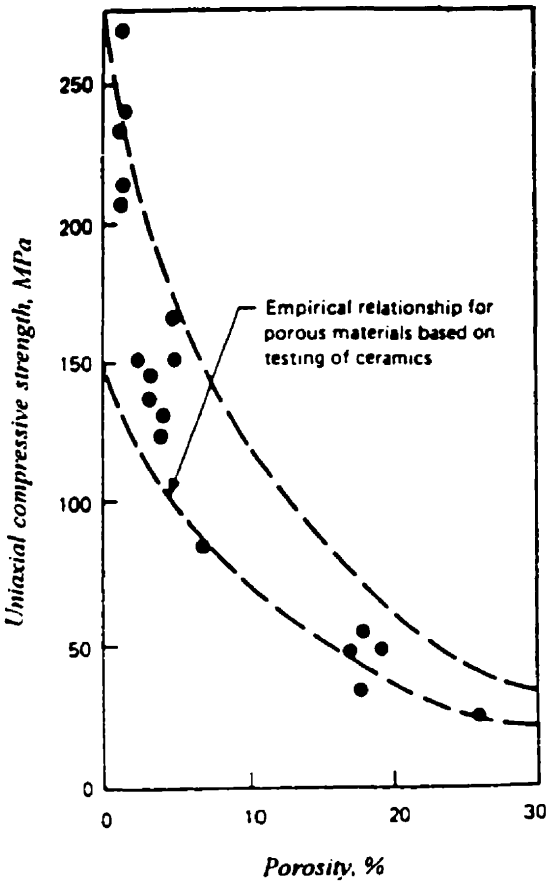

Figure 3.2: Effect of porosity in reducing the strength of rocks and other brittle porous material. Data relate to tests on a vesicular lava from California, after Franklin and Dusseault (1989).

3.5 Strength and deformability (static)

Strength or deformability is the resistance against applied force. It may be represented in terms of strength, hardness, modulus of elasticity etc., depending upon what is being tested and the test method employed. For example the resistance of a rock (in terms of stress) at failure is denoted as its strength. The resistance of material to regain its original shape (stress increase or decrease for unit change in strain) is denoted as its modulus of elasticity. The resistance of a smooth surface to scratching, cutting, drilling and indenting (in terms of load per unit area) by a mechanical tool is denoted as hardness. The time dependent resistance of material against wear is called abrasivity.

3.5.1 Strength

The strength of rock, besides its microstructure, is also influenced by intensity, direction and duration of load; size and shape of sample; confining pressure, moisture, water content and temperature of the test conditions. The strength of rock increases with increasing loading rate and confinement; however, it decreases with increase in moisture content and temperature. Compressive, tensile and shear strengths are three types of strength measured in three different types of load application. Generally, rocks have very low tensile strength, moderate shear strength, and high compressive strength. Table 3.1 shows the general strength values of some typical rock types. The high compressive strength is due to the loss of energy attributed to friction, plastic deformation, and generation of microcrack. The continuous crack resulting from compressive failure

remains intact, and such failure results in creation of fine particles at the weakest inclined plane. In tension, on the other hand, there is no friction involved between the grains, and

Table 3.1: General strength values of some typical rock types (after Farmer, 1968).

Types of rock	Compressive strength (MPa)	Shear strength (MPa)	Tensile strength (MPa)
Basalt	143.4	5.9-49.0	5.9-29.4
Gabbro	147-294	3.9-8.3	4.9-29.4
Granite	98-275	4.9-49.0	3.9-24.5
Dolomite	14.7-245	2.5-6.9	2.5-24.5
Limestone	3.9-245	1.5-49.0	1.0-24.9
Sandstone	49.0-167	2.9	19.6-24.5
Gneiss	78.0-245	12.4-31.0	3.9-19.6
Quartzite	85-353	19.2-57.4	2.9-4.9

failures leads to separation of relatively large sizes. Only cohesion comes into picture and that too at the weakest point. The various strength tests can be conducted on small or very large cores or blocks, either in the laboratory or in the field. The choice of specimen size is determined by design requirements, rock conditions and time and cost. The compressive strength is most commonly measured under unconfined uniaxial load conditions. It can also be determined under hydrostatic compressive environment, biaxial compression, axisymmetric tri-axial and poly-axial tests. In the field, the compressive strength is measured using flat jacks alone or in combination of jacks with the specimen prepared by line drilling or cutting with a saw. The tensile strength is measured in

uniaxial tension using epoxy to bond the rock sample to the steel platens. The most common method for measuring tensile strength is by Brazilian test in which load is applied over a disc specimen, diametrically. The load at failure is used to calculate the tensile strength. The tensile strength can also be measured by 3-point, and 4-point bending methods. The same is measured in the field by dilatometer method. The dilatometer consists of a flexible tube, a pump to inflate the tube and instruments to measure pressure and volume. The shear strength is measured for a joint or plane of weakness by applying a constant stress normal to the plane and then steadily increasing the tangential stress (perpendicular to the normal load) until sliding occurs due to failure of rock under shear. In tri-axial tests, this is determined from Mohr-Coulomb's failure envelope by measuring large sets of minor an major principal stresses at failure. However, the bulk of these tests are carried out under static or very low strain rate conditions. The present work aims at measuring strength at high strain rate, more appropriate to dynamic fracture behaviour of rock.

3.5.2 Deformability

Deformability is expressed by respective elastic constants i.e. Young's modulus, shear modulus, bulk modulus, Poisson's ratio, and Lame's constants. For isotropic material, only two of these elastic constants are independent. The rest of the parameters can be calculated from two known values. These constants are used in evaluating rock deformation under various loading conditions. It can be calculated under uniaxial, biaxial or tri-axial stressed environments. The ratio of stress to strain under uniaxial stress

application, shear stress application and compressibility gives Young's, shear and bulk moduli, respectively. With respect to the conservation of volume relationship under compression or tension, there is always a strain perpendicular to the direction of stress or strain application. The Poisson's ratio is defined as the ratio of the transverse strain to the corresponding axial strain, when the load applied is axial and within the elastic limit.

In a typical stress-strain diagram, the modulus of elasticity is low in the beginning (due to crack closure), then it becomes high and fairly constant for a linear stress-strain conditions. Further loading leads to catastrophic failure in a brittle rock. Whereas, in rocks exhibiting plastic deformation, the modulus may actually decreases before failure. Failure is essentially the result of the generation of irreversible microcracks and their coalescence. In layered rock, the modulus of elasticity is usually greater in direction normal to the layers as compare to that along the parallel direction.

The strength and deformability properties of a rock, calculated under static load conditions, are not very useful in predicting the behaviour under dynamic conditions. Dynamic failure is related to the rate of stress or strain applied, during breakage. In the context of dynamic fracture, as in blasting, the rates are in the range of 10^{-2}-10^{4}/sec.

3.6 Dynamic behaviour of rock

Under blasting conditions the maximum stress applied to the rock is very high. Since the duration of the stress applied is very small, the strain rate is thus very high. Intitutively, the dynamic moduli would therefore be higher under high dynamic loading conditions than under static ones. Since moduli and strength correlate approximately, it

also implies that dynamic strength would be higher than its static counterpart. The sudden application of load through explosives also leads to generation and propagation of shock waves in the rock. The velocity of shock waves (which later degenerate into seismic waves), as will be discussed later, is much higher than the rate at which a fracture in rock can travel. This energy imbalance leads to the creation of multitude of cracks resulting in intense fracturation of rock.

3.6.1 Energy transfer under dynamic loading

Elastodynamic theory states that only two types of wave can propagate in an unbounded elastic medium. These are body waves, e.g. the longitudinal (primary or P) and transverse (secondary or S) waves. In bounded structures (e.g. an open pit bench, drift etc.) several types of waves are generated. The most important waves are the body waves and the surface waves and their multiple reflections from the free surfaces. The surface waves travel along the surface or the interface between individual layers. The most important surface waves are Raleigh wave. In blasting, the body waves are more important near the explosive source. The P wave travels faster than the S wave. The velocities of P and S waves can be expressed in terms of elastic constants as follows.

$$V_p = \sqrt{\frac{(\lambda + \mu)}{\rho}} = \sqrt{\frac{(K + \frac{4}{3}\mu)}{\rho}} \qquad (3.4)$$

$$V_s = \sqrt{\frac{\mu}{\rho}} \qquad (3.5)$$

where V_p and V_s are velocities of P and S waves, respectively, ρ the density of the rock, K the bulk modulus, and λ and μ are Lame's constants. The P wave velocity, V_p, is a function of bulk modulus (K) and the shear modulus (μ), whereas, the velocity of the S wave, V_s, is a function of shear modulus (μ) only. The stress associated with wave propagation velocity can be represented in terms of density and particle velocity, v, at the wave front. For a plane wave, the stress associated with the wave can be expressed as,

$$\sigma = \rho . \ V_p . \ v \qquad (3.6)$$

The P and S wave velocities, in the laboratory, are measured using a resonant frequency method or by ultrasonic wave transmission tests. The wave velocities, in the field, are measured by inducing seismic waves, either by detonating explosives on the surface or in the borehole or by mechanical impacts. The wave velocities are affected by varius factors such as: anisotropy of the rock, stress condition or confinement, grain size, porosity, moisture content, and temperature of rock. The dynamic modulus of elasticity in the laboratory is determined by measuring P and S wave velocity and the density of the medium. Table 3.2 (Rinehart, 1965) shows some typical moduli for a quartzite rock under static and dynamic loading conditions.

Table 3.2 Comparison of static and dynamic elastic properties (Rinehart, 1965).

Property	Dynamic	Static
Poisson's ratio	0.19	0.22
Young's modulus (GPa)	85	72
Shear modulus (GPa)	36	29

3.6.2 Dynamic strength

Intitutively it can be assumed that the breakage in the vicinity of the blasthole ensues when compressive stresses associated with the outward propagating stress waves exceed the dynamic strength of the rock. Since the detonation pressure of the explosives in the borehole is at least an order of magnitude higher than the typical strength of rock, a zone of intensely crushed region is formed immediately around the borehole. The crushing is due to the collapse of the inter-crystalline or inter-granular structure; the intense crushing is due the dynamic compressive effect as cracks branch and multiply to dissipate energy. The dynamic compressive strength in rocks or rock like materials can be measured by the Hopkinson bar apparatus. The details of tests are discussed in a later section.

The dynamic tensile fractures in a blast consist of the radial cracks around the borehole and the fractures due to 'spalling' near a free face. Due to the detonation of explosives radial compressive stresses and tangential tensile stresses act on the surrounding rock masses. Whenever the latter exceed the dynamic tensile strength of the surrounding rock, tensile fractures ensue. Also, reflection of compressive stresses from a free face transforms it to a tensile stress which if of sufficient amplitude can lead to

failure in rock. Some examples of static versus dynamic tensile strengths measured in different rock types are shown in Table 3.3.

Table 3.3 Comparison of static vs. dynamic tensile strengths for different rock types.

Rock types	Dynamic (MPa)	Static (MPa)	References
Bedford limestone	26.9	4.1	Rinehart (1965)
Yule Marble, perpendicular to bedding	18.6	2.0	"
Yule Marble, parallel to bedding	48.3	6.2	"
Granite	39.3	6.9	"
Taconite	91.0	5.9	"
Granite	32.0	8.0	Mohanty (1987)
Greisen (Altered granite)	67.0	16	"
Limestone	51.0	11	"
Quartz diorite	56.0	15	"

3.7 Conclusions

The strength of rock depends on its mineralogy, grain size, microscopic and macroscopic structures and the loading rate. Microstrucural properties play a more critical role in determining the strength of various rock types than the macrostructures, especially, when large blocks of rocks have to be fragmented into very small fragments, as in blasting. The former also affect cohesion, transmission of stress waves through rock and hence the deformational behaviour and strength. Macroscopic structures are usually regular, while microscopic structures are usually random. The strain rates associated with blasting operations are very high, and for a proper understanding of the fracture

behaviour the usual strength properties obtained under static properties are inapplicable. This applies particularly to dynamic behaviour of material under blasting and comminution operations. The aim of the present research is to establish a correlation between microstructure of rock with its dynamic fracture behaviour through experimental and analytical means.

CHAPTER 4

FUNDAMENTALS OF ROCK FRAGMENTATION

The following review encompassing the whole field of fracture mechanics and material failure falls outside the scope of the present study. Nevertheless, it is considered essential in defining the main thrust of this investigation and laying out the foundation for future and continuing work initiated by the present work.

Fragmentation of rock consists of stress or energy application by some means till its strength is exceeded. Obviously, higher stress is needed when the strength is higher. If the rocks are broken by a machine or a tool then the strengths are referred as hardness. The process of fragmentation brings many synonymous terms such as the stress or strain at failure, fracture and failure, hardness etc.. A brief definition of some of the standard terminology used in the process of fragmentation is given here.

4.1 Definitions of fundamental terms

4.1.1 Stress and strain

Stress is defined as the load acting on an unit area. The stress increases when either the load increases for a given cross-sectional area or the cross-sectional area decreases for the given load. Strain is always associated with the stress. It is related to the change in dimension or deformation of the material when stressed. Although all the dimensions of the material get changed, but many times the interest is in the direction of the stress axis only. Thus, the strain is defined as the change in length per unit original length in the direction of the stress. Usually, higher the stress applied, higher is the strain developed in the material. If the strain developed in a stressed body is traced back to zero upon unloading, the reversible strain is called the elastic strain. The initial strain response to a stress is generally linear and recoverable. The limit beyond which the stress-strain curve begins to deviate from linearity is called the elastic limit. If the material is stressed beyond the elastic limit, a permanent change in the shape of the body (either the external surface or the interior in the microstructure) take place. The strain developed is irreversible. The non-recoverable strain is called the plastic strain. The total strain is the sum of the elastic and plastic strain.

In the portion of the stress-strain diagram the yield stress is the stress level beyond which there is a residual strain (upon unloading). The stress-strain curve begins to deviate from linearity beyond this stress. The specimen undergoes strain-hardening upto a point of maximum stress level. The strain-hardening means increasing resistance from inner micro-structural rearrangements for further rearrangements. For the same additional stress

change, more deformation has to be accomplished, thereby material posing as harder and harder. The maximum stress which the material can support is called the critical stress (strength) of the material, the corresponding strain is called the critical strain. These are characteristic to the rock type but get influenced in presence of external and internal environment. It can be also be expressed in terms of energy absorbed in achieving this stage.

The strength is generally expressed in terms of stress in the unit of MPa or N/m^2. Stress is always associated with deformation or strain, which is related to displacement. The product of stress and displacement is work and the capacity of doing work is energy. Therefore, stress and energy are interrelated. A term analogous to strength is expressed in energy form in the unit of Joule. The energy may further be classified in terms of strain energy, surface energy and kinetic energy.The strength in the unit of energy is more common in comminution where energy spent in the process is easier to measure as compared to stress in rock samples.

4.1.2 Fracture and Failure

Very often fracture and failure are used interchangeably in the process of fragmentation. The fracture is a process of failure under the influence of tensile or shear stresses, either applied directly or indirectly. The tensile or shear stresses are generated indirectly under compression. The process of fracture and failure involves crack initiation or extension of pre-existing cracks and their propagation. At first, a stable fracture propagation takes place, which in the presence of continuing load, changes to unstable fracture propagation and finally to failure.

Failure on the other hand, is a global term. Failure is said to occur when there is a decrease in load carrying capacity. The overall failure process (say in case of uniaxial compression) can be divided into three stages with respect to the characteristic stress-strain diagram. The first stage may consist of a non-linear stress-strain region with continuously increasing slope. In this zone an appreciable seismic activity may be noticed associated with pre-existing crack closure. The second stage represents linear elastic relationship between stress and strain. Almost negligible seismic activity is observed in this zone with a uniform modulus of elasticity. The third stage of stress-strain diagram consists of a non-linear elasto-plastic relationship. Strain hardening takes place in this range. Slope of the line decreases continuously, and the seismic activity increases exponentially till failure. The overall fracture and failure can be said to be brittle when a significantly low level strain is developed till the ultimate stress with little or no plasticity. Ductile failure is associated with considerable amount of plasticity between yield stress and ultimate stress.

4.1.3 Toughness

The toughness is another important material property which includes elastic and plastic strain energy absorbed till failure in the sample. The concept of toughness can be explained by various ways. For an un-notched tensile bar it is represented in terms of total area under stress and strain curve till the material fails. For a brittle material the area is small while for a tough material it is large. The former requires less energy or strains for fracture, while the latter needs a large expenditure of energy or strains for fracture. A brittle material shows very high sensitivity of notch i.e. the ratio of tensile strength for a notched and un-notched specimen is very much less than that corresponding to a tough

material. Most rock exhibit brittle behaviour and thus are represented by low toughness. However, some rocks may exhibit a ductile behaviour, resulting in relatively higher toughness. There are standard methods to determine the toughness of a material which are described in more detail in a latter chapter.

4.2 Material parameter under different approaches

In the previous section different terms have been used for representing the behaviour of a rock in a breakage process e.g. modulus of elasticity, critical stress or strain, strength (compressive, shear or tensile), toughness etc.. This could be misleading. Fundamentally, there is only one term representing the strength of a material which is expressed in different form depending upon what we are measuring and how we are measuring. For example, the modulus of elasticity represents the elastic stiffness before breakage, the yield stress represents the stress level beyond which irreversible strain is developed, the ultimate stress or strain represents the strength at failure etc.. The different mechanisms of stress application also bring material parameters in the form of compressive, shear or tensile strengths. The strength at high loading or strain rate are dynamic compressive or tensile strengths. All these parameters are global in concept. However, the local aspect, from where the fracture will start and along which direction it will propagate, uses the material parameter called surface tension or surface energy (a basis for Griffith's law (1921)). This is the energy consumed in creating an unit surface area. In case of brittle fracture, the surface energy, and in case of ductile fracture the elastic and plastic energy (Griffith law modified by Orowan (1955)) are used as a measure of strength in this localised concept. Irwin (1957) labelled this combination of elastic and

plastic terms as fracture toughness. The fracture toughness may also be expressed in terms depending on the nature of stress application, e.g. that due to crack opening, shearing along the crack plane and tearing away from the crack front.

The above mentioned parameters are the subjects of the various approaches employed in modelling a breakage process accomplished by different means. For example, the strength of material approach uses compression, shear, and tensile strengths measured by static or dynamic means; the fracture mechanics uses the fracture toughness; the continuum damage mechanics uses the critical damage. The following section gives a brief description of these approaches.

4.3 Strength of material approach

Under strength of material approach the rock failure is explained by the global material properties such as the compressive, shear or tensile strengths depending upon the way stress is applied. The strength values are largely influenced by the local environmental conditions e.g. the loading rate, the confinement, the temperature and the moisture conditions. Suitable environment is maintained while measuring the strength so that the failure represents the same condition as the objective of the test.

4.3.1 Fracture under different stresses

Fragmentation is the result of creation of simple or multiple fractures in rock. In simple terms it is the separation of rock into two or more parts. It involves initiation of new cracks or extension of pre-existing cracks through the application of suitable stresses. The latter can be compressive, shear or tensile, and can be applied to rock samples by various means.

The different modes of breakage process can be classified on the basis of primary breakage actions, namely, compression, shear and tension, either under static or dynamic conditions. The corresponding stresses at failure are called compressive, shear and tensile strength of the material. In compression, considerable amount of energy is wasted in friction or plastic deformation. However, it is the most economic method of industrial breakage process due to the ease of stress applications. The broken particles consist of a wide range of fragment sizes. The larger fragments are due to crack propagation and crack coalescence within the rock material, while fine fragments are due to friction or shearing-off of the broken pieces. Some of the cracks present after breakage remain unconnected within the material. Rock materials can also be broken by shear, as usually done in shear strength tests. This results in relatively more efficient use of energy. It has, however, certain operational problems when used on an industrial scale. The shear force is applied by mechanical tools which are made up of brittle iron alloys. These tools are subjected to large tension during operation, resulting in high rate of tool failure. Therefore, this method is applicable in breaking rock material of only intermediate strength. Breaking rock, in tension requires as little as 10 % of the stress required for compression breakage. Here breakage takes place at the weakest part of the material. Fragment sizes obtained are in narrow range with very less amount fines. The major problem with this method of size reduction lies in suitably anchoring of the rocks. Compression, shear or tensile stresses can be applied on low to very high rate of loading depending upon the requirements. Shatter or high impact breakage is dynamic in nature where a very large amount of stress is applied in a very short time. This method of fracture is more typical of rock blasting.

Dynamic breakage normally results in the creation of large number of fine fragments as the time available for the crack growth is limited.

4.3.2 Fracture under different strain rates

The stress or energy application in a breakage process may be associated with low, intermediate, or high strain rates. The examples are, mechanical breakage in tension or compression, breakage in crushing or grinding, and breakage by dynamic means or blasting, respectively. It should be noted that the phenomenon of creep is also a low strain rate fracture process, but it is not considered as a practical fragmentation process, hence omitted in the present work. Some examples of typical loading time, the nature of stress and the associated strain rates are shown in Table 4.1. Although the classification is somewhat arbitrary, it does provide us with a useful guideline to classify various fracture processes under different strain rates.

Table 4.1: Example of loading time and strain rate for different fracture processes.

Property	Low rate	Intermediate	High rate
Loading time (Sec)	$10^{6}-10^{4}$	$10^{4}-10^{2}$	$10-10^{-6}$
Strain rate (Sec^{-1})	$< 10^{-8}$-10^{-6}	$10^{-6}-10$	> 10-10^{4}
Type of Stress	Static load	Mechanical load	Impact or explosion
Example	Standard tests	Crushing & grinding	Blasting

4.3.2.1 Fracture at low strain rate

In this process, the rate of strain applied to rock material is low (~10^{-6} per second). Failure takes place by propagation of single or a few cracks. Therefore, the fragments produced are larger sized and fewer in numbers. The relevant strength properties of rocks are measured either in the laboratory or in the field in terms of tensile, shear, or compressive strengths depending upon how the stresses are applied. The measured parameters are specific to the internal rock structure (minerals, grain network, anisotropy etc.) and the external environmental conditions (confinement, temperature, moisture etc.). The measured values are used further in various failure criteria to predict stability, deformational behavior or failure in rocks under some predominant behavior of rocks or rock masses. The classical failure criteria are the Coulomb (for cohesive but frictionless material), the Mohr (for cohesion less but frictional material), and a combination of these in the Mohr-Coulomb. The latter expresses the failure condition in terms of stresses applied and the compressive and tensile strength, or shear and frictional angle. The other standard failure criteria of common use are the maximum tensile stress, or shear stress criteria utilizing the tensile and shear strength, respectively. All these failure criteria are based on stress approach in which strengths are expressed in terms of a critical value of stress applied. The failure behavior of rocks is also explained using energy point of view, the Griffith (1921) theory. This criterion explains the unstable extension of a crack in a material in terms of a balance between changes in mechanical and surface energies. The useful energy utilised during a fracture process can be correlated with strain energy, fracture surface energy, and kinetic energy. Most of the energy is dissipated as heat, and

vibration. The strain energy (force x deformation) consists of energy spent in deforming the material. Energy is also used up in initiation of cracks and its propagation. This can be grouped under 'fracture surface energy'. If the energy associated with the crack front is more than the intra-crystalline molecular strength, fracture propagation will take place. The critical stress,σ, needed at the outer surface of body is expressed as:

$$\sigma = \sqrt{\frac{2E.\gamma_s}{\pi.a}} \qquad (4.1)$$

where, γ_s, is the surface energy, a, is the half crack length, and E is the Young's modulus of elasticity. Orowan (1955) modified the Griffith's theory by incorporating a plastic energy term which is more appropriate in metals or some rock exhibiting non-linear fracture at the crack tip. The excess amount of energy at the crack front is utilised in rock displacement and in the kinetic energy imparted to the rock fragments. The rest of the strain energy is wasted in the form of heat (or friction), and ground and air vibration.

The strength related parameters (e.g. compressive, shear, or tensile strengths, and surface or elastic, and plastic energy etc.) and the various failure criteria are the subjects of conventional rock mechanics. The details of it can be found in any text book on rock mechanics such as- Jaeger and Cook (1979), Brady and Brown (1993). There are various other empirical or curve fitting failure criteria in terms of stresses applied and the strengths of the materials. Although these failure criteria are global in nature but are suitable for many engineering problems. Among them the most important and the widely used is the Hoek and Brown (Brady and Brown, 1993) criterion. This criterion is based upon a large number of data available from laboratory and field test of rocks and rock masses. It takes

into account of major (σ_1) and minor (σ_3) principal stresses, compressive strength, σ_c, and the degree of interlocking, S, between blocks in a jointed rock mass. This is given as:

$$\left(\frac{\sigma_1}{\sigma_c}\right) = \left(\frac{\sigma_3}{\sigma_c}\right) + \sqrt{\left(\frac{m.\sigma_3}{\sigma_c} + S\right)} \qquad (4.2)$$

where, m, varies with the rock type. The term 'S' indicates the brokenness of the rock mass before the application of failure stresses (S equals 1 for intact rock and 0 for broken rock). Hoek and Brown further suggested a failure envelope based on a large amount of experimental data on compressive (σ_c), tensile (σ_t), and shear (τ) strengths, and some curve fitting parameters such as A and B in the following equation.

$$\left(\frac{\tau}{\sigma_c}\right) = A\left(\frac{\sigma}{\sigma_c} - \frac{\sigma_t}{\sigma_c}\right)^B \qquad (4.3)$$

Most of the failure criteria of rock mechanics provide a good engineering tool to predict the behavior of rocks, however, they do not always provide a physical basis for explaining the failure process. They also fail to explain fracture behavior in the presence of cracks, discontinuities, and also under different loading rates.

4.3.2.2 Fracture at intermediate Strain Rate

Crushing or grinding operations are example of intermediate strain rate processes. Fracture may be caused by a single impact as in crushing or a large number of impacts as in grinding. The strength of a material or the energy needed in its breakage is determined in pilot plant tests using a strength related parameter called the work index. This originates from the Bond's theory (1952) of comminution and is measured in the laboratory using a

standard procedure (the details are discussed in the later chapter). Alternatively, the use of work index in the pilot plant tests gives the efficiency of the crushing or grinding operations by measuring the actual energy consumed in the given comminution process. The work index is further used to estimate the size of the fragmentation in a given comminution process. These size distributions obtained in a crushing or grinding process are further used to develop the kinetics of breakage in a comminution processes.

4.2.2.3 Fracture at High Strain Rate

Rock breakage by high strain rate (~10^1 to 10^4 per second) involves propagation of stress waves and imparting kinetic energy to the rock material. Independent crack nucleation takes place as the velocity of stress wave is much higher than the rate of crack propagation. The input of energy to the rock by stress wave is much higher than the dissipation of energy (cracked surface). The surplus energy causes independent crack nucleation and crack branching. The resulting fragments are smaller in size but larger in numbers, thus producing more fines. The crack branching is also enhanced by the interaction of reflected stress wave from the free face.

The dynamic nature of stress conditions around a borehole has been known for a long time. The dynamic stresses are found to be much higher before decaying and approaching to the stress level calculated for a static solution, Mohanty (1982). The fracture strength and the fragment sizes in such situations have been analyzed both numerically and experimentally in detail by Grady and Kipp (1989). The dynamic fracture models based on the strain rate, the strength and the fracture toughness have been found to be very close to that obtained by high strain rate laboratory and field results. The

following paragraph describes the work briefly.

Dynamic fragmentation is explained by means of two approaches. The first approach uses stress or stress intensity factor in combination with the existence of distribution of flaws or sites of weakness. The second approach uses kinetic energy rather than strain energy contributing to the fragmentation. The flaws are considered to be idealized and penny shaped. The flaw distribution is assumed to be given by the two parameter Weibull distribution:

$$n = k\,\varepsilon^{m} \tag{4.4}$$

where, n is the number of flaws per unit volume which can activate at or above a tensile strain level ε, the constants, k and m, are characterized as material parameters for fracture activation which could be determined experimentally. The original damage (ω) before the load application is simply the volume times the number of flaws. However, the dynamic damage due the various crack growths is calculated by integrating the number of flaws which get activated in the specified time, t. The basic assumption is that, as soon as the crack gets activated, it reaches the crack velocity, C_g, and the radius of crack growth is the product of crack velocity and the time duration. The simplified equation for the damage is expressed in terms of k, m, the constant strain rate of ε, C_g, and time t.

$$\omega(t) = \frac{8\pi C_g^3 k}{(m+1)(m+2)(m+3)}\,\varepsilon_o^m t^{m+3} \tag{4.5}$$

By using the continuum damage mechanics, the stress is given as the reduced modulus of elasticity times the strain.

$$\sigma(t) = E\,\varepsilon_0 t\left(1 - \frac{8\pi C_g^3 k}{(m+1)(m+2)(m+3)}\,\varepsilon_o^m t^{m+3}\right) \qquad (4.6)$$

The dynamic strength is the highest level of stress achieved at the critical damage, ω_c, occurring at the critical time, t_c. For a strain rate of 100/sec, k=1.7 x 10^{27} m^3, m=8, and C_g = 1300 m/s, the time resolved stress and commulative damage is shown in Figure 4.1.

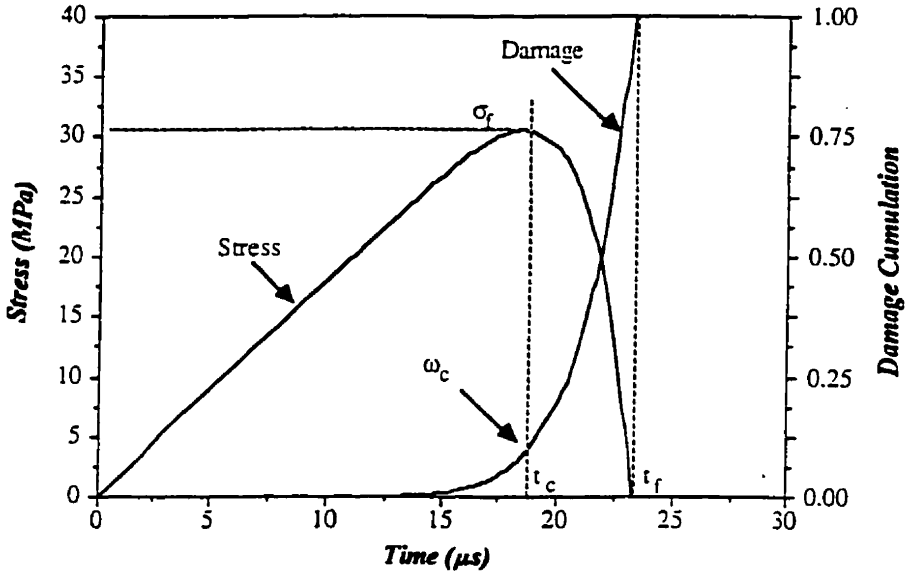

Figure 4.1: Stress history and damage cumulation for oil shale under a constant strain rate loading of 100/sec (after Grady and Kipp, 1989).

As the loading time increases the stresses applied also increases till failure. The stress in the material, thereafter, decreases. The damage remain unaffected below a threshold limit of strain. It increase exponentially with time after the limit. Almost constant strain rate loading has been noticed in early time, followed by rapid stress relaxation as damage

accumulates. The crack velocity is considered as an additional tensile fracture property which governs the rate of damage growth during dynamic fracture. The damage is dependent on the transient strain, strain rate and crack velocity. The critical tensile stress, the critical time and the critical damage comes to be 30.6 MPa, 18.5 microseconds, and 0.083, respectively.

The fragment size corresponds to the time, t_f, at which the stress reduces to zero and the damage, ω_c, becomes 1 (fully fractured). The fragment size, X, is assumed to be twice the radius of crack growth. The strain rate dependent maximum size of the fragment is given as:

$$X(\max) = \frac{6C_g}{m+2}\left[\frac{8\pi C_g^3 k}{(m+1)(m+2)(m+3)}\right]^{-1/(m+3)} \varepsilon_o^{-m/(m+3)} \tag{4.7}$$

The fracture strength and the fragment size for the measured properties (crack velocity, Weibull parameters, k m etc.) of oil shale are given in terms of the strain rates:

$$\sigma_{fracture} = 8.7\,\varepsilon^{0.27} \tag{4.8}$$

$$X_{size} = 0.48\,\varepsilon^{-0.73} \tag{4.9}$$

For the large set of experimentally measured dynamic tensile strengths at strain rates ranging from 10^1 to about 10^4/sec, the dynamic strength has been found to be dependent on the strain rates raised to the power of 1/3, (Grady and Kipp, 1989). A similar strain rate dependency on the tensile fracture stress to the strain rate (10–30/sec) for quartz has been found by Birkimer (1970).

The dynamic strength has also been modeled using the fracture toughness. The fracture toughness in the dynamic case was obtained by multiplying the static fracture toughness, K_{IC}, with a function of normalized time. The normalized time is expressed in terms of the shear wave velocity, C_S, and the time duration of fracture for a crack of length 2a in an infinite plate under dynamic stress. The dynamic stress is expressed in terms of dynamic strain times the modulus of elasticity, E. The strain rate dependent fracture stress for an isolated crack is given by

$$\sigma_c = \left(\frac{9\pi E K_{IC}^2}{16.N^2.C_s}\right)^{1/3} \cdot \varepsilon_0^{1/3} \qquad (4.10)$$

where N is a geometric co-efficient equal to 1.12 for penny shaped crack, and ε, the strain rate. Equation 4.10 has been verified to hold good for a sufficiently flawed medium also. In a body consisting of a large number of flaws, cracks beyond a characteristic length 'a' (equal to $(C_s K_{IC}/E\ \varepsilon_0)^{2/3}$) are expected to propagate. Though the above model relies on the presence of flaw distribution, it cannot explain all the observed effects in dynamic fracture and fragmentation. The energy balance principle in contrast still play a role in the process. Attempt has been made to model dynamic fragmentation by energy approach (Grady, 1982). In this approach, the kinetic energy rather than elastic strain energy is considered to be the primary source of driving the fracture process. The surface tension associated with the newly created surfaces resists the fracture process. Assuming spherical fragments of equal size, the fragment size, d, can be given in terms of fracture toughness, K_{IC}, density, ρ, and wave velocity, C_1.

$$d = \left(\frac{\sqrt{20}\, K_{IC}}{\rho C_1 \varepsilon .}\right)^{2/3} \qquad (4.11)$$

The above equation has been successfully verified to predict the fragment size in oil shale in dynamic fragmentation. The energy approach of fragmentation has been found to be more reliable in estimating the fragments in fully broken rock mass. However, flaws activation approach is found to be more suitable in predicting the fracturation i.e. surface creation.

4.4 Fracture toughness in rock breakage

Under this approach, breakage depends on the size, orientation and spacing of pre-existing cracks and the rock's resistance to crack extension. The material property associated with its ability to carry loads or resist deformation in the presence of a crack is defined as the stress intensity factor, K. The concept of K was first introduced by Irwin (1957). The stress intensity factor is analogous to the stress developed in the material. The critical stress at which a material fails (strength) is similar to the critical stress intensity factor (also called fracture toughness).

4.4.1 Introduction to fracture toughness

The phenomenon of lower strength of a material in comparison to its theoretical strength, and the decrease in strength with increased size led the foundation of fracture mechanics. Griffith explained the above behaviour due to the presence of cracks, flaws, micro-cracks and other discontinuities. The presence of micro-cracks in rock could be seen under optical or electron microscopes. These microstructures are distributed

randomly and act as stress concentrators which cause low strength. The concept of stress concentration around a circular or an elliptical opening was first given by Inglis (Atkinson, 1989). The stress concentration near the crack tip in an infinite plate under remote tensile stress is given by:

$$\sigma_{max} = \sigma(1 + 2\sqrt{a/\rho}) \qquad (4.12)$$

where σ_{max} is the maximum stress at the end of the major axis of the elliptical crack; σ is the stress applied to the plate at remote end normal to the major axis of crack; a is the half of major axis of the crack; and ρ is the radius of curvature of the end of the crack which is equal to b^2/a in terms major, a, and minor, b, axis lengths of the crack. The stress concentration effect increases with the crack size which is more likely to be found in a bigger sample of material. Also, the stress concentration is higher near a fresh sharp crack and is less in blunt or larger crack radius. Consequently, the ultimate stress or strain supported by the material is low due to higher stress concentration effects at the crack tips. Cracks and flaws in rock are found even at the microstructural level around grain boundaries or within the grains depending on the nature and rock type.

4.4.2 Definition of fracture toughness

As mentioned earlier, fracture toughness is the resistance of a material against crack extension. Therefore, it is defined in the vicinity of the crack tip only. The stresses, strains and displacements near a crack tip can be determined by Airy stress functions (Whittaker, 1992). For an infinite plate subjected to uniform biaxial tension of stress, σ, along both directions at infinity, Figure 4.2 illustrates the crack tip co-ordinates and stress

state in terms of both cartesian and polar co-ordinates. The stresses, σ_{yy} , σ_{xx}, and σ_{xy} surrounding the sharp crack tip are given as:

$$\sigma_{yy} = \sigma\sqrt{\frac{a}{2r}}\cos\frac{\theta}{2}\left(1 + \sin\frac{\theta}{2}\sin\frac{3\theta}{2}\right)+\ldots \tag{4.13}$$

$$\sigma_{xx} = \sigma\sqrt{\frac{a}{2r}}\cos\frac{\theta}{2}\left(1 - \sin\frac{\theta}{2}\sin\frac{3\theta}{2}\right)+\ldots \tag{4.14}$$

$$\sigma_{xy} = \sigma\sqrt{\frac{a}{2r}}\left(\sin\frac{\theta}{2}\cos\frac{\theta}{2}\sin\frac{3\theta}{2}\right)+\ldots \tag{4.15}$$

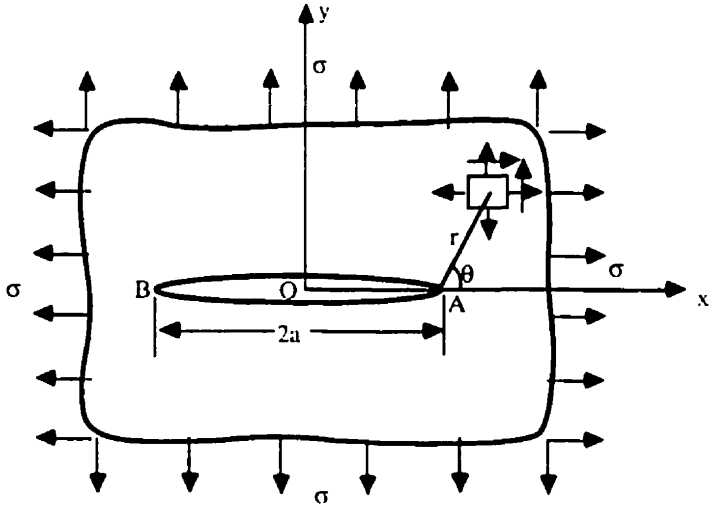

Figure 4.2: Infinite cracked plate in a biaxial stress of state (after Whittaker, et al., 1992).

For uniaxial application of stress in one direction the stresses are obtained by super-positioning '$-\sigma$' state of stress in the other direction. This superposition does not affect the above stress distribution. The stresses are expressed in terms of polynomials containing distance r from crack tip and angle θ from the plane of the crack. At close vicinity of a crack the high order 'r' terms may be neglected. The '$\sigma\sqrt{a}$' term in equation 4.13, 4.14, and 4.15 is equivalent to a material property as per Griffith's criterion (equation 4.1). Irwin (1957) defined this term as 'stress intensity factor' K_I. The subscript, I, refers to mode I (crack opening or failure in tension). Thus, the stress distribution around a crack can be represented in terms of $K_I/r^{1/2}$ terms. In other words, stresses, strains and displacements near a crack tip can be represented in terms of the stress intensity factor, K_I. The stress intensity factor (similar to stress distribution) depends on the stress level applied, the crack size and the geometry of the specimen. For an infinite thin plate with elliptical and through crack at the centre, and loaded at remote ends The stress intensity factor in generalised form can be expressed as:

$$K_I = Y.\ \sigma\sqrt{\pi a} \qquad (4.16)$$

where, Y is a dimension-less parameter depending upon the loading geometry and the crack type, σ, the stress applied on the specimen and, a, the half crack length. With the change of size of the plates and the position and types of crack, the equation is multiplied by a material independent, dimension-less parameter. The later is calculated in the terms of the crack and specimen sizes. A large number parameters (near about unity) have been calculated for different crack geometry and specimen dimensions, Sih (1973). For an

infinite length of plate the value of Y is unity. When the remote stress reaches a critical value, say σ_c, fracture ensues at the crack tip. Crack initiation or fracture propagation takes place when the stress intensity factor, K_I, near the crack tip reaches a critical value, called critical stress intensity factor, K_{IC}. This is also called the fracture toughness. The K_{IC} is a material parameter and is independent of size and loading geometry. It is denoted in terms of MPa $m^{1/2}$ or $MN/m^{1.5}$. The distinction between stress intensity factor, K_I, and fracture toughness, K_{IC}, is analogous to the distinction between stress and yield strength.

The subject of fracture mechanics deals with the crack geometry, the stress level applied, and the characteristic material property, the fracture toughness. Nevertheless, other factors such as temperature, loading rate, stress concentration, residual stresses etc. also influence these three primary factors. The fracture mechanics approach gives an insight of breakage process i.e. where and when the fracture will start depending upon the crack size and its sharpness (leading to the stress concentration effects), the stress level applied and the material property, fracture toughness. The fracture toughness is thus defined as the resistance of material associated with the ability to carry loads or resist deformation in the presence of a crack. This explains, a) the critical stress needed for failure in a given crack geometry, b) the critical crack size at which material fails for the given stress level, and c) the time required for a crack to grow from some initial size to the critical size.

4.4.3 Fracture toughness modes of fracture

Irwin postulated that failure at crack level can be divided into three possible mode which are necessary and sufficient to describe any crack behaviour. Crack tip can be

subjected to tension or a normal stress σ_{yy}, an in plane shear stress σ_{xx}, or anti plane shear stress σ_{zz}. Figure 4.3 shows the three basic mode, Mode I, Mode II and Mode III of crack tip deformation under the three stress field σ_{yy}, σ_{xy}, and σ_{yz} respectively. A combination of any two of the three mode constitutes a mixed mode such as Mode I-II, Mode I-III, Mode II-III. The most complicated mode of fracture is Mode I-II-III. Fracture toughness determined in pure mode I is called K_{Ic}, in pure mode II is called K_{IIc}. For the mixed mode of I+II we have to specify the crack and loading geometry.). The current work is limited to fracture toughness of mode I only, as it is the most dominant failure mode in rock mechanics.

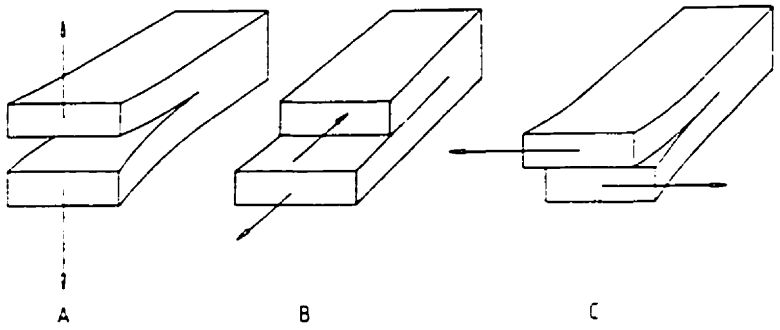

Figure 4.3: Schematic drawing illustrating three fundamental modes of fracture; A: mode I, tensile or opening mode; B: mode II, shear or sliding mode; C: mode III, anti-plane or tear.

4.4.4 Crack tip fracture process zone (FPZ)

With reference to Inglis formula (equation 4.12), or that given by the Irwin for the stress intensity factor (from equation 4.13, 14 or 15) it is observed that stress concentration becomes infinity at the crack tip for a closed crack (i.e. the radius of curvature is zero). This means that a sharp crack will no longer be in stable condition even with infinitesimal stress. This, however, is not true. Actually, a material sustains a load below its yield stress. Accordingly, a small plastic (or non-linear elastic) zone is assumed to be present around the crack tip in which stresses are released non-elastically. This zone is referred to as the plastic zone in metal, and crack tip micro-cracking or fracture process zone, FPZ, in rocks. The presence of a FPZ near the artificially created notch has been demonstrated by Atkinson (1989); and Labuz, et al. (1985). A schematic development of fracture process zone in rock is illustrated in the Figure 4.4. It includes four stages of its development, followed by the final crack growth. In the first stage a few fresh micro-cracks are generated near the tip of the notch. As the load is applied increases, more micro-cracks are generated. The behaviour is elastic in the stress-strain diagram. This completes the second stage. In the third stage more micro-cracks are created and the behaviour of the rock is non-elastic. The slope of the stress-strain curve decreases. At stage four, the ultimate stress is reached and the crack propagation from the notch tip takes place together with the severe micro-cracks. The crack growth is always preceded by this FPZ. The size of this zone is theoretically calculated by the distance at which the radial stress reaches yield stress (in metal) or tensile strength (in rocks). In terms of fracture toughness, K_{IC}, and the tensile strength, σ_t, it is assumed to be extended upto a

distance of $(K_{IC}/\sigma_t)^2/\pi$ ahead of crack tip. This is a material parameter (Ouchterlony, 1980) and is much larger in rocks than that in the metals.

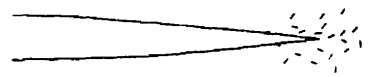

Stage 1: Developement of microcrack near a notch

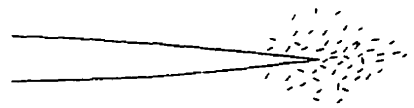

Stage 2: Further generation of microcrack near the crack tip
linear behaviour of material under stressed condition

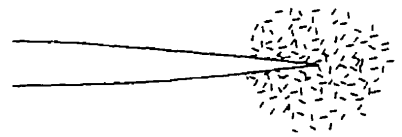

Stage 3: Further generation of microcrack near the crack tip
non-linear behaviour of material under stressed condition

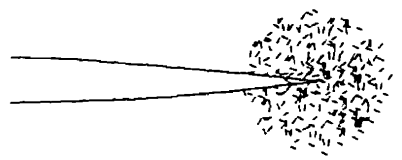

Stage 4: Developement of a critical fracture process zone, FPZ
the radius equals to a distance at which the effective stress is tensile strength

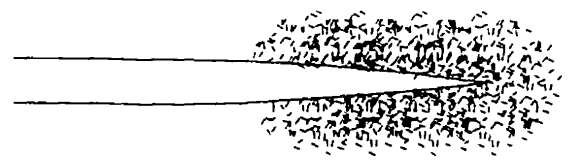

Stage 5: Cross linking of the weak cracks along the path of crack,
crack propagation from the crack tip led by the critical FPZ

Figure 4.4: Schematic drawing illustrating the development of a FPZ and its influence on macrocrack growth. (after Atkinson, 1989).

Labuz et al. (1987) have estimated this zone to be about 40 mm and 90 mm in Charcoal and Rockville granite, respectively, using the ultrasonic probing and acoustic emission technique. The size of the FPZ limits the minimum dimension of sample to be tested in a fracture toughness test. The former should be sufficiently less as compared to the other dimensions of the specimen. Traditionally, this was assumed to hold true by keeping the minimum size to be more than the10 times the grain size. However, with the present level of knowledge about crack propagation ahead of the FPZ, this 10:1 ratio is not always true. The solution, therefore, is either maintain sufficiently large sample (hence costly and time consuming) or use low size sample as compared to FPZ and use a correction factor of the non-linear zone. Barker (1979) and Ouchterlony (1986) have shown that by loading and unloading samples during the test of the fracture toughness, the non-linear effect is compensated to the apparent value of the fracture toughness.

The above sections described the principles of strength of material and the fracture mechanics approach. The former uses the measured values of compressive, shear or tensile strengths to predict the failure in rocks. This approach is global in nature i.e. it does not account for the presence of crack or crack geometry within the rock. However, the strengths values measured for the rock consisting crack or crack geometry can be used to represent the behavior of cracked rock or rock mass. The fracture mechanics approach describes the mechanics or mechanism of crack growth in presence of a dominant crack either present at microscopic scale or at macroscopic scale. The failure, thus could be explained by knowing fracture toughness and the dominant crack size and the stress level applied. The limitation which this approach is when there is a large number of cracks

which is true many times, especially, in rocks. The next section describes the behaviour of rocks in the later case.

4.5 Micro-structural damage mechanics

Microstructure of rock may be defined by a large number of entities such as pores, voids, cracks, discontinuities, inclusions, grains networks etc.. All of these may originate from the origin of the rock or part of it may be induced during the phase of transformation of rocks to the current status. The cumulative effects of these factors on the behavior of rock are difficult to analyze individually (details are discussed in a later chapter). However, the de-bonding of microstructure upon loading (creation of cracks, voids, re-alignment of grain network producing further cracks or discontinuities) can be expressed in a global term, such as 'damage.' This is used to describe, collectively, the effect of material change on the macroscopic mechanical properties. It is the volume fraction of material that has been stress relieved by multiple micro-crack interaction and growth. Damage, D, can be represented in the scale of 0 to 1. Intact rock represents D=0, whereas, fully damaged (separated) rock represents D=1. The critical damage must be in between and would depend on the material and stress environment.

$$D = 1 - \frac{undamaged\ area}{total\ area} \tag{4.17}$$

The scalar representation of damage was given by Kachanov (Whitakker et al., 1992). It was assumed as a global index being distributed all along the material, thereby predicting the strength of a rock type. With increase in damage, D, (decreasing supporting surfaces) the effective stress, σ_e, can be written in terms of stress, σ and D.

$$\sigma_e = \frac{\sigma}{1-D} \tag{4.18}$$

The effective stress increases under constant load till full separation of the faces takes place. Damage accumulation is also reflected in continuous degradation of modulus of elasticity and Poisson's ratio, as has been shown analytically by Budiansky and O' Connell (1976) in terms of crack density.

$$D = \frac{16}{9}\cdot\frac{(1-\bar{\nu}^2)}{(1-2\nu)}\cdot C_d \tag{4.19}$$

If the crack density, C_d, is known the effective Poisson's ratio can be calculated and thus damage, D can be estimated (Taylor, 1986).

$$C_d = \frac{45}{16}\cdot\frac{(\nu-\bar{\nu})(2-\bar{\nu})}{(1-\bar{\nu}^2)[(10\nu-\bar{\nu}(1+3\nu)]} \tag{4.20}$$

For a typical value of Poisson's ratio for an undamaged rock specimen, a large sets of crack density was calculated by assigning arbitrarily different values to the reduced Poisson's ratio values. The change in Poisson's ratio, the consequent change in crack density and the calculated damage has been shown in the Figure 4.5. The Poisson's ratio of the original rock was assumed to be 0.23. As seen in the figure, the crack density and the damage both increases with decrease in Poisson's ratio. At about 50 % of decrease in Poisson's ratio, the crack density approaches 32 % and the damage approaches 1 i.e. material is almost failed.

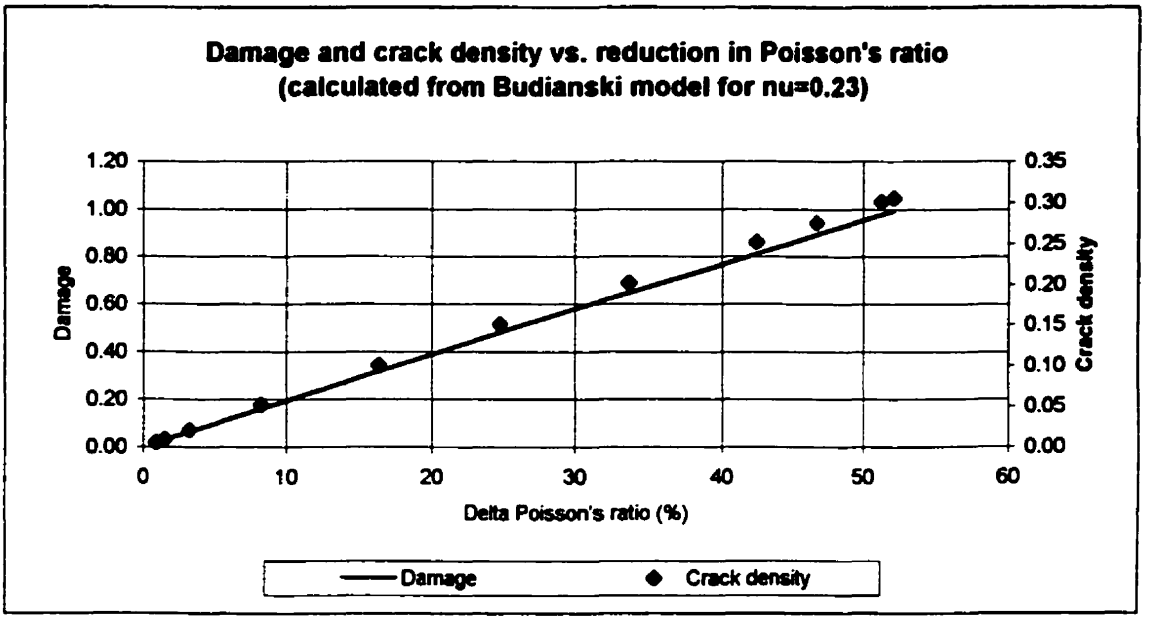

Figure 4.5: Degradation of Poisson's ratio, crack density, and damage profile.

The crack density is thus an important microscopic parameter affecting various physical and mechanical behaviour. A knowledge of it would assist in quantifying the role of micro-crack on the strength properties of rock. The crack density for this figure was calculated using equation 4.20. However, it may also be calculated independently using micro-structural measurements in the laboratory.

4.6 Limitations of the various approaches

The strength of material approach is very convenient when material is homogenous and isotropic. However, it is known that rocks are an-isotropic and consist of large amount of cracks or microstructure. Furthermore, rock may contain a dominant crack a relatively large crack. In such cases use of the strength of material approach would be

limited to a specimen size much larger than the size of the defects in it so that the material could be assumed isotropic despite its presence.

The use of fracture mechanics is very helpful in predicting the failure mechanism, especially, when one predominant crack is present. In case of a large number of cracks, some numerical techniques have also been developed to calculate the maximal stress intensity factor which indicates the origin of fracture under the given stress level. However, the analysis is complex. The use of fracture mechanics is limited by the size of the specimen and the crack size. The prediction of failure is valid well beyond the fracture process zone, but sufficiently close enough to the crack tip when linear elastic fracture mechanics hold good.

Microstructural damage mechanics has been used successfully to understand the growth of damage in a material before failure. It could be measured easily by indirect means such as acoustic events monitoring or the reduction in wave velocities etc. However, it is not known how the damage level will predict the failure process in presence of a weak plane or joints under mechanical loading.

The fracture mechanics and the continuum damage mechanics have been applied to explain the fracture process in presence of a large number of cracks. The first approach predicts the most critical weak plane where the cracking will start; the second predicts the complete failure or collapse of material when overall damage or the reduction in modulus of elasticity exceeds a critical level. The latter approach has achieved more success in modelling material failure due to the ease in measuring the crack density either directly or

through indirectly by measuring degraded modulus of elasticity or Poisson's ratio. However, it has been demonstrated by Kachanov (1990) that these two disciplines are independent and there is no direct correlation between the two.

4.7 Conclusions

Fragmentation of rock is achieved by applying stress or energy beyond a limit. The stress beyond this limit, the strength, and the energy absorbed beyond this limit are inter-related. The strength is usually measured in terms of stress, and it is conveniently measured during a test. However, in comminution it is expressed in terms of energy measured by energy spent in the process. The work index is considered as a relevant material property under intermediate strain rates. The strength of a material under a suitable environmental condition is a global engineering term which is used to predict the deformation or failure of a material. The fracture toughness approach, however, represents the strength of a material in the presence of a crack. The presence of fracture process zone which exists before the crack tip is very critical in the application of the fracture mechanics principles. In the presence of a large number of cracks, the micro-structural damage approach is used to predict ultimate failure in a material. All the three concepts (strength of material, fracture toughness and the micro-structural damage) have been developed independently to model the fracture process at different scales.

The stress or energy application may be accomplished by low, intermediate to high strain rate. There are a large number of rock properties influencing these breakage processes. The modulus of elasticity, compressive, shear and tensile strengths are examples of it. The wave velocity, the crack velocity and the fracture toughness have also

been used to model the dynamic breakage process. In addition, there are other macro- or micro-structural rock properties which greatly control the fracture processes. The following chapters describe in detail some of these parameters, how they have been measured in the laboratory in the present study, and how they affect the strength properties. Since the investigation has been conducted on laboratory scale specimens, the microstructural aspects have been elaborated in detail, and the macrostructural aspects ignored.

CHAPTER 5

MATERIALS AND METHODS

5.1 Materials Selected

Altogether, twelve different rock types were selected with the objective of measuring their fracture related properties in the laboratory, and later, correlating them with their respective microstructural properties. The following section gives a brief background for the rock types selected for this investigation.

The rock types have been identified by the names of their respective locations. An descriptor for the colour or texture has been used to emphasise its predominant character. The selected rocks types consisted of a wide variety of mineral and textures ranging from near isotropic and homogenous to sedimentary and an-isotropic. The nearly isotropic rocks consist of four granites, namely, the light grey coloured Stanstead granite, the Lawrentian pink granite and gneissic granite, and the grey coloured Barre granite. The an-

isotropic rocks consisted of three different blocks of marble from the Noranda Copper mine of Gaspé region of Quebec; Limestone from Kingston and St. Catherines regions of Ontario; Gneiss from the Hemlo region of Ontario; and Quartz from Bastakong region of Quebec.

The Stanstead area belongs to the Beebe region of eastern townships in Quebec near the international border of Vermont. This region is a part of the plain beside lake Memphremagog situated at about 45 km south of Sherbrooke. The surface topography is gently rolling with minor hills while the granite deposit is a continuous massive batholith with unconnected outcrops or masses at the surfaces. The deposit is of the Devonian period when the Appalachian region was subjected to mountain building forces. The folded and faulted strata was invaded by the intrusive deposit of granite. The length of the deposit along the north-south is about 2-3 km and the associated sediments are slate, quartzite, and limestone. The granite (A) is of medium to coarse grained texture. In almost all occurrences the rock is a biotite, or biotite-muscovite granite, depending upon the content of the biotite which ranges from 3 to 14 % and rarely as high as 20 %. The colour is white, pale, grey, to a dark colour depending upon the content of the mica. The Stanstead area is one of the oldest source of commercial granite in Quebec or in whole Canada. One of the companies supplying this rock is the Stanstead Granite Quarries Company Limited, which sells different rocks under different trade names such as pale, light grey, or dark granite.

The Lawrentian region is a part of the Grenville province of the Precambrian Canadian shield. It lies north of St. Lawrence and north-west of Quebec city. The Lawrentian granites and granite gneiss are the dominant formations to the north of the Lac St-Jean as far as Mistassini river. The rocks are pink, grey, or graintoid gneiss with quartz, orthoclase, oligoclase, biotite, and hornblende as its essential constituents. The gneissic granite (K) appears homogenous with the dark and light mineral bands, but the individual structure is obscured by complicated drag-folding, injection or segregation of pegamitic and aplitic facies. The irregularity of the banding formation is uniform as a whole but complex in details. The granite deposits are of two types, namely the grey and pink coloured. The former is associated with feldspar of oligoclase, whereas, the later has feldspar of microcline and albite. The pink coloured granite (H) has a coarse grained texture. The joints are sufficiently widely spaced so that the large blocks of granites are easily extracted. The pink granite and the gneissic granite are supplied by the Canadian Red Granite Company Limited. It is located in the vicinity of village Rawcliff at about 8 km north of Grenville station on the Canadian Pacific railway line between Montreal and Ottawa.

The Barre region is located at about 50 km south-west of Burlington in the state of Vermont, USA. This granite (J) is an intrusive deposit of Devonian age, concordant on a regional scale but discordant at local contacts. The deposit is the result of slow cooling of magma under the upper Paleozoic sediments. The outcrop of the deposit is bifurcated and is somewhat elliptical shape with about 7.1 km long and 3.0 km wide. It is surrounded by

Silurian Westmore formation consisting primarily, of various inter-bedded micaceous and quartzose schist. A small portion of the north east boundary is in contact with the younger rock formation consisting of calcareous rocks with inter-bedded mica schists. The overall formation varies from 0.9 to 1.2 km. The deposit is invaded by 2-3 predominant fractures except with some exceptions in the south-eastern part of the lower quarry. The granite consists of 26 % quartz, 35 % plagioclase, 19 % potassium feldspar, 18 % mica and less than 2 % accessory minerals.

The Noranda Copper mine is in the Gaspé region in the province of Quebec. The geological settings belong to the Appalachian orogen of Phanerozoic period. It lies east of the Candian shield and the St lawrence platform. The rocks are mostly, carbonate, shale, quartzite and graywacke. The carbonate rock samples were acquired in two phases. In the first phase, the samples were brought in the cored form (rock-B). These are very homogenous equi-granular white to greyish-white calcareous marbles with less than 3 % of disseminated sulphides. The rock specimens, F, and G belonged to the later phase of shipments in the form of irregular blocks. The rock, F, consists mainly of quartz and mica, whereas, the rock G is a foliated gneissic marble.

The Kingston and the St. Catherine areas lie in the eastern and the western parts of the Lake Ontario, respectively. These regions belong to the St-Lawrence platform adjacent to the Grenville province of the Canadian shield. The St-Lawrence platform is the result of the warm and shallow seas covering of about 1-3 km width. The predominant rocks are quartz-rich sandstone, overlain by inter-bedded carbonates and shales. The

Kingston limestone (C) is from a quarry located at about 5 km east of the Kingston city, whereas, the Vineland limestone (E) is from the country side of Vineland in the region of St-Catharines.

The Hemlo gold region is located near the north-east shore of Lake Superior, 35 km east of Marathon, adjacent to Trans-Canada Highway 17. The deposit is a part of Wawa subprovince of the Superior province of Ontario, a sequence of Archean meta-sedimentary and volcanic rocks. The rocks are folded into a broad doubly-plunging syn-form, called Hemlo-synform. The cored samples (D) from Page Williams mine consist of well defined foliation planes. The grains exhibit a sugary texture.

The quartz (I) is from a small quarry, located in the Baskatong reservoir and located at about 40 km north of Ottawa and about160 km north east of Montreal. The area lies in Grenville province. The rocks are of Precambrian sedimentary formations. Beds of sandstone and quartzite are widely distributed in most parts of the province. The other important rock formation consists of marble, amphibolite, biotite parageniss, and pink granite. The quartz is milky white in colour and totally re-crystallised. The foliation is apparent only if sufficient impurities are present.

The rock types employed in this investigation along with their respective alphabetical symbols are shown in Table 5.1.

Table 5.1: Rock samples with their symbols.

Rock samples	**Symbols**
Stanstead granite (Quebec)	A
Altered marble (Gaspé region, Quebec)	B
Limestone 1 (Kingston, Ontario)	C
Gneiss (Hemlo region, Ontario)	D
Limestone 2 (St. Catharines, Ontario)	E
Marble 2 (Gaspé region, Quebec)	F
Gnessic marble (Gaspé, Quebec)	G
Lawrentian granite (Quebec)	H
Quartz (Baskatong, Quebec)	I
Barre granite (Vermont)	J
Gneissic granite (Lawrentian, Quebec)	K

The details of the microstructure such as mineralogy, grain size and grain structure and their measurement are presented in chapter 6. The measured values of the fracture related properties are discussed in the following sections.

5.2 Physical properties

The physical rock properties measured are porosity; density; longitudinal (P) and transverse (S) wave velocities; the dynamic Young's, bulk, and shear moduli of elasticity; Compressibility; and the Poisson's ratio. The following section describe the details of these measurements.

5.2.1 Porosity

Porosity is the ratio of pore volume consisting water and air trapped in the solid to total volume. It can be expressed as:

$$\%P = \frac{V_w + V_a}{V_s + V_w + V_a}$$

where, V_w, is volume occupied by water, V_a is volume occupied by air, and $V_S+V_W+V_a$ is the total volume constituting solid, water and air. The porosity for the rock specimen were determined by water saturation method as suggested by International Society of Rock Mechanics, ISRM (ISRM, 1977). The shape of the sample varied from right circular cylinder to irregular such that the minimum dimension was more than the 10 times the grain sizes and the weight of each pieces was 50g or more. The pore volume occupied by water and air trapped was calculated by difference of weight in water- saturated surface-dry samples and oven dried samples. The first was measured by saturating the samples with water while running the suction pump for at least an hour with intermittent agitation of the samples to remove the trapped air. Saturation is considered to be achieved when a vacuum of about 800 Pa is maintained for an hour. Samples were then cleaned on the

surface with moist cloth and weighed to get saturated, surface-dry weight. The second, oven dried weight, was weighed after heating the samples in the oven at a temperature of 105^0 C for 24 hours. The total volume was calculated by the measuring the length and the diameters of the samples as the samples were in cylindrical shapes. The total volume of the saturated-surface dry samples were also measured by loss in weight when immersed in water. The ratio of these two gives the porosity. The porosity for all the samples are shown in Table 5.2.

5.2.2 Density

Density of a rock is the intrinsic physical property that denotes the heaviness of the mineral content of the rock in its unit volume. This is influenced by the type of minerals, discontinuities, and the type of fluid saturation. The density of the samples was measured by the standard water immersion method. The measured values are shown in Table 5.2.

Table 5.2: Porosity and density of the selected rock types

Rock type	Porosity (%)	Density (kg/m^3)
Kingston Limestone-C	0.18	2705
Quartz-I	0.21	2630
Gneissic Marble-G	0.24	2735
Marble-F	0.25	2720
Altered Marble-B	0.27	2865
Stanstead granite-A	0.60	2680
Barre Granite-J	0.69	2630
Gneissic Granite-K	0.78	2750
Lawrentian Granite-H	0.96	2650
Gneiss-D	0.68	2780
Vineland Limestone-E	2.32	2685
Vineland limestone-L	2.33	2640

The table shows the rock types with increasing order of porosity. The lowest porosity value is obtained for the Kingston limestone (C). This is because of the greater degree of packing of extremely small grains sizes. On the other hand Vineland limestone (L) yielded an exceptionally high porosity value and comparatively lower density because of the relatively larger grain sizes and weak inclusions. The low porosity in the quartz (I) is due to the absence of grain boundary, weak planes, and any other inclusions. All the marbles (G, F and B) are of similar porosity but relatively high density is due to the very fine grained minerals and their higher packing density. The granites (A, J, K and H) are of comparatively similar porosity and density except the pink granite, H, having a high porosity. This may be due to the biggest difference in grain sizes whereas, the comparatively low porosity and high density in gneissic granite is due to the filled grain boundaries. Higher density in case of gneiss, D, for its moderate porosity is due to some of the heavier minerals which could be identified by the metallic lustre.

5.2.3 Stress wave velocity

There are two principal types of elastic waves: body waves and surface wave. The body waves propagate through the solid medium and are divided into longitudinal (or primary, P) and transverse (or secondary, S) waves. The particle motion due to a P wave is compression or rarefaction with no rotation of material. The particle motion in S wave is transverse, thus causing shearing or rotation. The S wave changes the shape of the material while also compressing it. The P wave travels faster than the rod and S wave. The deformation of material due to P and S wave and their particle motion is shown in Figure

5.1. The shape of the P and S wavefronts depends on the characteristics of the source that is used to generate the waves.

The surface waves are generated when the solid body is limited by a free surface. They travel along the surface or the interface between individual layers. The particle motion is both along and perpendicular to the direction of waves, typically in elliptical shape. The intensity diminishes very rapidly perpendicular to the free surface or the depth (zero at one and half times the wavelength). The velocity of the surface wave is about 0.9 times the shear (S) wave velocity.

If the solid medium is infinite, the waves generated are P and S, as discussed. If the solid medium is in the form of a plate with the thickness of the order of the wavelength, the wave velocity is called plate velocity. If the solid medium is in the form of a rod, the wave propagated is called rod wave. The diameter of the medium in the latter case should be of the order of one third than the wavelength of the wave (Kolsky, 1963). The details of the generation and its use is discussed in dynamic compressive measurement section.

5.2.3.1 Measurement of wave velocity

The ultrasonic pulse velocity technique was used for measuring P and S wave velocities in the laboratory. The principle behind the instrument is that a piezoelectric transducer (such as barium titanate) converts a mechanical deformation into electrical charge and vice-versa. An equipment with a frequency range up to of 300 kHz was used to generate P and S waves in the rock specimens.

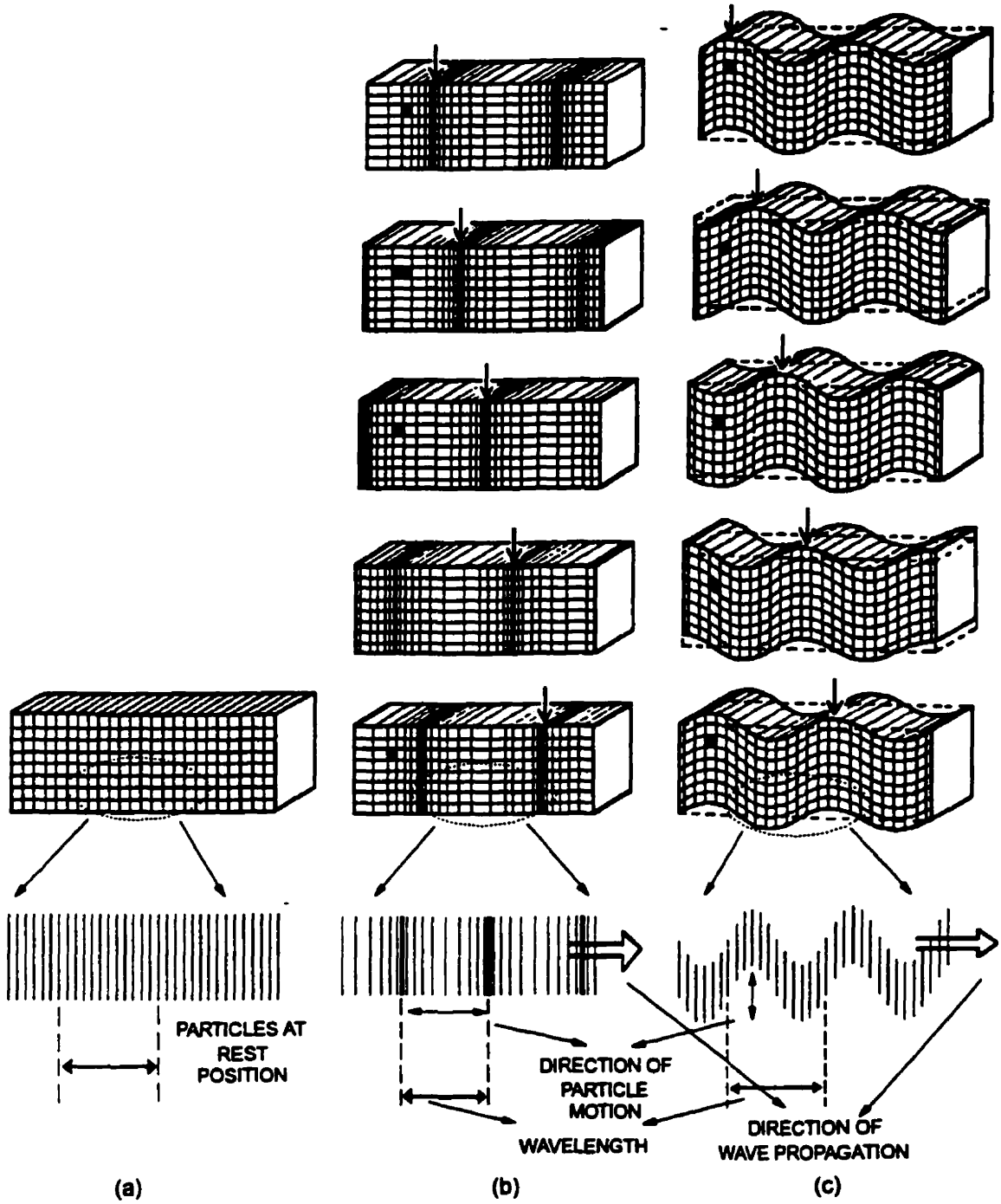

Figure 5.1: Successive stages in the deformation of a block of a material by P- and S-waves and their particle motion. The sequences in progress with time from top to bottom, a) the block of material, b) P-waves, c) S-waves. (after Sadri, 1996).

The minimum lateral dimension of the specimen was kept longer than the 5 times the wavelength of the pulse, λ, and the wavelength was longer than 10 times the average grain sizes of rock samples as suggested by ASTM standard D-2845-99. The miniature transmitting and receiving transducers are coupled to the rock specimen using a high vacuum grease. A portable grinder was used often to make the small contact points (~ 1 cm diameter) flat and smooth for efficient energy transfer between the transducer and the rock sample. The wave is collected by a receiving transducer. The wave trains consisting of P, S and surface wave can be seen on the oscilloscope screen. A typical wave train showing the arrival of P and S wave is shown in Figure 5.2 .

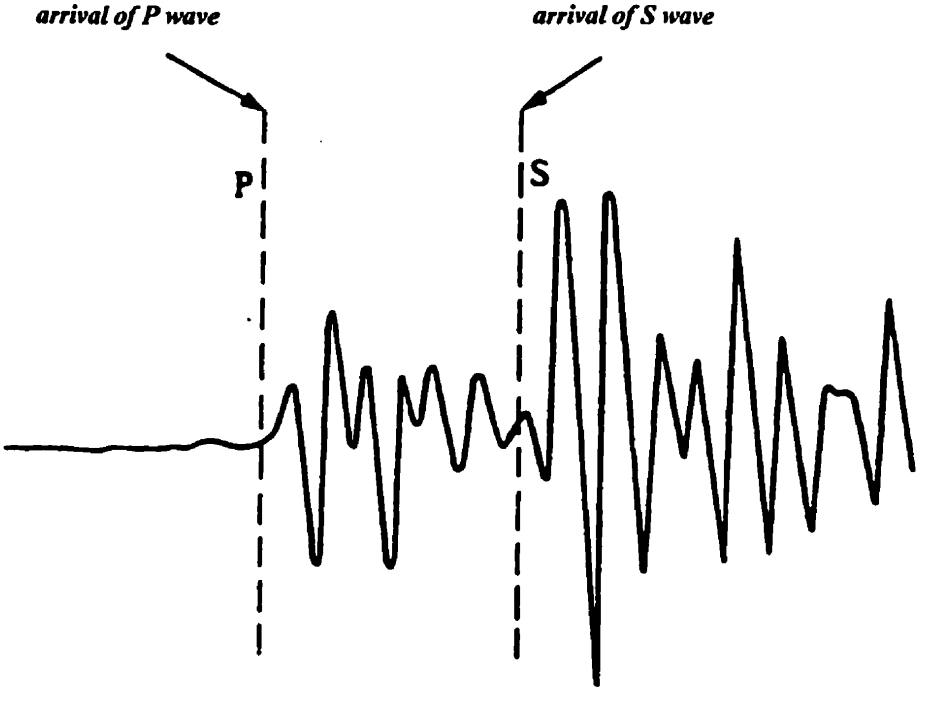

Figure 5.2: A typical wave train showing P and S wave in an ultrasonic tests (Prasad, 1994).

The very first wave arriving at the second transducer is easily detected as a P wave. The recognition of S wave arrival is less straightforward. The transducers were placed selectively along suitable orientations so that the surface wave would face long travel paths and thus S wave would be detected more easily. The distance between the two transducer divided by the delay (arrival) time of the P and S wave gives their corresponding wave velocity in the rock specimen. The wave velocities measured were at room temperature and with unconfined rock samples. The values obtained are presented in Table 5.3.

5.2.4 Dynamic elastic properties

The Young's modulus, E, the bulk modulus, K, the shear modulus, μ, and the Poisson's ratio, ν, are function of P-wave velocity, V_p, the S-wave velocity, V_s, and the bulk density, ρ, of the medium. These can be calculated by using following equations.

$$E = \frac{\rho V_S^{\,2}.(3V_P^{\,2} - 4V_S^{\,2})}{V_P^{\,2} - V_S^{\,2}} \tag{5.1}$$

$$K = \rho.(V_P^{\,2} - \frac{4}{3}V_S^{\,2}) \tag{5.2}$$

$$\mu = \rho.V_S^{\,2} \tag{5.3}$$

$$\nu = \frac{V_p^{\,2} - 2V_S^{\,2}}{2(V_p^{\,2} - V_s^{\,2})} \tag{5.4}$$

The compressibility was calculated as inverse of the bulk modulus.

5.2.5 Results

Table 5.3 summarises all the dynamic elastic properties i.e. the wave (P and S) wave velocity, the Young's modulus, shear modulus, bulk modulus, compressibility, and Poisson's ratio.

Table 5.3: Measured dynamic elastic properties of the test rocks.

Rock Type	P wave m/s	S wave m/s	E G Pa	μ GPa	K GPa	Compressibility (1/GPa)	Poisson's ratio 'ν'
Stanstead granite-A	4170	2670	44.04	19.11	2645	0.05	0.15
Altered Marble-B	5430	2830	60.28	22.95	2930	0.02	0.31
Kingston Lst.-C	5340	2900	58.73	22.75	2480	0.02	0.29
Gneiss-D	4770	3080	60.26	26.37	2760	0.04	0.14
Vineland Lst.-E	5300	3250	67.99	28.36	2750	0.03	0.20
Marble-F	4650	3075	57.20	25.75	2765	0.04	0.11
Gneissic Marble-G	4770	3080	59.28	25.95	2575	0.04	0.14
Lawrentian Granite-H	4330	2800	47.40	20.78	2610	0.05	0.14
Quartz-I	4420	2600	43.93	17.78	2520	0.04	0.24
Barre Granite-J	4250	2715	44.79	19.39	2625	0.05	0.16
Gneissic Granite-K	3750	2370	36.07	15.45	2765	0.06	0.17
Vineland Lst.-L	4665	2880	52.21	21.90	2700	0.04	0.19

The scatter in the above experimental data is mainly associated with sample extraction, sample preparation and measurement. For example, the effect of first two can be seen in the case of Vineland limestone (E and L) and marble from Mine Gaspe (B, F and G), even though these belong to the same family of limestone and marble, respectively, and from same region but from different blocks. The scatter due to measurement is common to all the specimen. However, errors due to the measurement are minimised by using a large number of repeats and relatively large test samples.

5.3 Compressive and tensile strengths

The commonly measured compressive and tensile strengths of a rock in the laboratory are known as unconfined compressive strength and Brazilian tensile strength, respectively. The former employs a standard cylindrical core sample for which load at failure per unit area of the core gives the unconfined compressive strength. In the latter case a cylindrical core in form of a disk is loaded diametrically. The load at failure is used to calculate the tensile strength. Failure is considered to take place when a sudden drop in applied load is observed and no further load can be supported. The load in compression for both the tests is applied by a servo-controlled hydraulic stiff machine which releases all the energy to the rock samples immediately after the failure. The machine is augmented with the digital control which facilitates the recording of data before and after the failure accurately.

5.3.1 Servo-controlled testing machine

The servo-controlled hydraulic stiff testing compression machine (R.D.P. Howden 2500 kN), employed in this investigation, was designed primarily for monitoring post failure characteristics of various geological materials. It was later modified by MTS to augment with TestStar II technology i.e. with digital control technology, application software and mouse driven graphical user interface. It provides an extremely versatile tool for investigation of the complete deformation behavior of rock and concrete over a wide range of testing conditions. Lowering of the cross-head is achieved by the hand held panel. It gets hydraulically clamped at the desired level so that the specimen can be placed

beneath the loading platen. An actuator piston attached to the cross head is capable of applying load to a maximum of 2500 kN in compression and 1250 kN in tension over a total working stroke of 100 mm. The applied load is measured by a pressure transducer giving differential pressure across the double acting piston. When testing very weak materials, or smaller specimen, a more precise load cell of 250 kN maximum capacity is attached as a subsidiary unit. The complete system has been designed to achieve a minimum stiffness rating of greater than 2500 kN/mm. This maintains a maximum continuous actuator velocity of 150 mm/sec. A computer provide a link between the TestStar control system and the user. Its mouse-driven graphical interface system finds and displays the information needed to run the tests quickly. It also stores the test applications data for further analysis. The system software gives quick access via the computer to all the controls for setting up a test. Using the menus on the main TestStar window one can assign transducer, define control modes, sets limits, auto-zero sensors, select readout signals and when necessary, set up parameters such as error limits or turning off the system.

5.3.2 Compressive strength measurements

This is measured by applying an uniaxial stress to a standard geometry of specimen under standard conditions. The procedure as suggested by US Bureau of Mines (1974) was selected as a reference because it gives more flexibility in selecting shorter sample length and smaller diameter. Also, the length to diameter ratio (2:1) as suggested in this standard was more appropriate for uniaxial compressive tests of very small samples. The

small test samples were used for comparing the corresponding dynamic compressive strength in which a similar length to diameter ratio was a necessity. Although, the standard ignores the effect of the sample sizes and the micro- and macro-structure which control the measured strength to a great extent. However, a sample diameter of more than 10 times the maximum grain size has been suggested in the standard.

The compressive strength of the rock samples was determined at various diameters. This is because a part of the present work is to compare the compressive strength measured in a static condition to that measured in a dynamic condition. The later is measured in small diameter (9 mm) samples at a strain rate of 10^3 /sec. The compressive strength values have been compared with the fracture toughness measured in 29 mm diameter samples. However, the sample geometry and the loading conditions are maintained as suggested by the standard procedure. The length of the samples was maintained at about a 2:1 of length to diameter ratio. The end faces were made perpendicular to the axis of the core using the diamond cutting saw and then followed by grinding with the help of lapping machines. The length of the sample represents a balance. The excessive length ensures pure compressive stresses at the centre of the test piece but may cause failure in bending. On the other hand an excessively short specimen length will not allow the sample to fail in shear which is a common mode of failure in compressive tests. The load was applied using a spherical seating at the top of the specimen. The diameter of the steel swivel arrangement was 2-3 mm more than the core being tested. The loading geometry is shown in Figure 5.3.

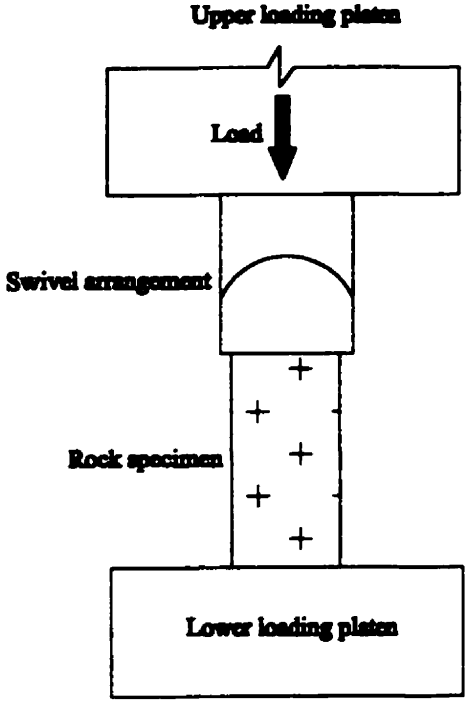

Figure 5.3: A typical loading geometry in an unconfined compressive tests.

The stress rate was maintained within the range of 0.5 – 1.0 MPa/sec as suggested by ASTM. However, this could also be achieved in applying load at a in displacement rate of about 0.001-0.003 mm/sec or causing failure in 5-10 minutes from initial loading. The load was recorded using a load cell with an ultimate capacity of 250 kN. The ultimate compressive stress beyond which it cannot sustain the load gives the unconfined compressive strength. In the present tests, samples as received were used; no special measures were taken to eliminate the presence of moisture in the ambient state. The static strength tests conducted for the rock samples were performed at random orientation with

respect to the bedding planes when present as the core samples drilled from the rock could not be made consistent with respect to the planes of weakness. This resulted in larger than normal scatter in data but it was in keeping with the intention of obtaining 'global' properties rather than that along any specific direction. Table 5.4 shows the compressive strength of selected rock types. The table also shows the standard deviation and number of tests performed on each rock type.

Table 5.4: Compressive strength measured at 29 mm and 9 mm diameters for comparison with fracture toughness and dynamic compressive strength.

Dia.	Diameter~29 mm & L/D ~1.8-2.0			Diameter~9 mm & L/D ~1.7-1.9		
Rock Type	σ_c (MPa)	SD (MPa)	No. of Tests (#)	σ_c (MPa)	SD (MPa)	No. of Tests (#)
A	75	10	11	48	13	15
B	189*	115	8	185	42	8
C	87	25	7	83	27	10
D	58	33	6	40	20	6
E	167*	12	4	77	31	3
F	47	9	6	32	9	10
G	50	9	6	34	13	12
H	132	28	6	67	17	7
I	64	33	6	67	17	5
J	118	12	4	61	16	4
K	82	17	8	52	13	5
L	43	16	4	49	8	4

* represents the compressive strength at 63 mm diameter (Prasad, 1994).

The compressive strength measured at 29 mm and at 9 mm diameter (columns 2 and 5) varied widely due mainly to the larger sized microstructure. The effect of the latter was proved with the help of some additional tests including some test results carried out in

the past. The details of it is presented under analysis and discussion section (chapter 8). Two important conclusions derived from the above data are following. The standard deviation of compressive strength is the highest for the marble and the gneiss samples, due to the well defined weak planes in the former, and the large number of foliation planes present in the latter. For the granite sample, which was reasonably homogenous and free from weak planes, the standard deviation was much lower. In the limestone sample, the compressive strength was measured normal to the prominent bedding planes, and therefore, had very low scatter. The compressive strength of coarse grained rock such as Stanstead granite, A, Lawrentian granite, H, Barre granite, J, and gneissic granite, K, decreases for smaller diameter sample. However, the strength of fine grained rocks such as marble, B, limestone, C, remains more or less constant. The compressive strength of some intermediate grain size such as the gneiss, D, the marble, F, and the gneissic marble, G, varied to a lesser extent than the coarse grained rock samples. The standard deviation in larger diameter samples is due to the weak joint planes and foliation whereas in smaller diameter samples it may be due to their micro-structure. The latter essentially consists of microcrack and grain size characteristics. These influences are further dealt with in chapter 7. This is dealt with in detail in Chapter 8.

5.3.3 Tensile strength

The tensile strength of the rock samples was determined by the Brazilian method. The load is applied in compression. The indirect tensile stress resulting from this arrangement at right angle to the direction of load application gives the tensile strength.

The justification behind this indirect procedure is the experimental fact that most rocks in biaxial stress field fail in tension at their uniaxial tensile strength when one principal stress is tensile and the other finite principal stress is compressive. The test result is, therefore, valid only when the fracture starts from the centre. A schematic layout of the loading geometry is shown in Figure 5.4.

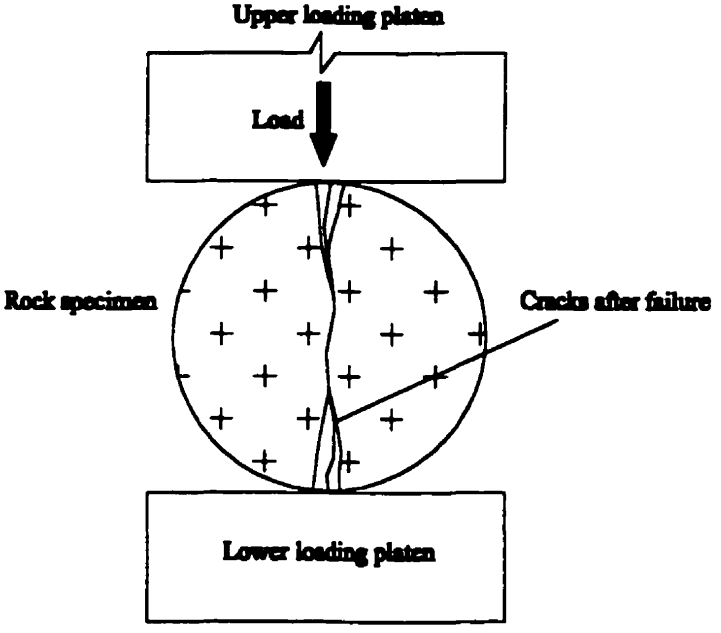

Figure 5.4: Schematic loading geometry in the Brazilian tensile test.

The value of tensile strength as with the compressive strength may be affected by factors such as geometry, environment, rate of loading and the intrinsic properties of rock specimens. Disc specimens with diameter to thickness ratio of 0.3-1 are recommended to minimise the effect of these factors (Hassani, 1980). The cylindrical rock specimen, lying

on its curved side, is loaded diametrically under compression. The load was applied using the same RDP-2500, the servo controlled hydraulic stiff compressive machine. A load cell with capacity of 250 kN was used to record the load. A vertical fracture plane develops along the applied load due to the tensile stress. A sudden decrease in load of 5 % from the maximum load achieved is considered as failure, and is used to stop the loading process. The loading ram is then immediately retracted so that the failed specimen can be taken out without any further crushing. The loading rate is under displacement control (0.0005-0.001 mm/sec) which is sufficient to break the specimen in 10-30 second as suggested by ISRM. The corresponding rate of loading is about 200 N/sec. The tensile strength (σ_t) of the rock in this test is calculated by equation:

$$\sigma_t = \frac{2.P}{\pi.D.t}$$

where P is maximum load at failure, D is diameter of the specimen, and t is height or thickness of the specimen. The Table 5.5 shows the measured tensile strengths for the various rock types, along with the number of samples tested and the respective standard deviation. The measured tensile strength of the specimen containing more discontinuities such as gneissic granite-K, marble-B, gneissic marble-F etc. exhibited a high standard deviation. These variations are probably due to the same considerations as for the

compressive strength test. However, the tensile strength depends on the weakest plane present in the rock rather than the distribution of weak planes in the rock. This is may be the reason that no correlation was found between tensile strength and porosity.

Table 5.5: Tensile strength (Brazilian) for the rock types.

Rock Type	Avg. Dia. (mm)	Avg. Width (mm)	Avg. Strength (MPa)	SD (MPa)	Number of tests
A	51.3	28.9	8.2	1.4	3[3]
A	28.7	15.6	8.5	0.5	3
B	63.2	29.5	15.5	5.3	6[3]
C	28.6	13.0	10.7	2.8	5
D	63.1	32.6	5.6	4.5	5[3]
D	28.7	12.8	12.3	3.0	5
E	27.3	13.6	13.7	1.5	3
F	28.6	14.5	8.9	3.4	5
G	28.7	13.4	11.0	2.5	5
H	28.8	14.9	17.4	2.1	3
I	28.7	14.2	13.9	3.0	5
J	28.8	13.6	11.5	1.0	4
K	28.7	13.4	10.0	3.6	5
L	28.6	12.9	12.9	1.6	3

3-Prasad (1994)

5.3.4 Summary

The compressive strength largely depends on the structure of the sample and its orientation with respect to the direction of loading. In the presence of foliation planes and weak joints a high standard deviation is to be expected. As the size reduces, the weak joints or discontinuities diminish thus resulting in a lower standard deviation. The

measured tensile strength values are also affected due to the presence of discontinuities, and the direction of load applications with respect to joints or foliation, resulting in high standard deviation. However, the strength depends on the weakest plane present with respect to the applied load rather than the distribution of weak planes in the rock.

5.4 Dynamic Compressive strength

5.4.1 Introduction

Rocks are subjected to high dynamic stresses during extraction of ores and minerals, or creation of an open space underground. The same dynamic stresses are also encountered in the process of mining and mineral processing, e.g. cutting, drilling, crushing and grinding. These processes affect greatly the economics and safety aspects of the mining operations. Better understanding of the behaviour of rock under these dynamic conditions is, therefore, essential in selecting the optimum amount of suitable explosives, the design of blast geometry, and the use of this information in modelling the blasting process. Also a knowledge of the dynamic response of rocks would help in the development of improved design of cutting tools and drill bits.

Modelling of blasting process and prediction of blast results are becoming increasingly common practice due to both economic and environmental pressures. However, compared to our knowledge base on the detonation properties of commercial explosives, the properties of rock which control the fracture process are relatively poorly known. The strength properties of a subject rock under high strain rate conditions prevailing during the blasting process constitutes one such example. Due to a general paucity of dynamic strength data, the analytical modelling of the blasting process normally employs either the strength data obtained under static load conditions or some arbitrary extrapolation of the later. Many times the behaviour of rock under dynamic conditions are inferred from corresponding behaviour of metals, ceramics or cements.

5.4.2 A review of dynamic strengths of rocks

The phenomenon of enhanced strength of rock under dynamic condition has been known since the early work of Rinehart (1965), in which the dynamic tensile strength of rocks was determined by reflection of a stress wave generated by a detonator. Since then various means have been used to measure the dynamic strength of rocks over a wide range of strain rates (Grady and Kipp, 1989). The dynamic strength and the fragment sizes resulting at different strain rates generated by a variety of means (i.e. a gas gun, a capacitor, a Hopkinson bar, and a tensile bar) in oil shale are shown in Figure 5.5a and 5.5b.

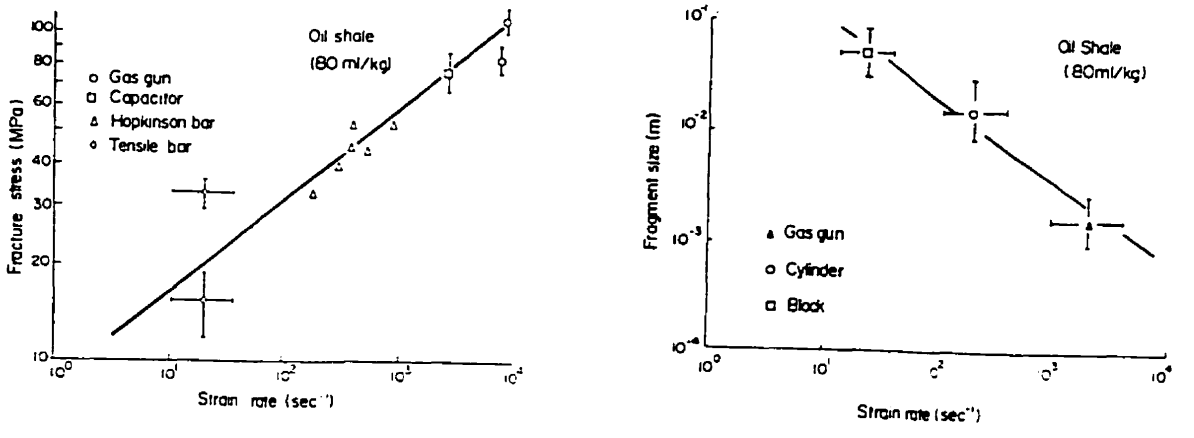

(a) (b)

Figure 5.5: Dynamic fracture strength (a), and fragment size (b), obtained at different strain rates, after Grady and Kipp (1989).

The figures show the increase in dynamic strength and decrease in fragment sizes, respectively, with an increase in strain rates. The plate impact induced spall in rocks have been used by Shockey et al. (1974), Grady and Kipp (1979). The Hopkinson bar or some alteration of it has been used in the past to investigate the dynamic behaviour of rock; under compression by Kumar (1968), Hakalehto, (1969), Lindholm (1974), Lundberg (1976), Buchar and Bilek (1981); under tension by Birkimer (1971), Mohanty (1988); and under torsion by Lipkins et al. (1980). The higher dynamic strength with respect to their corresponding static strength has been clearly demonstrated. However, the details of the comparison between the dynamic and static strength in many cases, especially, the geometry of the samples in the latter case are not available. Table 5.7 shows the dynamic compressive strength measured by split Hopkinson bar, the strain rates achieved, and the ratio of dynamic to static strengths.

Table 5.7: Ratio of dynamic and static compressive strengths of some selected rocks

Rock Types (Reference)	$\sigma_{c\,(dynamic)}$ **(M Pa)**	**Stain rate**	$\sigma_{c\,(dynamic)}/\sigma_{c\,(static)}$ [1]
Grey Basalt (Kumar, 1968)	190	~ 1300	2.2
Grey Granite (,,)	200	~ 1300	2.4
Bohus Granite (Lundberg, 1976)	283	n. a.	1.8[2]
Solenhofen Lst. (,,)	342	n. a.	1.3[2]
Basalt (Buchar & Bilek, 1981)	520	~ 1000	3.0
Granite (,,)	274	~ 1000	3.7
Limestone (,,)	188	~ 1000	3.9
Graywacke (,,)	203	~ 1000	4.0

1 Details of static strength i.e. sample size, diameter etc., are not mentioned in the references
2 Stain rates and the equilibrium of stresses in 50 mm x 25 mm samples are not given.

The dynamic strength of a material can be tested by a variety of means such as drop weight, pendulum, and spring or explosively driven hammer etc.. However, the state of stress or strain at the ends of the specimen is not uniform. Also the problem lies in measuring strains in the sample. The strain rate achieved in all these experimental set-ups are also limited. In contrast, the dynamic strength testing by Hopkinson bar or split Hopkinson bar has led to a very significant advance in high strain rate testing of materials. These techniques yield the highest possible strain rates in uniaxial compression tests under controlled and uniform deformation conditions. The strength of a specimen is calculated indirectly by transmitting and reflecting a one dimensional wave in the specimen as against the usual method of using load cells for measuring stresses and monitoring the change in length for measuring strain.

5.4.3 Split Hopkinson Pressure Bar (SHPB)

The foundation of high strain-rate strength measurement was first laid by Hopkinson in 1872 (Kosky, 1963). His original experiment involved a cylindrical steel bar several feet in length and about one inch in diameter suspended in such a way that it was free to swing in a vertical plane. An impulse was imparted to one end of the long bar, and the test sample was bonded at the other end. The compressive pulse travelling through the bar towards the end gets reflected from the free end as a tensile wave travelling back towards the impacted end. If the net tensile stress developed in the joint between the bar and the end piece exceeds the strength of the joint, the latter fails and the specimen detaches (spalls) at a specified velocity. The momentum of the sample in this case was determined by capturing it in a ballastic pendulum and the momentum associated with the

bar was determined from the amplitude of the swing. Davies (Kolsky, 1963) with the help of strain gages and related electrical transducers, measured the pressure-time relationship more accurately. Kolsky (1963) further modified the instrument by employing two steel bars. The target specimen are sandwiched between the two steel bars and the dynamic stresses and strains within the specimen are measured. The instrument is thus called, split Hopkinson pressure bar (SHPB). The development of SHPB by Kolsky and the measuring devices such as capacitors, amplifiers, strain gauges, oscilloscope etc., led the ground work for measuring dynamic strength upto a strain rate of about 10^4 /sec. Until now, there have been more than 1000 works on the measurement of dynamic strength on metals and composites, more than 200 on soil, cements and concrete, but much fewer on polymers and rocks (Field et al., 1994).

5.4.3.1 SHPB assembly

The SHPB assembly consists of four basic parts: an incident bar, a transmitted bar, a specimen, and a gas gun together with a striker bar. Two strain gauges are soldered at the middle of the incident bar and transmitted bar, respectively, and connected to a data acquisition system. The data acquisition system consists of a wheatstone bridge, a power supply to the bridge and a digital oscilloscope. The steel bars are supported on Delrin bushings and aligned accurately in a line. A schematic diagram of the SHPB assembly is shown in Figure 5.6. The striker bar, incident bar and the transmitted bar are selected to be of the same wave propagation, and also at least twice as long as the incident wave so that the incident and the reflected waves from the end of incident rod do not interfere. The

diameter and the length of the incident and transmitted bars were 9.5 mm and 1 m, respectively.

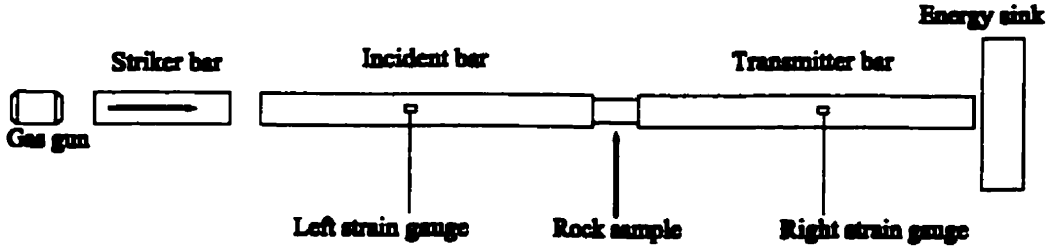

Figure 5.6: Schematic diagram of the Split Hopkinson Pressure Bar apparatus.

The specimen to be tested are of nearly the same diameter (~ 8.3-9.2 mm) as of steel bars and is placed between the incident and the transmitted bars. The length of the specimen (~1.2-1.5 times the diameter) is decided by balancing two opposite constraints. Smaller length (about half of the diameter) ensures multiple reverberations (about 4-5 are needed) of stress pulse to achieve equilibrium of stresses at the end faces of the specimen before breakage. Higher length (about 2 times the diameter as suggested in ASTM tests for static compressive strength tests) allows the rock piece to fail in shear in addition to splitting tension which are common breakage phenomenon during a standard rock mechanics test. For the measured value of the bar velocity, density, and the area of cross section of both

the steel bar and the rock sample; the stress level at the end faces of the specimens were found to be varying by 40%, 27%, 12%, 8% and 5%, respectively, after successive passage of stress pulse. The schematic of the stress reflections and transmissions through the rock and within the steel bar are shown in Figure 5.7.

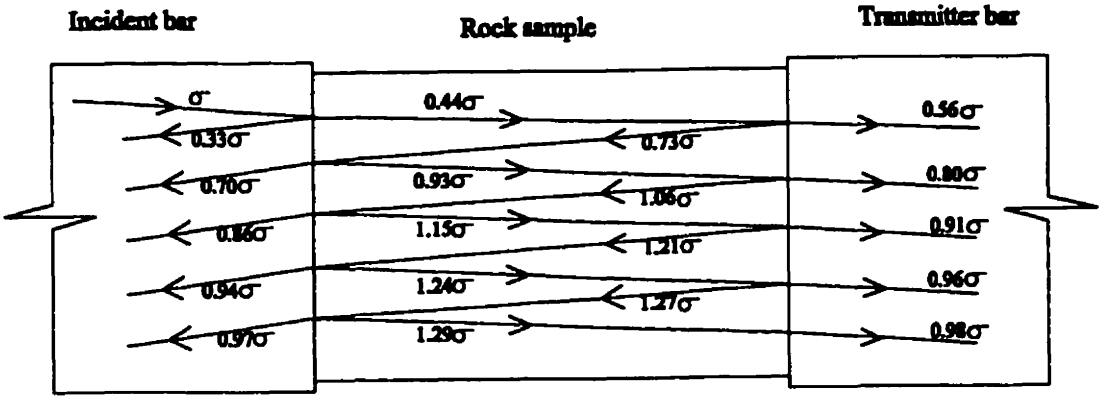

Figure 5.7: Schematic diagram showing stress levels at various reflections and transmission of pulse.

The stress level resulting at various stages are also shown in the Figure. It can be seen that the nearly equilibrium condition of stress is achieved after 4 passes of the stress pulse in the rock sample. The length of the specimens selected in the present work satisfies the requirements of 4 or more reverberations before fracture. For example, in a typical fracture time of 25 μs as observed during the experiments the stress wave passes more than 8 times the length of the sample(rod velocity of 4 mm/μs, and 12 mm sample length in a Stanstead granite sample). Therefore, the selected length of the samples is sufficient

for the assumption in deriving the equation by which the dynamic strength is calculated. The gas gun which supplies energy to the striker rod works in two stages. In the first stage the striker bar is pushed to touch the inner sabot of the assembly and pushed all the way back. Then the first valve is opened which releases pre-purified nitrogen from the tank and fills the outer chamber of the gas-gun assembly upto a desired pressure (700 kPa in this case). The inner chamber still stays at the atmospheric pressure as there is no path for the gas to enter into it. In the second stage the second valve is opened which apply pressure directly behind the sabot pushing it ahead. This movement frees the vent hole between the two chambers, and the pressure accumulated in the outer chamber reaches the back of the sabot. The sabot is then rapidly accelerated pushing the striker in front of it. At the end of the barrel, the sabot is stopped and the bar continues by itself. The speed of the striker bar is directly related to the pressure used in the gas-gun. If friction and wave propagation effects are neglected, the work done by the pressure equals the kinetic energy of the sabot and the striker bar. The velocity of the striker bar is calculated by knowing the pressure, P, cross section area of the sabot, A, the barrel length, ΔS, the mass of the sabot and the striker bar, M_s, M_b, respectively.

$$P.A.\Delta S = \frac{(M_s + M_b).V^2}{2} \qquad (5.4.1)$$

The velocity of the striker bar may also be measured more accurately using optical methods. The gas-gun is very safe, its maximum pressure incorporating a factor of safety of 5. The gas gun is bolted at one end of the table from where energy is applied. The other

end of the table consists of a momentum trap to receive the residual energy by penetration of the bar into a wooden plate. The velocity of the striker bar is controlled by the pressure from the gas gun, and the length of the stress pulse is controlled by the length of the striker bar. The two strain gauges mounted at the center of the incident and the striker bar are connected with the wheatstone bridge which is connected to the oscilloscope. The strain gauges (gage length: 6.35 mm, resistance: 350 ohms, type: CEA-06-062WT-350) are supplied by Measurement Group Inc..

5.4.3.2 Theory of a SHPB operation

The theory behind the use of a SHPB is based on a one dimensional stress wave propagation in a rod. The one dimensional wave justifies the condition of stress prevalent in either compressive or tensile strength tests as the strength measured under the influence of multiple waves may not be uniaxial strengths. In a SHPB test the specimen is placed between the incident and transmitter bars and a one dimensional stress wave is introduced in the left rod either by spring, gas gun or explosives. A part of the stress wave is reflected back from the first end of the specimen and the rest is transmitted through the specimen. The following calculations show how the stress (the maximum value being its strength) is derived from the test. The one dimensional wave equation in terms of displacement, u, and direction, x, is,

$$\frac{\delta^2 u}{\delta t^2} = C^2 \frac{\delta^2 u}{\delta x^2} \qquad (5.4.2)$$

where, C is the wave velocity in the rod. The solution of this equation can be represented by two superposing waves travelling in opposite directions. One solution along the positive direction is given as:

$$u = \int (C.t + x) \tag{5.4.3}$$

$$\delta u/\delta x = \int' (C.t + x) \tag{5.4.4}$$

$$\delta u/\delta t = C \int' (C.t + x) = C\, \delta u/\delta x = C\, \varepsilon \tag{5.4.5}$$

$$u = C \int \varepsilon\, dt \tag{5.4.6}$$

Thus if we know the strain, ϵ, at a point, the displacement can be easily obtained. The strain at the left end of the specimen is the algebraic sum of the incident and reflected strain recorded in the incident bar. The strain at the right side of the specimen is the strain recorded in the transmitter bar. The displacement at the left end of the specimen, u_1, and that at the right side of the specimen, u_2, can be expressed in terms of the strains recorded at the incident and the transmitter steel bars, assuming negligible attenuation in the bars. The corresponding loads at two ends of the specimen, F_1, and F_2, can be represented in terms of strains by following equations.

$$u_1 = C \int (\varepsilon_I - \varepsilon_R) dt \tag{5.4.7}$$

$$u_2 = C \int \varepsilon_T\, dt \tag{5.4.8}$$

$$F_1 = E\, A\, (\varepsilon_I + \varepsilon_R) \tag{5.4.9}$$

$$F_2 = E\, A\, \varepsilon_T \tag{5.4.10}$$

where, ε_I, ε_R, and ε_T are the strains due to the incident, the reflected (tensile) and the transmitted stress wave, respectively; E, the Young's modulus of elasticity; and A, and A_s, the area of cross section of the rod and specimen. The average stress and strain in the specimen can be represented by following equations.

$$\sigma_S = \frac{F_1 + F_2}{2 A_s} = \frac{E}{2}\frac{A}{A_s}(\varepsilon_I + \varepsilon_R + \varepsilon_T) \qquad (5.4.11)$$

$$\frac{d\varepsilon}{dt} = \frac{u_1 - u_2}{l} = \frac{C}{l}(\varepsilon_I - \varepsilon_R - \varepsilon_T) \qquad (5.4.12)$$

when the specimen is deformed uniformly, the stress at the incident bar and the specimen interface equals that at the specimen and the transmiter bar interface (i.e. equation 5.4.9 and 5.4.10). Thus

$$\varepsilon_I(t) + \varepsilon_R(t) = \varepsilon_T(t) \qquad (5.4.13)$$

Using the above relationship in equation 5.4.11 and 5.4.12, the stress and the strain rate become:

$$\sigma(t) = \frac{EA_0}{A_s}\varepsilon_T(t) \qquad (5.4.14)$$

$$\frac{d\varepsilon}{dt} = -2\frac{C}{L}\varepsilon_R(t) \qquad (5.4.15)$$

Thus stress, strain rate, and strain (integral of strain rate) can be calculated by knowing the transmitted and reflected strains which are monitored in two steel bars. The next section shows the use of the above principle and how the strength is calculated by measuring strains in the two steel bars of SHPB.

5.4.3.3 Operation of SHPB

The SHPB has been used widely to measure compressive, tensile and shear strengths under high strain rate conditions for metals, composites, concrete, and soil etc.. The fundamentals of all the testing methods are the same except in the method of sample placement. Since the present work is limited to dynamic compressive testing, the details of operation is limited to this compressive set up only.

The amplitude of the incident stress pulse is determined by the impact velocity and characteristic impedance of the striker bar while the duration of the pulse is dependent on the length and the stress wave velocity in the striker bar. The striker bar at a velocity of about 19 m/s is unloaded from the incident pressure pulse when the compression pulse travelling through the striker bar reflects at the free surface as a tensile pulse and returns to the impact face. Therefore, the pulse in the incident bar is dependent on the wave velocity in the bar (≈5.2 km/sec) and is thus twice the wave travel time through the length (40 cm) of the striker bar (≈160 μs). The impact is sufficient to produce high stress in the incident bar (about 600 MPa). The stress level achieved is well above the strength of rocks, but well below the yield strength of the steel bars (~1500 MPa). When the stress wave reaches an interface with the connecting specimen (after about 200 μs in the 1 m

bar), a part of it is transmitted and the rest is reflected. The relative magnitudes of the reflected and the transmitted pulse are dependent on the physical properties of the specimen. Because of the numerous internal reflections (time of fracture is about 25 μs in which the stress wave can travel about 7 to 8 times in the specimen), the stress distribution along the specimen is smoothed out and the stress can be considered uniform along the specimen. The algebraic sum of the incident and the reflected pulse is recorded by the two strain gauges in the incident bar, and the transmitted pulse by the two gauges in the transmitted bar. The location of the strain gauges at the center helps in recording the data independently as the trailing incident wave and leading reflected wave do not interfere. The signals from the strain gauges are recorded using a Nicolet Pro 40 digital oscilloscope. The sampling of data was 0.5 micro-seconds for a total of 1000 data points (i.e. 0.5 milli-seconds) to ensure completion of all the events. These signals are in turn related to the displacements occurring at the interfaces of the steel bar faces in contact with the specimen by assuming negligible losses in the steel bars due to attenuation. The actual data recorded in the left and the right strain gauges of the steel bars are in terms of voltage signals at 0.5 microsecond time intervals. The voltage signals recorded are multiplied by a gage factor of 2/21 as pre-calibrated to calculate the reflected and transmitted strains, respectively. With the use of equation 5.14 and 5.15, the stress and stain at various time intervals are calculated. Typical voltage signals corresponding to the reflected and transmitted strains at the left and right steel bars are shown in Figure 5.8 a. The stress and strain calculated from voltage signals are shown in Figure 5.9 a. A sudden decrease in the transmitted pulse shows the failure of specimen The maximum stress

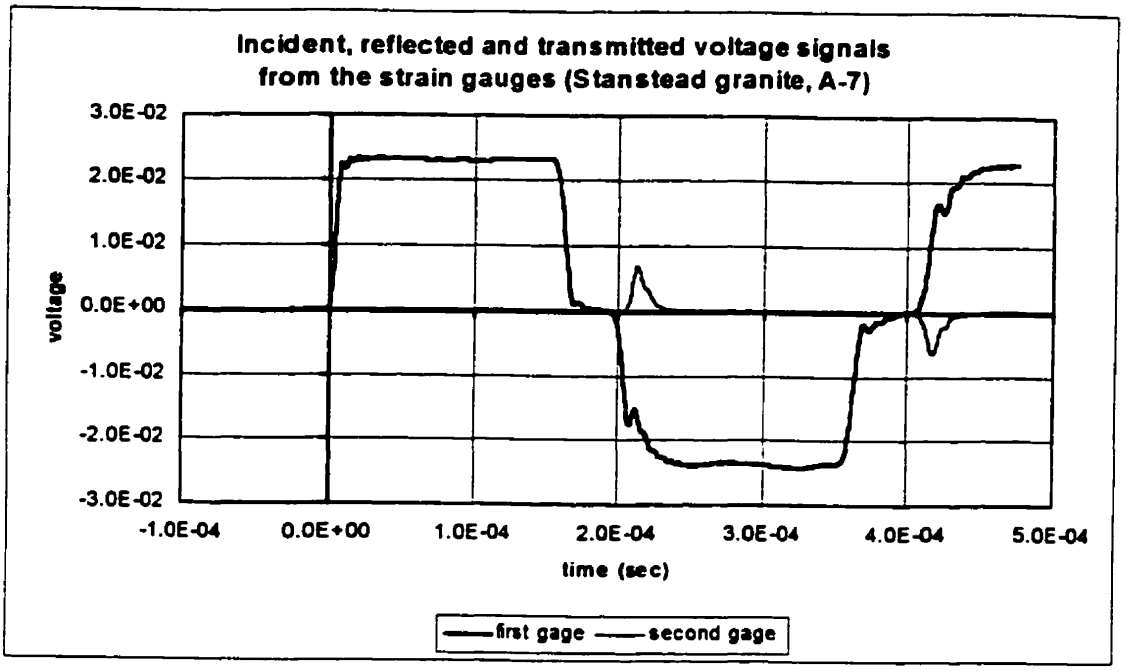

Figure 5.8 a: Typical voltage signals corresponding to the incident, reflected, and transmitted Strains recorded in incident and transmitter bar of the SHPB assembly.

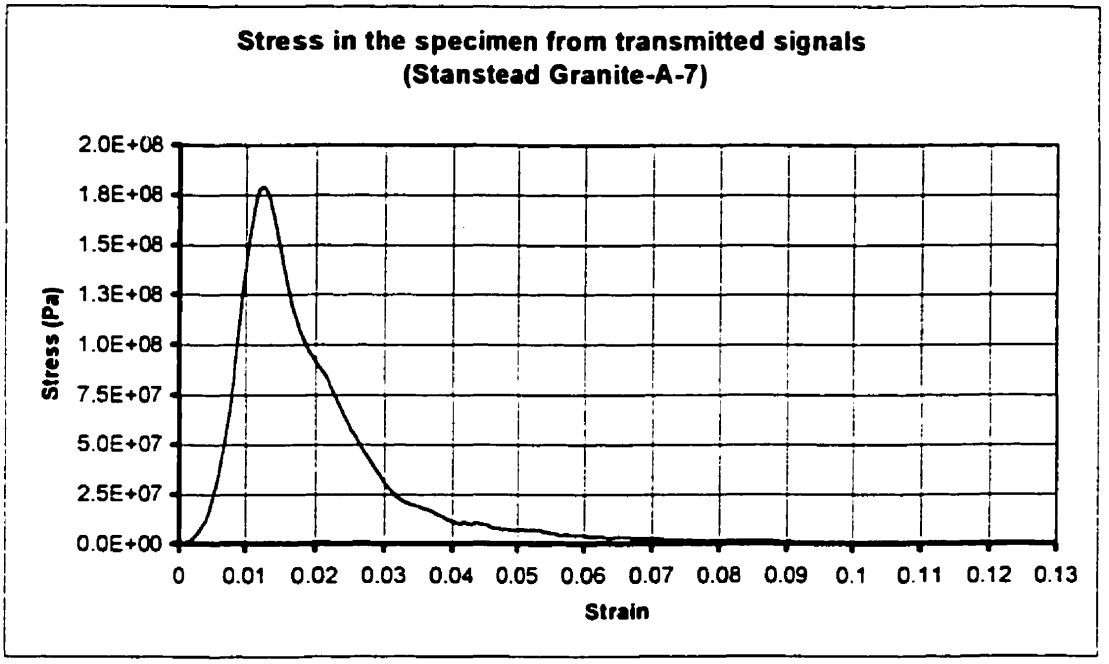

Figure 5.9 a: Typical dynamic stress and strain curve in split Hopkinson pressure bar test.

sustained by the specimen gives the dynamic strength. Strains recorded at varius time intervals is used to calculate the strain rate at failure, Figure- 5.10a. A similar diagram obtained a test sample of Barre granite (J) is shown in 5.8 b, 5.9 b, and 5.10 b, respectively.

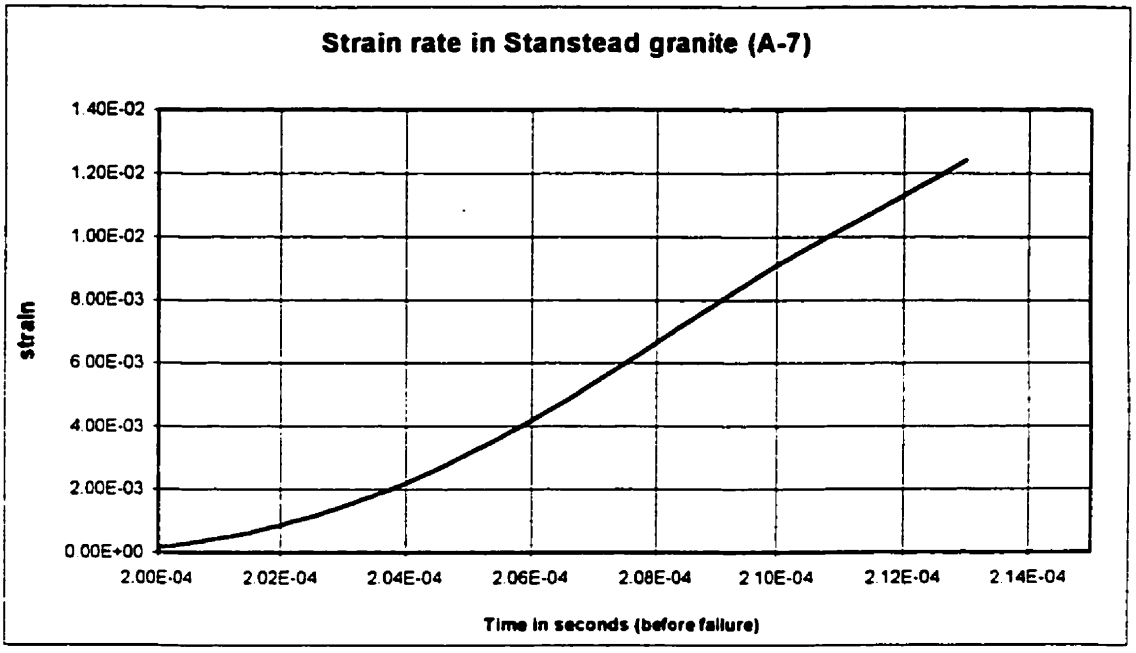

Figure 5.10 a: Typical strain rate during a compressive strength measurement by SHPB.

5.4.3.4 Strain rate in dynamic testing

It is desirable to obtain almost constant strain rate to evaluate the strength of material at low or high strain rates. In static tests it is easily achieved by conducting tests on displacement control with servo-controlled stiff compression machine. However, in dynamic case such as this SHPB set-up, it is difficult, if not impossible to achieve the constant strain rate for different types of rocks. The strain rate in this case is governed not

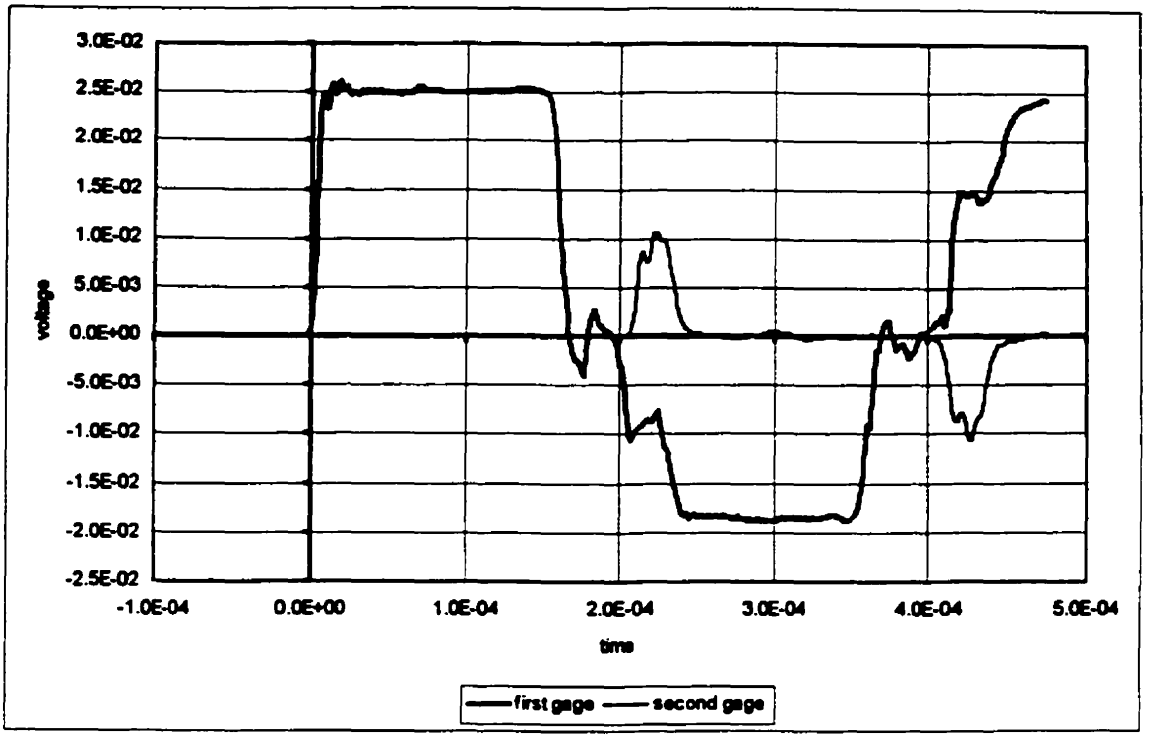

Figure 5.8 b: Typical voltage signals corresponding to the incident, reflected, and transmitted Strains observed in a sample of Barre granite (J).

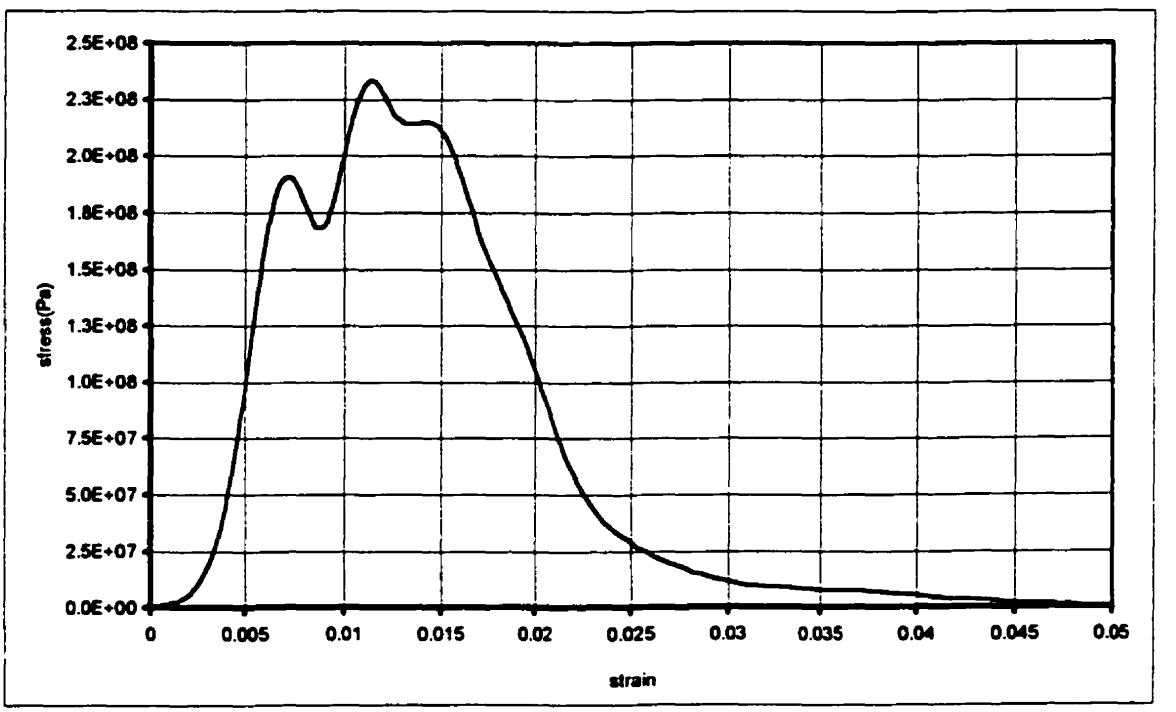

Figure 5.9b: Typical dynamic stress and strain curve calculated from wave propagation in SPPB.

only by the apparatus but also by the material response. The strain rate developed in the specimen depends on the diameter of the steel bars, impact velocity of the striker bar (or the rise time of pulse), length of the specimen and the reflected strain histories. The strain rates in the present case varied from 600 to 1200 per second compared to 10^{-6}/sec in case of static tests. The dynamic strain rate was calculated at 25-70 % of the ultimate strength. It has been noticed that the strain rate after increasing to a maximum value during the rise time, generally decreases during the remainder of the test. Although attempts have been made to obtain a constant strain rate by using a striker bar of non-uniform cross section designed for a particular material (Takeyama et al, 1985), propelling of such a striker raises practical problems.

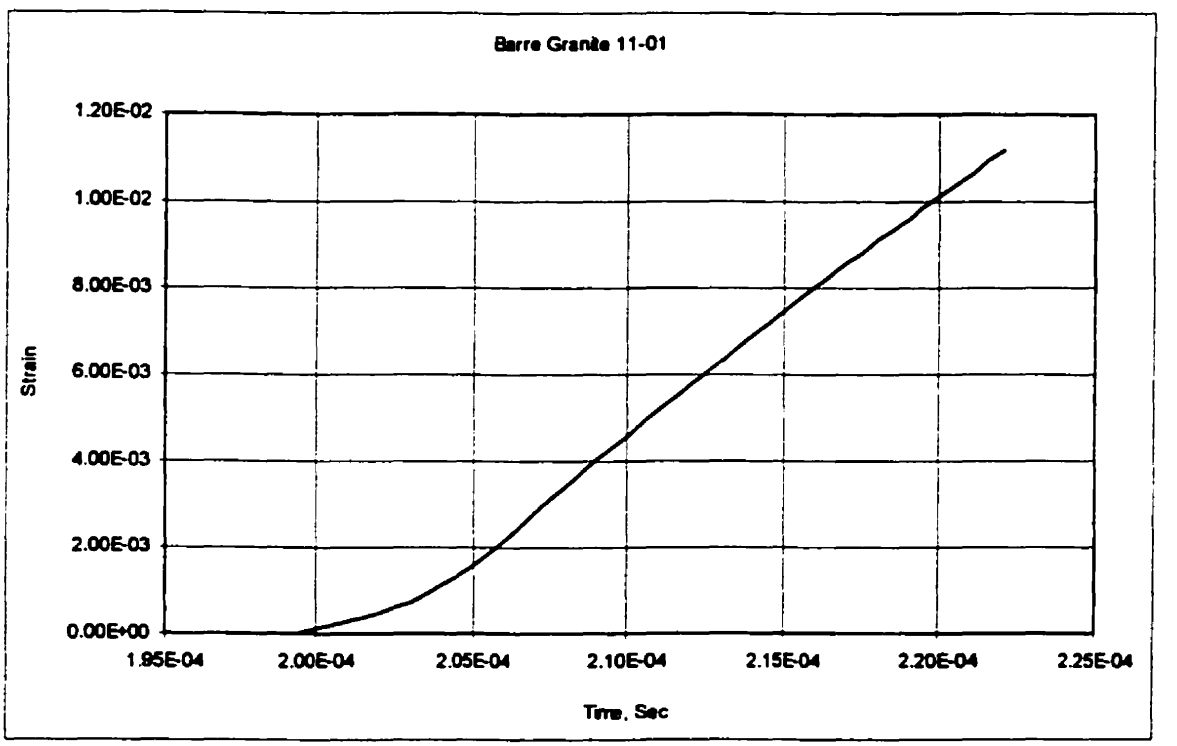

Figure 5.10 b: Strain rate at failure observed in Barre granite (J) in a SHPB test.

5.4.4 Results

5.4.4.1 Dynamic and static compressive strength

The diameter of test specimen for the dynamic compressive tests was 8-9 mm, as dictated by the existing SHPB test facility. For comparison, the static compressive strength was also measured in the same rock types with samples of identical dimensions as those employed in the dynamic measurements. A minimum of 8 to12 samples were tested for their strengths in each case. The strain rate during the static tests was of the order of 10^{-6} per second. The static tests were conducted using a RDP servo-controlled stiff compressive testing machine, as described before. The average value for static and dynamic compressive strengths, their standard deviations, and the ratio of dynamic strength over the static values; measured in the laboratory are shown in Table 5.7. The dynamic strength was found to be significantly higher than its static value. For the dynamic strain rate employed ($\sim 10^3$/sec), the ratio of the dynamic to static value ranged between 2.5 to 4.6. It was also observed that the ratio of the dynamic strength to the static strength decreases with increasing strength. This is shown in Figure 5.11.

5.4.4.2 Fines generation in dynamic breakage

After each experiment of dynamic and static compressive testing, all the rock fragments were collected for sieve analysis. The sieve sizes selected were the standard Tyler series with the screen sizes varying from 4.76 mm to 0.075 mm. Table 5.9 summarises the sieve analysis for the fragments obtained after dynamic and static compressive tests. The screen size corresponding to 80 % and 50 % passing sizes are also

calculated and shown in the Table 5.8. The size distribution of the resulting fragments corresponding to the 50 % and 80 % passing sizes are shown in Figure 5.12 and 5.13. The size of the fragments in dynamic loading is found to be consistently much lower than the fragments from static breakage. Furthermore, the dynamic compressive strength is found to have a definite correlation with the 50 % or 80 % passing sizes. As expected, the fragment size increases with increasing dynamic strength. In contrast, the resulting fragment size distribution for the 50 % or 80 % passing size is seen to have a rather weak correlation with the corresponding static compressive strengths for the twelve rock types tested (Figure 5.14, and 5.15). Though, the data points are more scattered in the figure with 80% size estimation, the trend is still the same as for the 50 % estimated passing size.

Table 5.7: Test results of dynamic and static compressive strengths with their Std. Dev.

Rock type	$\sigma_{c\ static}$ (MPa)	$\sigma_{c\ dynamic}$ (MPa)	$\sigma_{c\ (dynamic)}$ / $\sigma_{c\ (static)}$	Strain rate (/sec)	No. of test
Stanstead granite-A	48±13	160±27	3.3	1110±284	5
Altered marble-B	185±42	459±50	2.5	850±218	6
Kingston limestone-C	83±27	316±65	3.8	613±189	6
Gneiss-D	40±20	122±25	3.1	1034±56	5
Vineland limestone 1-E	77±31	272±59	3.5	1088±225	4
Marble 2 –F	32±9	128±14	4.0	1072±113	5
Gneissic marble 3 –G	34±13	153±32	4.5	900±120	5
Laurentian granite-H	67±17	245±36	3.7	798±159	6
Quartz-I	67±17	281±65	4.2	900±75	5
Barre granite-J	61±16	241±21	4.0	616±151	5
Gneissic granite-K	52±13	238±27	4.6	660±175	6
Vineland limestone 2-L	49±8	147±20	3.0	1125±101	6

Figure 5.11: Static and dynamic UCS

(for similar specimen sizes)

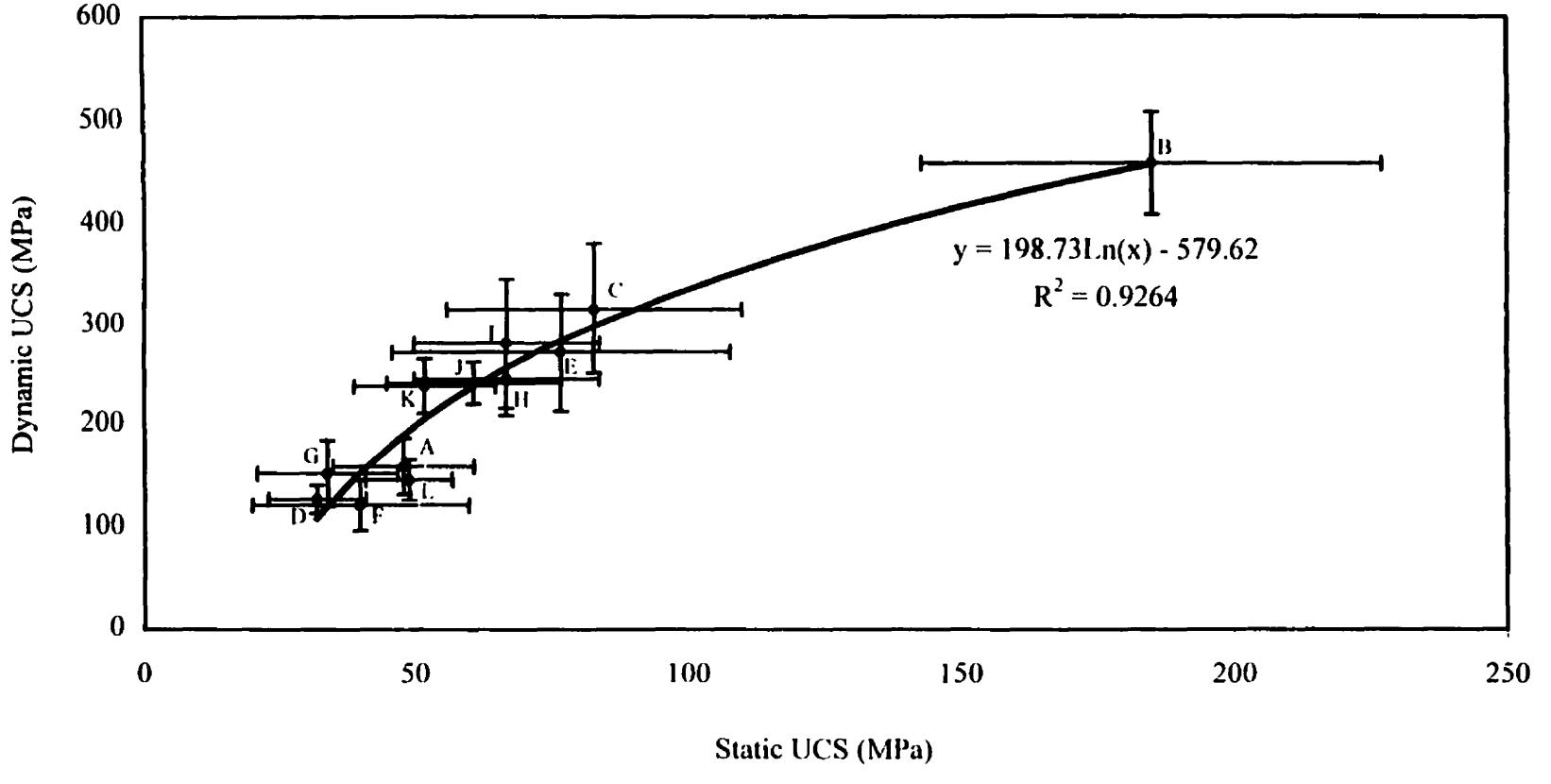

Note: Stanstead granite (A), Altered marble (B), Kingston limestone (C), Gneiss (D), Vineland limestone 1 (E), Marble 2 (F), Foliated marble 3 (G), Laurentian granite (H), Quartz (I), Barre granite (J), Gneiss granite (K), Vineland limestone 2 (L)

Table 5.9: Size distribution of the fragments after dynamic and static tests.

Cummulative size distribution (passing): after compressive strength test (dynamic)

Size (mm)	A	B	C	D	E	F	G	H	I	J	K	L
4.760	98.96	76.20	78.12	77.52	89.13	90.48	86.17	82.54	98.25	100.00	79.92	95.24
2.380	79.41	37.28	41.31	63.05	47.28	69.49	60.18	56.97	77.05	66.33	41.74	60.87
1.180	50.61	21.22	18.01	53.88	20.65	55.66	45.45	37.09	47.73	44.89	21.38	38.70
0.850	39.57	16.76	13.67	50.26	14.13	52.19	41.80	31.02	36.81	38.05	16.59	31.26
0.425	18.41	8.68	7.27	37.60	6.70	44.06	34.78	19.20	18.17	25.82	9.05	18.53
0.250	8.12	4.81	4.42	14.47	3.62	30.02	29.45	10.15	8.29	15.42	5.07	10.74
0.150	2.36	2.23	2.29	3.81	2.17	8.20	17.89	2.91	1.91	6.30	2.12	3.03
0.075	0.47	0.59	0.63	0.39	0.91	0.97	3.85	0.56	0.08	0.73	0.27	0.09
80% size	2.45	4.99	4.88	5.17	4.24	3.57	4.20	4.52	2.71	3.35	4.77	3.70
50% size	1.16	3.16	2.94	0.83	2.53	0.74	1.55	1.96	1.27	1.47	2.87	1.79

Cummulative size distribution (passing): after compressive strength test (static)

Size (mm)	A	B	C	D	E	F	G	H	I	J	K	L
4.760	56.22	47.23	54.81	6.10	58.42	20.20	15.02	37.93	39.35	44.74	17.14	27.31
2.380	32.14	26.95	13.78	4.69	18.56	8.39	6.87	18.75	6.09	18.71	7.59	10.83
1.180	18.38	14.81	6.16	3.28	9.28	6.08	4.87	12.63	1.52	12.07	3.99	6.57
0.850	14.18	11.54	4.31	2.63	7.04	5.14	4.17	11.03	0.76	10.17	3.13	5.09
0.425	6.79	7.14	1.77	1.88	4.30	4.02	3.29	6.87	0.11	6.81	2.19	2.78
0.250	3.30	4.60	0.77	1.31	3.26	3.31	2.76	4.10	0.00	4.22	1.25	1.57
0.150	1.37	2.60	0.31	0.84	2.41	2.19	2.11	1.97	0.00	2.07	0.70	0.56
0.075	0.33	0.93	0.23	0.38	1.20	0.47	1.00	0.48	0.00	0.26	0.16	0.00
80% size	7.33	7.70	7.40	8.49	7.22	8.31	8.38	7.97	7.94	7.78	8.36	8.20
50% size	4.15	5.08	4.48	6.98	4.34	6.26	6.53	5.37	5.30	5.03	6.42	5.91

Figure 5.12: Dynamic compressive strength vs. Fragment size

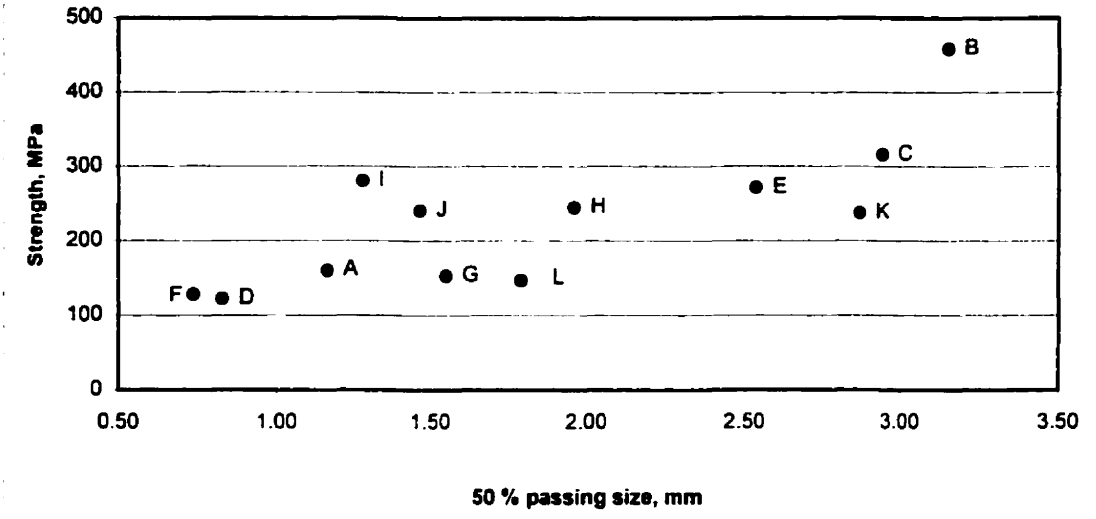

A: Stanstead Granite; B: Altered Marble; C: Limestone 1; D: Gneiss; E: Limestone 2; F: Marble 2;
G: Gneissic Marble; H: Laurentian Granite; I: Quartz; J: Barre Granite, K: Gneissic granite, L: Limestone 3.

Figure 5.13: Dynamic compressive strength vs. Fragment size

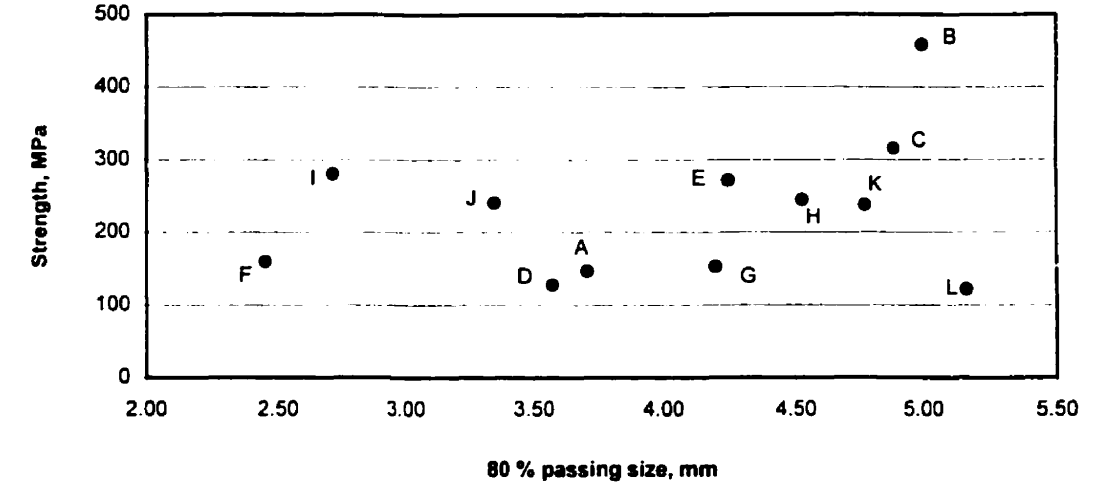

A: Stanstead Granite; B: Altered Marble; C: Limestone 1; D: Gneiss; E: Limestone 2; F: Marble 2;
G: Gneissic Marble; H: Laurentian Granite; I: Quartz; J: Barre Granite, K: Gneissic granite, L: Limestone 3.

Figure 5.14: Static compressive strength vs. Fragment size

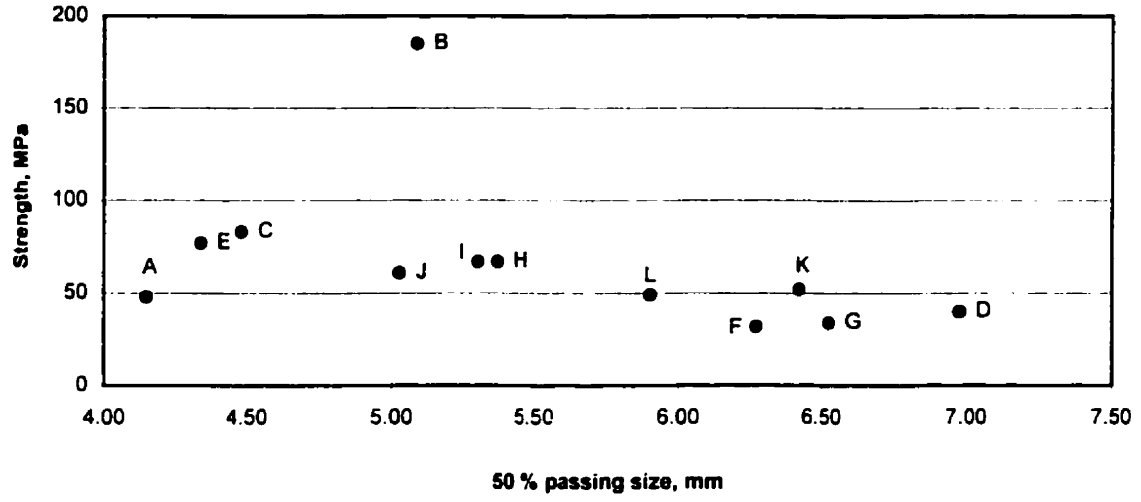

A: Stanstead Granite; B: Altered Marble; C: Limestone 1; D: Gneiss; E: Limestone 2; F: Marble 2;
G: Gneissic Marble; H: Laurentian Granite; I: Quartz; J: Barre Granite, K: Gneissic granite, L: Limestone 3.

Figure 5.15: Static compressive strength vs, Fragment size

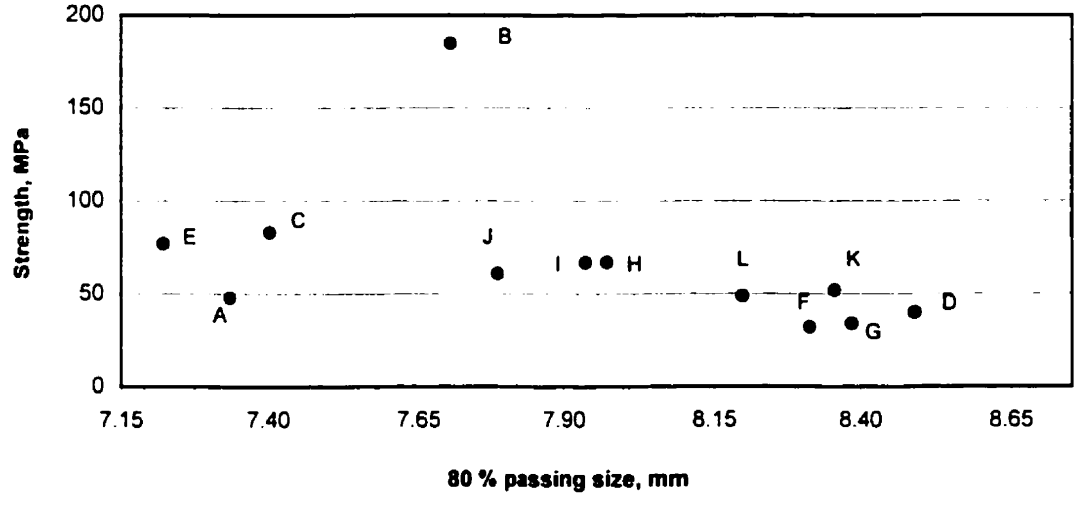

A: Stanstead Granite; B: Altered Marble; C: Limestone 1; D: Gneiss; E: Limestone 2; F: Marble 2;
G: Gneissic Marble; H: Laurentian Granite; I: Quartz; J: Barre Granite, K: Gneissic granite, L: Limestone 3.

The result with Altered marble (point B) appears anomalous when compared to other rocks. The higher strength is due to the absence of crack, joints, and re-melting of grain boundary zones. If one ignores the data for the Altered marble, the static strength shows a weak but inverse correlation with fragment size, whereas, the dynamic strength shows a strong and direct correlation with fragment size. The inverse correlation between the fragments size and the static strength may be explained by two plausible phenomena: shear failure, and splitting tensile failure; which are the most predominant mechanism of rock breakage in static compression. The weaker rock breaks rapidly along the weak plane resulting in fewer and larger fragments. However, the stronger rocks break more catastrophically resulting in more fines due to the crushing and frictional effects in the failure planes. In the dynamic compressive breakage, the stress is distributed over the entire wavefront in contrast to the localised planes in shear or tensile failure in static breakage. For identical levels of dynamic stress applied to all the samples, the stronger rocks yield larger size fragments.

It should be noted that the better fitness of the data should not be confused with the better correlation. The first reflects how the data appears in the plot showing the variation in the result obtained either due to the rock type or the random error involved in process while calculating the result. On the other hand, correlation represents the physical basis for the trend obtained irrespective of better or poor fitness of data. The plots of static strength with the fragment size distribution result better fitness of the data, however, the correlation is very poor. By ignoring the test result of Altered marble (B), the fitness

becomes poor but the correlation is better. In both the cases the nature of the trend is same demonstrating the physical basis involved in the breakage process.

The fitness of the data in 50 % passing sizes of the fragment size during the dynamic breakage is much better than that for the 80 % passing size. This is due to the lower degree of random error involved in estimating the passing size in the first case. The 80 % or 50 % passing size is calculated by linear interpolation of the two sieve sizes through which the desired amount (80 % or 50 %) of fragments passes through. Since the number of particles present in coarser sizes (80 %) considered random and few in number, compared to the finer sizes (50 %), the amount of error will be more in the first case. For example, in case of limestone (L) the 80 % passing size is calculated by interpolating the sieve size corresponding to 95 % and 60 % passing size. The 50 % passing size, on the other hand, is calculated by interpolating sieve sizes through which 60 % and 39 % of the material passes. The first covers 35 % of fragments in which countable number of fragments will be present. However, in the latter case, large number of fragments will be present covering only 21 % passing fragments. The number of fragments produced is random but few in the first case, whereas, they are very large in the latter case. Therefore, the estimated fragment size through which 50 % of the fragments pass would incorporate less random error, and therefore yield a better fit.

5.4.5 Summary

Rock breakage by dynamic means is a common and necessary process. However, our understanding of the failure process under high strain rate is limited due to a general

paucity of dynamic strength data. The dynamic strength of rock can be measured easily at high strain rate using Split Hopkinson Pressure Bar.

The dynamic compressive strength, measured under a strain rate of 10^3 /sec, has been found to be about 2.5-4.6 times higher than the compressive strength measured under static conditions (strain rate of 10^{-6} /sec) for a wide variety of rock types. It has also been found that this ratio is higher for low strength rocks, and lower for high strength rocks. The particle size distribution resulting from high velocity impact breakage is much smaller than in the static case. This is attributed to the transient nature of impact loading, which provides insufficient time for cracks to propagate and coalesce to produce larger fragments. The degree of fines (50 % or 80 % passing) generated under dynamic breakage is well correlated with the dynamic compressive strength; the coarser fragments corresponding to the higher strength for the same dynamic stress applied. In contrast, there appears to be a very weak but inverse correlation between static compressive strength and the corresponding fragment size distribution. The opposite trend in the static breakage is due to the completely different mechanism of stress applications. The dynamic breakage encompasses distributed stress application over the whole rock specimen. Whereas, the latter allows localised stresses condition along the weak failure plane and additional crushing and frictional effect, especially, in stronger rocks. It is concluded that the use of static strength values in predicting fragment size distribution in blasting can lead to significant errors.

5. 5 Fracture toughness

5.5.1 Review of fracture toughness of rocks

The material property associated with the ability to carry loads or resist deformation in the presence of a crack is defined as the fracture toughness. This is a powerful tool which describes when, where and why fracture takes place (Atkinson, 1989). By knowing this, the critical stress needed to fracture a material in a known crack geometry can be predicted. Alternatively, the size of the crack which will cause failure under a given load condition can be determined. The most common form of fracture is crack opening mode (mode I) and the corresponding toughness parameter is denoted by K_{Ic}.

The concept of fracture toughness has been used to model fracturing process in rock cutting, Hua Guo (1990); rock slope stability, Singh and Sun (1989); hydro-fracturing (Rummel, 1989) and blasting, Ochterlony (1974), Grady and Kipp (1979) and Kipp et al. (1980). In particular, fracture toughness is used as, a) a parameter for classification and characterization of rock material with respect to its resistance to crack propagation, b) an index of fragmentation process such as rock cutting, tunnel boring and blasting, c) as a material property in the process of modeling rock fragmentation. In some modeling examples, the fracture toughness value is not the only strength property which is taken into account, but it is more relevant than the other strength properties when the effect of a relatively few dominant cracks is being modeled.

Measurement of fracture toughness is a relatively new procedure compared to the other established rock mechanics tests. Table 5.9 shows the range of published fracture toughness values determined by the standard method of three point bending method as recommended by the International Society of Rock Mechanics (ISRM). The table shows the values of the fracture toughness designated as K_Q or K_{IC}. The former represents the approximate value of fracture toughness by assuming the fracturing process being purely brittle. The latter incorporates the necessary correction for non-brittle behaviour, if any, during the fracturing process. For most brittle rocks, the difference between K_Q and K_{IC} is minimal (<5%).

T able 5. 9 : Fracture toughness values for some selected rocks, by 3-point bending (after Atkinson, 1989)

Rock types	K_Q or K_{IC}, MPa$\sqrt{m}$	References
Granite	0.65-2.78 (K_Q)	Muller (1984, 1986), Olfsson (1978)
Limestone	0.82-2.21 (K_{IC})	Bearman et al. (1989), Hua Guo, 1990)
Sandstone	0.68-3.01 (K_{IC})	Hua Guo (1990), Muller (1984, 1986)
Marble	0.96-2.09 (K_{IC})	Hua Guo (1990), Ouchterlony & Sun (1983)
Salt	0.23-0.57 (K_Q)	Rummel & Muller (1984)
Diorite	2.22-2.77 (K_Q)	Bearman et al. (1989)
Quartzite	2.38-2.44 (K_Q)	Bearman et al. (1989)
Dolomite	0.88-1.82 (K_Q)	Bear and Barr (1977)

Note: K_Q and K_{IC} are approximate (level I) and corrected (level II) fracture toughnesses values.

It has been observed that the fracture toughness values of rocks are an order of magnitude lower than that for metals. For example, the fracture toughness of iron is of the order of 120 MPa $m^{1/2}$. The low value of fracture toughness in rocks is due to the low level of plasticity at the crack tip which in tern is due their brittleness. The same is reflected in their respective measured tensile strength.

In the above paragraph the fracture toughness of rock is compared with that of metal. This is because the measurement of fracture of rock originates from ASTM E399 (1988) being used for the metals. The following section reviews the various methods used for measurement of fracture toughness of rocks and justifies why a separate method was necessary for rocks.

5.5.2 Fracture toughness tests

All fracture toughness tests of rocks (in crack opening mode) are essentially derived from the standard ASTM E-399 method (ASTM, 1990). The latter, normally is used to determine the fracture toughness of metallic materials, has been extended to rocks, especially, for hard rocks. This test is conducted on a variety of samples e.g. bend specimen, compact specimen, arc-shaped specimen, and disk-shaped compact specimen. A schematic diagram of different shape of the sample is shown in Figure 5.16. The specimens are notched and further pre-cracked at the tip by cyclically loading the specimen under fatigue so as to give reproducible, sharp and narrow crack from where the crack grows. The specimens are loaded in tension, either directly or indirectly, under three point loading. The load applied in tension and the displacement measured across the notch

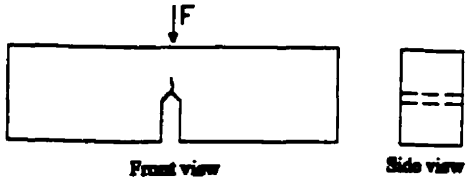

Bend specimen

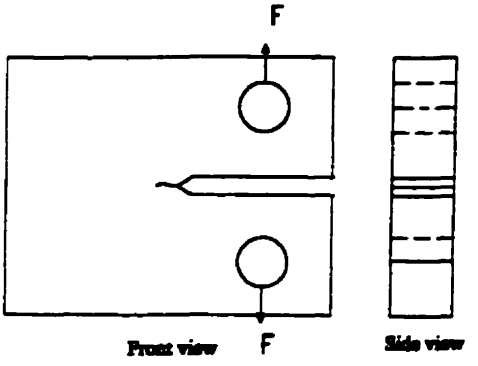

Compact specimen

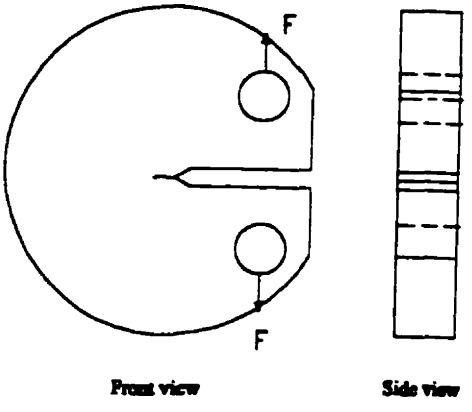

Disk-shaped compact specimen

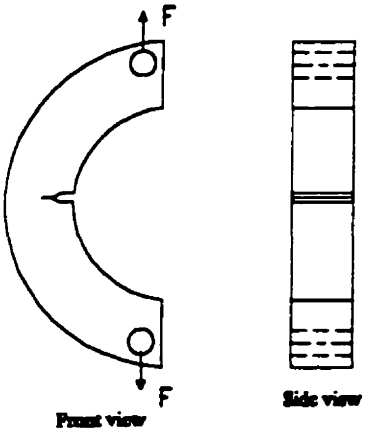

Arc-shaped compact specimen

Figure 5.16: Schematic diagram showing different shapes and loading geometry of samples while measuring fracture toughness for metal as per ASTM method E-399.

is recorded in the form of a graph. The geometry of the sample, i.e. thickness, width, loading span etc. is used to calculate a dimension-less functional variable which in tern is used to calculate the stress intensity factor. The fracture toughness is calculated by measuring the load corresponding to 95 % of tangent modulus of elasticity on load-displacement diagram, or the maximum load experienced by the specimen (whichever is less). The calculated fracture toughness is assumed to be plain strain fracture toughness under the condition that the thickness and the crack length are more than or equal to $2.5(K_{IC}/\sigma_y)^2$. However, these standard methods, developed for metal, produce acceptable values for only hard rocks. Also it requires unreasonably large and impracticably shaped specimens, as well as a testing procedure that is not adaptable to rock. Therefore, these methods have been modified by ISRM for application to rocks.

There are two methods for determination of fracture toughness of rocks as suggested by ISRM. The first method uses a chevron bend specimen which is loaded under three point bending to break apart at the central chevron notch. The second method uses a short rod which is loaded under tension to tear apart the two sides from the chevron notch. In both methods the load at failure is used to calculate the fracture toughness under LEFM (linear elastic fracture mechanics) considerations. However, the size independent and duly corrected fracture toughness (due to the non-linear or plastic effect) is calculated by the use of the load and the crack mouth opening displacement record. The later is recorded by a clip gauge attached to the crack opening or alternatively, by the load point displacement record in three point bending method. In the

present work the first method is selected for the determination of the fracture toughness in keeping with the specifications of the available loading machine in the laboratory.

5.5.3 Three- point bending method test

The three point bending method uses a cylindrical specimen with a chevron or a 'v' shaped notch cut perpendicular to the axis of the sample. The samples in the form of a core are easily available from exploration log samples, or are easily prepared with a minimum of machining. A schematic diagram of the specimen geometry, the chevron notch, and the load being applied is shown in Figure 5.17.

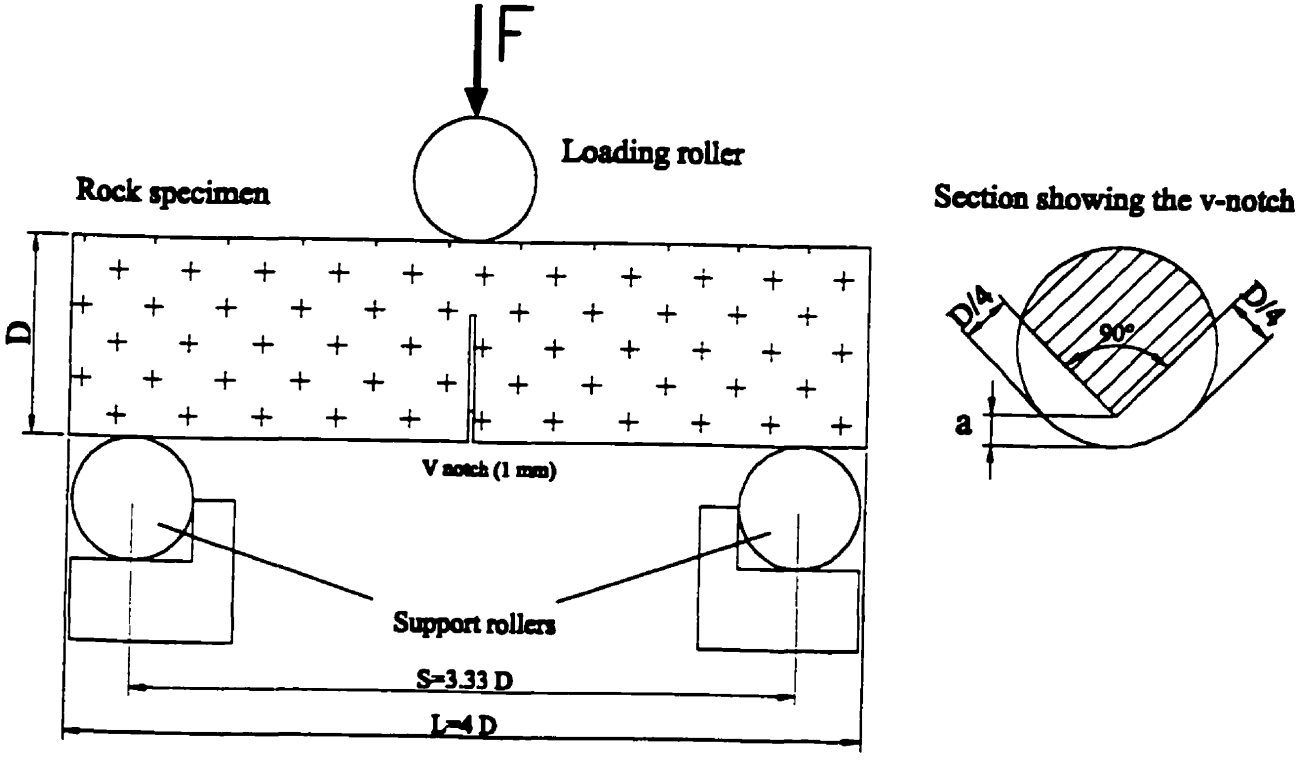

Figure 5.17: Chevron Bend specimen with bend fixture and basic notation.

The specimen rests centrally on two support rollers at a fixed span length. The support rollers are anchored by springs to a base plate. The spring allows some deflection during loading so that the latter is free from any constraints. The base plate is anchored to the lower loading platen and is rigid. The load is applied to the sample using a roller placed on the surface of the specimen just above the notch so that specimen breaks into two parts due to indirect tensile failure. The chevron notch causes crack propagation to start at the crack tip of the 'v' which proceeds transverse to the core axis in a stable fashion until the point where the fracture toughness is evaluated. This is a pre-requisite for the method. The specimen dimensions and their tolerances, as suggested by ISRM, are shown in Table-5.10. The experiment may be repeated with rock samples cored in orthogonal directions to take into account of rock variability and isotropy.

Table 5.10: Specimen dimensions and its tolerance value for CB method.

Geometry parameter	**Value**	**Tolerance**
Diameter, D	35-50 mm	> 10x grain size
Length, L	4 D	> 3.5 D
Support span, S	3.33 D	± 0.02 D
Chevron angle, θ	90°	± 1.0 °
Chevron V tip position, a_o	0.15 D	± 0.10 D
Notch width, t	<0.03 D or 1 mm	Whichever is greater

5.5.4 Specimen geometry and alignment

A standard AX drill coring bit was selected for making the core samples. The diameter of the resulting cores was 28-29 mm. A fixed length of 4 times the diameter of the sample is cut from the core pieces. The end faces are ground to make the face normal to the axis. A chevron notch of specified dimension (i.e. 1 mm in thickness and an apex angle of 90 degree) perpendicular to the axis of the core is made in each sample using a specially prepared fine diamond saw blade and the two specially designed holding devices. These devices hold the core sample after being tightened with the help of four screws at suitable places. The holding devices, designed and assembled in the laboratory, are shown in Figure 5.18.

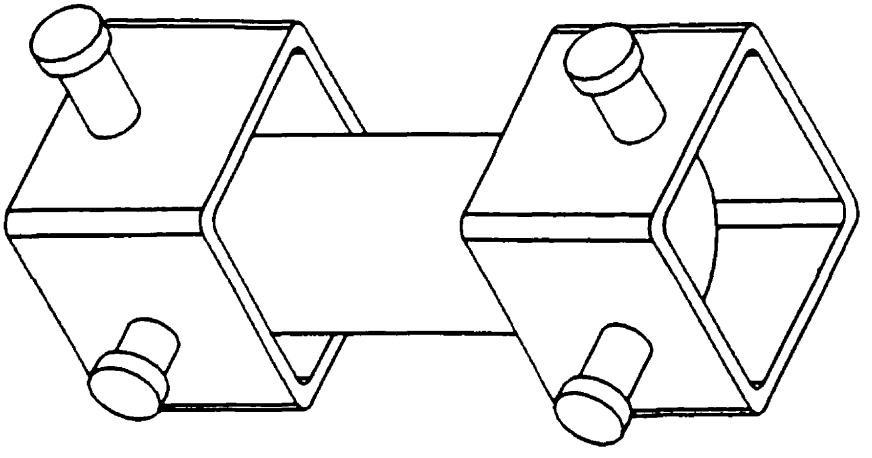

Figure 5.18: Two similar holding devices used in making the suitable 'v' notch at the centre of the core specimen and perpendicular to the axis.

The two perpendicular cuts at the centre of the specimen and perpendicular to the axis are achieved by sliding the whole assembly through the cutting wheel. The specified depth of the notch from the surface of the core is achieved by lowering the wheel to a suitable depth. A large number of samples for different rock types were prepared using the above mentioned techniques. The specimens were placed on the two support rollers for loading with the help of a special loading assembly. Two different alignment kits has been suggested in the ISRM method for suitably and stably loading the specimen in a fracture toughness test. The necessary conditions for an alignment kit in a loading assembly are that: a) the loading roller should rest on specimen just above the chevron notch and at the middle of two support rollers, b) the chevron notch should be centered such that the tip points vertically downward, c) the axis of the specimen remains perpendicular to the rollers.

An alignment kit suitable for the existing machine was assembled in the laboratory. A fly-out diagram for the whole loading assembly is shown in Figure 5.19. Although, this assembly satisfies the necessary conditions with the help of some additional fixtures, the stability in the loading assembly was difficult to achieve while loading. A modification in the above loading assembly was necessary for successful execution of the tests. The new specimen alignment kit was similar to the other alignment kit as suggested by ISRM except with some minor modifications. A fly out diagram showing the different parts are shown in Figure 5.20. This new alignment kit helps to achieve the necessary conditions. The design of the kit is in two pieces so that it can be removed when the specimen is

secured in loading position. This allows :

- the loading roller to rest on the specimen just above the chevron notch and at the middle of two support rollers using a 'U' cut in the alignment kit
- the chevron notch to be centred such that the tip points vertically downward using a 45° edge touching the chevron notch from both sides, and
- the axis of the specimen to remain perpendicular to the rollers using a flat side at the back of the alignment kit.

5.5.5 Measurement procedure

The fracture toughness testing is performed under two levels, namely, level-I and level-II. The level I is used to calculate the fracture toughness as an approximate value without taking into account the non-linear or plastic behaviour (if any) of rock specimen. The level II is used to calculate the same by taking into account the energy dissipation in the non-linear fracture process zone at the crack tip (Ouchterlony, 1989). If the specimen behaves elastically till failure and there is negligible cracking near the crack tip till failure, then level-I gives accurate results and level-II is not then needed.

At level I, the objective is to determine the load at failure during the stable crack growth takes phase. The specific sample geometry and the specified load assembly employed helps achieve this. The load is applied in load control mode till failure. The loading history is recorded every half a second; the maximum load at which specimen fails

is used to calculate the fracture toughness.

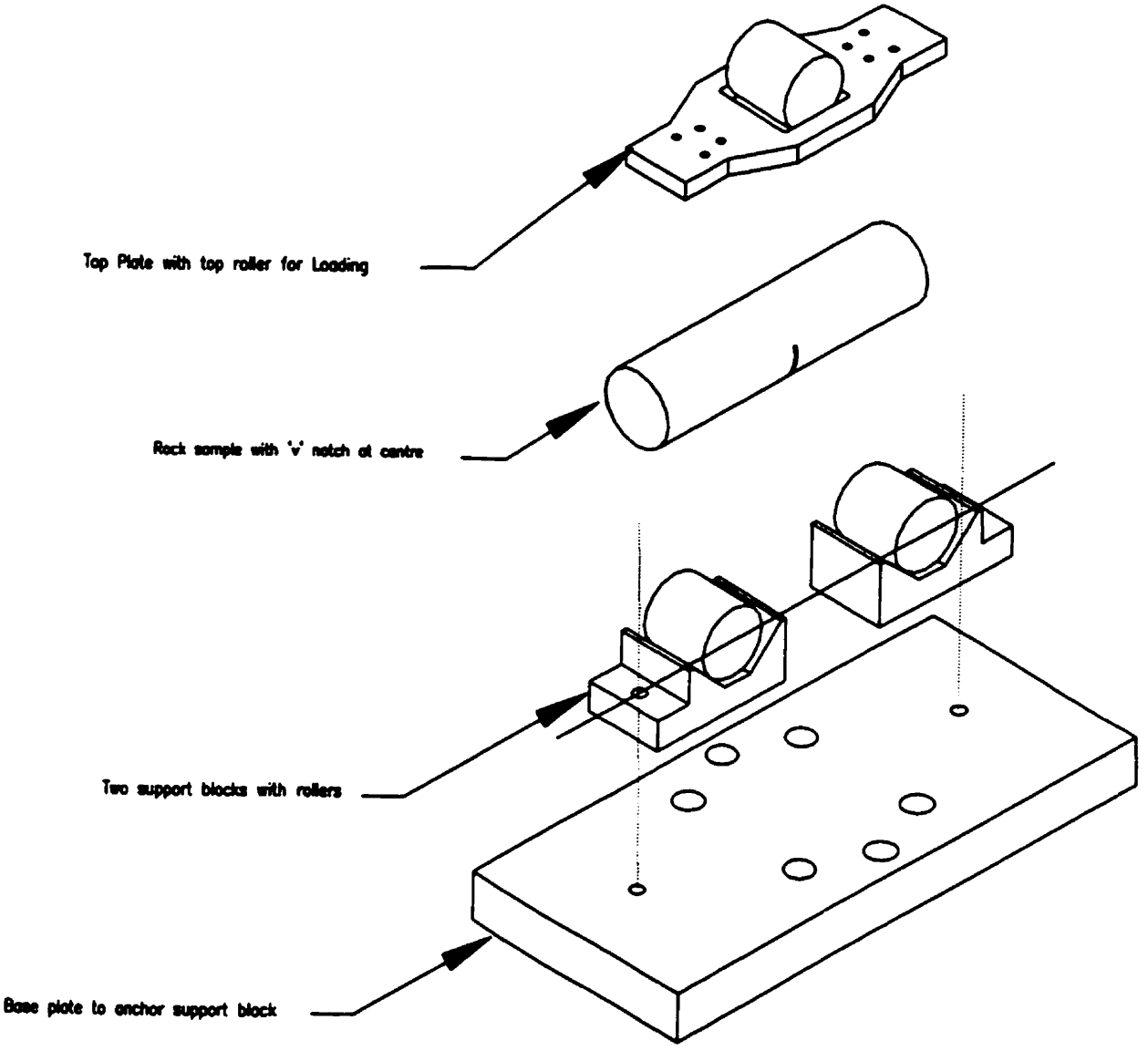

Figure 5.19: A fly-out diagram for the whole loading assembly as per ISRM for the measurement of fracture toughness by three point bending method.

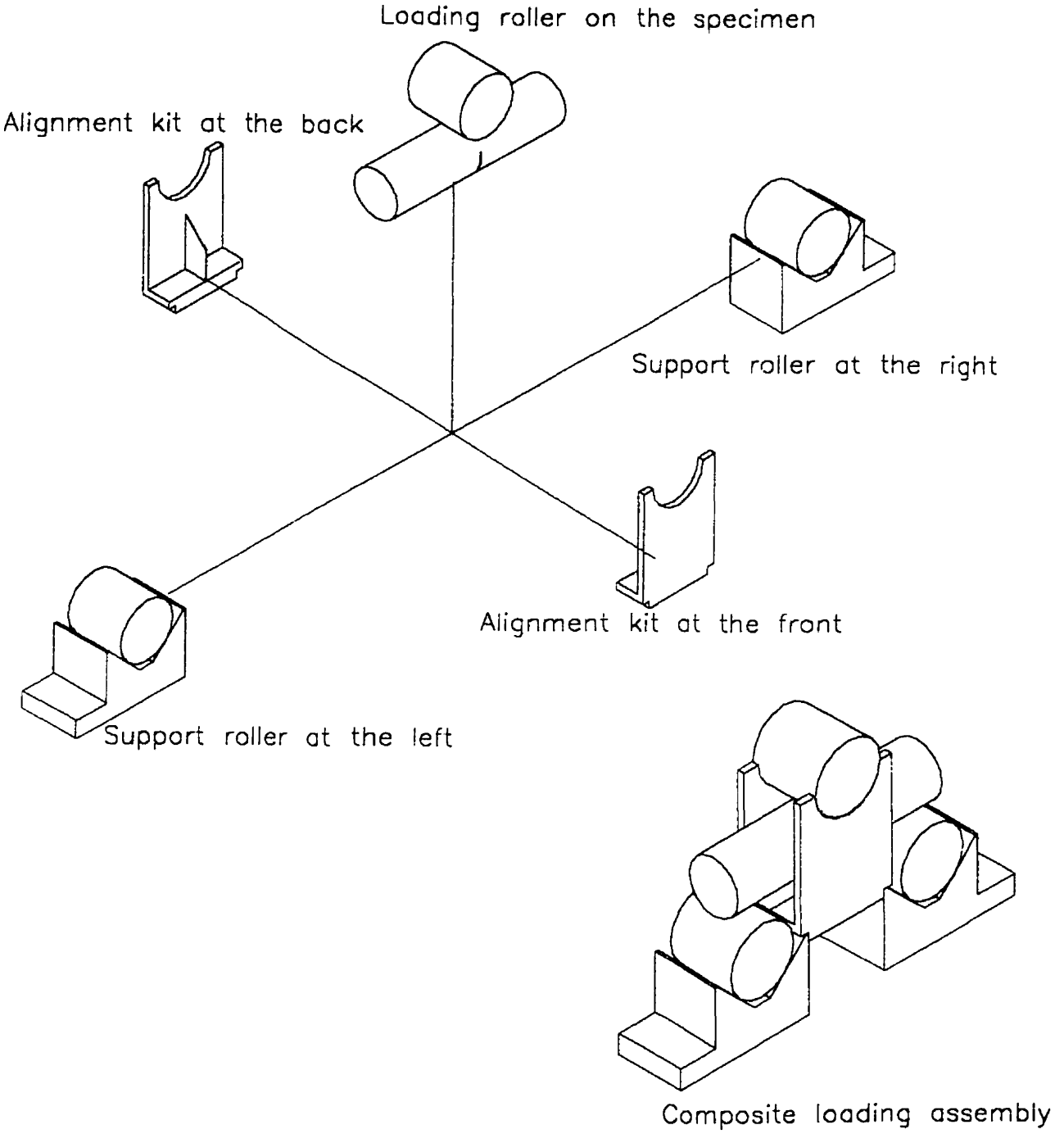

Figure 5.20: A fly-out diagram of the modified loading assembly for the measurement of fracture toughness by three point bending method.

The parameters used in the calculation of fracture toughness at level I are:

- specimen diameter, D
- depth of the notch, a_0,
- span of support rollers, S, and
- Maximum load, F_{max}

For a particular assembly of a test apparatus, the first three parameters should be fixed but is not the case in reality. Even though the same set of equipment (the coring bit of specified diameter, the same cutting wheel, and the same holding devices) was used in making the specified samples, the diameter, the width, and the depth of the notch did vary to some extent. These variations are however small (usually less than 2.5 %), and are due to the relative weaknesses of the rock samples used for coring and cutting. The diameter and the depth of cut of each rock samples were noted individually. The depth of the notch was noted after each test as it is more convenient to measure it in free face than to estimate it in 1 mm wide notch. The support span of rollers was changed after each tests. This is brought back to original position at the start of the tests for each sample. Loading was applied using the RDP servo-controlled stiff compression testing machine, as described before. The loading rate was maintained at 60 N/sec for all the samples. This results in sample breakage in about 10-20 seconds as recommended by ISRM. The load history was recorded at every half a second using a load cell with a maximum capacity of 250 kN. The formula used to calculate K_Q are:

$$K_Q = \frac{A_{min} \cdot F_{max}}{D^{1.5}} \qquad (5.5.1)$$

where, F_{max} is the maximum load at failure, D is the diameter of the specimen, and A_{min} a dimensionless parameter representing geometry of the sample. A_{min} is given as:

$$A_{min} = [1.835 + 7.15(a_0/D) + 9.85(a_0/D)^2]S/D \qquad (5.5.2)$$

where, a0 is the chevron tip depth from the free end of the cylinder, and S the distance between support rollers. If the failure load, Fmax, is in kN and the specimen diameter, D, is in cm; the fracture toughness calculated is in MPa m0.5 or MN/m1.5. Sometime the breakage does not start from the tip of the chevron notch and therefore, the fracture toughness calculated is not acceptable as the formula used for calculating fracture toughness does not hold good in this case. This was noticed in some of the samples of gneiss and quartz, and these results thus was rejected. The calculated fracture toughness by level I is represented as a tentative value, KQ. The KQ value is further modified using the non-linearity correction, p, as determined in level II testing:

In level-II testing, the load is applied in displacement mode, and load and displacement are recorded for 4 repeated loading and unloading cycles to calculate non-linearity behaviour of rock samples. The additional parameter to be recorded is load point displacement, LPD. The LPD was recorded using a LVDT connected to the actuator which has a range of 100 mm of span in compression loading. The template in the

TestwareSX software was designed for each rock type by knowing their maximum load measured while testing at level-I. The first loading was continued from zero load to 50 % of maximum load as determined in level I, the second cycle of loading was continued till 70 % of maximum load, the third cycle of loading was continued till 85 % of maximum load, the fourth loading cycle was continued till 90 % of maximum load and finally, in the last cycle the loading was continued till failure. The unloading ends and reloading begin when the load is about of 10 % of the maximum load. The load from the load cell and LPD from the LVDT of the actuator are recorded at every half a second. A linear line for a cycle of unloading and loading is plotted using the standard procedure. This is shown in Figure 5.21. Each line is defined by two points, H, and L. The high point (H) is where the displacement starts to decrease on the unloading parts of the cycle and the corresponding load is F_H. The lower points (L) lies on the reloading part of the cycle and is defined at the load level, $F_L=0.5F_H$. A line is joined from the high point, H, and the low point, L, and is translated vertically downward to half the vertical hysterisis. The above procedure is repeated for two successive cycles, one before the failure and the other, after the failure. However, in the present investigation the cyclic unloading and loading was not possible after the maximum load. Therefore, the two cycles nearest to the load at failure were used to calculate the non-linearity factor. The difference of the residual displacement, x_u, at zero load and, x_f, at the highest load (between two successive linearized lines) is calculated with the help of load and LPD plot. The non-linearity factor,

p, is defined as the ratio of the former over the later, x_u/x_f. The ISRM guidelines suggests the acceptable non-linearity, p, for rocks should be less than or equal to 0.05. The corrected fracture toughness, K_{IC} thus can be calculated using following equation:

$$K_{IC} = \left(\frac{1+p}{1-p}\right)^{1/2} K_Q \qquad (5.5.3)$$

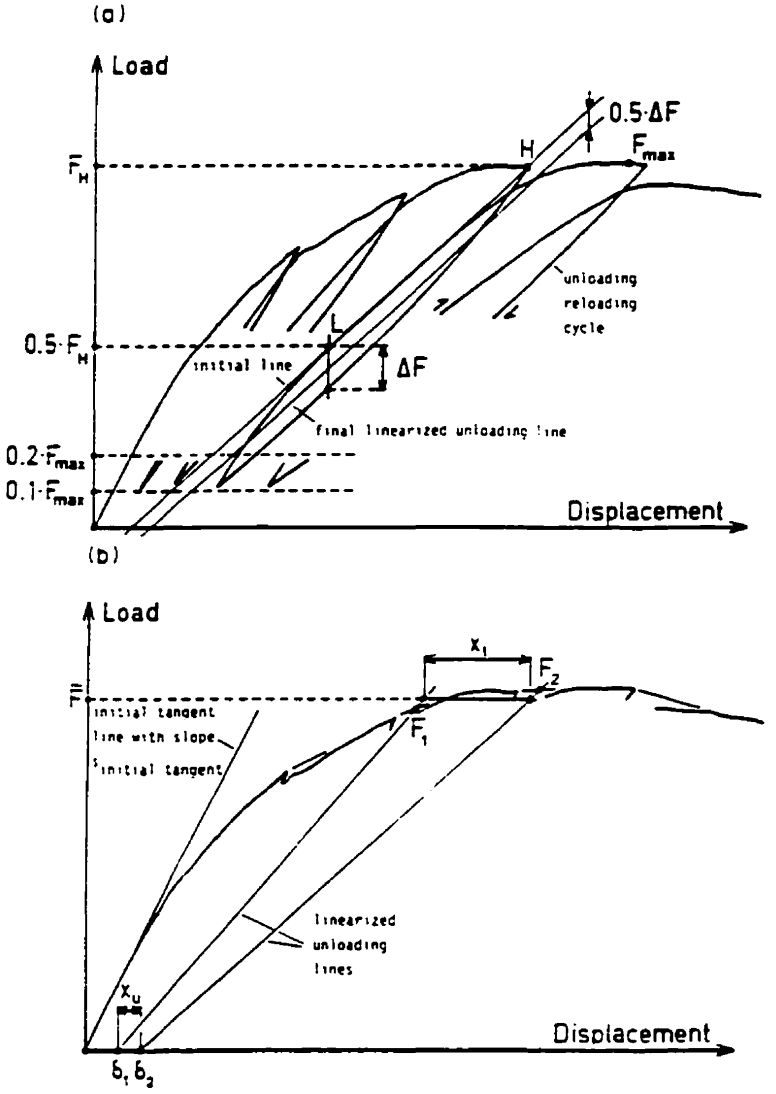

Figure 5.21: Construction of linearized unloading line, (a) and calculation of net displacement at zero load and that at the maximum load , (b). (after ISRM, 1981).

5.5.6 Results

5.5.6.1 Fracture toughness, K_Q (level I)

The fracture toughness is calculated by level I test using the formula given in above section. This does not take into account the non-linearity behaviour of rock specimen. Altogether a total of 32 tests on 10 different rock types were conducted. The details of specimen geometry and their calculated, K_Q are shown in Table 5.12.

Table 5.12: Fracture toughness, K_Q, by 3-point bending method for the rock types.

Rock Sample	a_0 mm	A_{min} -	F_{max} kN	K_Q $MN/m^{1.5}$	No of Tests
Stanstead granite-A	1.6	7.73	1.008	1.593 ± 0.184	4
Kingston limestone-C	1.8	8.05	0.966	1.559 ± 0.129	9
Gneiss-D	0.0	6.27	1.061	1.367 ± 0.163	3
Marble-F	3.0	9.30	0.941	1.751 ± 0.023	2
Foliated marble-G	1.0	7.18	1.487	2.200 ± 0.227	2
Laurentian granite-H	3.9	10.28	0.820	1.687 ± 0.156	4
Quartz-I	3.5	10.35	0.615	1.240	1
Barre granite-J	2.8	9.03	0.860	1.588 ± 0.119	3
Granite gneiss-K	3.5	9.74	0.628	1.258 ± 0.459	2
Vineland limestone-L	2.8	8.96	0.640	1.153 ± 0.309	2

5.5.6.2 Fracture toughness, K_{IC} (level II)

Altogether 32 different tests on 10 different rock types were conducted for the calculation of the non-linearity factor so that the true fracture toughness, K_{IC}, can be obtained from the apparant fracture toughness obtained in the level I test shown above. The details of specimen geometry and the number of cycles before failure and the

maximum load achieved are shown in Table 5.12. Table 5.11 and 5.12 show the average values of the notch depth, a_0, the calculated dimensionless coefficient, A_{min}, the maximum load at failure, F_{max}, the tentative value of fracture toughness, K_Q, and the number of tests. Table 5.12, also gives the value of number of cycles before failure for level I tests. The average values of the depth of notch is shown to be different for different rock types. This is because the notch of 1 mm thickness was created by two different diamond tipped saw blades.

Table 5.12: Results of level II testing showing number of cycles, F_{max}, and, K_Q

Rock Sample	a_0 mm	A_{min} -	F_{max} KN	K_Q $MN/m^{1.5}$	Cycles # before fail	No of tests
Stanstead granite-A	4.7	11.10	0.724	1.647	3	6
Kingston limestone-C	4.6	11.10	0.567	1.295	3	8
Gneiss-D	4.5	10.92	0.603	1.354	3	2
Marble-F	4.5	10.96	0.437	1.001	2	8
Foliated marble-G	4.6	10.92	1.024	2.343	3	4
Laurentian granite-H	4.5	10.96	0.713	1.610	3	1
Quartz-I	4.0	10.35	0.595	1.271	3	1
Barre granite-J	3.0	9.19	0.794	1.503	3	1
Granite gneiss-K	3.5	9.74	0.442	0.886	3	1
Vineland limestone-L	5.0	11.58	0.624	1.489	3	1

The diameter of these two blades were of 75 mm and 150 mm, respectively. After making notches in some of the samples, it was realised that the small diameter blades did not give the specified notch depth of 4.5 mm under existing equipment set-up. The larger diameter cutting wheel resulted in a notch depth in accordance with ISRM standard, with only a

small variation due to different rock types. It was assumed that the wide variation in notch depth (a_0) would be compensated by different values of A_{min}. The latter is a dimensionless parameter calculated from the former with the fixed loading span, S, as shown in equation 5.5.2.

The apparant fracture toughness as shown in the above tables vary within a narrow range, except for the very high value of foliated and gneissic marble (G), and a lower value for quartz. The values for Stanstead granite (A), Laurentian granite (H), Barre granite (J), Kingston limestone (C), gneiss (D), and gneiss granite (K) fall in the mid-range in decreasing order of fracture toughness. In general, the higher toughness values were associated with more irregular crack paths thus producing larger surface areas as compared to fine grained rocks giving less crack surface areas. High toughness values are characteristic of more non-linear or ductile failure associated with a large number of crack generation. Low toughness values means fast and brittle failure with almost negligible non-linear work. The crack growth in high fracture toughness material is accompanied with more crack branching, trans-granular cracks and meandering crack paths, whereas, the low fracture toughness is associated with inter-granular grain boundary cracks (Swanson, 1983). Further, it is not known if the same trend would be valid even after correcting the values of fracture toughness for the non-linearity behaviour of rocks. The following paragraph describes how the correction is applied using level II test results.

For each test the load being applied and the corresponding load point displacements are recorded using the same 250 kN load cell and the LVDT transducer. A typical layout of the load and load point displacement during cyclic loading is presented in Figures 5.22, 23, and 24 for three granite samples. A large variation in displacement is observed for unit change in load. This made it very difficult to distinguish different loading and loading cycles. An arbitrary load value of 1, 2 and 3 kN was added to the recorded load value in three successive loading cycles so that each cycle can be identified separately. Furthermore, each cycle was assigned a straight line as per the procedure discussed above so that the net displacement at zero load and that at maximum load be calculated. This was the most difficult task, especially, when the data points overlapped to a great extent. Nevertheless, approximate linear lines were drawn for each cycle of unloading and loading. A typical non-linearity calculated for the Stanstead granite #3 comes out to be 0.4. This value is much more than the accepted value of 0.05 as suggested by ISRM. Also, the graphical representation of load cycles by hand results in a large error even for the same set of data points. For example, the calculated non-linearity factor for the Stanstead granite # 4, yields values of 0.3 and 0.4 in two different diagrams. None of the test results gave the result accepted by ISRM. The data obtained for Barre granite (figure 5.23) and Laurentian granite (figure 5.24) clearly shows similar patterns. The details of the test results are summarised in Table 5.12 in terms of the notch depth. The dimensionless A_{min}, the maximum load at failure, the calculated K_Q based on the maximum load, the number of cycle of loading and unloading before failure, and the

number of tests.

The above methods and results are given only for the sake of completeness. As already stated, for brittle fracture in rocks, the difference between 'apparent' and 'true' fracture toughness values is minimal. Therefore, the fracture toughness values measured in this study, although lacking the plasticity correction factor obtained with level II testing, can be taken to represent true toughness values. Henceforth, no distinction will be made between the two values.

The present work has analysed the fracture toughness determined by static means only. The fracture toughness in dynamic condition is traditionally obtained by multiplying it with a normalised time factor expressed in terms of shear wave velocity in rock, the crack length, and the time interval for fragmentation process (Chen and Sih, 1977; Grady and Kipp, 1989). The dynamic fracture toughness increases upto 25 % than the corresponding static values. A preliminary result on dynamic fracture toughness measured by varying load rate has also confirmed the higher level of dynamic fracture toughness (Zhang el al , 1999).

5.5.7 Summary

The fracture toughness of rocks (in crack opening mode) can be determined by various methods depending upon the shape of the test specimen used. The three point bending method is one of those as suggested by ISRM. The methodology prescribes a specific dimension of a chevron notch in a core sample, a specified loading assembly, and an ultimate load at failure. Although the measured fracture toughness (level I) does not

Figure 5.22: Fracture toughness at level II
(non-linearity factor: 0.26; Stanstead graniteA2)

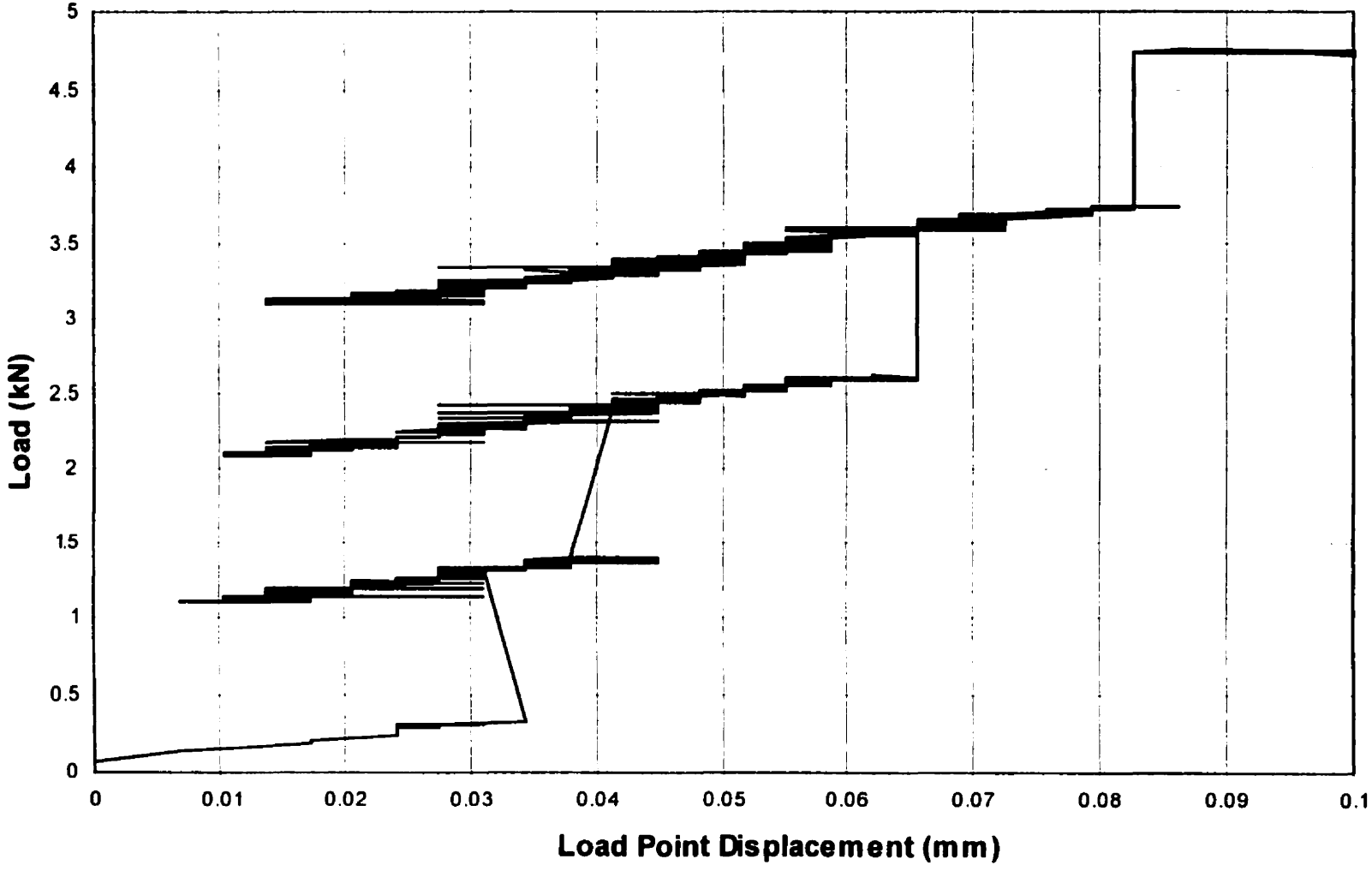

Figure 5.23: Fracture toughness Level II
(Non-linearity factor: 0.44; Barre granite J1)

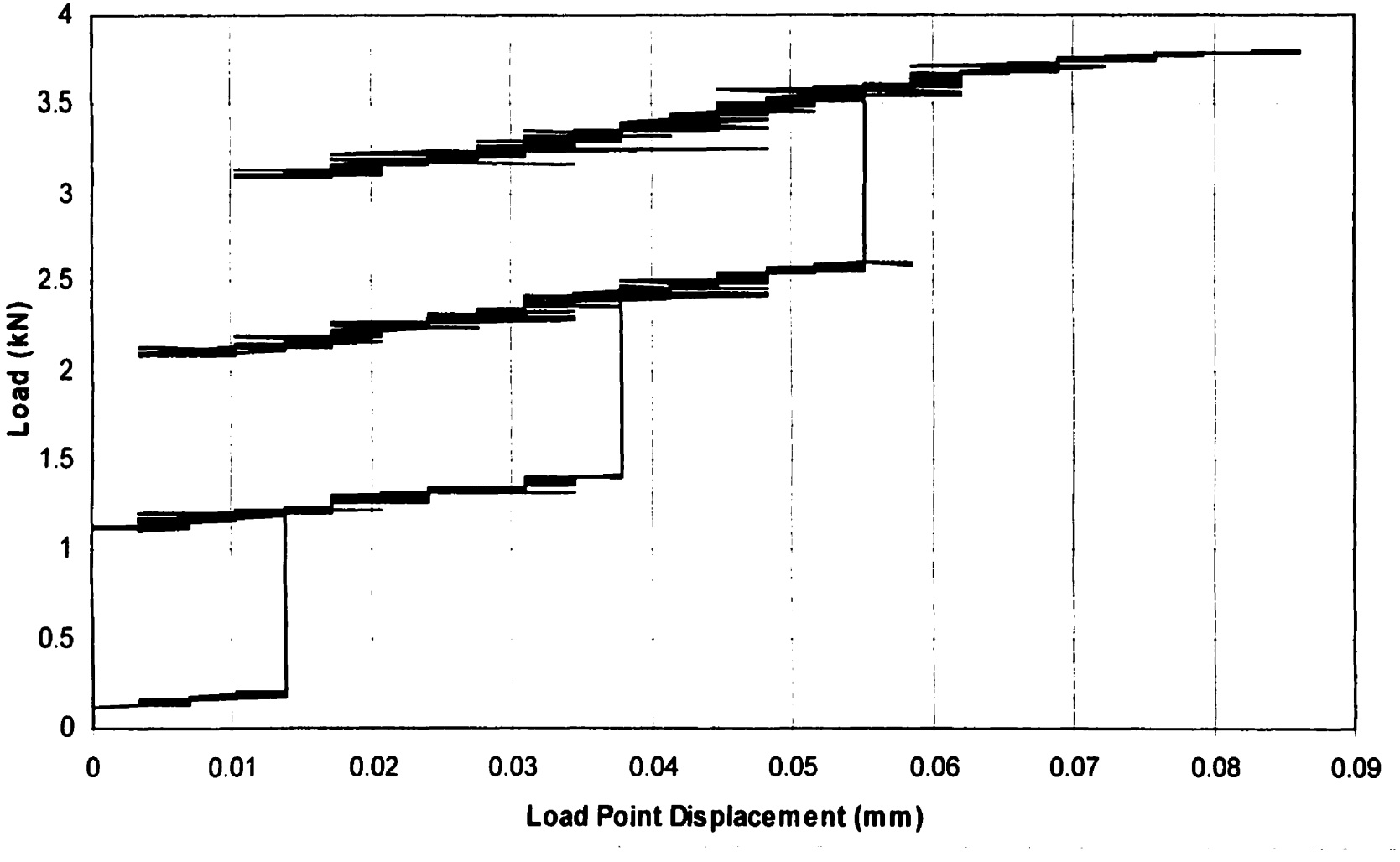

Figure 5.24: Fracture toughness Level II
(non-linearity factor: 0.35; Laurentian granite H2)

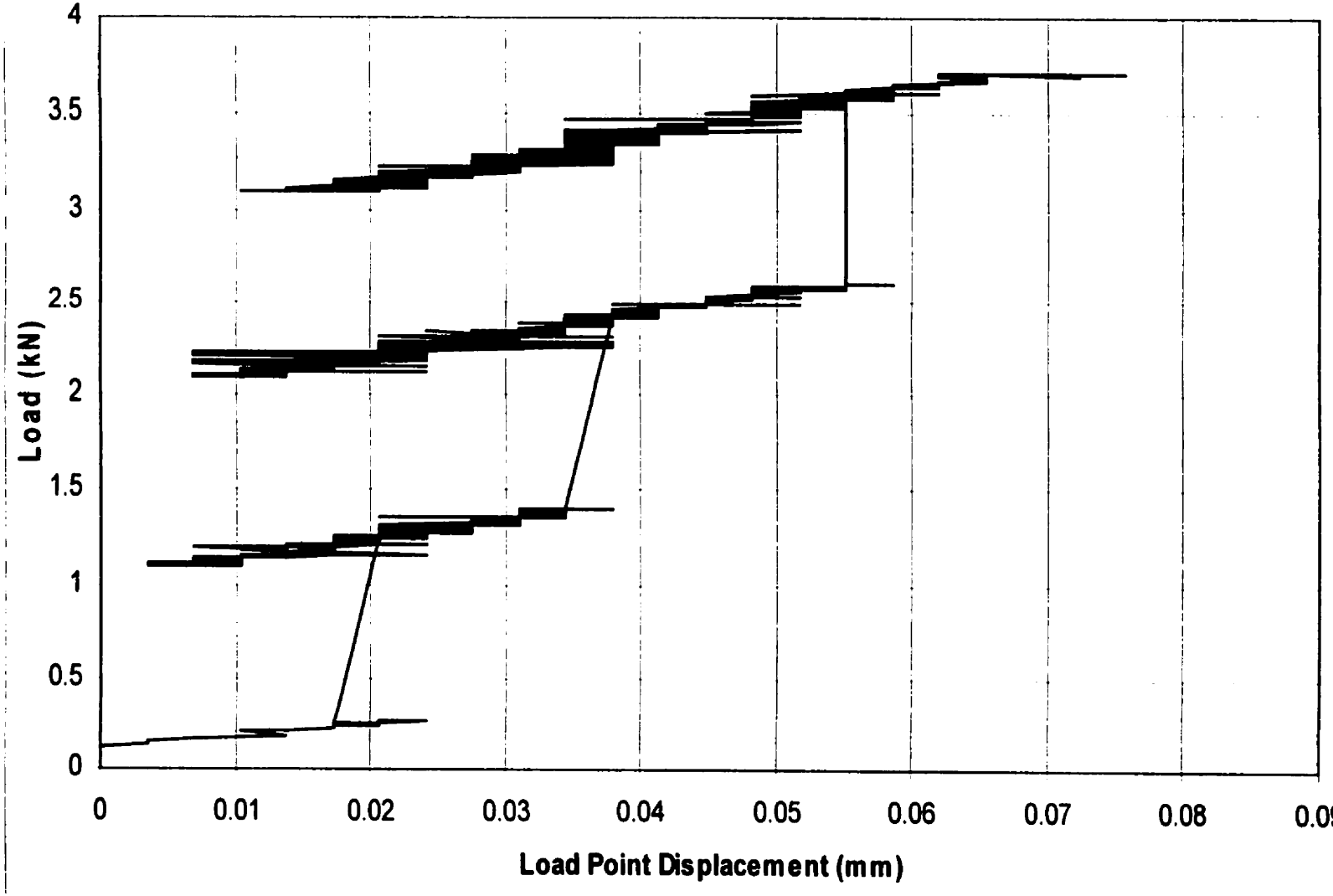

an ultimate load at failure. Although the measured fracture toughness (level I) does not incorporate the plasticity factor, because of the brittle nature of the fractures, the measured values are considered representative of the true toughness values. The test procedure at both the levels is complex. This is because the selected specimen geometry and loading assembly assembled for a test can be used for only one diameter of the rock specimen. Further, the test method becomes more complex during the calculation of the non-linearity factor by smoothing load displacement data by hand. A low capacity load cell (5-10 kN) and a precise clip gauge capable of measuring 0.2 to 0.5 mm in crack opening might have been useful but was not available.

5.6 Conclusions

The compressive as well as the tensile strength both depends largely on the structure of the sample and its orientation with respect to the direction of loading. However, in absence of weak joints of foliation planes, the compressive strength depends more on the distribution of weak zones or extent of cracks whereas, the latter strength depends more on the weakest plane present with respect to the applied load.

The dynamic compressive strength, measured under a strain rate of 10^3 /sec, has been found to range between 2.5 to 4.6 times the compressive strength measured under static conditions (strain rate of 10^{-6} /sec), for a wide variety of rock types. It has also been found that this ratio is higher for low strength rocks, and lower for high strength rocks. The particle size distribution resulting from high velocity impact breakage is much smaller than in the static case. The degree of fineness (50 % or 80 % passing) generated under

dynamic breakage is well correlated with the dynamic compressive strength: In contrast, there appears to be a very weak but inverse correlation between static compressive strength and the corresponding fragment size distribution.

The fracture toughness of rocks (in crack opening mode) can be determined by various methods depending upon the shape of the test specimen used. The three point bending method is one of those as suggested by ISRM. The measured fracture toughness (level I) is an apparent one and is rue only under linear elastic fracture mechanics (LEFM) considerations. The test procedure at both the levels is complex. This is because the selected specimen geometry and loading assembly assembled for a test can be used for only one diameter of the rock specimen. Furthermore, the test method becomes more complex during the calculation of the non-linearity factor by smoothing load displacement data by hand. However, for brittle fractures, the plasticity correction factor obtained with level II test is very small, and therefore, the toughness values obtained with level I test in the present study can be considered to be the representative toughness values for the rock types tested.

CHAPTER 6

COMMINUTION WORK INDEX

6.1 Introduction

The objective of the present research is to analyse the dynamic breakage process in great detail. The fracture related properties measured at low strain rate (10^{-6}/sec) and that at a very high strain rate (10^{3}/sec) are analysed. The analysis of different strain rate fracture properties will not be complete unless some fracture related comminution characteristics have also been studiied, as it involves a strain rate intermediate to static and high dynamic conditions.

The breakage energy associated with any comminution process can be explained by two approaches: stress or energy based. The stress approach is used to explain the strength of the rock or material on macroscopic scale such as compressive, shear or tensile strength. The fracture stress or the strength (in MPa) depends on many factors such as

macro- and microstructure of the material, amplitude and rate of stress, and the method of stress application. Due to an inability to uniquely quantify the strength of a heterogenous and anisotropic material, stress and energy criteria are often lumped together. The energy approach is also a macroscopic scale of representing fracture strength but it takes into account the crack size present in the material (the Griffith theory). With the knowledge of the strain energy (energy absorbed under stress application) and the surface energy (work done in creating unit surface area), the minimum work required in a comminution process can be estimated. Alternately, if the actual energy used is measured, one can estimate how efficiently it is used.

6.2 The energy-size relationships

The first energy-size relationship was postulated by Rittinger (Austin, 1984). It is also known as the surface theory. It states that the energy required for breakage in a material is proportional to the surface area over which it acts. The specific energy consumed in the process is, therefore, proportional to the inverse of the size. The drawback of this theory is that it does not consider deformation done during breakage. Kick (Austin, 1984) postulated that the specific energy consumed or work done in a comminution process is proportional to reduction in the volume of the particle. This is known as volume theory. The work done is same for the same reduction ratio irrespective of the size range. It takes into account only strain energy, which is correct only before fracture propagation takes place. When it does, the surface energy has to be taken into account. These two theories could not explain the size reduction process over the full size

range and to the energy consumed upto the final failure. The third theory of comminution known as Bond's law was developed subsequently. Bond (1952) summarised the three comminution principles as follows: a) it may be assumed that the energy content of a particle is inversely proportional to the square root of its size. The required energy in the course of size reduction is added to the initial energy content of the feed to produce the energy content of the product. Therefore the net energy required is the difference between the energy content of feed and product; b) the second principle states that the useful work in the size reduction process is proportional to the length of new crack produced. In ordinary comminution processes, particles absorb strain energy and are deformed under compression or shear until the weakest flaw in the particle fails with the formation of a crack. The slight deformation causes other crack tips to develop at other flaw sites, and particles break thereby releasing strain energy as heat. The strain energy required to break is proportional to the length of the crack formed; c) the third principle deals with the relationship of particle flaws to material breakage. A flaw is defined as any structural weakness which develops as a crack under strain. Flaws are always present in a brittle material and may cause wide variations in breaking strength. The weakest flaw in a particle determines its breaking strength in comminution. It also controls the number of particles after breakage.

Though Bond tried to correlate his law with crack theory, in actual sense he did a compromise between the earlier two theories. The concept lies in the fact that the energy consumed is proportional to the initial size of the rock (Kick's theory) till the stage of fracture is reached. Once the stage of fracture is reached the energy consumed further by

fracture is proportional to the surface area created (Rittinger's theory). The total specific energy is thus inversely proportional to the square root of the initial size. The generalised relationship in a size reduction process is give as:

$$E = 10 W_i \left(\frac{1}{\sqrt{X_p}} - \frac{1}{\sqrt{X_f}} \right) \qquad (6.1)$$

where, E (in kWh/t) is the specific energy consumed in the process of size reduction, W_i is the work index (intrinsic property of a material, relating energy input in kWh/st (1 kWh=3.6 MJ), required to break a given material from a theoretically infinite size to 80 % passing 100 micrometers), X_f is the feed size, and X_p the product size (both 80% passing) in micro-meter.

Austin (1984) modified the original energy size relationships by using 80 % passing sizes to the initial size and the product sizes instead of the previously used hypothetical differential sizes. This is because the products of a breakage must contain small fragments even if the original particle is only slightly broken in a comminution process. Hukki (Austin, 1984) suggested that the relationship between energy consumed and particle size is a composite form of Rittentiger, Bond and Kick's laws. The value of the constant varies depending upon the initial size and the breakage mechanism considered. Charles (Austin, 1984) gave a variable parameter to the exponent of the initial size and verified it experimentally. He further, combined the famous Gates-Gaudin-Schumann equation (G-S-S), a statistical size distribution equation to represent fragment size distribution, with the generalised size-energy relation. He concluded that if the size

distribution of the product of a comminution process follows the G-S-S equation with a slope 'n' then the energy size relation plot on log-log plot will follow the same slope, but with the opposite sign.

The energy approach plays a significant role in explaining the phenomenon of breakage in a fragmentation process. The fragmentation studies of Rittinger, Bond, and Charles, reflect, at least qualitatively, the energy aspects in the breakage process (Grady and Kipp, 1987).

6.3 Work Index (WI)

The work index, referred as the comminution work index, W_i, originates from Bond's law and takes into account the material characteristics, the method of size reduction and the efficiency of the operation. This could be assumed as a representative of the macro- and micro-structural and physico-mechanical properties of material, lumped into one term and derived from the grindability. The grindability, or the ease of grinding is quantified in terms of an amount of undersize (with respect to a specified size) produced in a specified machine, from a known starting size, and for a given energy input (e.g. per revolution of a calibrated rod or ball mill). The grindability of the material is widely used in comminution engineering to determine energy requirements and scale-up equipment.

Bond (Austin, 1984) used this index to model grinding circuits by assuming that an almost negligible change occurs in work index during grinding. Thus, the energy requirement for a material in a standard grinding mill (2.44 meter inner diameter overflow mill operating under a given set of standard condition) can be predicted for a specified

feed and product size. He made use of separate bench-scale laboratory tests both for rod and ball mills and determined the laboratory scale work index (W_i) by equating the work applied in the 2.44 meter mill to the number of revolutions to obtain the same size reduction. On the other hand the work index calculated from the mill based on the power draw from the motor and the feed and product size is known as operating work index[1] (W_{io}) (Bond, 1952). The ratio of operating work index, W_{io} to laboratory-scale work index, W_i is called the efficiency factor of the size reduction process (Austin, 1984).

The work index measured takes into account, at least implicitly, strain energy (elastic and plastic energy), surface energy, kinetic energy (some of the kinetic energy is translated into heat, material and machine vibration, sound, electricity and light generation) and finally material-material and material-machine friction. The work index is thus a measure of breakage performance in a defined piece of equipment according to a strict procedure.

Due to typical use of work index in comminution, it is being measured at various sizes at which a particular liberation process is undertaken using a specified machine. Although, the specific energy consumption increase with the finer comminution (3-4 kWh/t in coarse crushing, and 20-30 kWh/t in fine grinding), the work index remains fairly constant for each comminution processes. However, the work index below the natural grain size of the minerals increases (Bond, 1961). This increase is attributed to the absence

[1] The operating work index during blasting is calculated by the explosive energy (kWh/t) spent in obtaining a desired product size (80% passing in μm) with the assumption of feed size to be infinity.

of grain boundary which used to be the major source of stress concentration. At scales smaller than the grain size, breakage of the grain may require excessive energy input.

6.4 Measurement of work index

A fixed amount of samples by volume, less than 12.5 mm size in size, is ground in the standard laboratory Bond rod mill. The undersize (less than 1.2 mm) fines are discarded. Fresh sample is added to make up the amount of fines discarded. The mixture is ground in the mill so as to achieve 100 % circulating load. The process is repeated till a constant amount of grindability is achieved. The sequential steps are shown in form of a flow chart in Figure 6.1. The 80% passing size of the fresh feed, F_{80}, is determined by screening. The grams per revolution (GPR) is determined at steady state, when the desired circulating load, 100%, is achieved; the 80% passing size of the undersize, P_{80}, is determined by screening the product of the last cycle. The work index, W_i, is then calculated from following formula:

$$W_i(kWh/t) = \frac{1.102 * 62.5}{GPR^{0.25} \cdot p^{0.23} \cdot \left(\frac{1}{\sqrt{P_{80}}} - \frac{1}{\sqrt{F_{80}}}\right)} \qquad (6.2)$$

where p is the product size at which W_i is determined (1180 mm in the present tests).

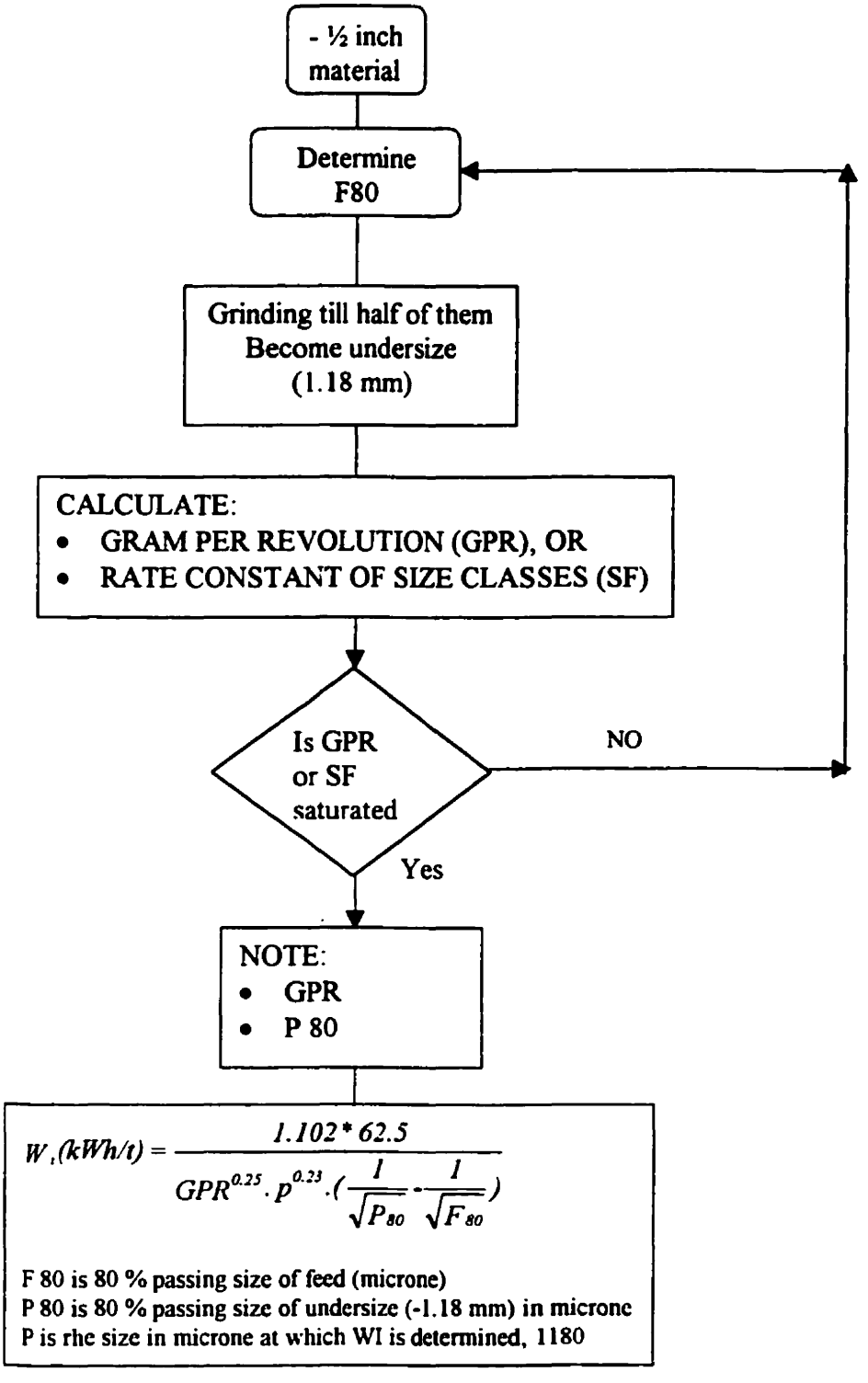

Figure 6.1: Methodology of W_i determination using Bond Rod mill.

6.5 Results

A summary of the important variables –the constant grindability (gram per revolution, GPR), feed and product size, F80, and P80 – and the work indices of the four rock types is shown in Table 6.1.

Table 6.1 Work Index for selected test rocks (Prasad, 1994).

Rock type	Const. GPR	P_{80}	F_{80}	Work Index
Unit	(g/rev.)	(mm)	(mm)	(kWh/t)
Stanstead Granite-A	25.30	0.93	9.74	7.8
Gneiss – D	14.31	0.84	8.46	10.8
Limestone –E	7.82	0.96	9.20	17.0
Marble -B	6.03	0.91	9.20	19.2

6.6 Conclusions

The breakage associated with any comminution process can be explained by stress or energy approaches. The later approach is used extensively to predict requirements or the efficiency in a comminution process. The work index, a constant of proportionality in Bond's law, takes into account of the strain energy, the surface energy, the kinetic energy and finally material-material and material-machine friction. This is determined in the laboratory by a standard Bond rod mill in which a fixed amount of rock aggregates is ground till a constant grindability is achieved.

Up until now, various fracture related rock properties, and their methods to measure in the laboratory have been described. This was done with the objective of analysing the dynamic fragmentation process in detail. The fracture related properties e.g.

compressive strength has been measured at a very high strain rates of about 10^3/sec (with an SHPB test apparatus) to a very low strain rates of about 10^{-6}/sec (static compressive strength measurement). Determination of work index was necessary as it is the fracture property at intermediate strain rates, albeit using a completely different approach. This bridges the gap of strain rates from static compressive or tensile breakage to a dynamic compressive breakage at a very high strain rates. It is expected that these fracture related properties are directly controlled by the inherent microstructural characteristics of rocks. The next chapter describes how to characterise and measure some of these microstructure for rocks.

CHAPTER 7

MICRO-STRUCTURAL MEASUREMENTS

7.1 Microstructure of rocks

The micro-structure of rocks is one of the principal features that sets rocks apart from other materials. However, compared to other materials, the micro-structural aspect of rock failure has received much lower attention. It has been often inferred indirectly from similar behaviour of other brittle materials such as ceramics, concrete, glass, brittle metals etc.. The microstructure of rocks may be broadly divided into two categories:

- Minerals
- Textures

The first one represents the type of minerals constituting the grains, the grain boundaries and the cementing materials between two or more minerals. Further, at the lower scale, it relates to the specific type of atoms, molecules, or ions constituting the specified minerals.

However, the textural features represent the arrangement of the mineralogical details within the rocks. This includes dislocations in atoms of the minerals, cracks or fractures in the crystals constituting the mineral grain, size and shape of the grains or grain-boundaries, cavity or pores in a mineral grain or between mineral grains.

7.1.1 Minerals

Minerals in a rock are naturally occurring inorganic compounds. Contrary to the fixed proportions of atoms, molecules or ions as dealt with in chemistry, rocks are mainly solid solutions of silicates, carbonates, oxides, etc.. Some of the inorganic elements get replaced in course of rock formation and thus both the elements are represented in parenthesis to represent rock as nearly as possible. For example, in Fe (Mg) Sio_3, K (Na) Al Sio_2 the magnesium and sodium replaces some of iron and potassium, respectively, to the extent depending upon the local environmental condition. The exact proportion is difficult to represent. Therefore, it is difficult to represent them by a unique chemical formula. Formulas or symbols are given to common minerals only. When minerals are in molten or dissolved state, molecules of the mineral roll or slip past each other. But when molten minerals solidify or dissolved mineral settle down from the solution. Individual minerals get crystallized or get crowded until they make a rigid mass of shapeless lump called grains. The minerals, which settle first, are developed well as compared to the remaining mineral solutions. The minerals assumes crystalline arrangement in the space where they are squeezed even if they do not get time to crystallize properly. Most of the minerals are silicates e.g. quartz, feldspar, micas, clay, olivine, garnet, pyroxenes and

amphiboles. Minerals are also found in carbonates, sulfides and oxides form but in limited amount. The basic building block of silicates is the silicon-oxygen tetrahedron consisting of silicon atom surrounded by four oxygen atoms with covalent bond at the corner of the tetrahedron. The tetrahedron, in turn, may be linked in single chain, double chain, sheets, three-dimensional network or not linked at all. Table 7.1 below shows the most important mineral group of silicates and carbonates. Their compositions, their characteristic cleavage (further explained in later paragraph) and their specific gravity are also shown to highlight their fracture properties and their heaviness, respectively. One or two cleavage shows the weakness in a mineral, whereas the absence of a cleavage plane makes a mineral stronger due to its relative intactness. The three cleavages show their resistance in fracture due to

Table 7.1: Rock forming minerals of silicates and carbonates and their characteristics.

Types	**Structural type**	**Minerals**	**Composition**	**Cleavage**	**Sp Gr.**
Silicates	Single tetrahedron	Olivines	$Mg(Fe)_2Sio_4$	None	3.2-4.1
		Garnet	$Fe_3Al_2(Ca_3Fe_2)(Sio_4)$	None	3.8-4.3
	Single tetrahedral chains	Pyroxenes	$Ca(Mg,Fe,Al)[(Al,,Si)O_3]_2$	Two	3.2-3.5
	Double tetrahedral chains	Amphiboles	$Ca(Mg, Fe)_3(Sio_3)_4$	Two	3.0-3.2
	Tetrahedral sheets	Micas	$K\,Al_3Si_3O_{10}(OH)_2$	One (platy)	2.7-3.2
		Clays	$Al_2Si_2O_5(OH)_4$	One(platy)	2.5-2.7
	3-D tetrahedral networks	Feldspar	$(K, Na, Ca)Si_3O_8$	Two-three	2.6-2.8
		Quartz	Sio_2	None	2.65
Carbonates	Ionic	Calcite	$CaCo_3$	Three	2.7-2.9

interlocking of cleavage planes, thus generating additional friction between the planes. A brief outline of the important minerals is presented in the next paragraphs.

Quartz is one of the most common mineral found in igneous or magmatic rock. Quartz crystals are pure silicon dioxides with straight edges of crystal which are easily identified in thin sections. These are unaltered, lack cleavage and show grey and white interference of colors under crossed polarized light. An alternating white and black band of colors in quartz indicated that these have been strained which is stored as memory. Quartz crystals are found in interlocking positions thereby imparting more strength to minerals, and in turn to the rocks. This is a hard mineral and resistant to the process of weathering and physical breakdown. While growing, quartz minerals may enclose silicate liquids which is turned into a ground mass of very fine crystals.

Feldspars are the most common rock forming minerals. These can be categorized into alkali-feldspar and plagioclase. The former consists of potassium-aluminum silicate (orthoclase) or sodium-aluminum silicate (albite) while the latter contains minerals ranging from sodium-aluminum silicate to calcium-aluminum silicate. The feldspar minerals show two good cleavages. However, in thin section we may not notice the cleaves if their orientation is parallel to the thin section made. Most of the feldspar minerals show alternate color change (twining) in polarized light due the difference in refractive index of crystals. Feldspar has a tendency to alter to fine grained crystals of quartz, mica or clay which imparts weakness in rock in due course of time. Also, these fine altered particles are difficult to identify in thin sections. Higher resolution techniques such as scanning electron

microscope or X-ray diffraction are used to identify these fine minerals.

The mica group of minerals are hydrous aluminum-silicates of magnesium and iron in addition to potassium, and often fluorine. These are mainly divided into two types namely, biotite and muscovite. The former is dark green, brown or black color due to the presence of iron and magnesium while the later is colorless or light pale in absence of them. The third type, chlorite, is common in metamorphic rock, and consists of hydrous magnesium and iron aluminum silicates. Both are platy pseudo-hexagonal crystals and show perfect cleavage in sheets which may be bent but spring back into shape again. Mica may undergo hydration or alter to clay minerals easily.

Pyroxenes are a coherent group e.g. the properties are true for most of its member types. They are all meta-silicates of iron, magnesium and calcium, and are in the alkaline group of sodium, iron and aluminum. These gives dark color to the rock types. Pyroxene crystals are prismatic but with no recognizable straight edges. Alkali pyroxenes are rather acicular crystals. All the pyroxenes have two good prismatic cleavages at right angle to each other. Many pyroxenes also exhibit a good parting sometimes more regular and persistent than the cleavages. Alteration usually starts from these places and are often marked by flakes of ilmenite,, magnetite and hematite. The altered minerals are mostly chlorite.

The amphiboles group of minerals contains a large number of different solid solutions but all of them have similar crystal structure despite the great variety of substitution which are possible. Essentially, amphiboles are meta-silicates of magnesium,

iron, calcium, sodium and aluminum. These form acicular or fibrous crystals. They have got perfect cleavage characteristic of prismatic type which distinguishes them from all the other minerals. The commonest amphibole is hornblende. The amphiboles on alteration results in talc or chlorite.

Calcite and dolomites are calcium and calcium-magnesium carbonates. Calcite is relatively pure and is found in limestone. Dolomite is a secondary mineral it may replace calcite or form a cement. Both are rhombohedral crystals with irregular or curved edges in thin sections. Both shows cleavages and multiple twining when rotated under polarized light. Calcite may be in different forms, especially, in sedimentary and metamorphic rocks. In limestone, the organized aggregates of carbonate minerals may be of circular or elliptical shapes with concentric laminae of fine grained carbonate minerals in the surroundings called ooids. The hard parts of carbonate secreting organism called bioclast remain either in complete or fragmented forms or even in fine grained carbonates lacking any recognizable internal structure called peloids. The coarse grained sparry calcite (also called sparite) consists of calcite which are in the form of cement with its crystal of diameter 5 μm or more which occasionally fills the pores. The fine grained micro-crystalline calcite (sometimes also called as carbonate mud) are micrite which are formed from disintegration of secretions of calcium carbonate associated with organism such as algae. The micrite surround the outer parts of ooids, peloids and bioclasts. The crystal size of micrite is much smaller than the thickness of normal thin sections, and hence difficult to analyze under polarizing microscope. The function of polarizing microscope is elaborated

in subsequent section.

The clay minerals are fine grained soft hydrous aluminum silicates with varying amount of iron, magnesium, and alkali. They are pseudo-hexagonal like mica and chlorite or forming blade-like or even tubular flakes. They may occur as amorphous dusts in impregnations or patches as aggregates. Due to their fine grains they cannot be identified accurately in thin sections. These are formed by hydro-thermal alteration of feldspar, weathering of igneous rocks and sediments under acid conditions.

7.1.2 Textures

The textural aspect of microstructure consists of the arrangements of atoms, ions, or minerals, in terms of its shape and size; cracks, fractures or cleavages and their inter-locking in and around a mineral in a rock type. There are a large number of textural entities in rocks. In order to simplify the representation of these entities with respect to their relevance in fracture process they can be classified into volumetric, planer, linear, and point structures. These structures represent three dimensional (3D), two dimensional (2D), one dimensional (1D), and zero dimensional textures or defects in space.

The 3D textures consist of arrangements of minerals, grains or grain aggregates (solid part), and pores, voids or cavity (vacuum part). The volume of these features corresponds to the grain volume and the porosity, respectively. The weight-volume relationships of it represents the physical properties on macroscopic scale. If the pores or voids are interconnected, permeability is the term to represent them physically. Altogether, there are large number of parameters which describe the interrelationships among grains,

pores, and the fluid content in it (e.g. porosity, density, void ratio, bulk, dry, or grain density, water saturation, etc.). Most of these parameters which correspond to the macroscopic physical properties, are measured by volumetric or water displacement methods. However, the microscopic measurement, such as the size and shapes of the grains or pores are done using a large number of two dimensional sections or photographs. Inferring 3D features from these sections or photographs has limitations but is relatively easy and quick. The relationship between actual 3D objects and an apparent 2D objects are shown in Table 7.2.

Table 7.2: Actual object in 3-D and its apparent look in 2D.

Actual 3 D objects	**Apparent 2D object, or objects**
Sphere	Circles
Cubes	Triangles, Squares, Hexagons
Disks	Ellipse, Circles
Needles	Ellipse, Circles, Rectangles
Flakes	Strips, Irregular polygons

For an example, a spherical shaped mineral or pores will show a circle in 2D pictures. However, the circle in the photograph may be due to the spherical, disk, or needled shaped minerals or pores. These problems can be minimised by taking large number of pictures at different sections. The fraction of a 3D microstructure in a rock aggregate or rock sample can be estimated by its area fraction in two-dimensional photograph.

The two dimensional textures include grain boundaries, grain areas, or the inter-phase boundaries between two minerals. It also include the surfaces of pores, cracks, or cleavages etc.. Inferring 2D objects by photograph also has limitations. For example, a square plane can be viewed as a line, a rectangle, or a square depending upon the angle it is being viewed. However, again the large number of sections or photographs will reduce the chances of error.

Faces of grains meet along common edges, called grain edges at which three or more grains are joined. The one dimensional structure consists of the content of these edges as well as any discontinuities along these edges. These 1D features are in the same scale as the mineral sizes. However, there are also linear defects (dislocations) at the atomic level which is at much lower scale than the above mentioned textures. In dislocations, atoms or ions are aligned differently than their regular alignments. These are identified by Burger vector (it describes the displacement associated with a dislocation) and tangent vector (it describes the geometry of dislocation). The zero dimensional features are the defects in atoms or its vacancy in the lattice structure. These are also in the same scale as the dislocations.

Overall the mineralogical and the textural features are due to the type of formation, the source of origin and, its evolution to the present condition. The former primarily controls the size of individual atoms, the density of the rock type and the bonding strength between the minerals depending upon the grain size, shape and its packing. The later represents the geometry of minerals and the presence of defects, if any, in rock. Both are

subject to change due to change in environmental conditions (temperature, pressure, corrosive fluids etc.). Also, certain minerals are more prone to micro-structural degradation in such situations. This results in further increase in cracks and fractures and even conversion of some minerals into weak fine clays. Therefore, It can be said that the textural details in a rock are also the result of mineralogy of microstructure. The textural feature, or more appropriately, the microstructure (as discussed above) plays a significant role in the strength behaviour of rocks.

7.2 Microstructure

As discussed in the above paragraph, there are a large number of entities in 2D textures. It also include 3D objects as well as 1D features in the specific 2D plane, section or photograph. The 2D texture, thus includes grain size, grain shape, surfaces of crack or fractures, linear cracks, fractures or point defects. These are termed collectively as micro-structure. Visual assessment of microstructure using the terms such as, many, few, large and small can mislead quantitative representation and are no longer used in present day. The extent of a mineral or a phase can be represented in terms of the specific surface area per unit volume, the perimeter line per unit area, or the number of grid points falling per unit of the scan line. These can be assessed or directly measured from large number of thin sections (or photographs) representing the 3-D objects. The precision of estimate in point counting is no worse than the other two methods. The degree of orientation of individual phase can be said to be the number of intersections per unit length in different direction. The degree of connectivity of a phase can be represented as the ratio of contact area

between those phases with the total contact area of all the grains. Shape, size and size distribution of a particular phase can also be determined. The measurement of dislocations as well as the vacancies in atoms or ions is complex due to the very high magnifications required and the large number of these features frequently observed in minerals like rocks. Moreover, it is not known how the linear and point defects affects the fracture process in an intact material, especially, when larger and more critical defects in two or three dimensions are already present. The focus of the present work is, therefore, to characterise those microstructure features which control the fracture process significantly.

Due to the large number of contributing factors in microstructure it is sometime difficult to quantify its role on overall rock fracture process. In micro-structural damage mechanics these microstructure features are lumped under one term, damage, especially when similar mineralogical features are present. The damage is used to quantify the continuous degradation of material i.e. generation of micro-cracks, pores and voids. An increase in damage is associated with the decrease in the effective modulus of elasticity, Poisson's ratio, and finally load bearing capacity. The kinetics of growth of microstructure before reaching the level of well defined crack is the subject of damage mechanics. Crack growth from a well developed dominant crack, on the other hand, is the subject of fracture mechanics. Further, no matter whether one or more well defined cracks are developed or not, the subject of rock under a given load, whether it will fail or not, is covered under strength of material or rock mechanics. The distinction among rock mechanics, micro-structural damage mechanics and fracture mechanics is due to scale i.e. macro-level,

micro-level and a size intermediate between them, respectively. The boundary line between micro-structural and macro-structural is sometimes ambiguous. In this work micro-structure refers to the scale at or below which hetrogeneity exists in the rocks.

7.3 Influence of microstructure on strength

7.3.1 Strength due to mineral bonding

The ideal or theoretical strength is due to the type of bonding between adjacent atoms or molecules of minerals in a rock. The individual atoms or ions in a mineral are bonded by inter atomic bonding. The bond may be of ionic, covalent or combination of ionic and covalent bond. The ionic or covalent bonds are characteristics of sharing of electrons and directional bonds. This is evident as rock behaves as a non-conductor in the absence of free electrons, and the directional bond causes brittleness. The equilibrium separation of atoms or ions correspond to a the minimum in potential energy, E. This is associated with balance of attractive and repulsive forces existing between two opposite charged ions and similar charged ions, respectively. The form of this relationship is given by $E=-\alpha/x^m+\beta/x^n$, where $-\alpha/x^m$ and $+\beta/x^n$ correspond to energies of attraction and repulsion, respectively, and $n>m$. The force acting on the particles at equilibrium separation, x_0, is zero. The second derivative of potential with respect to distance (alternatively, the first derivative of the force with the atomic separation) is given as stiffness or relative resistance of separation. The stiffness is highest at the equilibrium position of atoms. It reduces upon atoms separation and reaches zero with respect to increasing separation of atomic distances.

Mineral grains are, however, connected with physical bonds consisting different cementing materials and the microstructure in and around it. For similar microstructures, the cementing materials have profound effect on the strength of rock specimens. Stronger minerals lead to higher strengths in rock samples. Price (1960) found the unconfined compressive strength of coal measure rocks to be increasing with increase in the quartz content of the cementing materials. He also found that the strength increases with the high compaction (low microstructure) for rocks having similar mineral content.

7.3.2 Strength and microstructure

As mentioned in the earlier section the textural features contribute significantly to the strength of the material. It may change the microstructure almost completely from origin of rock to the present stage. If a large amount of cracks and fractures are generated during transformation, rock becomes weak. If a part of the original grain boundary or cracks is healed, it results in higher strength. The presence of voids, cracks and defects can easily be seen under microscope under high magnifications. Nucleation of stresses take place at pre-existing cracks or flaws. The nucleation may also take place at the mismatch of different grain types, grain sizes, grain orientations and grain cavities. The growth of these cracks take place until the stress applied at the microscopic level is above a threshold limit. For a particular type of mineral, this threshold limit is dictated by the fracture toughness i.e. the stress applied and the size of the microcrack. Consequently, the growth of a crack takes place at the largest cracks or cavities or at the grain boundaries, whichever is larger. The weakness in grain-boundary is due to the impurities, porosity,

second phase particles, and imperfect bonding prevailing at this zone. Sanga et al., (1974) have demonstrated experimentally that the grain-boundaries are weaker than the grains themselves, as failure in compression takes place preferentially at the weak grain boundary zone irrespective of the stronger or larger mineral grain sizes. Furthermore, the grain-boundary of larger grains are more weaker because of higher concentration of grain boundary defects. The inter-granular cracks, therefore, consume less stress or energy than the trans-granular crack for crack propagation. A large amount of energy can be stored in grain boundary crack growth before any macro-crack growth is noticed. This is true, especially, when the crack growth is at subcritical level and occurs over a very long time (Swanson, 1984). For very fast crack velocities, such as those generated by loading cracks close to the critical stress intensity factor, the trans-granular fracture becomes more dominant (Swanson, 1984). This causes multiple crack formation and branching at barriers to release the energy to the nearby grain boundaries. These barriers are more numerous in highly heterogeneous or micro-structurally complex materials and lead to more tortuous crack paths (Swanson, 1984, Atkinson, 1989). This is the reason for fracture energy of some of the larger grained rocks to be higher than the smaller grained rocks. The direction of growth is dependent upon stress applied, material type and the environment of the crack. Cracks after sufficient growth, coalesce and make fragments. The crack coalescence is dependent on the crack growth velocity and spacing between cracks and flaws. The microscopic aspect of crack nucleation, propagation and fragmentation has been discussed in detail also by Curran and Seaman (1996), and Curran et al. (1987).

The actual strength of an intact rock sample is much lower than its theoretical values due to the cracks or the voids causing the stress concentration effect. This is the reason for the sedimentary rocks to have low strengths in general. Price (1960) has investigated the effect of pores in coal measure rocks in which mineral content of rocks were of similar content. He found a reduction in strength by 4 % when the porosity increased by 1 %. Brace (1961) has investigated the effect of grain sizes on the hardness (Vicker's hardness) of minerals. The later has been found to increase inversely with a power factor of the grain size. The power factor varied from 0.5 to 0.3 depending upon mineral types. The effect of the grain size on the yield stress in marble has been investigated by Olfsson (1974).

Even though the microstructural characteristics of rocks have been observed and measured for a long time, much less effort has been spent in systematic analysis in relating these with the strength of rocks. This is because of the difficulty in quantifying the microstructure e.g. the large variations in grain sizes, crack sizes, it distributions and orientations. The largest grain size (the average grain size when grains vary in close range) have been used most often in the literature to study its effect on the strength of rocks. The crack sizes, more than a specified length, and falling in a regular spaced grid size and at particular orientation have been counted for quantitative correlation with strength values. The investigation of micro-structure using scanning electron microscope is more often limited to the identification of finer minerals, the crack growth of intra-, inter- or trans-granular etc. (Swanson, 1984). The microstructure measurements, therefore, are very

subjective and the actual procedure depends on the types of rock and types or work. The effect of microstructure on strength of rocks have also been investigated indirectly by measuring a global term called 'damage' as in the continuum damage modeling or monitoring the acoustic emissions (Bieniawski, 1967) during a continuous loading process. The extent of microstructure increases in such cases which are evaluated using damage and acoustic emissions. The former is measured easily by the reduction in the modulus of elasticity, Poisson's ratio, or the stress wave velocities with the increase in density of microstructure. The later is a technique in which the sub-audible or audible noise generated during crack generations is recorded using precise instrumentation.

7.4 Measurement of microstructure

Minerals and textures are distinguished optically by eye or with an optical microscope. Normal light reveals the grain size, shapes, cleavages and fractures. A polarised light reveals the identity of minerals by producing characteristic bi-refringent patterns and colours. Staining techniques make certain types of minerals more readily identifiable under microscope. A further detail of rock-fabric and pore structure is achieved by higher resolution as in the scanning electron microscope (SEM). Under SEM a topographical image of the rock is viewed. The back scattered electrons depending upon different content of the mineral in the specimen reveal the mineral types. The emission levels are different for different atomic numbers of the mineral phases. Differential thermal analysis and X-ray diffraction methods are used to quantify the clay content in the rock type. Clay content can also be identified by nuclear magnetic resonance or infrared

spectroscopy method.

The measurement of microstructure involves different subject areas of interests. The investigations may range from the origin of rocks, petrography of rocks, or the strength behaviour of rocks. The present work is related to the later e.g. exploring some of the microstructure which are expected to have significant influence on the strength related properties. In particular the microstructure measured are: the mineral types, their proportions, their grain sizes, the largest crack size and the crack density. This was carried out by means of optical microscopy.

Optical microscopy has been employed as the principal tool for these studies. The optical microscope has a provision of using it either as a transmitting microscope or as a reflecting microscope. The total magnification achieved is about 30 to 200 times. The microscope is equipped with a rotating stage and two polarizing filters, one below the stage and the other above it. Ordinary light is considered to consist of waves vibrating in all directions whereas polarised light consists of wave vibrating in one plane only. The two polarizing filters are set such that their polarization directions are right angle to each other and parallel to the cross wire in the eye-piece of the microscope. The polarising filter below the stage is called polarizer while, that lying above the stage is called analyser. The rock sample used in this study were in the form of thin sections (25 mm x 45 mm x 0.03 mm thick) mounted on glass slides. The thin sections can be studied either in plane polarised light (analyser is taken out from the path of the view) or in crossed polar or crossed Nicol. Most of the minerals are identified under transmitted light for its grain size,

grain shape, and the fractures or cleavages if present in the minerals. The two minerals formed at the same time but with different refractive indices are identified by alternate bright and dark bands in the grain. This phenomenon is called twining. Certain mineral changes its colour from dark to light and becomes invisible with the rotation of the stage. This is called extinction. Reflecting microscope is used to quantify microstructure of opaque minerals. Since the selected rock types in the present work had very limited amount of these minerals (iron and titanium oxides), microscopy was mostly carried out under transmitting light only. The microscope under reflecting light was used to calibrate the microscope for the measurement of grain or crack sizes either with the cross wire of the microscope, the computer screen attached with the microscope, or the photographs taken with the camera attached to the microscope. Calibration is achieved by placing a fine ruler under reflecting light. The magnification achieved by the microscope is verified by the cross wire readings of the eye-piece as well as from the photographs taken from the attached camera. The following section described the details of the measurement of microstructure.

The general microstructure measured in the present work consists of predominant mineral types, proportion of minerals, grain size range, presence of fracture and alteration of minerals if any. The minerals are identified by colours, grain shapes, presence of cleavages and the phenomenon of twining and extinction. The appearance of the most important minerals under transmission microscope has already been described. Since the selected rock types are mostly granites, limestone, and marble; the predominant mineral

types are: quartz, feldspar, mica, and carbonates. The quartz grains are identified by their colourless or light pink to grey colour in polarised light with straight grain edges. The feldspars are identified through the phenomenon of twining, two good cleavages, and transparent o translucent grey to pink colour grains. The mica is dark green to brown (biotite), or light yellow to brown (muscovite) with a shape cleavage in the grain. The carbonates are tested with dilute hydrochloric acid which yields carbon dioxide gas. The carbonate minerals have three planes of cleavages with three cleavage planes as identified in marble. However, in limestone the circular or elliptical shaped calcite are in the surroundings called ooids. A large amount of fossils makes the limestone devoid of any geometrical grain structure. The proportion of minerals are estimated qualitatively both by observing the thin sections and looking at the rock samples. The grain and crack sizes were measured by scanning the full thin sections under the microscope. The alteration in minerals e.g. from feldspar to mica was noticed by replacement of former by the latter. However, the alteration to clay could not be observed as they require much higher magnification obtainable only by SEM or X-ray techniques. Alteration in minerals were noted down as comments during microscopic examinations. Altogether 180 photographs were taken from 12 rock samples out of which 80 photographs were in black and white. The thin sections were scanned from corner to corner in x-y directions. This helped in obtaining a picture of biggest grain sizes and the biggest crack sizes. The following paragraph describes the details of the microstructure for each rock types.

Sample #A: Stanstead granite

The Stanstead granite is an intermediate grain sized rock. It consisted mainly of feldspar, quartz, mica, and traces of zircon, amphibole, and epidote. The quartz and feldspar are highly fractured. Figure 7.1a shows the extent of fractures in feldspar at a magnification of 50. One of the largest grain is shown in Figure 7.1b (a combination of two photographs) at a magnification of 32. The size of the photographs at a magnification of 50 is 3 mm x 2 mm. Similarly, the size of photographs at a magnification of 32 is and 3.1 mm x 2.3 mm. Table 7.1 highlights the other microstructural features in detail. It includes the mineral content, the range of their grain sizes, the approximate proportion of minerals, and the presence of fracture and alterations if any.

Table 7.3: Details of microstructure of Stanstead Granite -A

Minerals	Grain size (mm)	Mineral %	Fractures	Alterations
Feldspar				
a) Plagioclase	μm to 2 x 4	40-50	Fractured	To mica
b) Microcline	μm to 1 x 2.2	<2	Some grain fractured	To mica
Quartz	μm to 2 x 4	20-25	Mostly fractured	None
Mica				
a) Biotite	μm to 0.35 x 2	20-25	Good Cleavage	Marginally
b) Muscovite	μm sized	<0.5	Cleavage	In feldspar
c) Chlorite	μm sized	<0.5		To biotite
Amphibole	μm to 2 x 4	<0.5	Cleavage	By biotite
Zircon	0.06x0.23 to.35 x .92	<<0.1	None	
Epidote	μm to 0.12 x 0.21	<<0.1	Cleavage	

Sample #B: Altered Marble

The altered marble is a very fine grained rock with a few well defined foliation planes filled with fine grained minerals, including veins of calcite, chlorite and amphibole.

Figure 7.1a: A typical fracture in a grain of feldspar in Stanstead granite (50 x).

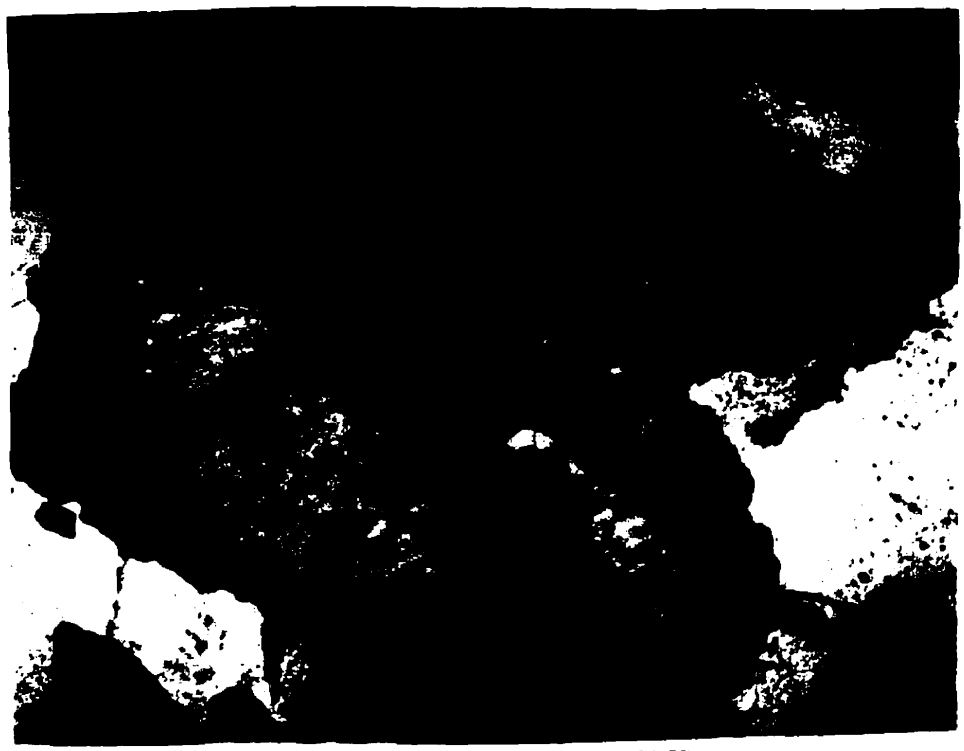

Figure 7.1b: One of the largest grain in Stanstead granite (32 X).

In the scale of the thin section the foliation planes are not visible. The fracture features in this scale appear perfectly healed and behave as part of the host rock. Figure 7.2 shows the usual grain network in the rock. It also shows healed cracks and the absence of any geometrical grains in the marble. The minerals, their proportions and their range of grain sizes are shown in Table 7.4. The extent of fracture and the alteration is also given in the table.

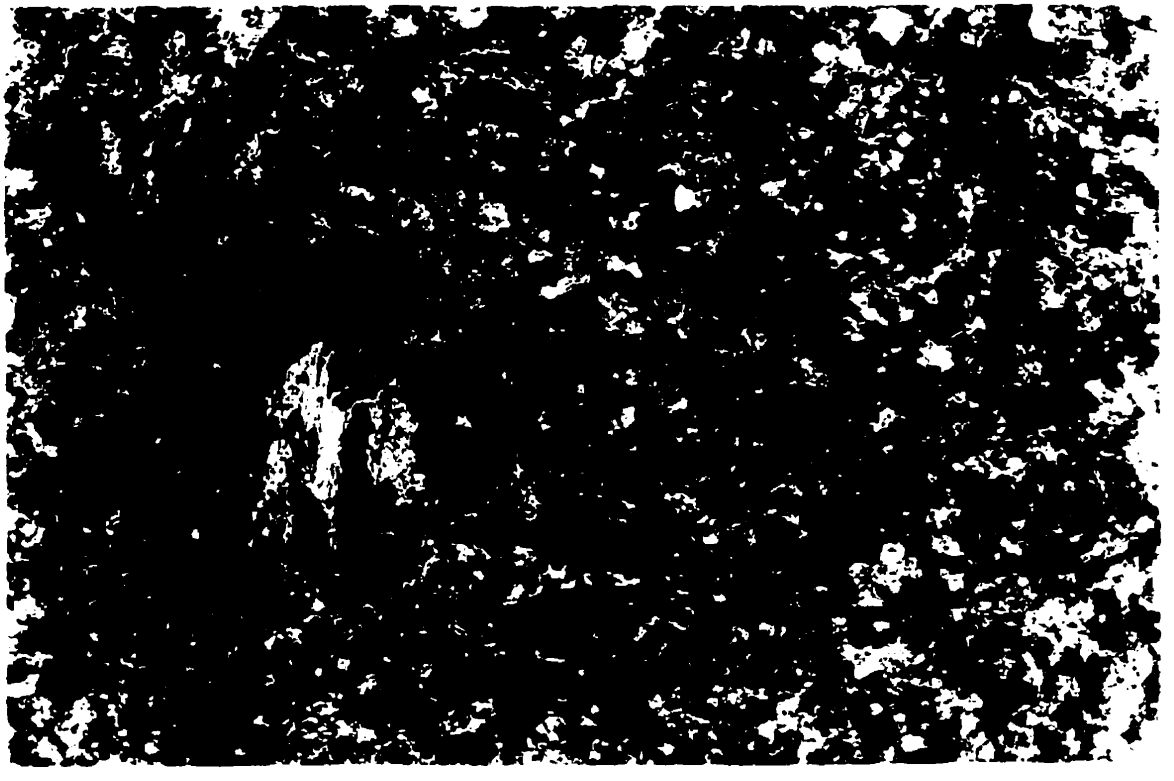

Figure 7.2: A typical microstructure of Marble-B showing no apparent grain or cracks (50 x).

Table 7.4: Details of microstructure in altered marble-B

Minerals	Grain size (mm)	Mineral %	Fractures	Alterations
Calcite	μm sized	50-55	None	None
Mica Muscovite & Chlorite	μm to 0.23 x 1.3	40-45	None	In amphible
Quartz	μm to <0.2	<10	Fractured	None
Feldspar	μm sized	<1	None	By sericite
Opaque Fe-Ti oxides	μm to 2 x 4	<1		

Veins of calcite, chlorite, amphiboles

Sample #C: Fossiliferous limestone

The fossili-ferrous limestone is oolitic marble. It is fine grained with the size of the ooids generally less than 0.2 mm. Thin sections prepared in two perpendicular directions (along the axis of the core on which compressive strength is evaluated and perpendicular to it) resulted similar grain sizes. A larger fossils of approximate diameter 0.7 mm has also been noticed in both the micro-photographs but are few. Figure 7.3 shows the common type of oolites and their grain structure. The details of the microstructure observation are shown in Table 7.5.

Table 7.5: Details of microstructure in limestone-C.

Minerals	Grain size (mm)	Mineral %	Fractures	Alterations
Microfossils & ooids	μm to 1.15 x 3.38	75-80	None	to sparicite
Bio-sparite	μm to 0.46 x 4	<5	None	None
Burrowing animal	μm to 0.2 x 4	Trace	None	By micrite
Matrix	Sum μm sized	10-20	None	To oomicrite
Quartz	μm to 0.07 x 0.09	Trace	None	None

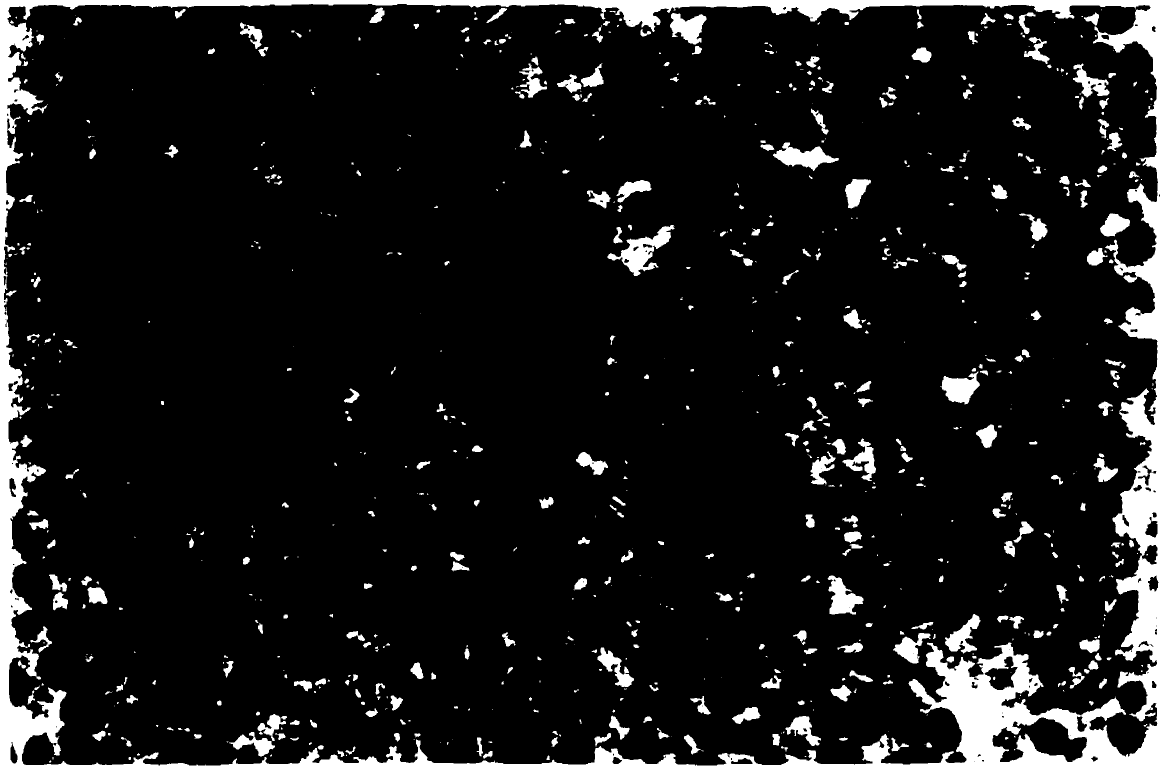

Figure 7.3: A typical microstructure of oolitic limestone-C obtained from Kingston (50 x).

Sample #D: Biotite Muscovite Gneiss

The gneiss is a metamorphic rock of intermediate grain size (see Figure 7.4). The minerals are mainly quartz, feldspar and mica with some opaque minerals like titanium oxides. Some of the feldspars and micas are altered into biotite and chlorite. A well defined foliation and a fractured grain can be seen in the figure. The Table 7.6 highlights the other minerals, their grain sizes, their proportions and the extent of fractures and alterations.

Table 7.6: Details of microstructure in gneiss-D.

Minerals	**Grain size (mm)**	**Mineral %**	**Fractures**	**Alterations**
Quartz	.02x.02 to .18 x .46	30-45	None pertinent	None
Feldspar				By biotite
a) Micorcline	µm to 0.23 x .58	<15	None pertinent	
b) Plagioclase	µm to 0.38 x .43	<10	None pertinent	
Mica				
a) Chlorite	µm to 0.23 x 0.46	<5	Cleavages	
b) Biotite	µm to 0.05 x 4	<0.5	Cleavages	By chlorite
c) Muscovite	µm to 0.02 x 2	<0.5	Defined foliation	To biotite
d) Sericite	µm to 0.02 x 0.06	<0.2	Cleavages	
Opaque Fe-Ti oxides	µm to 0.38 x 0.43	<1	None	To oomicrite
Amphibole	µm to 0.23 x 0.92	Traces	Cleavages	
Apatite	µm to 0.04 x 0.04	Traces	None	

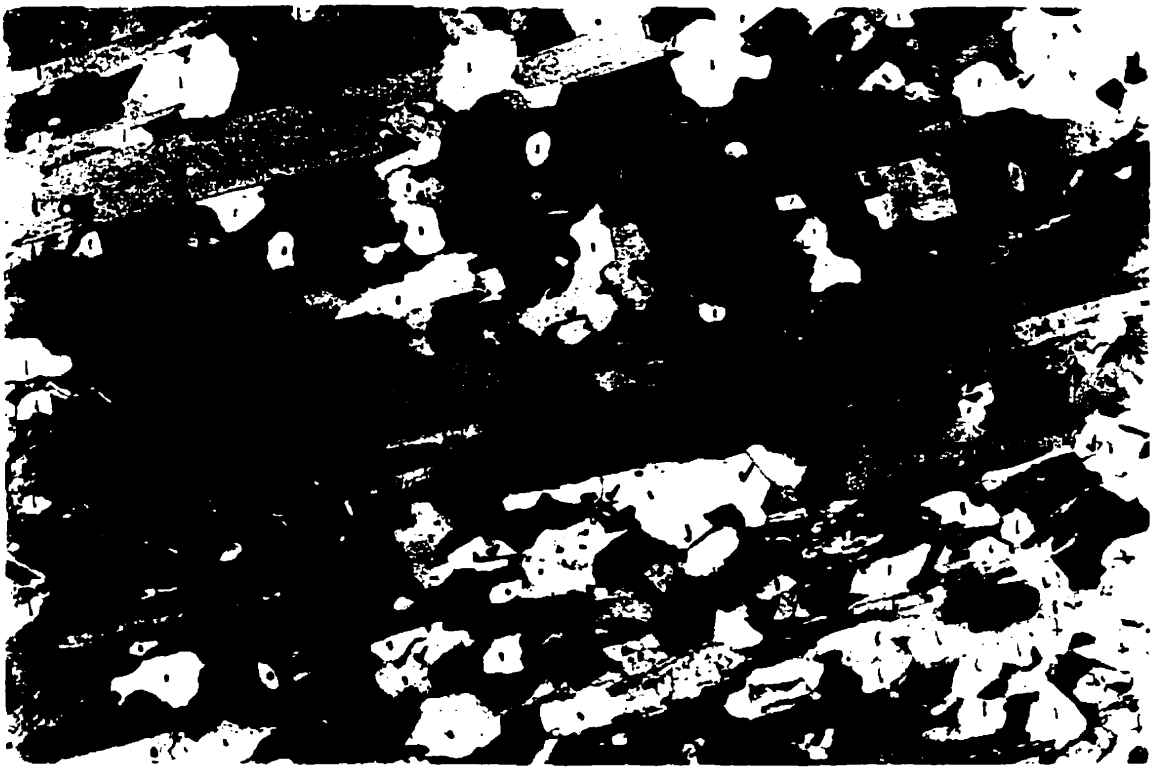

Figure 7.4: Foliated grain network of gneiss (D) from Hemlo gold deposit.A total of 231 grains are observed in the field of view with the largest grain size of 0.6 mm at the centre (50 x).

Sample #E: Micritic Limestone

The limestone is highly an-isotropic in nature, a well developed conglomerate of different minerals is present irregularly in this rock type. The host rock is fine grained with healed fractures in it. However the rock is invaded with coarse grained minerals. A typical photograph of fine grained altered calcite near a coarse calcite vein is shown in Figure 7.5. The details of the microstructure are shown in Table 7.7.

Table 7.7: Details of microstructure in Limestone-E.

Minerals	Grain size (mm)	Mineral %	Fractures	Alterations
Micrite (lime mud)	Sub μm sized	95-100	None	None
Quartz	~0.3 x 0.42	<1	Invariably fractured	None
Lithic clasts	5 x 20	<5	Vein-filled	By qz. veins
Feldspar	μm to 0.23 x 0.35	<0.5	None	By biotite
Sparite	0.5 x 1 to 3 x 3.5	<0.01	Strained	Traces

Veins of quartz varies in width from less than 1mm to more than 10 mm.

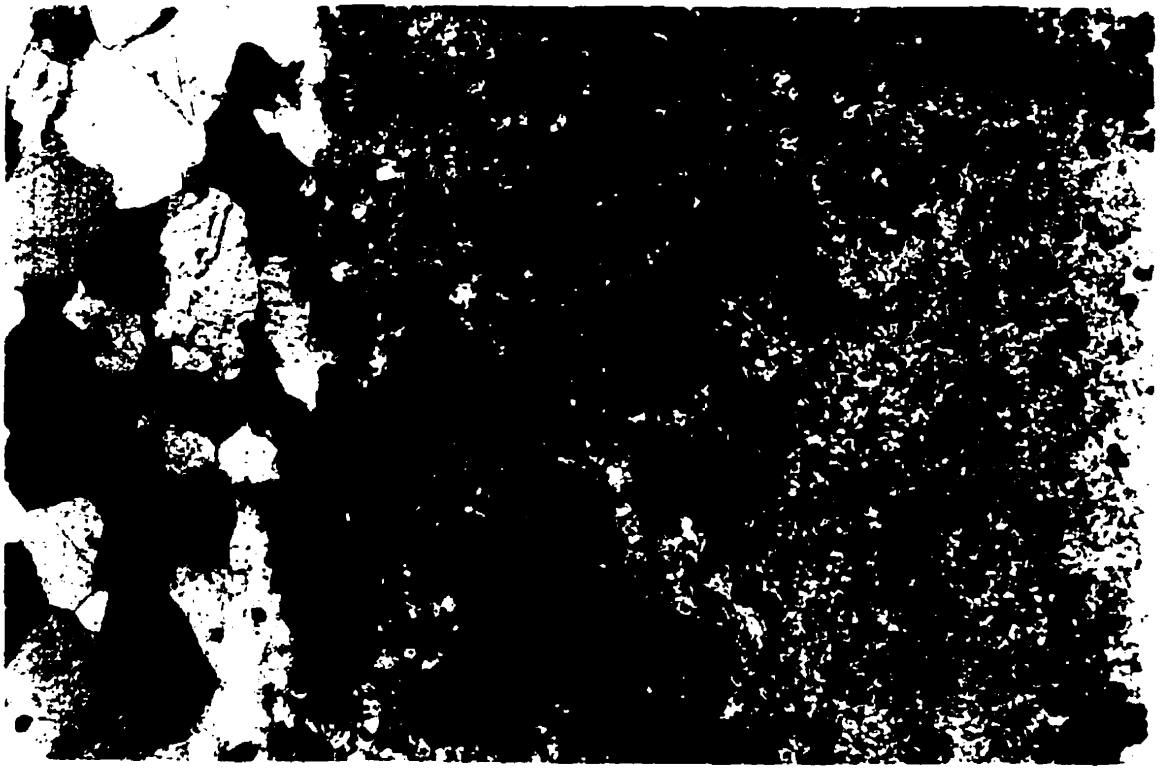

Figure 7.5: A typical micro-photograph of Vineland limestone (E), (magnification: 50X).

Sample #F: Marble 2

This is an intermediate to fine grained metamorphic rock with veins of quartz and calcite. The biggest grain is 1.6 mm with a few cracks lying along the grain boundaries. The largest crack was been found to be 0.47 mm as a geometric mean of length and width. The grain distribution is shown in Figure 7.6, which also shows the details of microstructure measurements as indicated in Table 7.8.

Table 7.8: Details of microstructure in marble2-F.

Minerals	Grain size (mm)	Mineral %	Fractures	Alterations
Calcite	~ 0.25 to .5 x 2	80-90	None	None
Mica Muscovite & sericite	μm to 0.13 x 0.45	<10	None	In amphible
Quartz	μm to 0.23 x 0.25	<5	None	None
Feldspar	μm to 0.2 x 0.32	<2	None	By calcite
Opaque Fe-Ti oxides	μm to 0.4 x 1.5	<0.5	None	By calcite

calcite rich veins with subsidiary opaque, quartz, and minor K-feldspar

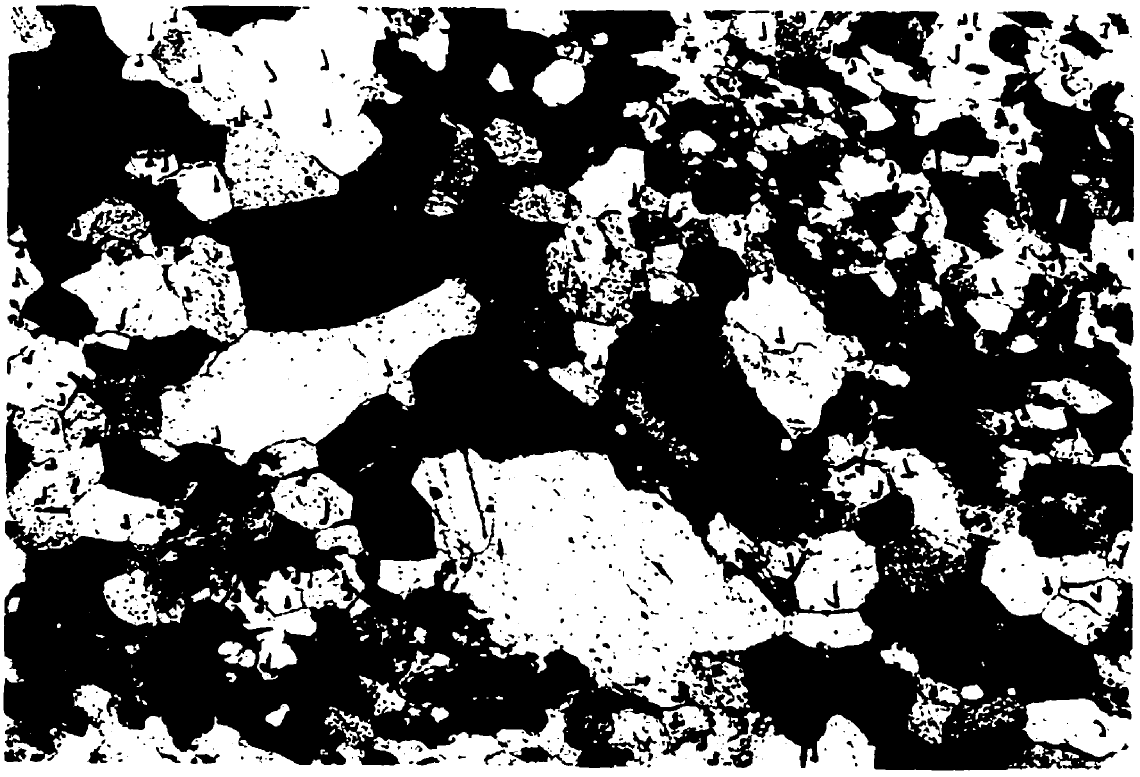

Figure 7.6: Grain network of feldspar, amphiboles and opaque minerals of Marble 2-F, (magnification: 50X).

Sample #G: Foliated Gneissic Marble

The foliated gneissic marble is a fined grained rock with biggest grain observed to be 0.78 mm as a geometric mean of length and width. The mineral contents are mostly calcite, feldspar, amphiboles and some opaque titanium oxide. The different foliation characteristics of the minerals are shown in Figure 7.7. The figure illustrates the problem in quantifying grain sizes. It also shows the feldspars being highly fractured. Table 7.9 shows the details of the microstructure observed.

Table 7.9: Details of microstructure in marble -G.

Minerals	Grain size (mm)	Mineral %	Fractures	Alterations
Calcite	μm to 0.12 x 0.43	75-80	Causes deformation	None
Feldspar	μm to 0.1 x 0.23	20-25	Invariably fractured	None
Amphibole	μm to 0.23 x 1	<10	Cleavage	Replaced
Opaque Fe-Ti oxides	μm to 0.35 x 2	<5	Good cleavage	Partly replaced
Quartz	μm to <0.1x 0.12	Traces	None	None

Figure 7.8: The grains distributions in the marble-F (x 50)

Sample #H: Laurentian red granite

The red granite is an intermediate grained rock consisting of quartz, feldspar, mica and some traces of other minerals. The usual grain size observed is 2.8 mm long, however the largest feldspar has been observed to 5 mm in length. The cracks are of the order of 1 mm in length. A typical grain structure and fracture in quartz are shown in Figure 7.8. The feldspars are altered to albite and some mica are altered to feldspar. Table 7.10 shows the other features of microstructure.

Table 7.10: Details of microstructure in red granite-H.

Minerals	Grain size (mm)	Mineral %	Fractures	Alterations
Feldspar c) Plagioclase d) Microcline	0.06 to 5 mm	65-75	Fractured	Alterations to- Albite
Quartz	0.08 to 3.2 mm	20-25	Few fractures	Deformed
Mica a) biotite b) Muscovite c) Sericite	 µm to 1.5 µm to 1.3 µm sized	10-15	 Good Cleavage Cleavage	 Marginally In feldspar To biotite
Accessory minerals a) Fluorite b) Zircon d) Epidote-allanite e) Apatite	µm sized	<5	Fractured	Associated With biotite

Rock is pinkish red, fine grained.

Sample #I: Quartz

There is only one mineral present in this rock type, that is quartz. There is no grain boundary in it as these have been re-melted and welded. However a pseudo-grain boundary of size 1.4 mm has been found under polarised light. A large number of fractures

Figure 7.8: An example showing a rare fracture in Lawrentian granite-H, (50 x).

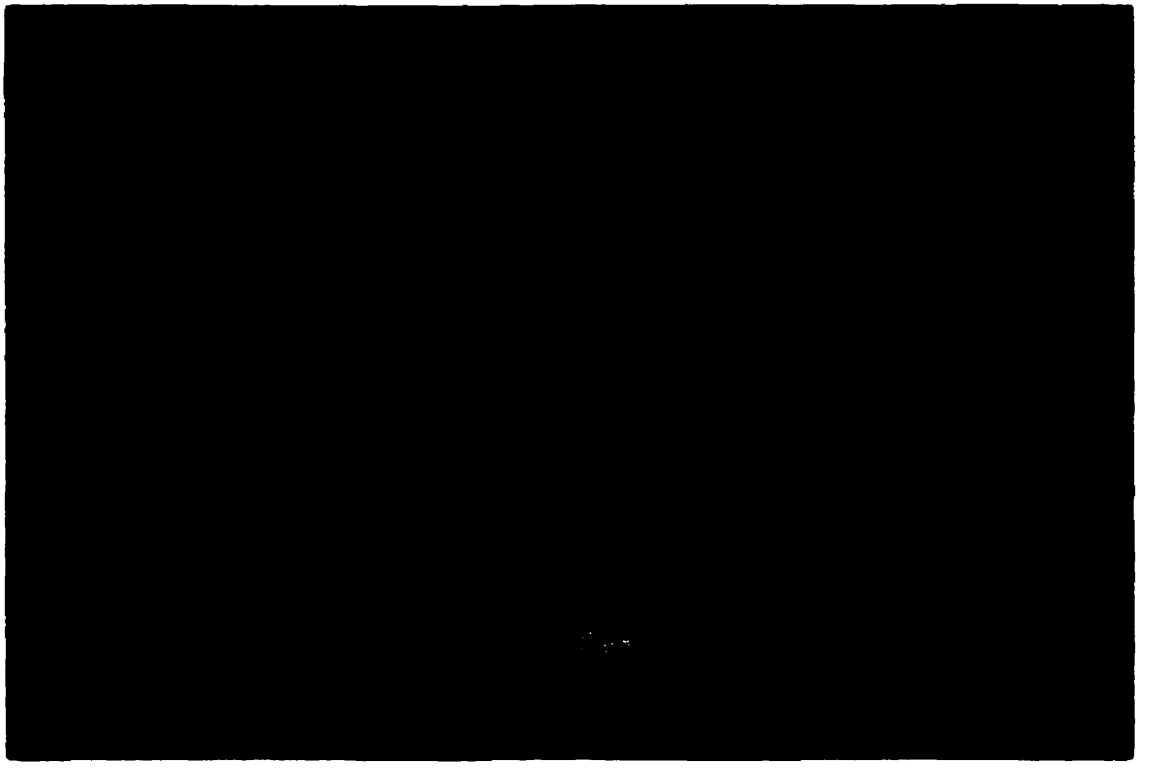

Figure 7.9: Presence of fractures and absence of grain boundary in Baskatong quartz (50 x).

are observed which are interlocked with each other. Figure 7.9 shows some of the fractures with dark spots as pressure solution causing meting of grain boundaries. Fracture network is extensive and passes through the whole section of the thin section. The Table 7.11 summarises the finding of the microstructure.

Table 7.11: Details of microstructure in quartz-I.

Minerals	Grain size (mm)	Mineral %	Fractures	Alterations
Quartz	No distinct grain	100	Interlocking fractures	GB remelted

Rock is milky colored annealed meta-quartzite with no individual grain boundaries. Incipient fracture occurs across the thin section. Veins and lenses of quartz are-crystallized by pressure solutions.

Sample #J: Barre granite

The Barre granite is a fine grained rock with minerals consisting of feldspar, quartz and mica with traces of other accessory minerals. The largest grain is of size 2.8 mm and the crack crack length of 1 mm. The details of microstructure is shown in Table 7.12.

Table 7.12: Details of microstructure in Barre granite-J.

Minerals	Grain size (mm)	Mineral %	Fractures	Alterations
Feldspar e) Plagioclase f) Microcline	µm to 2.6	60-70	Fractured	Alterations to- Albite Tartan twinned
Quartz	µm to 1.3	20-25	Few fractures	Deformed
Mica a) biotite b) Muscovite	 µm to 1.0 µm to 2.8	15-20	Cleavages	None
Accessory minerals a) Amphibole b) Zircon f) Epidote-allanite g) Opaque Fe-Ti oxide	µm sized	<1	Fracture emanates From zircon	Associated With biotite

Rock is fine grained, leucocratic granite. Plagioclase and quartz makes Myrmekite.

Some of the minerals coincide with the fractures. Figure 7.10 shows the typical grain network in intermediate to fine grained granite, along with the fractures in quartz.

Figure 7.10: Typical grains and fractures of feldspar and quartz in Barre granite-J, (50 x).

Sample #K: Gneissic granite

This is a coarse grained gneissic granite. The largest minerals is 4.4 mm long. The grain boundaries are healed with accessory minerals. Most of the quartz are fractured. The Figure 7.11 shows the healed grain boundaries and the fracture in quartz. Two thin sections made at mutually perpendicular directions gave similar results. The average grain size was difficult to predict from both the sections. The longest crack in quartz have been found to be 1.1 mm. The other details of microstructure are shown in Table 7.13.

Table 7.13: Details of microstructure in gneissic granite-K.

Minerals	Grain size (mm)	Mineral %	Fractures	Alterations
Feldspar g) Plagioclase h) Microcline	µm to 2.6	60-70	Fractured	Alterations to- Albite Tartan twinned
Quartz	µm to 1.3	20-25	Few fractures	Deformed
Mica a) biotite b) Muscovite	 µm to 1.0 µm to 2.8	15-20	Cleavages	None
Accessory minerals a) Amphibole b) Zircon h) Epidote-allanite i) Opaque Fe-Ti oxide	µm sized	<1	Fracture emanates From zircon	Associated With biotite

Rock is more like biotite amphibole granitic gneiss. Foliation is defined by streaks of dark minerals that pinch and swell; isolated clots produce eye-shaped, "augen-texture".

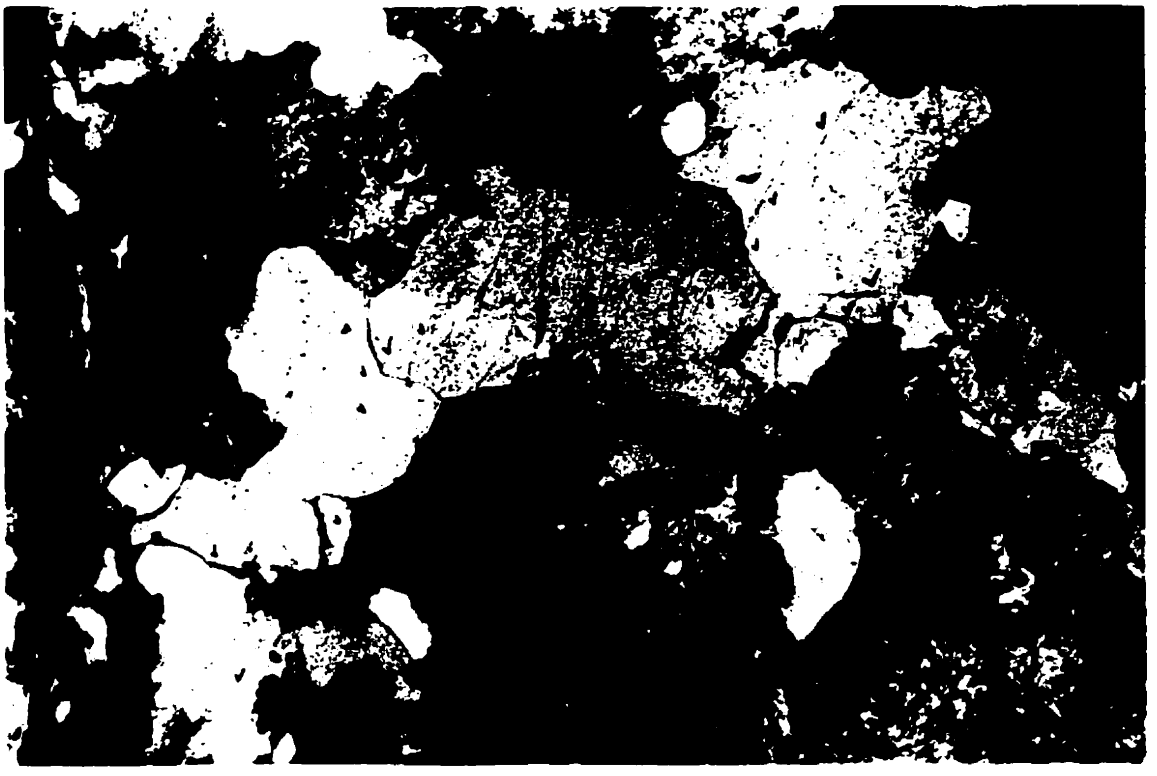

Figure 7.11: One of the few quartz minerals in gneissic granite-K, (50 x).

The microstructure of limestone (L) from Vineland was highly irregular and characterised as being very porous. Although the minerals were mostly calcite but the different layers were difficult to distinguish due to their fine grained nature. The details of the other minerals were not analysed.

7.4.3 Grain size characteristics

The grain size for all the rock types usually varied from a few micrometer to a few millimeters. Thus, it was difficult to give a representative value to it in most of the cases. However, the largest grain size was measured easily by scanning the whole thin sections under the microscope. The geometric mean of the approximate length and width of the grain size is referred as the largest grain size. The measurement of the average grain size was difficult. It was also not possible to determine its value in fine grained rocks and those devoid of any geometrical shapes in the grain network. The average grain size was determined by counting the number of grains in the known area of the photographs which were taken during the microscopic observation. An average of 10 photographs were used for this work. Table 7.14 shows the number of grains counted in the known areas of the photographs, the number of photographs used and the average grain size. The table above shows some of the measurements with the use of only 1 to 2 photographs. This is because in those cases it was very difficult to isolate the individual grains. The photographs at a very high magnification e.g. 212 to 300 times also did not give grain sizes. The measured value is an approximation in such cases.

Table 7.14: Results of the largest and the average grain size calculated from photographs.

Rock	**Largest grain size**	**Average grain size**		
Type	mm	Average grain, mm	Total area, mm2	Photographs
A-Stanstead Granite	3.3	1.34	109.9	17
B-Altered Marble	0.2	0.05	1.9	2
C-Kingston Limestone	0.7	0.17	60	10
D-Gneiss	0.8	0.26	13.3	4
E-Vineland Limestone 1	0.7	0.06	7.5	2
F-Marble	1.0	0.14	33.3	4
G-Gneissic Marble	0.4	0.16	1.5	1
H-Laurentian Granite	3.8	0.91	103.1	17
I-Quartz	0.9	0.90	No grain	5
J-Barre Granite	1.7.	0.59	76.9	13
K-Gneissic Granite	1.7	0.74	26.9	5
L-Vineland Limestone 2	0.4	0.38	8.1	4

7.4.4 Largest crack and crack density

The largest crack observed either inter-granularly or trans-granularly was measured to give the largest crack length in the rock type. It should be mentioned that this crack length represents the biggest crack at the grain level only. It is assumed that this length will reflect the largest weak zone existing in the grain level, especially, for the nearly isotropic rock such as granites. The crack length measured by this means is expected to influence the fracturing process in Brazilian tensile strength and fracture toughness in which cracking starts from the specified location (center of the disc, and near the notch end, respectively). However, this length may not have any influence on measured value of compressive strength as this does not represent the largest crack in the volume of the rock sample in which shear or splitting tensile failure may take place. Similarly, this crack would not be considered representative, if the tensile strength would have been measured by

uniaxial tension, when failure takes place at the much larger crack length present in the volume of the rock sample.

The crack density was measured using a simple stereological technique. It could be measured either by counting the number of times it intersects a linear or circular scan-line (in the unit of m^{-1}) or by measuring the total fracture length falling in unit area of the photographs (m/m^2). The later technique is used for the measurement of crack density which has the unit of m^2/m^3. Since the cracks observed were not consistent, the measured crack density is the maximum value observed from the investigation. Table 7.15 gives the measured values of the crack density.

Table 7.15: Results of the largest crack size and the nominal crack density .

Rock	**Largest crack**	**Nominal crack density calculations**			
Type	mm	Cracks length , mm	Area, mm^2	Photographs	Density, m^{-1}
A-Stanstead Granite	3.2	49.6	19.13	3	2.59
B-Altered Marble	0.03	0.1	0.63	1	0.16
C-Kingston Limestone	1.1	3.4	12.0	2	0.28
D-Gneiss	4.4	26.96	8.13	2	3.32
E-Vineland Limestone 1	0.1	0.4	0.17	1	2.42
F-Marble	0.5	21.55	6.17	2	3.50
G-Gneissic Marble	0.4	11.72	3.0	2	3.91
H-Laurentian Granite	1.0	15.36	19.13	3	0.8
I-Quartz	8.0	5.9	7.13	1	0.83
J-Barre Granite	0.8	17.9	13.93	4	1.29
K-Gneissic Granite	1.1	19.79	12.63	3	1.57
L-Vineland Limestone 2	6.0	0.9	0.17	1	5.45

The table also includes the details of the measurements i.e. the number of cracks observed, the length of the cracks measured, the area of the photographs, the number of photographs taken of the measurement. The table shows some of the measurements using only 1 to 2 photographs. This is because of similar reasons as discussed in the measurement of grain sizes. Some of rock have been are re-melted and the cracks healed. In such cases, it was very difficult to trace cracks in most of the photographs. The measured values are approximate in those cases.

7.5 Conclusions

Microstructure are the mineralogical and the textural details of rocks which make them anisotropic and heterogeneous in character. It is due to the nature of origin of rocks, the type of formation and the environmental condition which lead them to the present stage. The bonding among minerals contribute to the strength of a rocks, however, the texture makes it weak. The former upon degradation also add to the structure. The microstructure are largely the later part which consist of pores, cavity, grain sizes and shapes, surfaces of cracks or fractures, presence of linear cracks, fractures, and point defects. These are generally observed in a section or in photographs taken under microscope.

The rock sample used for the measurement of microstructure were in the form of thin sections and the instrument used was an optical microscope with polarised light. The general microstructure observed were the predominant mineral types, the proportion of minerals, grain size range, presence of fracture and alteration of minerals if any. The

largest grain size and the average grain size were measured by scanning the whole thin sections under the microscope and by counting the number of grains in the known areas of the photographs, respectively. The large number of photographs taken were used to measure the largest crack either inter-granularly or trans-granularly. The crack density, however, was measured using simple stereological technique i.e. by measuring the length falling in unit area of the photographs (m/m^2).

CHAPTER 8

ANALYSIS AND DISCUSSIONS

The response of rock under stress depends on what is being examined and how it is it being measured. There are various parameters characterising the fracture of rock depending on how the stress is applied and what is measured. Compressive and tensile strength are the fracture properties of rock when load applied in compression or tension, respectively. Fracture toughness reflects the failure strength of rock in the presence of a crack or a predominant crack. These properties can be further classified in terms of static or dynamic loading depending upon the strain rate specific to the process. A large number of fracture related properties of rocks has been measured and analysed to study the underlying mechanism (s) which govern dynamic fracture process. These also include the microstructural properties specific to each of the rock types investigated. The fracture

properties under low strain rate are obtained by the normal compressive and tensile strength tests; and fracture toughness tests. The very high strain rate properties are obtained by dynamic compressive strength tests using SHPB apparatus. The work index study encompasses intermediate strain rate phenomena. The micro-structural properties, measured by optical microscopy, include average and maximum grain size, inherent crack size, and crack density. In the following section the above mentioned properties of rocks are analysed and discussed with reference to the role of respective microstructures present.

However, since the term 'microstructure' may represent several independent facets of rock inhomogeneity and anisotropy, and which have been shown to affect many fracture related properties, it is considered appropriate here to start with a detailed description of the inter-relationships between these parameters.

8.1 Microstructure

Microscopic observation of the rocks shows the details of the microstructure. Rock are usually inhomogenous at high magnifications. The size and shape of the mineral content and their packing vary at different regions of the same rock sample. Even in the case of nearly isotropic rocks in which the arrangement of microstructure should have been independent of directions, inhomogeneity can still be observed. However, in a bigger scale the grain types, their packing, and their mineral content may be considered invariant, and the same rock may be considered isotropic. Orthotropic character is another variable typical to sedimentary rocks. In this the grain geometry and their packing vary in two

orthogonal directions i.e. along the bedding planes and perpendicular to it. The orthotropic effect could be minimised by making core samples perpendicular to bedding planes and applying stress along the appropriate direction. However, this could not be achieved in the various limestone rock types in this investigation, mainly due to the relatively small block of rock from which the cores had to be prepared. Although this resulted in larger scatter of strength values but it was so intended as it represented a global value of fracture property for the whole rock block.

The nearly isotropic and homogenous behaviour (especially, in igneous rocks) is reflected by the consistent value of seismic wave velocity along different directions, and the same values of density and porosity on macroscopic scale. The density is not only a measure of the relative heaviness of the minerals components of a given rock samples, but also an approximate measure of microstructure present in the rock in the form of cavities and porosity. For a highly porous material the decrease in density has been found to be exponentially decreasing with increase in porosity (Franklin, J. A. and Dusseault. 1989; Allison, 1987). However, for less porous materials such as the Portland limestone, the decrease is very nominal (Allison, 1987). A similar trend is obtained for rock which have low porosity. A very high porosity in two different blocks of Vineland limestone (E and L) is mainly due to its highly an-isotropic and inhomogenous character. In limestone, E, a well developed conglomerate of porous minerals, found throughout the volume of rock, contributes to its high porosity. In limestone, L, the larger grain sizes and possibly the porous layers, which could be easily seen by naked eye, might have resulted in high porosity. If the data points for these two rock types are ignored because of their extreme

nature, all the other rocks could be correlated easily with their micro-structure. The porosity is found to be increasing with larger grain sizes as expected. Both the largest grain size and the average grain size found in the rock specimens gave similar results. The trend of increase in porosity with increase in grain sizes is shown in Figure 8.1. The porosity increases with the increase in grain sizes. The increase in porosity is rapid in the beginning followed by a slow growth leading to a saturation values. This is not surprising as larger pores in the highly porous rock will be filled by finer particles or cements.

8.2 Unconfined compressive strength

The unconfined compressive strength of a rock depends largely on the presence of joints or bedding plane, the direction of stress applications, the rate of stress application, the sample size, and the microstructure of the test specimens. The other factors such as confinement, temperature, and moisture conditions refers to the test conditions which were not varied in the present study. The effect of the first among the above variables, did not arise in most of the selected rock specimens except limestone and gneiss. The effect of bedding or foliation plane in the tests was minimised by proper selection of test samples. The rock blocks used in the present work were not sufficiently larger to give large number of cored samples at orthogonal directions. However, care was taken to core the samples perpendicular to the bedding in layered rocks. The effect of loading rate is considered in the next section under dynamic compressive strength. The effect of moisture is ignored here since all the samples were tested at room temperature and as received conditions. The effect of microstructure and the sample size are discussed in the following.

Figure 8.1: Porosity vs. largest grain size

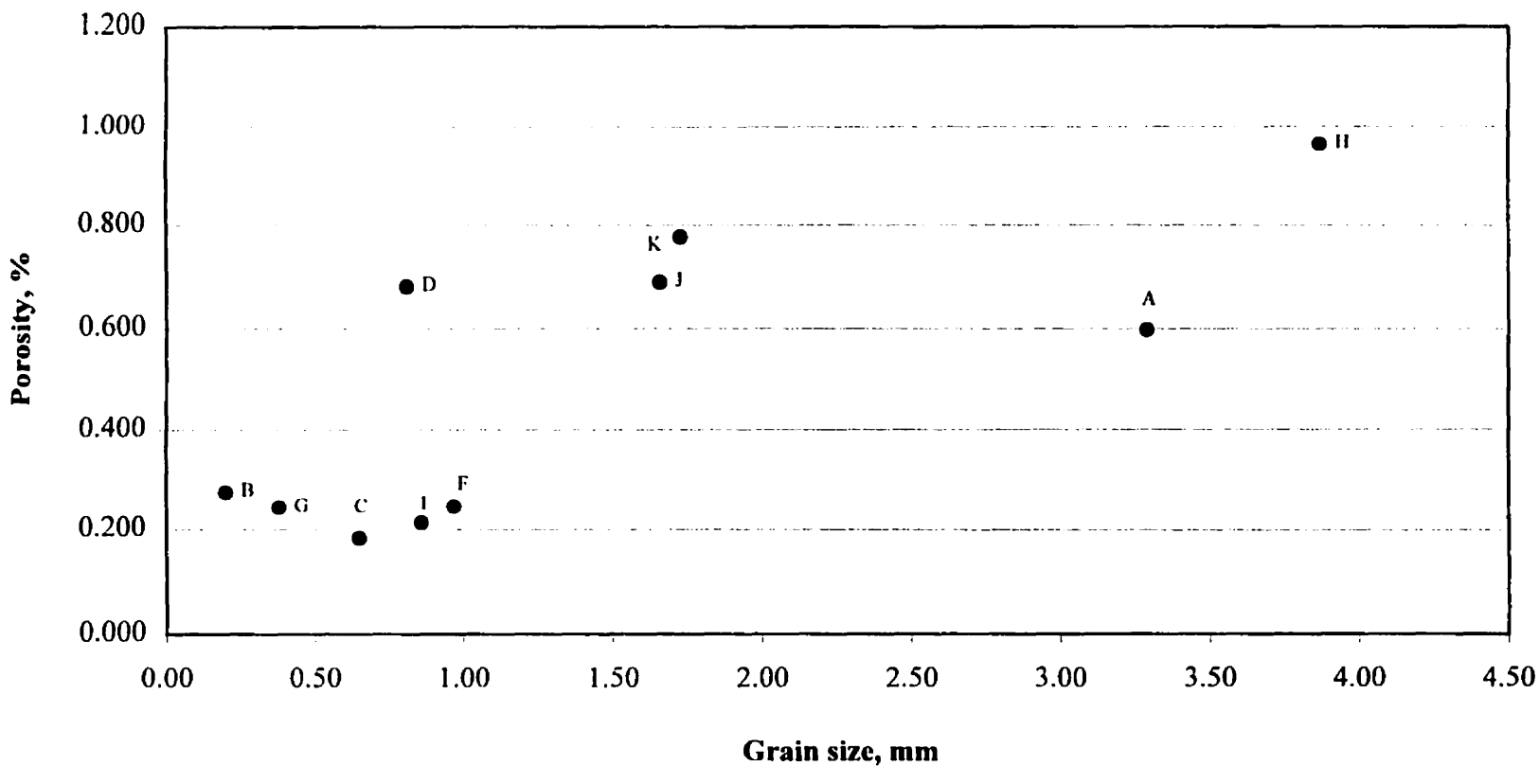

Note: Stanstead granite (A), Altered marble (B), Kingston limestone (C), Gneiss (D), Vineland limestone 1 (E), Marble 2 (F), Foliated marble 3 (G), Laurentian granite (H), Baskatong quartz (I), Barre granite (J), Gneissic granite (K), Vineland limestone 2 (L)

8.2.1 Role of microstructure in selection of sample size

The effect of macro-structure on unconfined compressive strength was confirmed by Bieniawski (1968), and those of micro-structure observed by Hoskins and Horino (1969), and Hassani (1980). The decrease of strength due to the former has been attributed mainly to the existence of joints and discontinuities within the internal structure of the rock and the probability of their increase with size. The decrease in strength was noticed up to a size of about 20 times the minimum joint spacing, beyond which it remained constant. The decrease in strength due the micro-structure, on the other hand, is presumed to be due to a combination of two factors: volume flaws and surface flaws. The first causes the usual size-effect as mentioned above due to the maco-structure. However, in the second, the grain size range becomes more predominant and reverses the trend of size-effect at higher specific surface areas (smaller diameters). The strength has been found to be higher for smaller sizes upto a specific diameter, beyond which it again reduces. It is possible that the specific diameter may be some factor (10 or so) of the largest grain sizes.

A detailed investigation on compressive strength was carried out over wide range of diameters for the coarse grained granites- Stanstead granite (A), Barre granite (J), and Laurentian granite (H). The diameters, the length to diameter ratio of the samples, the average value of the compressive strength and their standard deviations along with the number of tests performed are shown in Table 8.1.

Table 8.1: Unconfined compressive strength at different diameter.

Rock type	Avg. Dia. (mm)	Length/Dia (ratio)	Avg. Strength (MPa)	SD (MPa)	Number of tests
Stanstead Granite-A	50.8	2.0	143.3	6.0	3[a]
	39.2	2.0	132.4	3.9	20[b]
	37.2	2.0	129.9	4.6	10[c]
	28.7	1.8	74.8	10.3	11
	22.3	2.1	69.6	18.8	6
	12.8	2.0	49.1	9.1	6
	10.5	2.0	40.1	11.5	5
	8.3	1.9	47.8	13.6	15
Laurentian Granite-H	28.7	1.8	132	28	6
	22.6	2.1	92	23	6
	12.7	2.1	116	30	6
	9.2	1.8	67	17	7
Barre granite-J	28.7	1.9	118	12	4
	22.6	2.1	69	17	6
	12	2.0	105	26	6
	8.9	1.8	61	16	4

a-Afsin (1996), b- Momayezzadeh (1993), and c-Prasad (1994).

The loading rate was kept the same (0.5 to 1 MPa/sec). It should be noted that the compressive strength at diameter of 50.1 mm, 39.2 mm, and 37.2 mm were taken from previous work as indicated at the bottom of the table. However, to validate the previous work carried out with a different machine configuration, two tests in 51.3 mm and 28.7 mm diameters were carried out through another MTS compressive loading machine. The strengths measured were 150 MPa and 77 MPa which falls in the range of data obtained with the current machine, thus confirming the validity of this configuration.

The test results on Stanstead granite, A, (maximum grain size: 3.29 mm, and the maximum crack length: 3.2 mm) clearly show the influence of the largest crack or grain

size on strength. Figure 8.2 shows the influence of microstructure on the unconfined compressive strengths of Stanstead granite (A). It is possible that the largest crack size, which is also in the same range as that of the grain size, might have affected the compressive strength in granite. However, the influence of grain sizes on the compressive strengths in Laurentian granite (H) and Barre granite (J) confirms the role of grain size on strength. It should be noted that the largest grain sizes in H and J were observed to be 3.87 mm and 1.66 mm, respectively. The maximum crack sizes, on the other hand were only 1 mm and 0. 8 mm, respectively. The strength at 29 mm diameter of these two granites (Laurentian granite-H, and Barre granite-J) were considerably higher than that at 22 mm or smaller diameters. This confirms that the largest grain size does a play role in reduction of strength when the microstructure is of the same scale as the diameter. The reduction in strength due the presence of the largest crack size is evident by the test results on the Stanstead granite (A) only. Further work is needed to quantify the effect of the crack size exclusively. The effect of grain size was found to be negligible when the diameter tested was sufficiently larger that the grain sizes. This is evident on the basis of the nearly uniform strength obtained with fine grained marble (B), limestone (C), and fine to intermediate grained gneiss (D), when tested for different diameters, Figure 8.2. Even with the coarse grained rock type like Stanstead granite (A), the strength remains more or less uniform in the larger diameters (Figure 8.2). The average grain sizes for marble, limestone, and gneiss were 0.2 mm, 0.65 mm, and 0.81mm, respectively. This was much smaller than the sample sizes tested for the compressive strength. The very high standard deviation at large diameter samples, as compared to low variation in small samples in

altered marble (B), is also evident in the Figure 8.2. The consistent strength at two different diameters in case of Limestone (C) and at three different diameters in case of gneiss (D) is also shown in Figure 8.2. The results confirm the influence of micro-structure on strength.

8.2.2 Compressive strength and other fracture properties

This section deals with the measured values of compressive strength and other fracture properties. Also the role of microstructure measured in the present work is examined. The largest crack size, although measured at grain level only, is omitted for its role on compressive strength. This is because the compressive strength is known to be governed by the largest crack present in the rock volume, rather than that present in the grain level. The result of the regression analysis for the compressive strength (Y-variable) with respect to other fracture characteristics and micro-structural properties as X-variables are presented in Table 8.2. The co-efficient of correlation (R squared) is also shown.

Table 8.2: Coefficient of correlation between the Compressive strength (Y-variable) and other commonly measurable strength properties including microstructure (X-variable).

X-variable	Y-variable, static UCS (MPa)	R squared
Brazilian tensile strength, MPa	$Y = 11.4\,x - 45.45$	0.385
Fracture toughness, MPa $m^{0.5}$	$Y = 0.001\,x + 1.494$	0.004
Work index, kWh/t	$Y = 0.763\,x + 4.361$	0.888
Crack density (mm^{-1})	$Y = 92.43\,x^{-0.3016}$	0.435
Largest grain size (mm)	$Y = -22.23 \ln x + 90.97$	0.572
Average grain size (mm)	$Y = -18.406 \ln x + 70.567$	0.172

Figure 8.2: Compressive strength at different diameters

Stanstead granite-A, grain size 3.3 mm; altered marble-B, grain size 0.2 mm;
Kingston limestone-C, grain size 0.6 mm; gneiss-D, grain size 0.8 mm

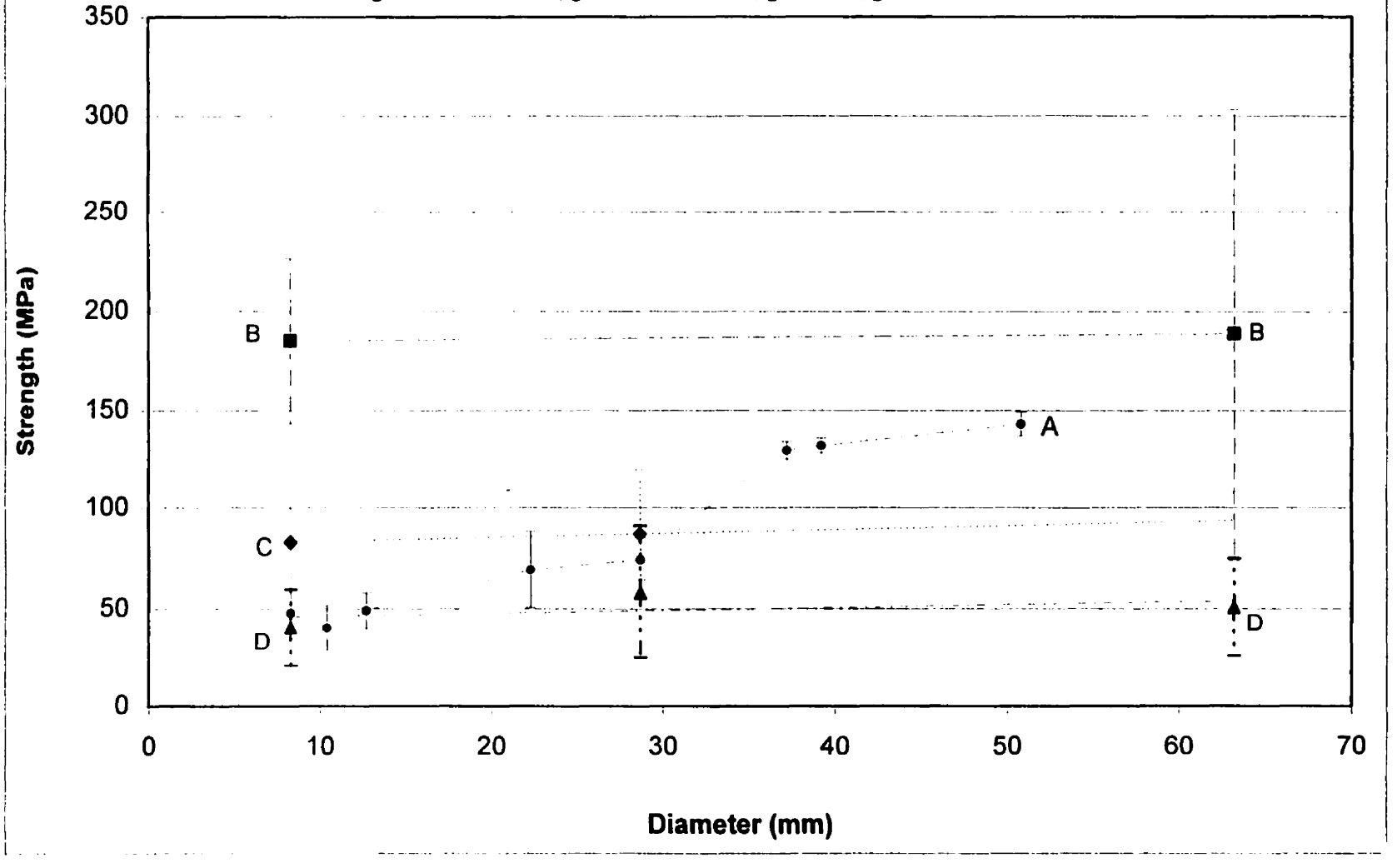

A comparison between the compressive strength and the tensile strength, measured at the same diameter for different rock types, yielded a nearly constant proportionality (~10:1). A similar trend of correlation has been found by various researcher (Hassani, 1980). The Figure 8.3 shows the trend obtained in the present work. However, the coefficient of correlation is poor. This can be explained to be due to the microstructure, especially, for coarse grained rock type. This has resulted in a wide scatter in measured data. Also, the fewer tests with tensile strength measurements may have contributed to the wider scatter of data. The compressive strength was found to be poorly related with the fracture toughness. The reason for this is due to the completely different mechanism of rock breakage in these two types of tests. A very good correlation was obtained between compressive strength and work index. This shows some similarity in breakage by a compressive means and that in a tumbling mill. The work index is analysed further in detail in later section. Since the work index used in the present analysis were for only four rock types, it opens a new area in which future work can be done.

Although, porosity is known to affect the strength in a general way, it is not known how exactly it will affect the latter, especially, in presence of more critical and sharp cracks. The latter act as stress concentrators and greatly alter the strength properties. In the absence of sharp cracks grain boundary also acts as a stress concentrator. A high correlation with the crack density followed by grain sizes is due to this reason. Figure 8.4 shows the decreasing trend of strength with increase in crack density.

Figure 8.3: Compressive strength (static) vs. Brazilian tensile strength

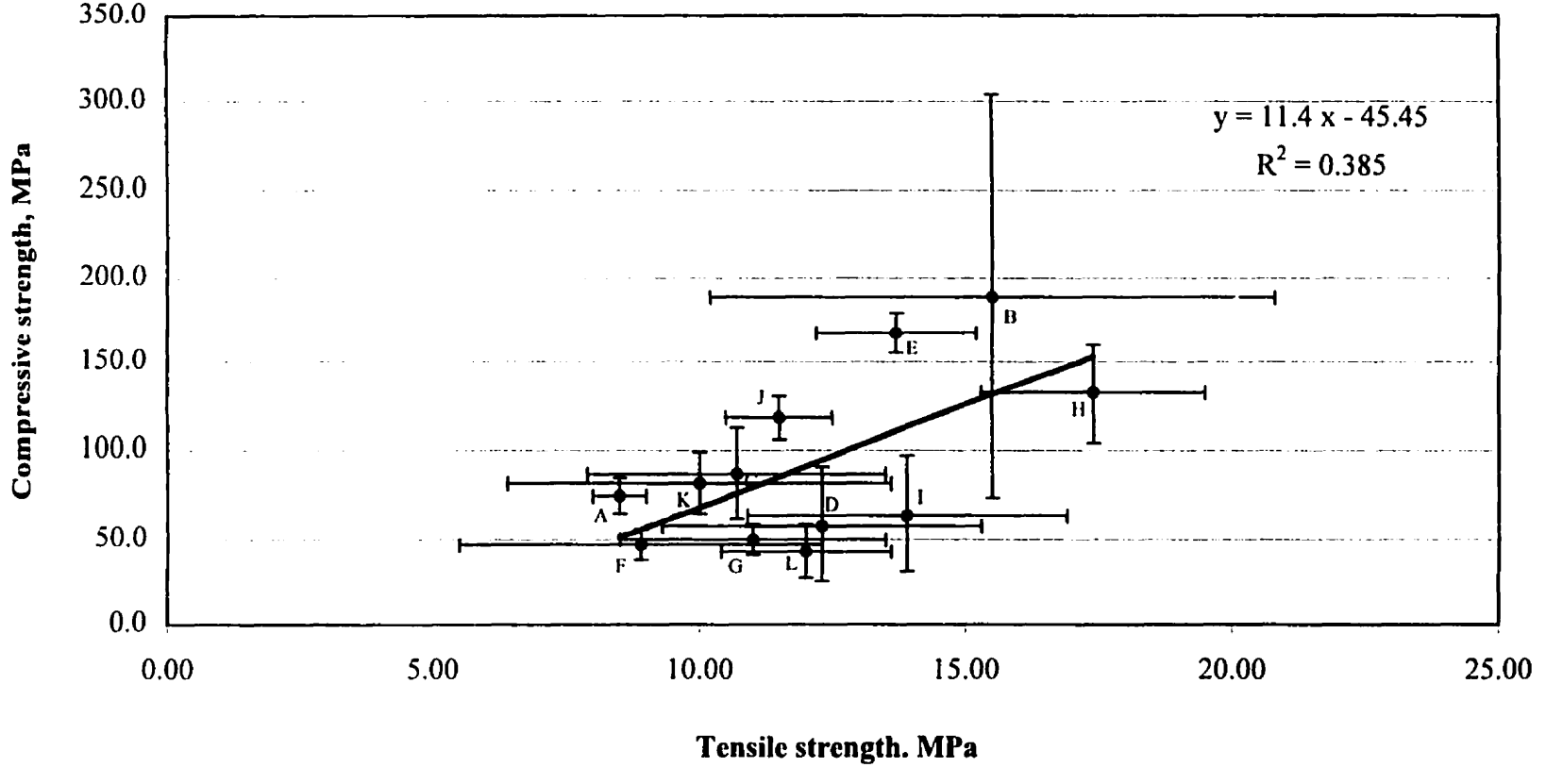

Note: Stanstead granite (A), Altered marble (B), Kingston limestone (C), Gneiss (D), Vineland limestone 1 (E), Marble 2 (F), Foliated marble 3 (G), Laurentian granite (H), Baskatong quartz (I), Barre granite (J), Gneissic granite (K), Vineland limestone 2 (L)

Figure 8.4: Compressive strength (static) vs. crack density

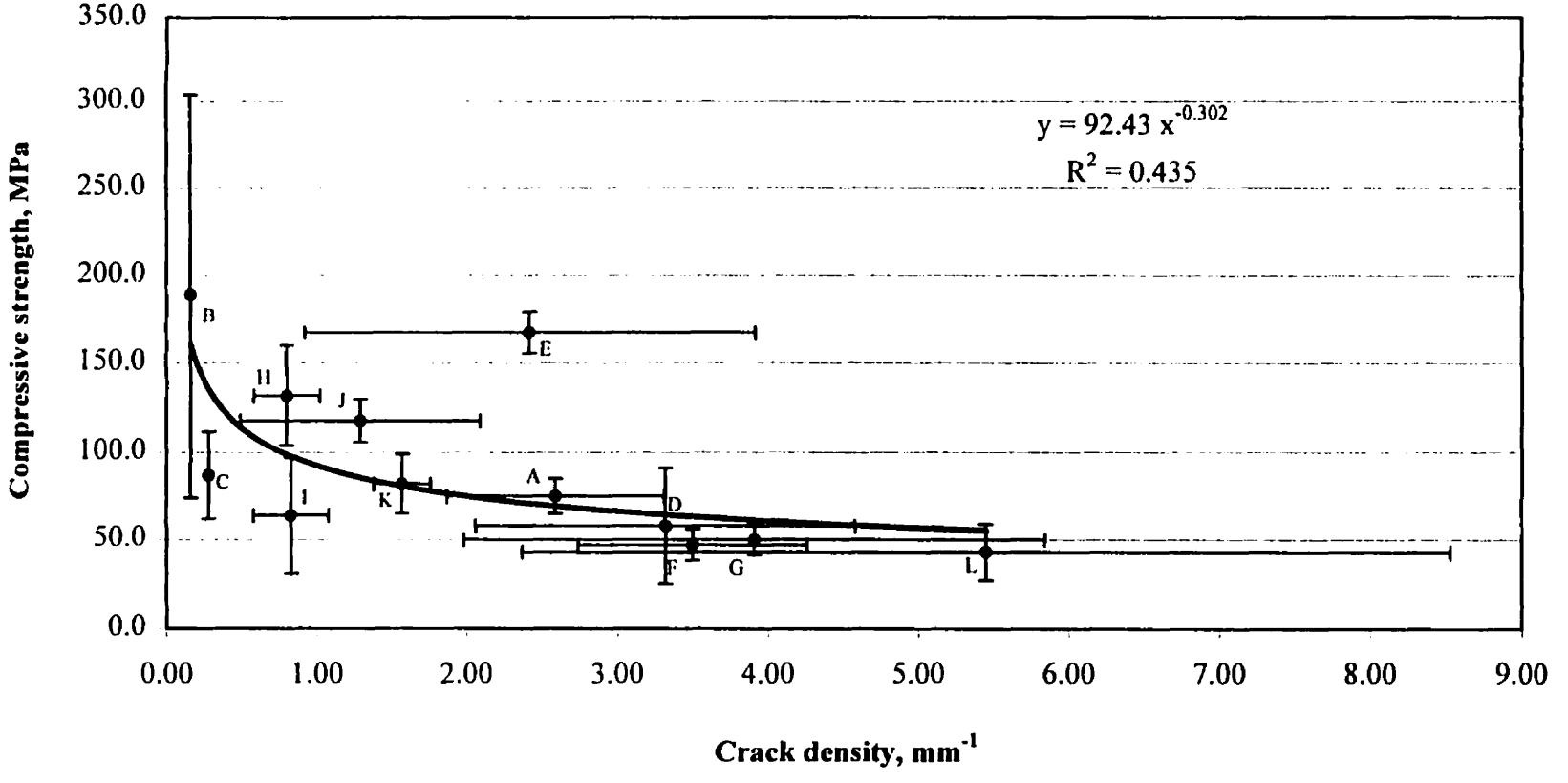

Note: Stanstead granite (A), Altered marble (B), Kingston limestone (C), Gneiss (D), Vineland limestone 1 (E), Marble 2 (F), Foliated marble 3 (G), Laurentian granite (H), Baskatong quartz (I), Barre granite (J), Gneissic granite (K), Vineland limestone 2 (L)

8.3 Brazilian tensile strength

The measured values of Brazilian tensile strength have been compared with the dynamic as well as the static compressive strengths, the fracture toughness, and the microstructure of selected rock types. Among the microstructure measured, only the largest grain size was investigated for its influence on the tensile strength. This is because in typical Brazilian failure it is known that crack will start from the center of the disc specimen. Therefore, the microstructure which are distributed all along the volume is ignored. The results of the regression analysis i.e. the best fit line or curve and the coefficient of correlation are shown in the Table 8.3.

Table 8.3: Coefficient of correlation between the tensile strength and other commonly measurable strength properties including microstructure.

X-variable	Y-variable, Tensile strength (MPa)	R squared
Dynamic UCS, MPa	$Y=19.87 x - 10.64$	0.290
UCS (29 mm diameter)	$Y=11.40 x - 45.45$	0.385
Fracture toughness (MPa $m^{0.5}$)	$Y= 0.866 x^{-0.1438}$	0.024
Work index (kWh/t)	$Y= 1.686 x -7.373$	0.892
Largest grain size (mm)	$Y= 11.04 x^{-0.15}$	0.436

It should be noted that a very high value of the tensile strength was obtained for Laurentian granite (H) based on three test results. Due to reasons beyond control it was not possible to repeat the experiment for a large number of test samples with this rock type, and therefore, it is omitted from the following regression analysis.

The tensile strength was found to be linearly related with the dynamic compressive strength (a factor of about 20 times less), however the correlation was poor (Figure 8.5).

Figure 8.5: Brazilian tensile strength vs. dynamic compressive strength

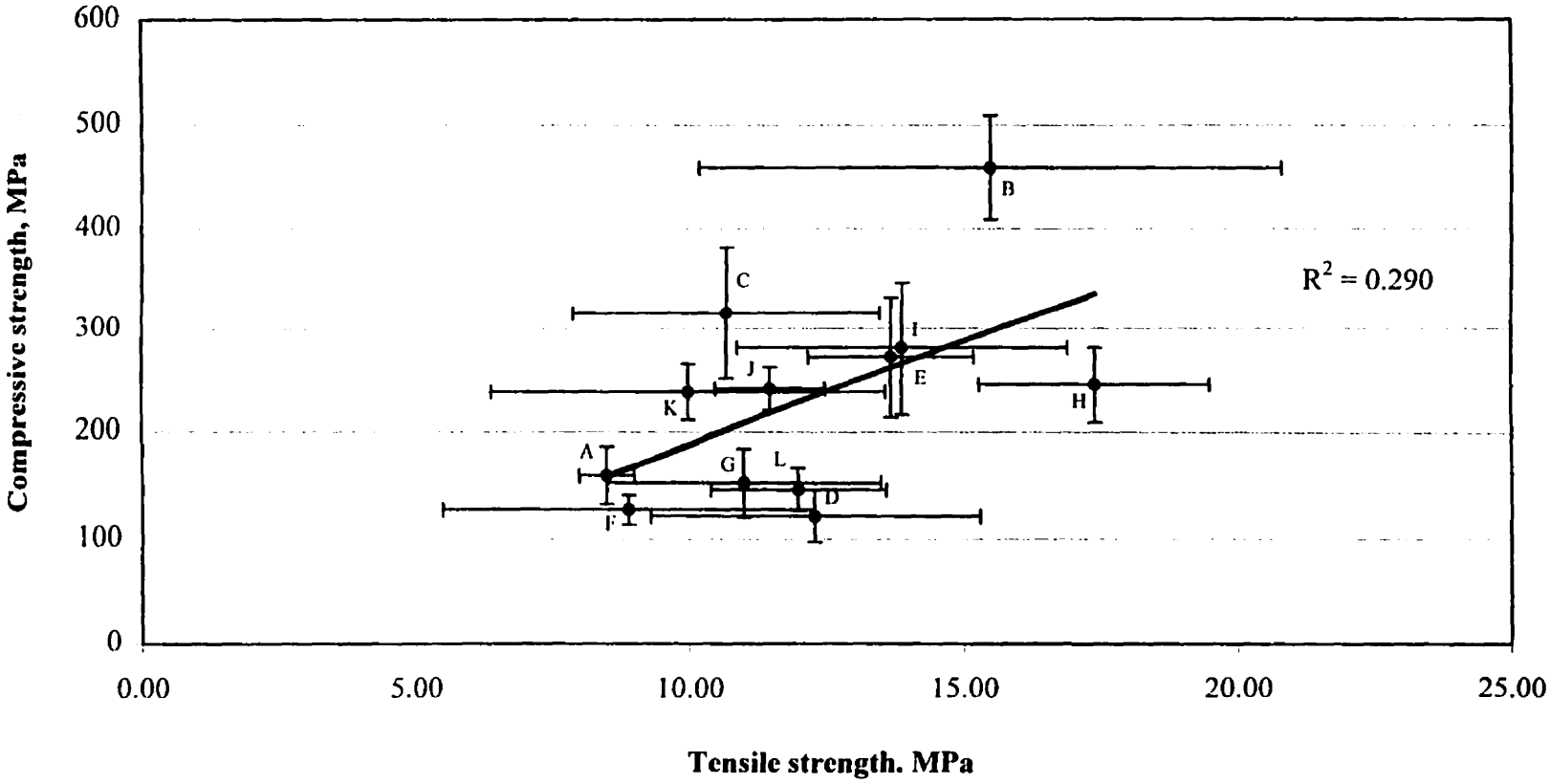

Note: Stanstead granite (A), Altered marble (B), Kingston limestone (C), Gneiss (D), Vineland limestone 1 (E), Marble 2 (F), Foliated marble 3 (G), Laurentian granite (H), Baskatong quartz (I), Barre granite (J), Gneissic granite (K), Vineland limestone 2 (L)

This is to be expected as the former is known to be less than about 10 times the static compressive strength, which in turn is much lower than the dynamic compressive strength.

The very poor correlation between the tensile strength and the fracture toughness was surprising. Although the mechanism of breakage in these two tests are different, much better correlation was expected. The scatter diagram for these two variables is shown in Figure 8.6. The result is not conclusive, as a very high scatter is obtained in the tensile strength data. More work is needed for both the tensile strength as well as the fracture toughness to get any conclusive result.

The tensile strength was found to be highly correlated with the work index. Figure 8.7 shows the correlation between the Brazilian tensile strength with work index. The increasing trend of work index with tensile strength demonstrates some similarity in these breakage process. The individual particle in the mill may be breaking in tension under indirect compressive stresses resulting from the impact of tumbling rods. This should however be viewed only as a trend, as only four data points were used for the latter property. This opens up another area in which more work should be done.

The tensile strength was found to be well correlated with the largest grain size in the rock, Figure 8.8. This is not surprising as the later provides the most critical flaw site for crack initiation. A similar correlation with the largest crack size was not seen as the orientation of the biggest cracks which could not be controlled in the present experiment, may have led to the larger data scatter.

Figure 8.6: Brazilian tensile strength vs.Fracture toughness

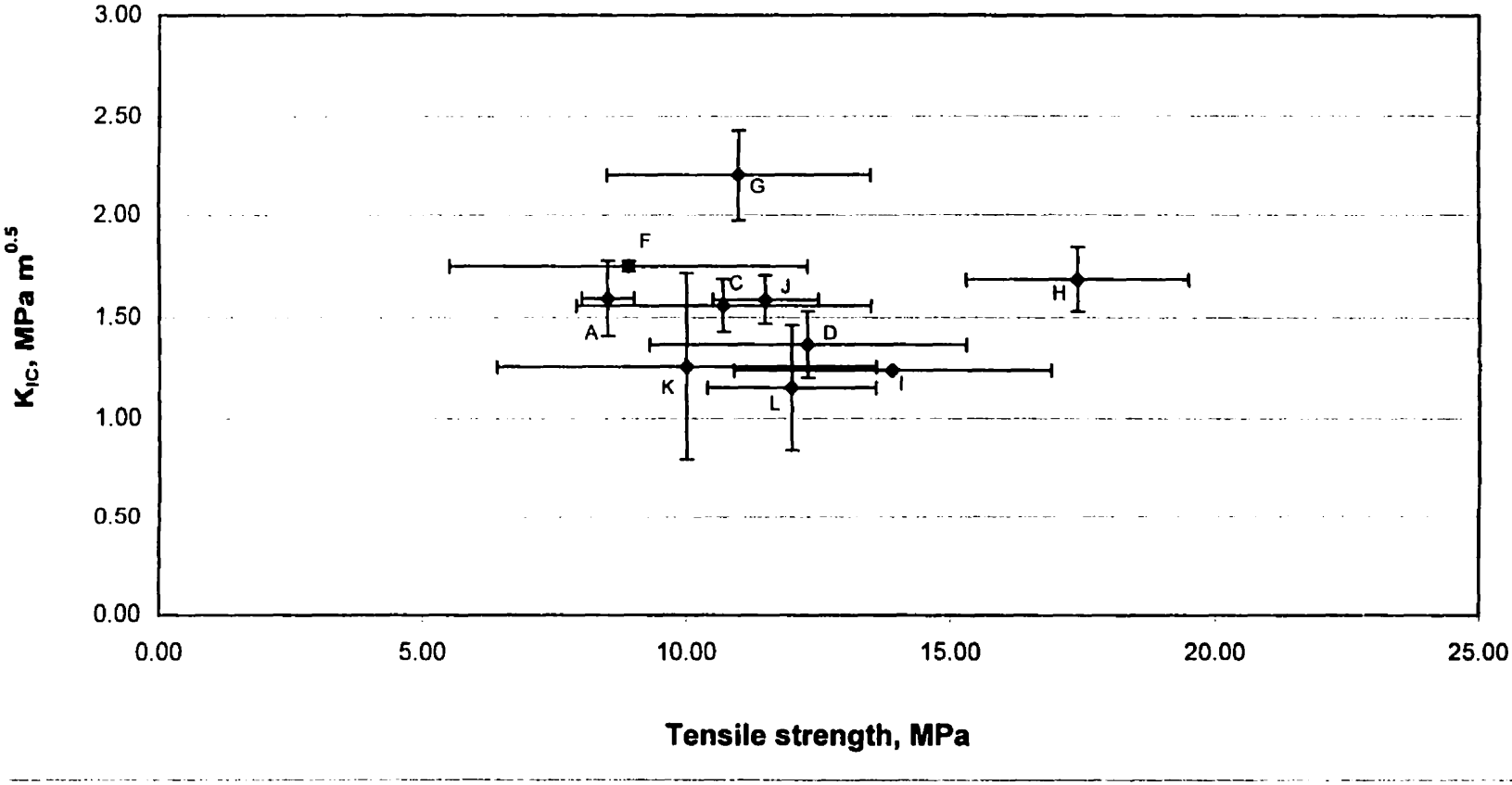

Note: Stanstead granite (A), Kingston limestone (C), Gneiss (D), Marble 2 (F), foliated marble (G), Lawrentian granite (H), Baskatong quartz (I), Barre granite (J), Gneissic granite (K), Vineland limestone 2 (L)

Figure 8.7: Work index vs. Tensile strength

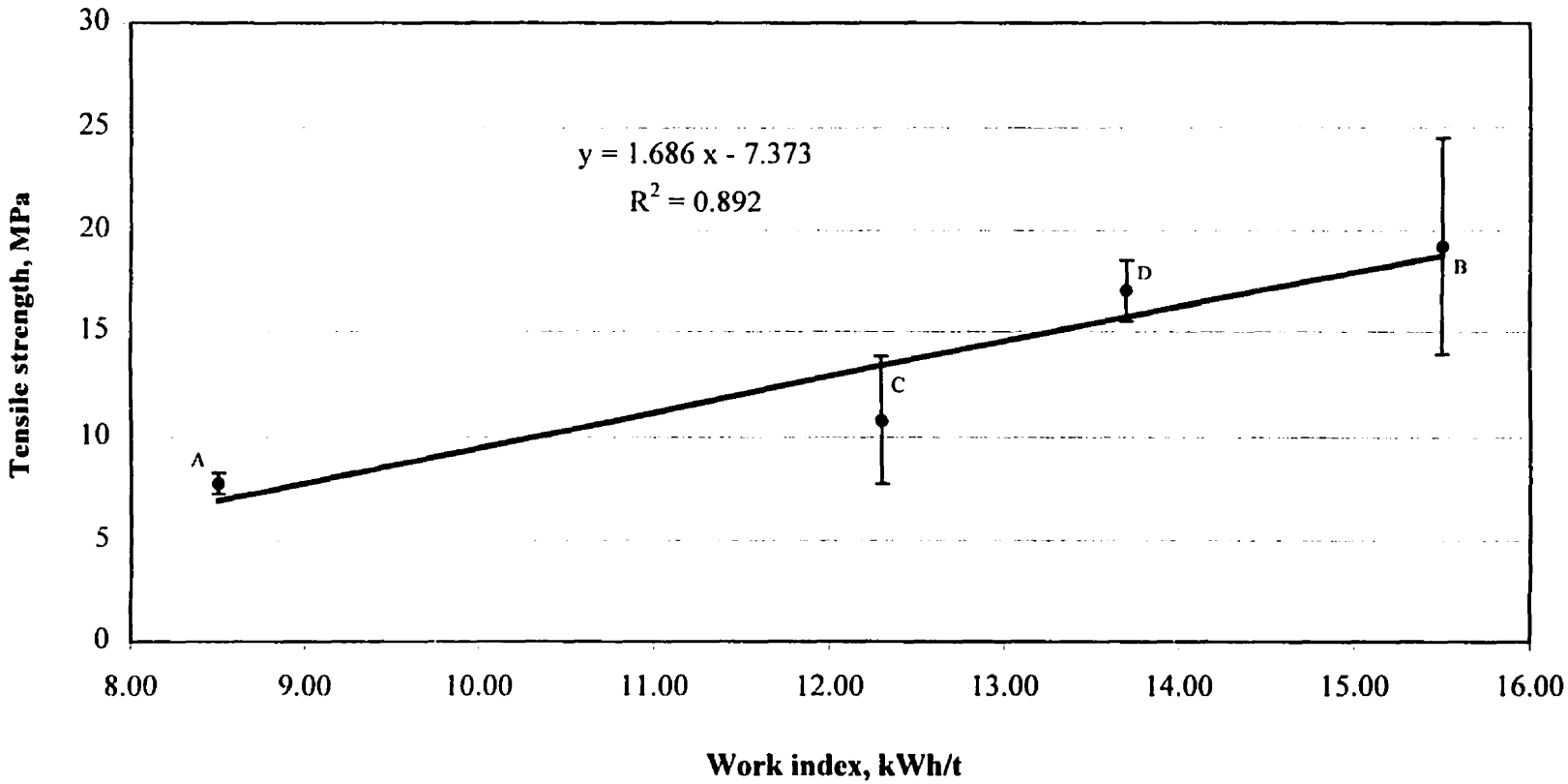

Note: Stanstead granite (A), Altered marble (B), Gneiss (D), Vineland limestone 1 (E).

Figure 8.8: Brazilian tensile strength vs. Largest grain size

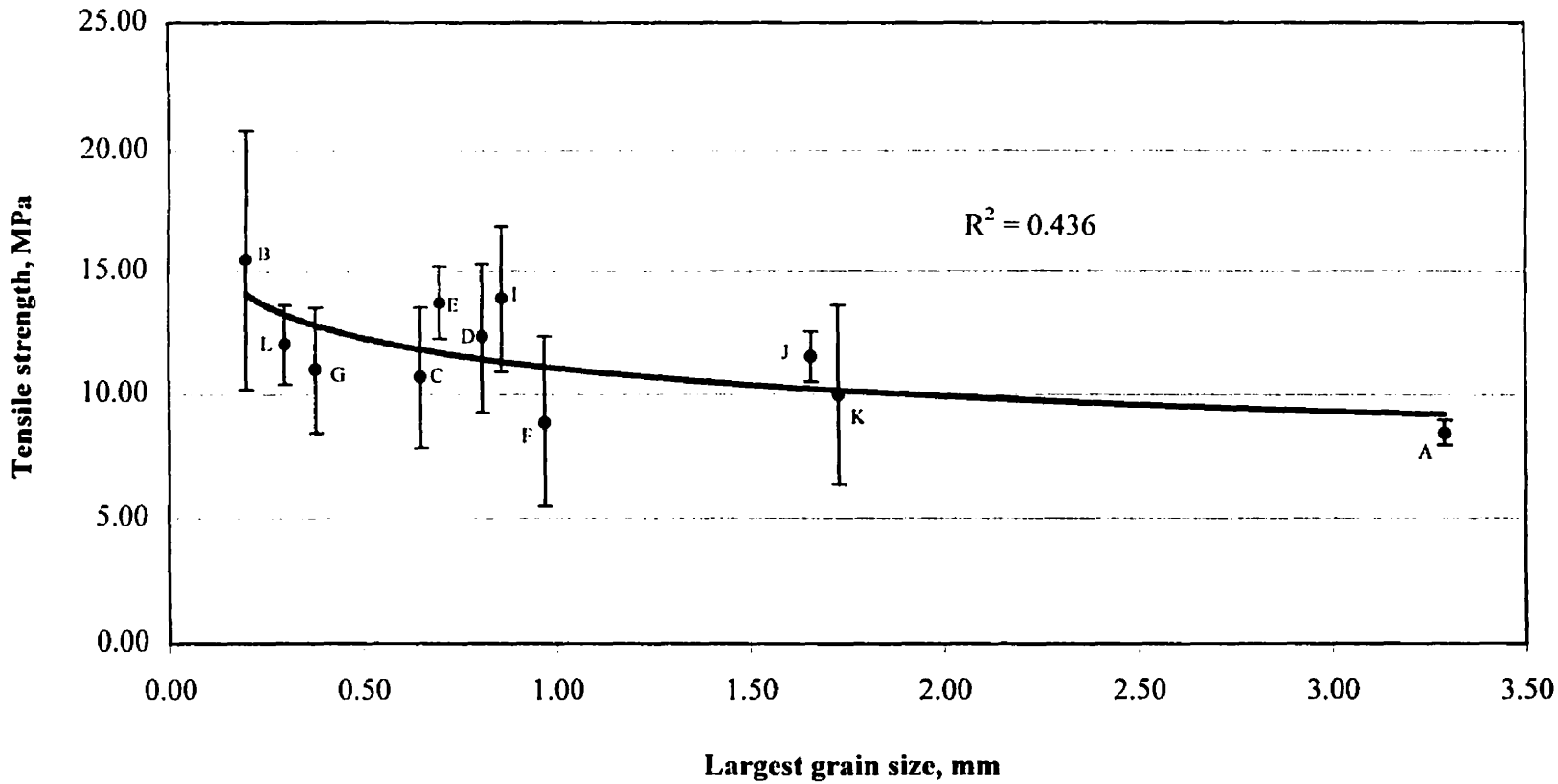

Note: Stanstead granite (A), Altered marble (B), Kingston limestone (C), Gneiss (D), Vineland limestone 1 (E), Marble 2 (F), Foliated marble 3 (G), Laurentian granite (H), Baskatong quartz (I), Barre granite (J), Gneissic granite (K), Vineland limestone 2 (L)

8.4 Dynamic compressive strength

The dynamic compressive strength was compared with the same mechanical and the microstructural properties. The regression analysis in terms of the best fit line or curve between the measured properties of rock (X-variables) and the dynamic strength (Y-variable) are presented in Table 8.4, together with the coefficient of correlation. The correlation between the dynamic as well as static compressive strength for similar dimension of the test samples have already been discussed in an earlier section. The issue of dynamic compressive strength and the static tensile strength has also been discussed in the previous section.

Table 8.4: Coefficient of correlation between the dynamic compressive strength and other commonly measurable strength properties including microstructure.

X-variable	Y-variable, dynamic UCS (MPa)	R squared
Static UCS at same dimension (MPa)	Y=198.73 ln x – 579.62	0.926
Tensile strength at 29 mm dia.(MPa)	Y= - 45.01 x + 272.39	0.040
Fracture toughness, MPa $m^{0.5}$	Y= 0.001 x + 1.494	0.004
Work index (kWh/t)	Y= 0.031 x + 5.859	0.780
Bulk modulus (GPa)	Y= 6.494 x + 36.831	0.530
Compressibility (1/GPa)	Y= - 4910.1 x + 412.25	0.303
Shear modulus (GPa)	Y= - 4.26 x + 324.87	0.029
Young's modulus (GPa)	Y= 1.049 x + 174.92	0.010
Poisson's ratio	Y = 1316 x – 15.717	0.727
Crack density (m^{-1})	Y= - 81.937 ln x + 261.15	0.839
Largest crack size (mm)	Y= - 34.535 ln x + 227.48	0.343
Average grain size (mm)	Y= - 32.165 ln x + 191.49	0.130

The dynamic strength was found to have no correlation with the measured values of the fracture toughness (Figure 8.9). This is because under dynamic condition, the breakage starts at a large number of pre-existing microcracks at which a large number of cracks are propagated. The strength is the largest stress sustained by the material. However, the later was calculated by allowing only a single crack to propagate through the sample thus the breakage is accomplished by propagating a crack from the tip of the previously created macro-crack.

The Young's modulus and shear modulus resulted in almost no correlation with the dynamic strength as compared to a very high correlation with bulk density, and its reciprocal (compressibility). The extent of correlation with dynamic elastic properties on the dynamic compressive strength corresponds to the extent of correlation of the former with the P and S wave velocity. For example, the S wave was found to be independent of dynamic strength, so was shear modulus. The Young's modulus resulted some correlation due to the P wave effect. The bulk modulus, and the compressibility resulted some correlation because of its dependence on the P wave. The Poisson's ratio is found to be highly correlated with the dynamic strength due the latter dependency on the crack density. Figure 8.10 and 8.11 show the correlation between dynamic compressive strength and Bulk modulus and Poisson's ratio.

The crack density parameter appears to be most controlling factor in the correlation with dynamic strength (Figure 8.12). The correlation is much superior compared to other parameters such as the average or the largest grain size or crack size.

Figure 8.9: Dynamic UCS vs. Fracture toughness

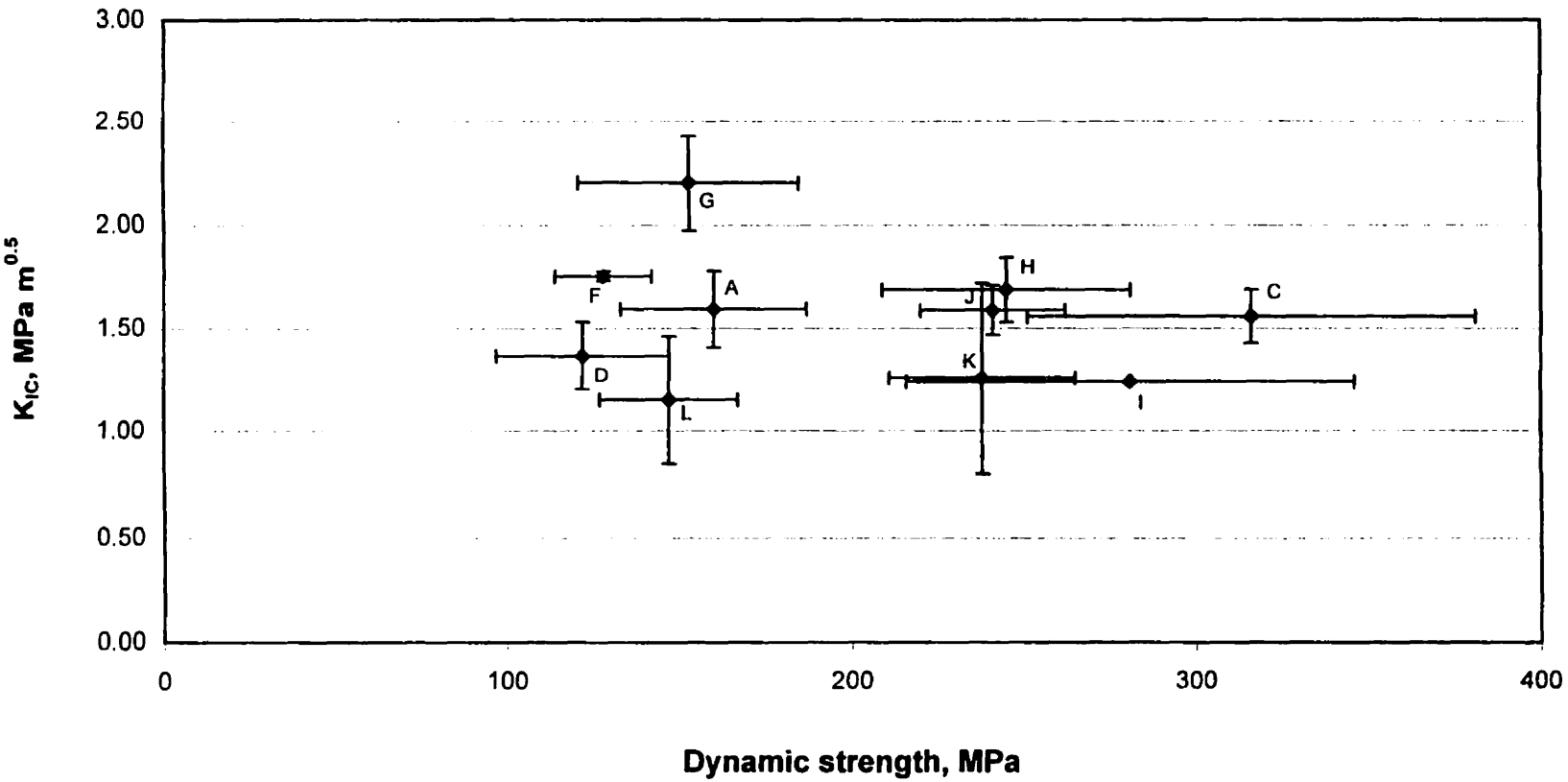

Note: Stanstead granite (A), Altered marble (B), Kingston limestone (C), Gneiss (D), Vineland limestone 1 (E), Marble 2 (F), Foliated marble 3 (G), Laurentian granite (H), Baskatong quartz (I), Barre granite (J), Gneissic granite (K), Vineland limestone 2 (L)

Figure 8.10: Bulk modulus vs. Dynamic compressive strength

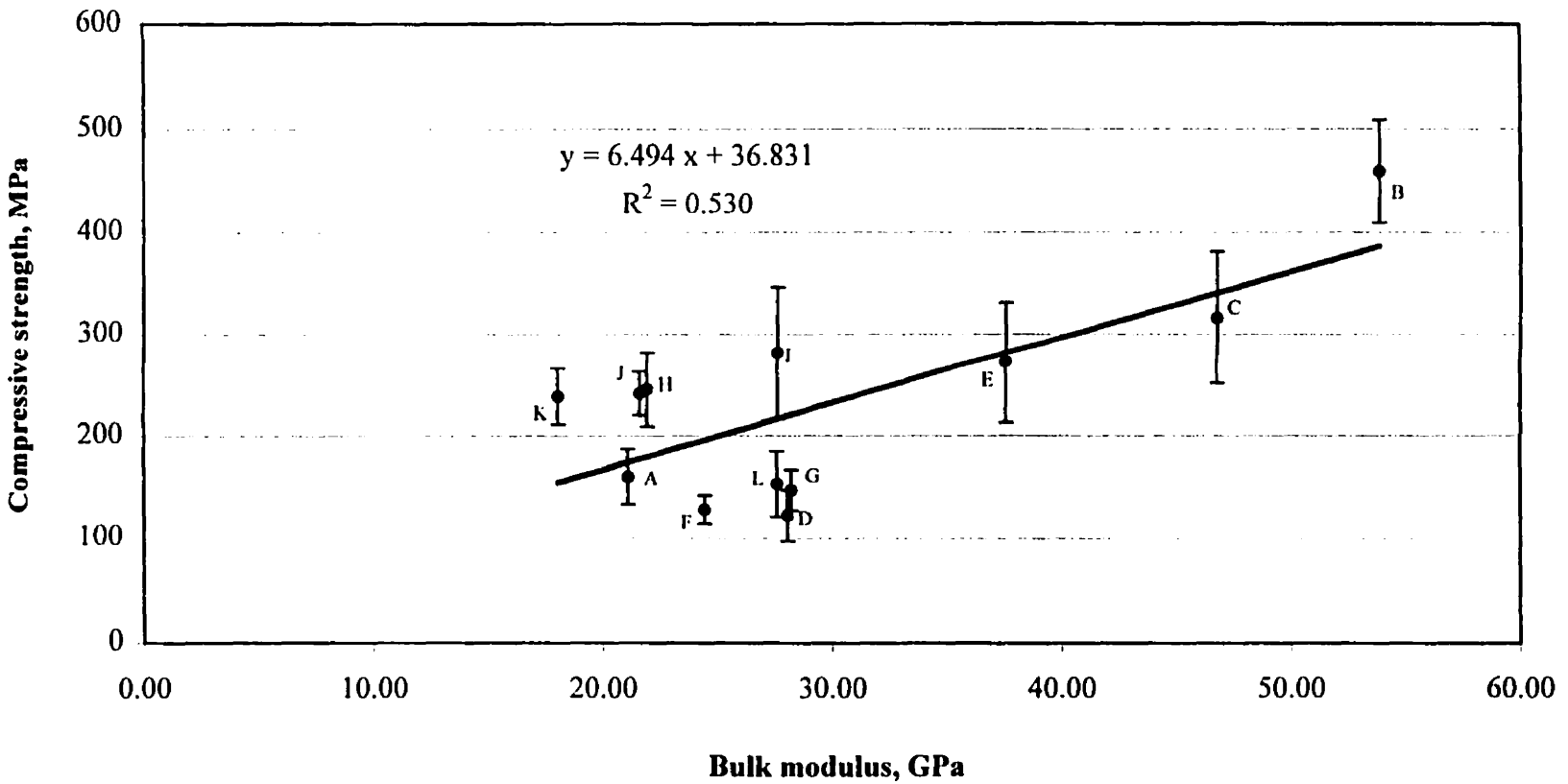

Note: Stanstead granite (A), Altered marble (B), Kingston limestone (C), Gneiss (D), Vineland limestone 1 (E), Marble 2 (F), Foliated marble 3 (G), Laurentian granite (H), Baskatong quartz (I), Barre granite (J), Gneissic granite (K), Vineland limestone 2 (L)

Figure 8.11: Poisson's ratio vs. Dynamic compressive strength

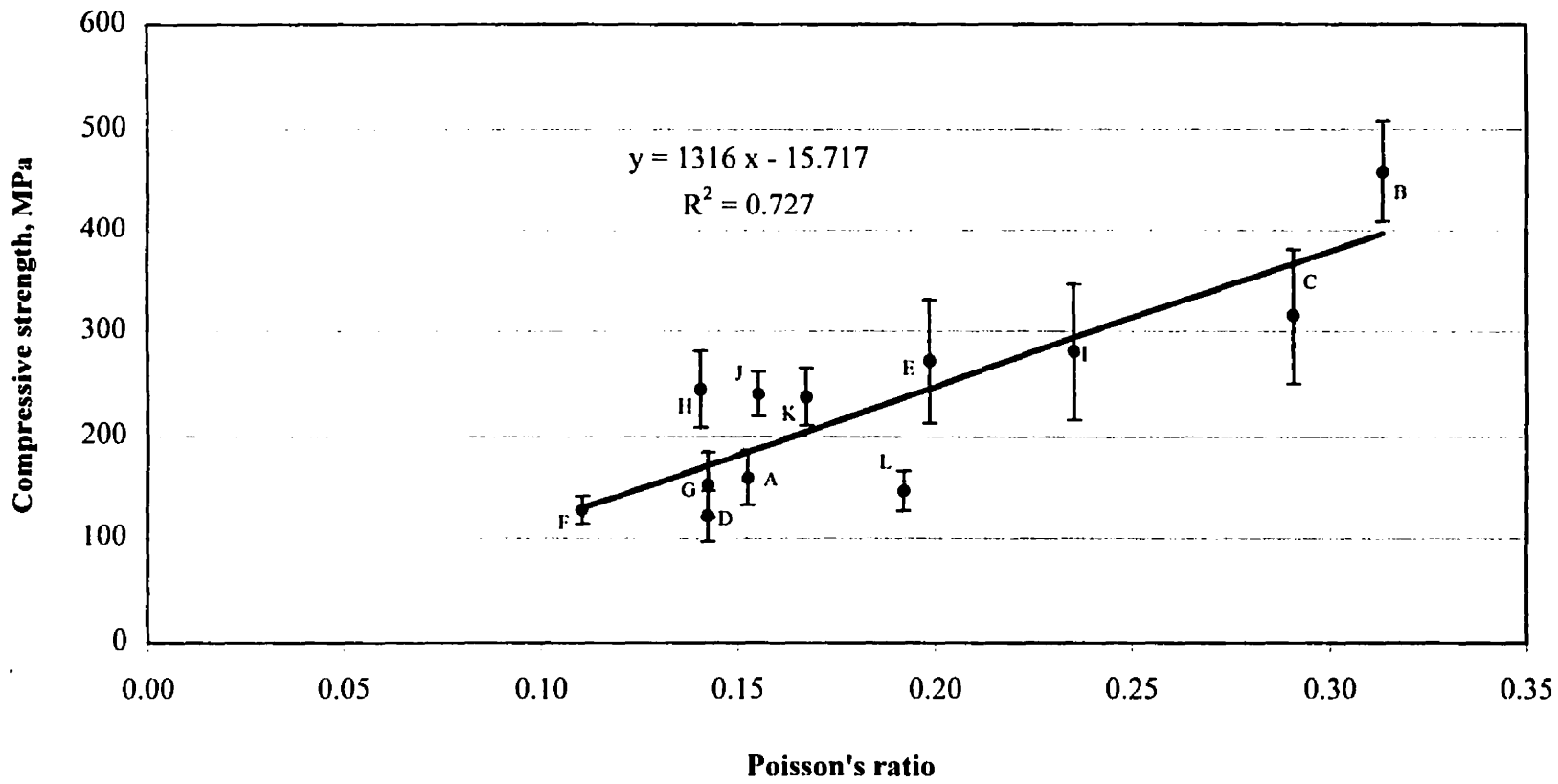

Note: Stanstead granite (A), Altered marble (B), Kingston limestone (C), Gneiss (D), Vineland limestone 1 (E), Marble 2 (F), Foliated marble 3 (G), Laurentian granite (H), Baskatong quartz (I), Barre granite (J), Gneissic granite (K), Vineland limestone 2 (L)

Figure 8.12: Crack density vs. Dynamic compressive strength

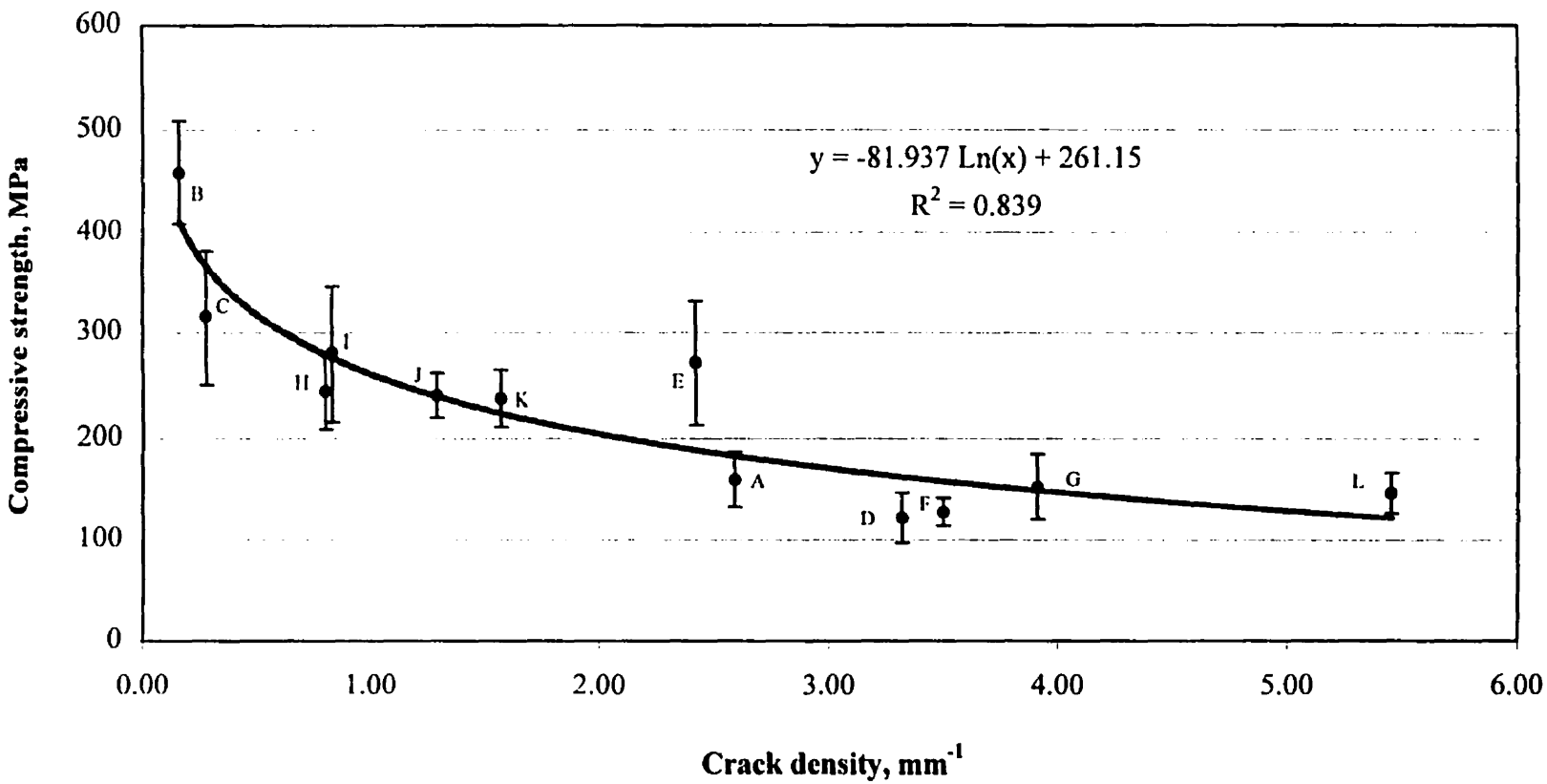

Note: Stanstead granite (A), Altered marble (B), Kingston limestone (C), Gneiss (D), Vineland limestone 1 (E), Marble 2 (F), Foliated marble 3 (G), Laurentian granite (H), Baskatong quartz (I), Barre granite (J), Gneissic granite (K), Vineland limestone 2 (L)

The correlation between the compressive strength (both static as well as dynamic) and the crack density is very similar unlike tensile strength. The largest grain size is found to be more controlling factor in tensile strength unlike the static and dynamic compressive strengths.

8.5 Comminution work index

A regression analysis for the measured values of work index and other fracture related properties of rock were performed. The coefficient of correlation and equation for the best fit line or curve is presented in the Table 8.5.

Table 8.5: Coefficient of correlation between the work index and other commonly measurable strength properties including microstructure.

X-variable	Y-variable, work Index (kWh/t)	R squared
Tensile strength (29 mm dia)	$Y = 1.686 x - 7.373$	0.892
Dynamic UCS, MPa	$Y = 0.031 x + 5.859$	0.780
UCS (29 mm dia)	$Y = 0.763 x + 4.361$	0.888
Compressibility (1/GPa)	$Y = - 420.77 x + 27.173$	0.961
Bulk modulus (GPa)	$Y = 12.912 \ln x - 31.492$	0.953
Young's modulus (GPa)	$Y = 0.0074 x^{1.842}$	0.677
Shear modulus (GPa)	$Y = 0.1558 x^{1.3903}$	0.338
Largest grain size (mm)	$Y = 11.869 x^{-0.3307}$	0.830
Average grain size (mm)	$Y = 8.113 x^{-0.269}$	0.979
Crack density (m^{-1})	$Y = -2.869 x + 19.789$	0.546

Overall, the work index is found have the best correlation with a majority of the fracture related properties. The correlation of work index with Brazilian tensile strength is already discussed. A better correlation of work index with static compressive strength than compared to the dynamic compressive strength is surprising. The result suggests that WI,

being associated with intermediate strain rate phenomenon, correlated well with the low strain rate (static loading) process compared to a very high strain rate dynamic breakage. However, Although, only four rock types have been used for this analysis, additional work needs to be done over a wider suits of rocks to confirm this correlation.

The Poisson's ratio, the Young's modulus and the shear modulus calculated from P and S wave velocities show some correlation with the WI which depends on the extent of the material dependence on P wave velocity. However, the work index was found to best correlated with the compressibility .

The work index is further compared with the average grain size, the largest grain and crack size, and the crack density. The former resulted in an excellent correlation with the work index (Figure 8.13), which is expected as the later is an average property showing average strength over a large number impacts. However, the crack density did not give better correlation with WI unlike both static and dynamic compressive strengths. This is obvious as the work index has been determined at a size of 1.2 mm at which most of the cracks, even some of the largest grains might have been broken or vanished. The work index could not be compared with the fracture toughness as the rock samples for which the former was determined, were exhausted during test works.

8.6 Fracture toughness

The fracture toughness measured for different rock types were further compared with some easily measurable common strength related properties of rock. The latter includes the physical properties, mechanical properties, and most predominant micro-

Figure 8.13: Work index vs. Average grain size

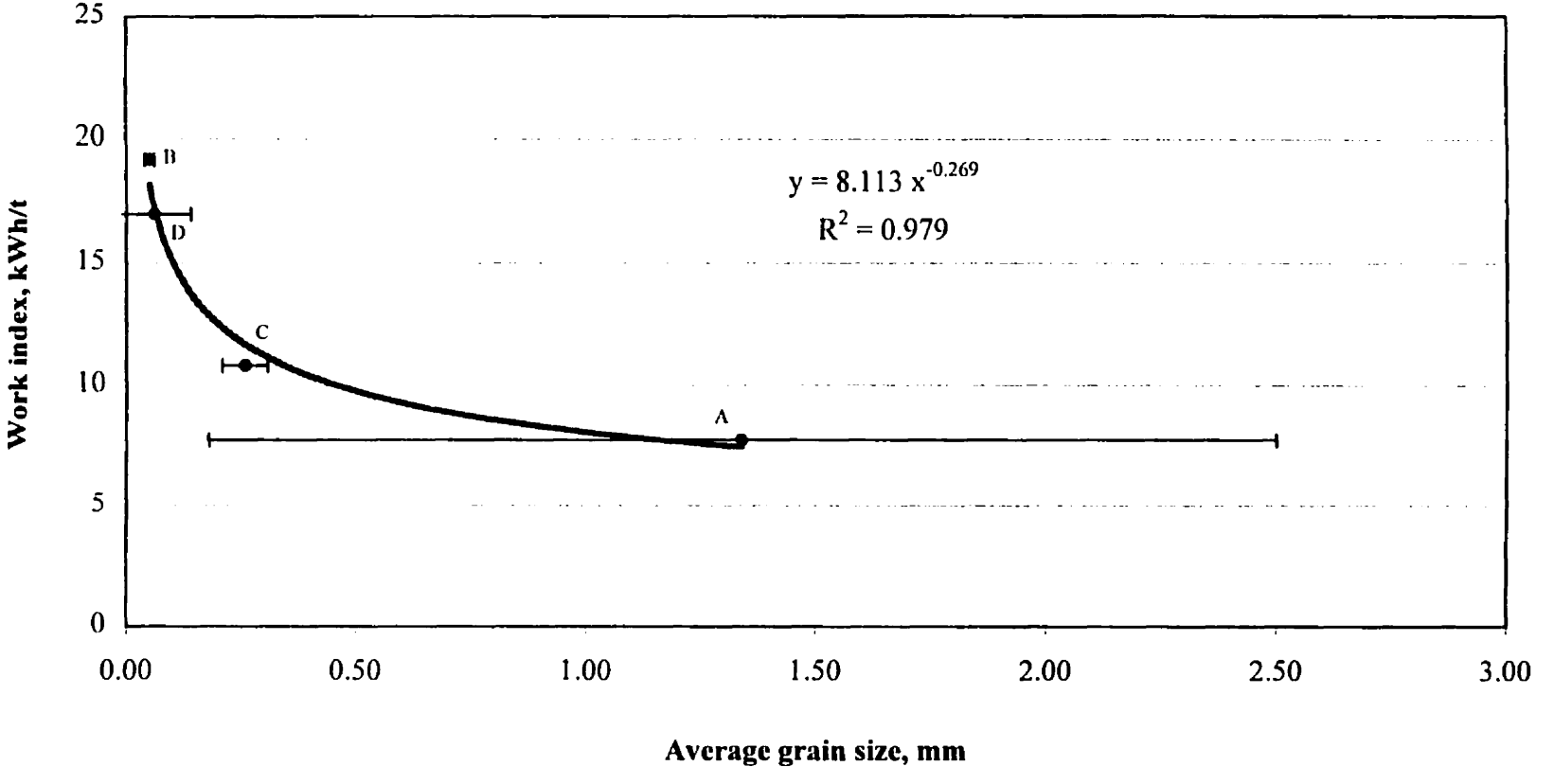

Note: Stanstead granite (A), Altered marble (B), Gneiss (D), Vineland limestone 1 (E).

structural properties. Table 8.6 shows the equation of the best fit line or curve and the coefficient of correlation.

Table 8.6: Coefficient of correlation between the fracture toughness (Y-variable) and other commonly measurable strength properties including microstructure (X-variable).

X-variable	Fracture toughness, Y (MPa $m^{0.5}$)	R squared
Dynamic UCS, MPa	$Y = -0.0009 x + 1.7218$	0.040
UCS (29 mm diameter)	$Y = 0.0006 x + 1.494$	0.004
Tensile strength (29 mm dia.)	$Y = 2.147 x^{-0.1438}$	0.024
Porosity (%)	$Y = - 0.2397 x + 1.706$	0.246
Largest crack size (mm)	$Y = 1.6241 x^{-0.145}$	0.628
Largest grain or crack size (mm)	$Y = - 0.2617 \ln x + 1.7516$	0.626
Crack density (m^{-1})	$Y = 0.135 x^2 - 0.463 x + 1.753$	0.529

The above analysis suggests that there is almost no correlation between fracture toughness and compressive or tensile strengths. This has been discussed in the earlier sections. The fracture toughness was found to be more correlated with S wave velocity than compared to P wave. This is not surprising as the S wave is more correlated with the surface waves which greatly control the crack propagation (the resistance of crack propagation is the fracture toughness). Further, the fracture toughness was found to be more related with the shear modulus as compared to Poisson's ratio, Young's modulus, bulk modulus and compressibility. The extent of the correlation corresponds to the extent of dependence of the latter on the S waves.

The fracture toughness is found to be well correlated with the porosity. This is shown in Figure 8.14. The decrease of toughness with increase in porosity is not surprising as the crack growth faces less resistance in case of higher values of latter.

Figure 8.14: Porosity vs. fracture toughness

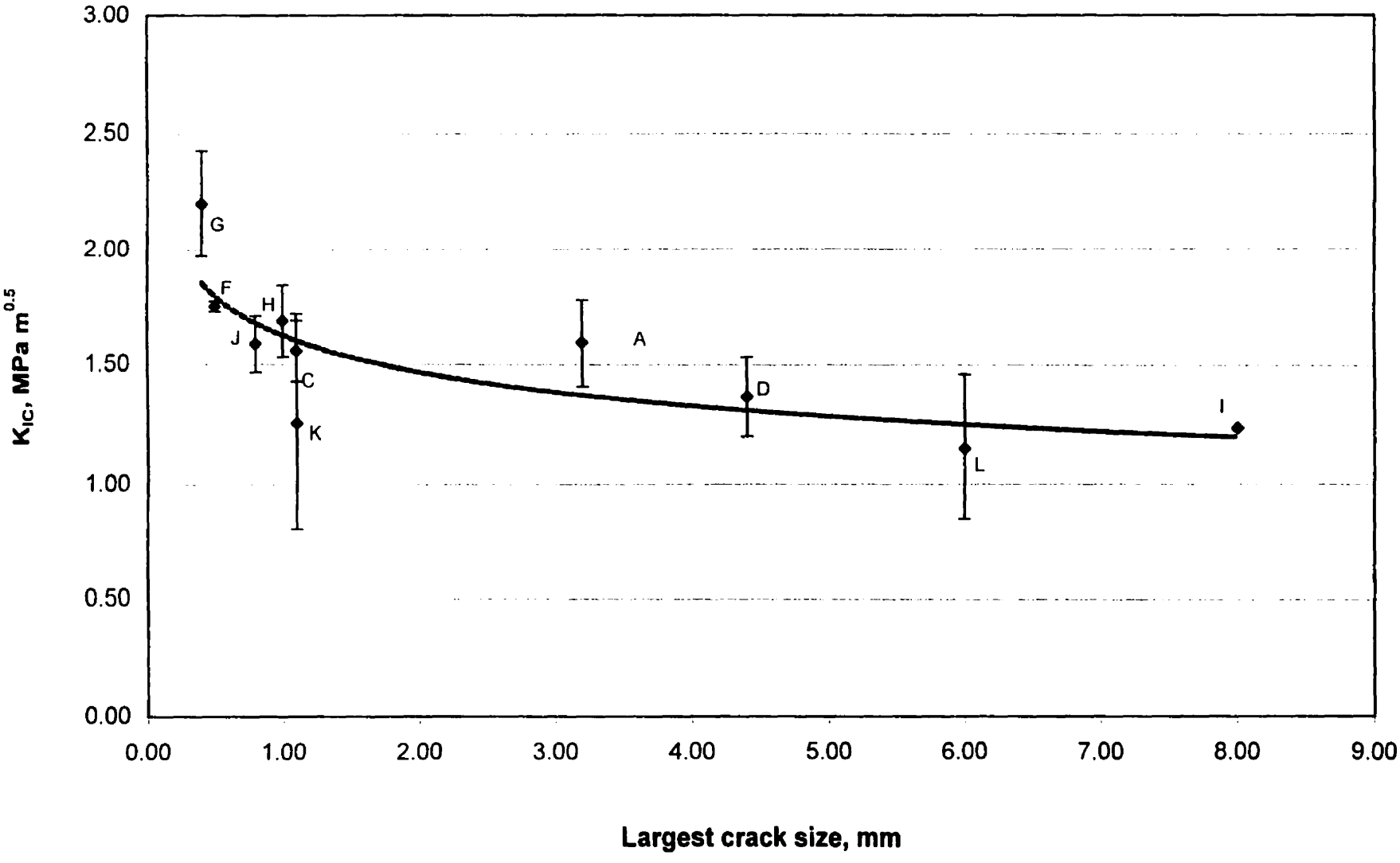

However, the porosity does not provide stress concentration effect as it is round and blunt in shape. The presence of sharp crack or the grain boundary crack, on the other hand, provide more stress concentration effect and the crack resistance is much lower. This is the reason the fracture toughness is found to well correlated with the largest crack sizes or the largest of either crack or grain sizes. This is shown in Figure 8.15 and Figure 8.16. It should be noted also that the decrease in toughness values in these cases are by power law or logarithmic. This means that smaller crack must be sharp and must have decreased the toughness very quickly. However, the larger cracks must be comparatively blunt and hence the decrease in toughness is only marginal. The plot of fracture toughness with the crack density appeared to have a very good correlation except for the values of Vineland limestone (L). This point lies at the rightmost part of the curve. A very limited number of photographs were available for this rock for calculating its crack density. By ignoring this point the best fit curve obtained is very typical (Figure, 8.17). The toughness appears to be decreasing in the beginning and then it increases. This can be explained by combination of two concepts, the stress concentration effect, and the effect of microcrack fracture process near the crack tip.

The decrease in toughness values at lower values of crack density is due to the first effect. However, the increase in toughness values at higher crack density is due to larger amount of resistance encountered in creation of microcrack process zone at large number of crack tips. The final crack growth in linking these microcrack process zone might have resulted higher resistance in crack growth. This phenomenon is opposite to the behaviour of rocks in its dynamic compressive breakage. In the latter case the large amount of crack

Figure 8.15: Largest crack size vs. Fracture toughness

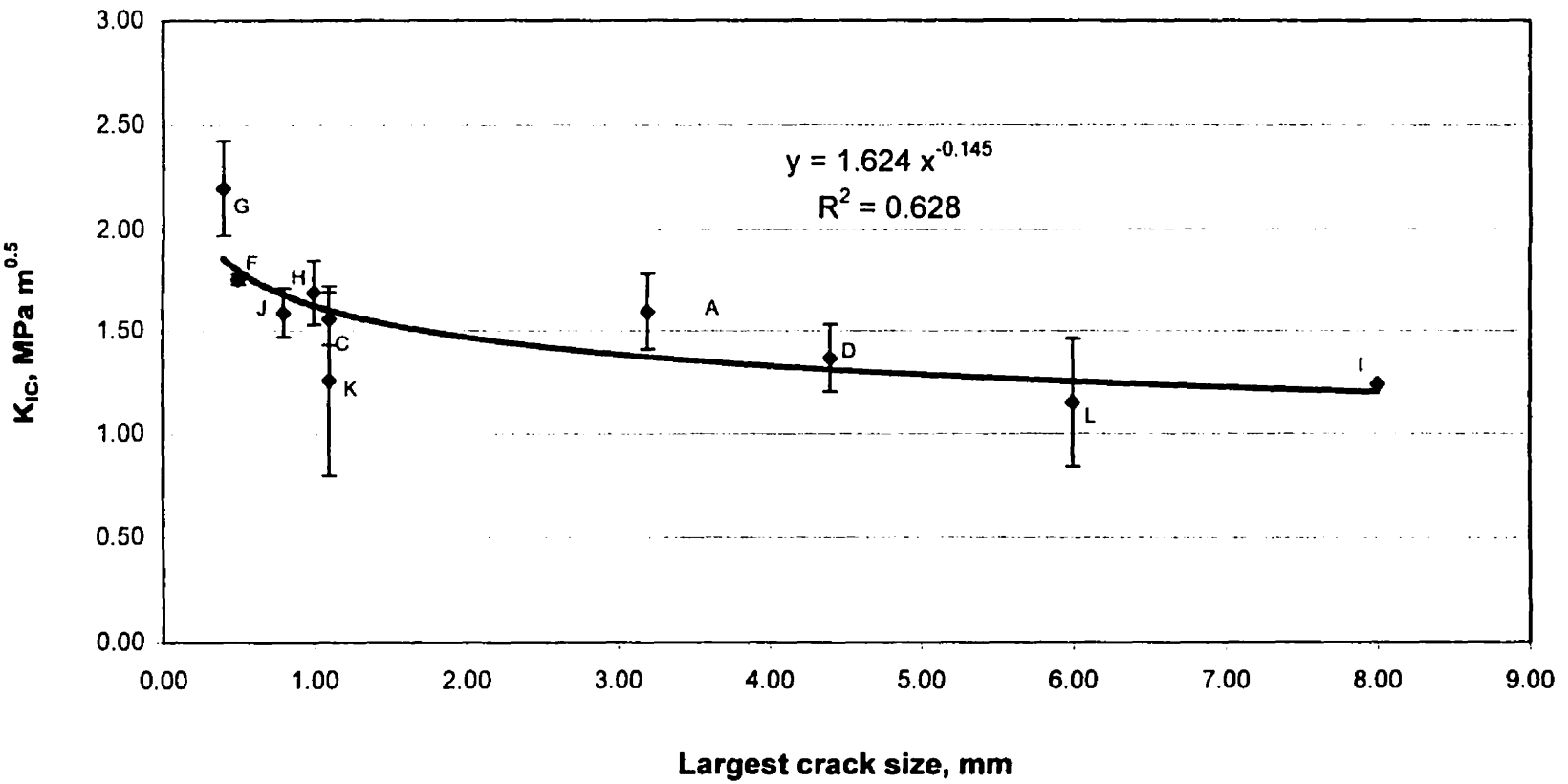

Note: Stanstead granite (A), Altered marble (B), Kingston limestone (C), Gneiss (D), Vineland limestone 1 (E), Marble 2 (F), Foliated marble 3 (G), Laurentian granite (H), Baskatong quartz (I), Barre granite (J), Gneissic granite (K), Vineland limestone 2 (L)

Figure 8.16: Largest crack or grain size vs. Fracture toughness

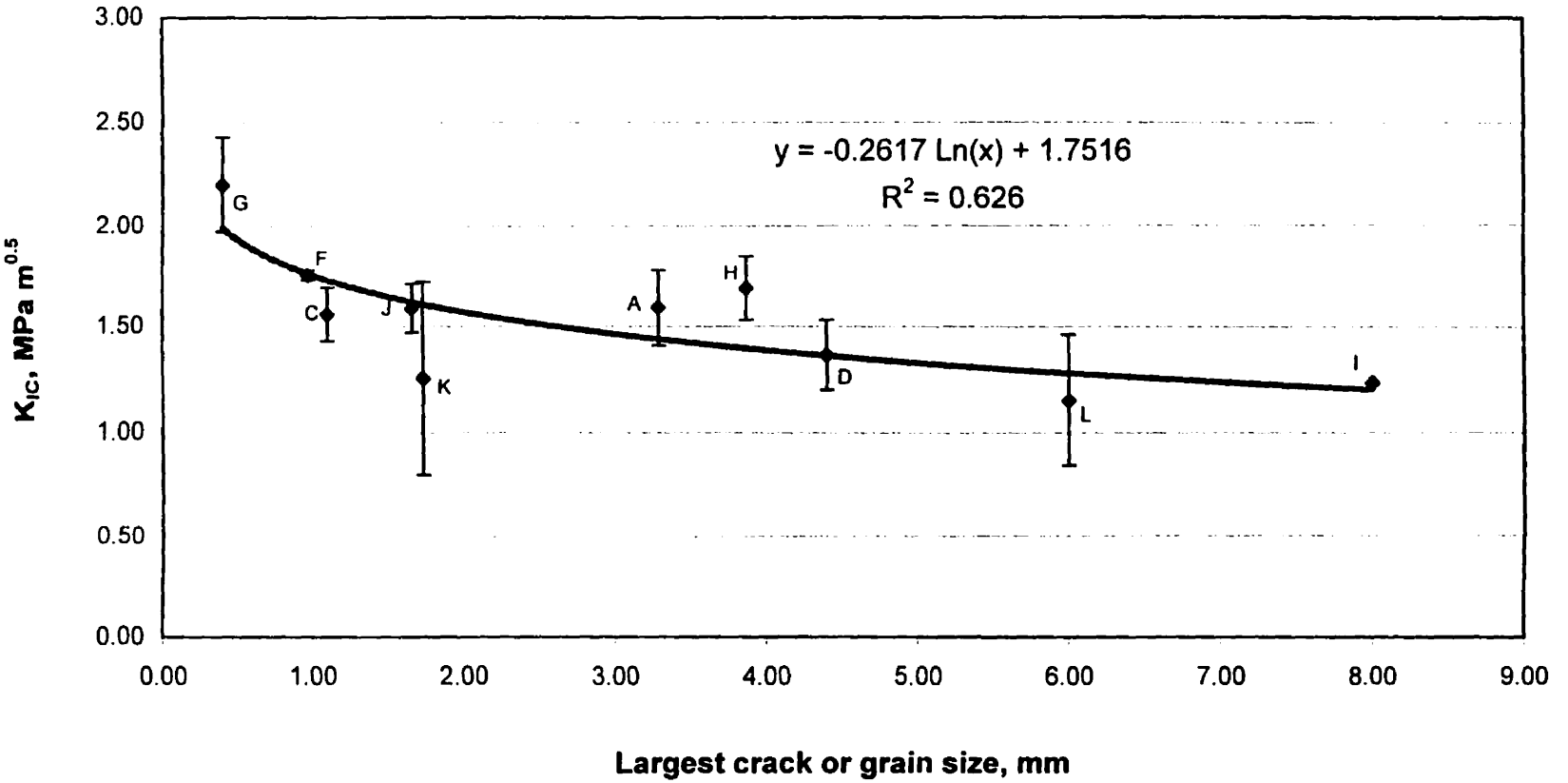

Note: Stanstead granite (A), Altered marble (B), Kingston limestone (C), Gneiss (D), Vineland limestone 1 (E), Marble 2 (F), Foliated marble 3 (G), Laurentian granite (H), Baskatong quartz (I), Barre granite (J), Gneissic granite (K), Vineland limestone 2 (L)

Figure 8.17: Crack density vs. Fracture toughness

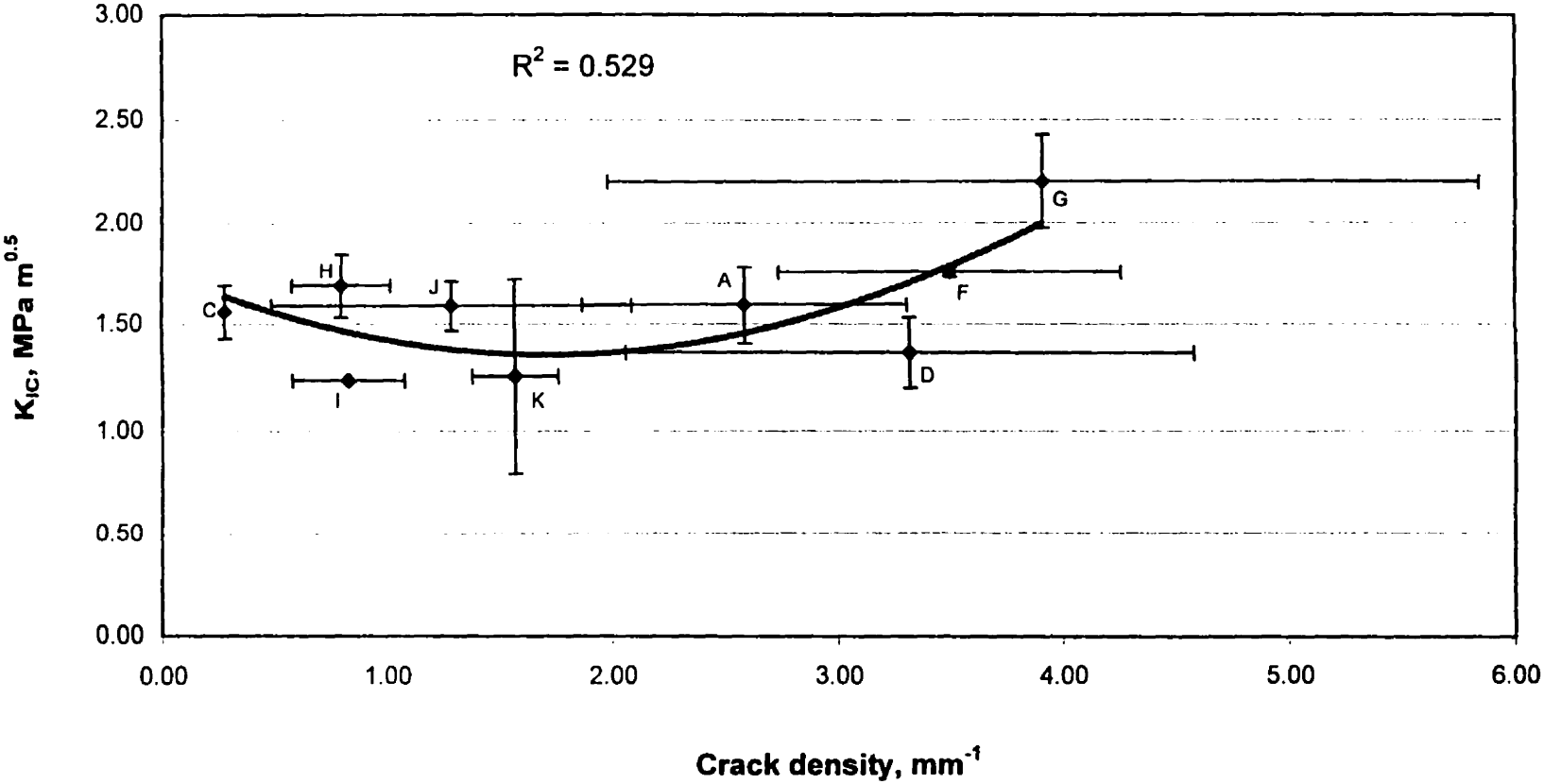

Note: Stanstead granite (A), Altered marble (B), Kingston limestone (C), Gneiss (D), Vineland limestone 1 (E), Marble 2 (F), Foliated marble 3 (G), Laurentian granite (H), Baskatong quartz (I), Barre granite (J), Gneissic granite (K).

density lowers the dynamic strength as these are the places for crack initiation and extension. The ultimate failure in this case is the result of large number of a large cracks being developed at different crack tips.

The above discussion concludes that the role of microstructure is very critical in all the fracture properties. However, the role of microstructure is different in different fracture characteristics. For example, the compressive strength (both static or dynamic) was found to be greatly controlled by the crack density, the tensile strength and the fracture toughness were greatly influenced by the largest grain sizes, and finally the comminution work index was governed by the average grain size distributions. The microstructure controls the critical stress or strain developed in the material. In compressive strength test the distribution of cracks leads to stress concentrations throughout the bulk of the sample, the extension of cracks takes place selectively lying at critical angles to the direction of loading resulting in tensile or shear failure. In the absence of any pre-existing cracks the largest grain may act as a weakest locale for stress concentration However, in fracture toughness or the Brazilian tensile strength test, the fracture is expected to originate from a specific place. A pre-existing crack may not be present always at that location. The largest grain, thus may serve the same purpose. The work index is more controlled by the average grain sizes as these are the only weak spots remaining in the relatively small rock fragments. In the small rock samples used for grinding, in the present study, both inter-granular boundaries and extensive network of microcracks would be largely absent.

In the absence of microcracks the modulus of elasticity, a ratio of stress over strain, is expected to be directly related to the fracture stress. However, it is known that microcracks greatly affect the stiffness of the material. The following section describe the effect of microstructure on the elastic properties of rocks.

8.7 Microstructure and elastic properties

The elastic properties of rock represent the stiffness of the material. It can be measured by different methods e.g. wave propagation through the rock, or measuring stress and strain during axial loading. The measured values represent the response of rocks under low levels of stress. In the present work these have been measured by the seismic wave (P and S) velocities and the density of corresponding rocks.

The measured values of elastic properties have been compared with the important microstructural properties measured in the rocks. The coefficient of correlation between the measured values of elastic properties with respect to the average and the largest grain sizes, the grain level crack size and the crack density are presented in Tables 8.7, 8.8, 8.9, 8.10 and 8.11, respectively. The degree of fitness of the curves correlating moduli and Poisson's ratio with these properties are also shown in the same tables.

Table 8.7: Coefficient of correlation between the Young's modulus and microstructure.

X-variable	Y-variable, Young's modulus (GPa)	R squared
Porosity, %	$Y = 2684\ x^{-0.0488}$	0.285
Average grain size, mm	$Y = -7.56 \ln x + 43.59$	0.775
Largest grain size, mm	$Y = -2.94 \ln x + 52.45$	0.268
Crack density, mm^{-1}	$Y = 0.0264\ x^2 - 0.204\ x + 51.23$	0.046

Table 8.8: Coefficient of correlation between the shear modulus and microstructure.

X-variable	Y-variable, Shear modulus (GPa)	R squared
Porosity, %	$Y = -4.96x + 24.04$	0.142
Average grain size, mm	$Y = -2.77 \ln x + 18.88$	0.601
Largest grain size, mm	$Y = -1.99 \ln x + 21.98$	0.213
Crack density, mm^{-1}	$Y = -1.52x + 22.987$	0.193

Table 8.9: Coefficient of correlation between the bulk modulus and microstructure.

X-variable	Y-variable, Bulk modulus (GPa)	R squared
Porosity, %	$Y = 19.751 x^{-0.3688}$	0.441
Average grain size, mm	$Y = -7.6296 \ln x + 20.598$	0.582
Largest grain size, mm	$Y = -8.387 \ln x + 28.82$	0.483
Crack density, mm^{-1}	$Y = -6.631 \ln x + 32.28$	0.437

Table 8.10: Coefficient of correlation between the compressibility and microstructure.

X-variable	Y-variable, Compressibility (1/GPa)	R squared
Porosity, %	$Y = 0.0506 x^{-0.3688}$	0.441
Average grain size, mm	$Y = 0.0078 \ln x + 0.0465$	0.613
Largest grain size, mm	$Y = 0.009 \ln x + 0.0381$	0.565
Crack density, mm^{-1}	$Y = 0.0048x + 0.0353$	0.226

Table 8.11: Coefficient of correlation between the Poisson's ratio and microstructure.

X-variable	Y-variable, Poisson's ratio	R squared
Porosity, %	$Y = -0.058 \ln x + 0.133$	0.277
Average grain size, mm	$Y = -0.0228 \ln x + 0.159$	0.156
Largest grain size, mm	$Y = -0.0379 \ln x + 0.1825$	0.296
Crack density, mm^{-1}	$Y = -0.0462 \ln x + 0.2043$	0.635

All the moduli of elasticity are found to be dependent more on the average grain sizes as compared to other micro-structure. The extent of correlation for the respective moduli are same as its dependence on the P and S waves. For an example, the correlation between the shear modulus and grain size is similar to that obtained between S wave and the grain size. A comparatively weaker correlation between the average grain sizes with the bulk modulus or the compressibility may be due to the scatter of the measured microstructure. The result of the present work shows only a trend. More work is needed to establish these findings. The variation of Young's modulus with respect to the average grain sizes is shown in Figure 8.18.

The variation in the dynamic elastic properties with porosity, as indicated in the above tables, are due to the similar reasons as discussed above. For an example, the bulk modulus and the compressibility varied with the porosity corresponding to their variation with P- and S-waves. The shear modulus followed the trend of that between the S-wave and porosity. The Young's modulus varied weakly with porosity and is the true reflection of its dependence on P- and S-waves.

The independent behaviour of Poisson's ratio with respect to the average grain size is because the former reflects the ratio of measured values of P and S waves. A slight error in detection and measured values of S wave makes a big difference in the calculated value of the same. However, the Poisson's ratio was found to be best correlated with an independently measured crack density. This is not surprising as similar nature of correlation has been shown analytically (Budiansky and O'Connell, 1976). The variation in Poisson's ratio with respect to the crack density is shown in Figure 8.19.

Figure 8.18: Average grain size vs. Young's modulus

$y = -7.559 \ln(x) + 43.59$

$R^2 = 0.775$

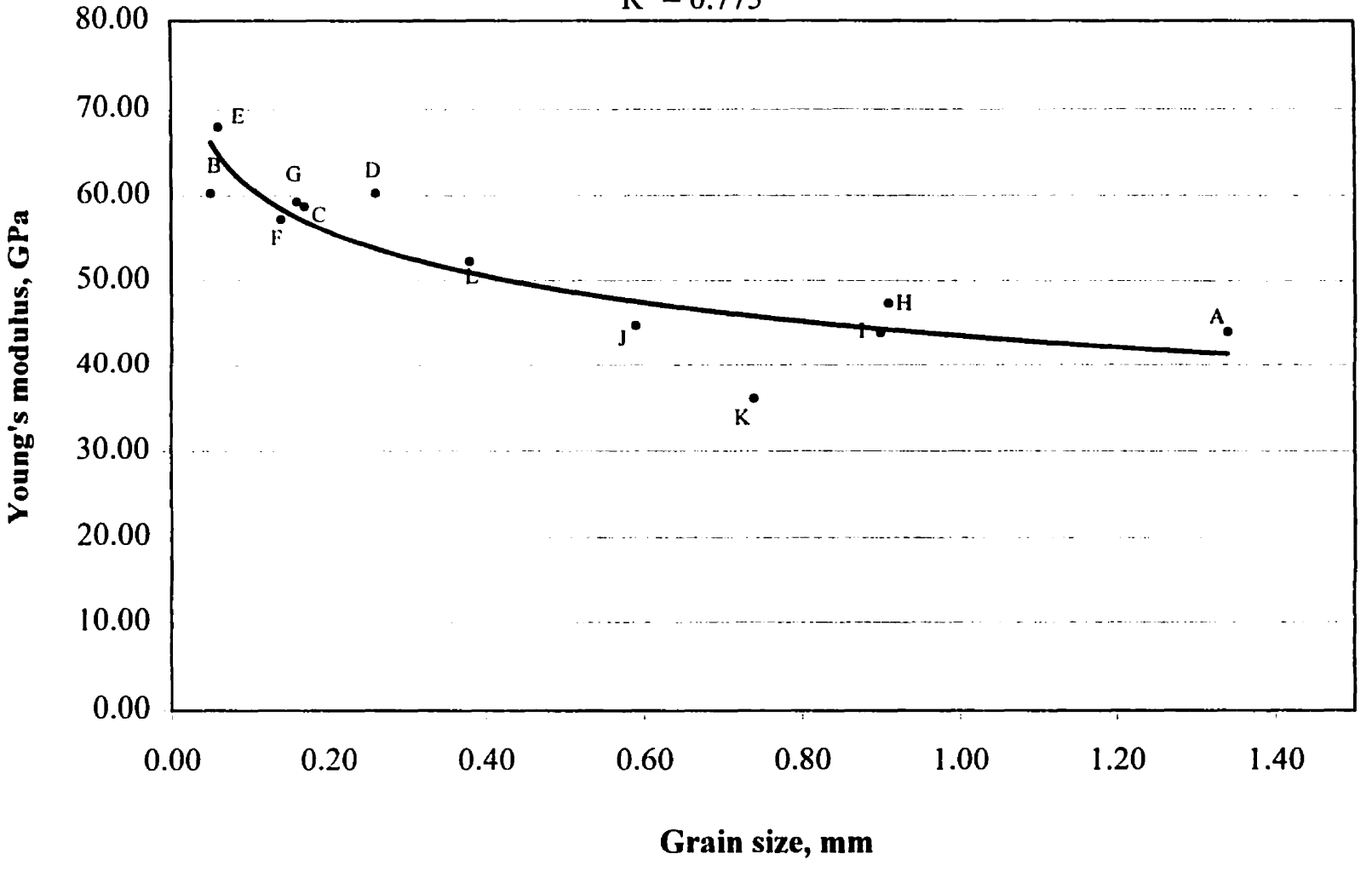

Figure 8.19: Crack density vs. Poisson's ratio

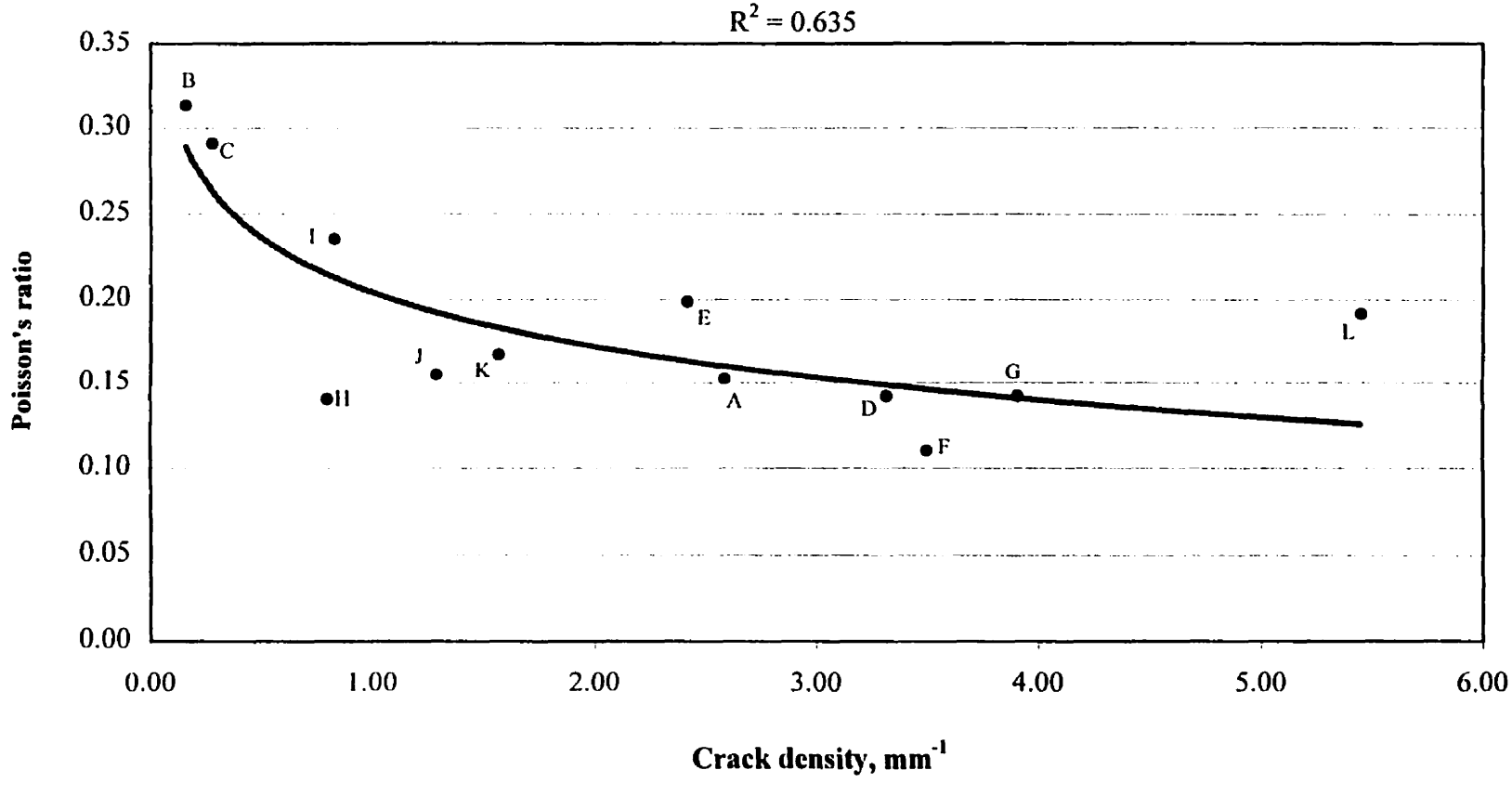

Note: Stanstead granite (A), Altered marble (B), Kingston limestone (C), Gneiss (D), Vineland limestone 1 (E), Marble 2 (F), Foliated marble 3 (G), Laurentian granite (H), Baskatong quartz (I), Barre granite (J), Gneissic granite (K), Vineland limestone 2 (L)

It is concluded, therefore, that among the different parameters representing the microstructure, only the average grain sizes affect the modulus of elasticity the most, especially, in the absence of major crack network in the test sample. This is in contrary to the effect of microstructure on the fracture properties. The measured values of elasticity cannot, thus be uniquely correlated with fracture strength due to the presence of microcracks.

CHAPTER 9

CONCLUSIONS

9.1 OVERALL CONCLUSIONS

Fragmentation by blasting is different from other methods of rock breakage due to the time scale involved. The time frame applicable to blasting ranges between tens of microseconds to half a second. This leads to very high strain rate loading of rock (10^3/sec to 10^{-1}/sec). The range of time scale or the strain rate corresponds to various breakage processes during blasting, e.g. breakage due to shock wave, gas pressure, rock mass collision and movement. The exact mechanism of dynamic fracture and the factors which control it are much less understood in rock than in similarly rate-sensitive fracture process in metals or composites. The main objective of the present work has been to investigate the phenomenon from a global perspective i.e. strength of material, comminution

principles, fracture mechanics, and micro-structural damage mechanics for a clearer understanding of this phenomenon under these various regimes of loading rates.

The strength of material, such as compressive or tensile strength is merely descriptive. It ignores the presence of crack in the material and the latter's role in the fracture process. The fracture toughness, on the other hand, explicitly exceeds the role of pre-existing crack (s), and represents the strength of a material in the presence of a crack. It predicts whether a material will fail or not at the specified stress level for the known crack and specimen geometry. In the presence of a large number of cracks, the micro-structural damage approach is used to predict ultimate failure in a material. The strength related parameter is the damage or the crack density which is calculated indirectly by measuring the reduction in moduli or Poisson's ratio.

The work index is also a relevant material property under intermediate strain rates. It is used routinely to predict the breakage characteristics in comminution and design of appropriate crushing and grinding circuits. The strain rate involved in this process is also a part of the blasting process, albeit more typical of the fragmentation behavior during the latter stages of blasting. The wave velocity, the crack velocity, and the fracture toughness values have been used to model the dynamic breakage process in rock (Grady and Kipp, 1989). The three concepts, strength, fracture toughness, and the damage, are quite distinct from each other, but can be very useful in explaining the phenomenon of rock breakage at different levels and scales.

The objective of the present work was to enhance our knowledge of fragmentation by considering the blasting process as a global event in which the whole fragmentation

process is assumed to be a strain-rate dependent process. The commonly designated rock properties normally used to describe these processes were measured in the laboratory and compared with the dynamic rock properties. Additionally, the fracture related properties of rocks were examined for correlation with respect to their physical, mineralogical and micro-structural characteristics. The physical properties measured were porosity, density, the seismic wave velocities, dynamic moduli, and Poisson's ratio. The mechanical properties measured were the compressive and tensile strength both under static conditions and the former under high dynamic conditions as well. The work index represented a fracture property at an intermediate strain rate. The fracture toughness corresponds to low strain rate but a fundamental fracture property. Since the present work was aimed at measuring the above fracture related rock properties in laboratory-scale samples, the effect of macro-structure was not considered.

The rock types, selected for the present work ranged from nearly homogenous isotropic rock to an-isotropic rocks. The nearly isotropic rocks were of three different types of granites. The an-isotropic rocks consisted of gneissic granite, gneiss, marble, limestone, and quartz. Based on the investigation of the above mentioned rock properties, several important conclusions have been drawn. The following section lists the salient ones of these:

1. The dynamic compressive strength, measured under a strain rate of 10^3 /sec, has been found to be about 2.5-4.6 times higher than the compressive strength measured under static conditions (strain rate of 10^{-6} /sec) for similar specimen sizes in a wide variety of

rock types. It has also been found that this ratio is higher for low strength rocks, and lower for high strength rocks.

2. The particle size distribution resulting from high velocity impact breakage is much smaller than in the static case. This is attributed to the transient nature of impact loading, which provides insufficient time for cracks to propagate and coalesce to produce larger fragments. The degree of fineness (50% or 80 %passing) generated under dynamic breakage is well correlated with the dynamic compressive strength; the coarser fragments corresponding to higher strength. However, there appears to be a very weak but inverse correlation between static compressive strength and the corresponding fragment size distribution. It is concluded that the use of static strength values in predicting fragment size distribution in blasting can lead to significant errors.
3. A great care should be taken into account when comparing compressive strengths at different diameters. This is because, the microstructure reduces the compressive strength significantly, when the minimum dimension of the specimen is some multiplication of the largest microstructure (~10 times the largest grain or crack sizes). Further, the present work suggests that the dynamic strength which is usually determined at much smaller diameter is more true for fine grained rocks.
4. The dynamic compressive strength resulted in almost no correlation with the fracture toughness, better correlation with the Brazilian tensile strength, and much better correlation with the static compressive strength.
5. Among the microstructural properties, the crack density parameter was found to have greatly superior correlation with dynamic strength over the other properties such as

the average or the largest grain size or crack size. The correlation between the compressive strength (both static as well as dynamic) and the crack density is very similar unlike tensile strength. The largest grain size is found to be more controlling factor in tensile strength and fracture toughness unlike the static and dynamic compressive strengths.

6. The work index, which represents a fracture process at an intermediate strain rate, is found to have the best correlation with a majority of the physico-mechanical properties. It had better correlation with the Brazilian tensile strength as compared to static and dynamic compressive strengths. The work index was also found to have very good correlation with compressibility of the test samples. This is expected due to the load characteristics typical to the rod mill employed in the study.
7. The work index is further compared with the average grain size, the largest grain and crack size, and the crack density. The former resulted in an excellent correlation with the work index which is expected as the later is an average property showing average strength over a large number impacts. However, the crack density did not give better correlation with WI unlike both static and dynamic compressive strengths. This is obvious as the work index has been determined at a much finer particle size (1.2 mm) at which most of the cracks, even some of the largest grains might have been broken or vanished.
8. The fracture toughness is found to be well correlated with the porosity as the latter allows more easy crack growth. However, the correlation with the largest crack or grain size is much better as the latter provide severe stress concentration effect, thus

easy propagation of crack. Further, the effect of crack density appeared to be non-linear. The fracture toughness initially decreases with increase in crack density, but further increase in the latter results an increase in toughness. This suggests the behaviour of rocks in dynamic compressive breakage is different than that due to static single crack growth. The first effect can be explained due to the stress concentration effect causing lower toughness, whereas, the second effect is explained due to the microcrack fracture process near the crack tips. The final crack growth in linking these microcrack process zone might have resulted higher resistance in crack growth. This phenomenon is opposite to the behaviour of rocks in its dynamic compressive breakage. In the latter case the large amount of crack density lowers the dynamic strength as these are the places for crack initiation and extension. The ultimate failure in this case is the result of large number of cracks being developed at different crack tips.

9. The effect of microstructure is found to be critical to all the fracture related properties. However, its role is different for different rock characteristics. For example, crack density is more influential in dynamic as well as static compressive breakage process. The tensile strength and fracture toughness are more influenced by the size of the largest grain or cracks representing the weakest sites for crack growth. The work index on the other hand, is strongly affected by the average grain size characteristics due to the latter's global nature under multiple impact loading. This is also because both intergranular boundaries and extensive network of microstructure are largely absent in the scale of grinding experiment in the present case.

10. In the absence of microcracks the modulus of elasticity, a ratio of stress over strain, is expected to be directly related to the fracture stress. However, as the average grain size characteristics affect the modulus of elasticity the most (especially in the absence of major crack network in the test samples) the measured value of elasticity cannot thus be uniquely correlated with fracture strength.
11. The structural characteristics are shown to be key parameters in all the fracture processes. In fragmentation process involving relatively small fragments, such as blasting, both micro- and macro-fractures play a dominant role. In crushing and grinding, involving fragmentation in the scale of grain size or smaller, the micro-structure would be represented better by specific grain size distribution than micro-fracture or crack density. However, in all non-static fracture process, such as blasting or comminution, the use of static strength values in predicting fragment size distribution can lead to significant errors.

9.2 RECOMMENDATIONS

Despite the detailed work on fracture properties of rocks at various strain rates in this present investigation, several important areas relating dynamic fracture behavior of rock still remain unanswered. To improve our understanding of the dynamic fracture process in rock, the following additional work is recommended for future work.

1. The present work has examined the dynamic compressive strength and the resulting fragment size distributions at two strain rates only. It is recommended that additional work be carried out for compressive and tensile strengths at intermediate strain rates to cover the full range of strain rates representative of the blasting process.
2. Crack velocity is considered an essential property of rock under dynamic breakage. Grady and co-workers (1989) have shown analytically the use of crack velocity for predicting fracture strength and fragment size distribution in blasting. It is recommended that detailed work be carried out to measure crack velocity as a function of dynamic loading conditions.
3. Estimation of 'damage zone' in rock due to blasting is a critical parameter in excavation work. This relates to, a) safe working conditions, b) greater control on dilution, and c) better control of the degree of the fragmentation. It is recommended that future work be focussed on estimation of 'damage states' in rock under dynamic loading following the work of Grady and Kipp (1989).
4. Dynamic compressive strength in the present work has been measured at one diameter, due to the limitation of the test apparatus. It is recommended that future work should

be carried out to measure the same at different diameters of rock samples to examine size-effect, if any.

5. In the present work fracture toughness was measured by static means. It is recommended that future work be carried out to examine the feasibility of measuring fracture toughness at different loading rates.
6. In the present work, a specific chevron notch was created for the measurement of fracture toughness by use of a cutting blade. It was assumed that the crack tip radius would be the same in all rock types. Future work should incorporate the effect of notch radius on the measured values of fracture toughness.
7. Excellent correlation was obtained between the work index and grain size characteristics in four rock types in the present work. Additional work needs to be carried out over a wider suite of rocks to confirm this correlation.

REFERENCES

Atkinson, B. K., 1989; "Fracture Mechanics of Rock," Atkinson, B. A. (Ed), Academic Press.

Austin, L. G., Klimpel, R. R. and Luckie, P. T., 1984; "Process Engineering," SME publication New York. pp 28.

Barker, L, M., 1979; "Theory of determining KIC from small, non-LEFM specimens, supported by experiments on aluminium." Int. J. of Fract., vol 15. No 6, pp 515-536.

Bear, T. J., and Barr, B., 1977; "Fracture toughness tests for concrete." Int. J. Fract. Vol. 13, pp 92-96.

Bearman, R. A., et al., 1989; "Use of fracture toughness testing in characterising the comminution potential of rock." Today's Technology for the Mining and Metallurgical Industries, Symp., of MMIJ/IMM, Kyoto, Japan, pp 161-181.

Bieniawski, Z.T., 1968; "The effect of specimen size on compressive strength of coal." Int. J. of Rock Mech. And Min. Sci. & Geomech. Abstr. Vol 5, No 4, pp 325-335.

Birkimer, D. L., 1971;. "A possible fracture criterion for the dynamic tensile strength of rock." 12 th US Symp. on Rock Mech. University of Missouri Rolla, Missouri. Clark, G.B. (editor), pp 573-590.

Bond, F.C., 1952; "The Third Theory of Comminution," Trans. SME/AIME; vol. 193. pp. 484-494.

Brace W. F., and Bombolakis, 1963; "A note on brittle crack growth in compression." J. G. R., No. 68, pp 3709-3713.

Brady, H. G., and Brown, E. T. (eds), 1993; "Rock mechanics for underground mining." Chapman and Hall.

Bucher, J. and Bilek, Z. 1981; "Application of Hopkinson split bar test to the mechanical and fracture properties to rock." Fracture for Ceramics, Rocks, and Concrete. ASTM STP-745. Freiman, & Fuller (eds.) pp 185-195.

Budiansky, B. and O' Connel, R. J., 1976; "Elastic modula of a cracked solid." Int. J. Solid and Structure; vol. 12, pp. 81-97.

Chen, E. P. and Sih, G. C, 1977; "A elastodynamic crack problems." (ed. Sih, G. C.) Noordhoff, 1983.

Curran, D. R., Seaman, L., Shockey, D. A., 1987; "Dynamic failure of solids." Physics Reports, 147, No. 5/6 pp 253-388.

Curran, D. R., Seaman. L., 1996; "Simplified models of fracture and fragmentation." High-Pressure Shock compression of Solid II. Dynamic fracture and Fragmentation. Springer-Verlag, NY, pp 340-365.

Designation: E -2845-95, 1999; "Standard test method for laboratory determination of pulse velocities and ultrasonic elastic constants of rock." Annual Book of ASTM Standard, Philadelphia, PA, vol. 4.08, pp. 257-262.

Designation: E -2938-95, 1999; "Unconfined compressive strength on intact rock core specimens." Annual book of ASTM Standards, Philadelphia, PA; vol. 4.08, pp 282-284.

Designation: E 399-83; "Standard test method for plane-strain fracture toughness of metallic materials," Annual book of ASTM standards, vol 2.02, pp 686-710, 1990.

Farmer, J. W., 1968; "Engineering Properties of Rock." E. and F. N. Spon, Ltd., London.

Field. J.E. et al., 1994; "Experimental methods at high rates of strain." Journal de Physique IV, Colloque C8, Suppl. au Journal de Phy., Vol 4, pp C8-3-C8-22.

Franklin, J. A. and Dusseault, M. B. 1989; "Rock Engineering." McGraw Hills Publishing Company.

Grady D. E. & Kipp, M. E., 1989; "Dynamic rock fragmentation." Fracture Mechanics of Rock, Atkinson, B. A. (Ed), Academic Press, pp. 429-473.

Grady, D.E. and Kipp, M.E., 1979; "The micromechanics of impact fracture of rock," Intl. J. Rock Mech. Min. Sc. & Abs.., 16, pp 293-302.

Grady, D.E., 1982; "Local internal effects in dynamic fragmentation." J. Appl. Phys., vol 53, No 1, pp 322-325.

Griffith, A. A ,1921; "The phenomenon of rupture and flow in solids." Phil. Trans. R. Soc. London, Series A, 221, pp 163-198.

Hakalehto, K.O. 1969; "The behavior of rock under impulse loads. A Study Using the Split Hopkinson Bar Method." Acta Polytechnica Scandinavica. Chap.81.

Hassani, F.P. 1980; "A study of the physical and mechanical properties of rocks and their discontinuities associated with open cast coal mining operations." PhD Thesis, University of Nottingham,

Hoskins, J. R. & Horino, F.G. 1969; "influence of spherical head size and specimen diameters on the uniaxial compressive strength of rocks". United States Department of the Interior, Bureau of Mines (USBM) R. I. 7234, pp 1-16.

Hua Guo, 1990; "Rock cutting using fracture mechanics principles," PhD Thesis, Univ. of Wollonggong, N.S.W. Australia, 1990.

Irwin, G. R., 1957; "Analysis of stresses and strains near end of a crack." Journal of Applied Mechanics, vol 24, pp 361.

ISRM: 1981; "Suggested methods of rock characterization, testing, and monitoring." ISRM Commission on Testing Methods, E.T. Brown, (Ed.) Pergamon, Oxford, pp. 211.

Jaeger J. C. and Cook N. G. E; 1979; "Fundamentals of rock mechanics," Fletcher and Son Ltd., Norwich, Great Britain.

Kachanov, M., 1990; "A damage mechanics in Engineering materials." The Winter Annual Meeting of ASME, Texas. Ju, J.W., Krajcinovic, D., and Schreyer, H.L. (Eds), pp 11-15.

Kolsky, H, 1963; "Stress waves in solids." New York Dover Publications Inc..

Kolsky, H. 1949; "An Investigation of the mechanical properties of materials at very high rates of loading." Proc. Royal Soc., Section B, Vol 62, pp 676-700.

Kumar, A. 1968; "The effect of stress rate and temperature on the strength of basalt and granite." Geophysics , Vol 33, pp 501-510.

Labuz, J. F., et al. 1985; "Experimental analysis of crack propagation in granite." Int. J. Rock Mech. min. Sci. & Geomech. Abstr., vol 22, No. 2, pp 85-98.

Labuz, J. F., et al. 1987; "The fracture process zone in granite." Int. J. Rock Mech. min. Sci. & Geomech. Abstr., vol 24, No.42, pp 235-246.

Langefors, U. and Kihlstorm, B., 1978; "The modern techniques of rock blasting." Third edition, Almquist and Wisksell, Stockholm, Sweden.

Lewis. W.E. & Tandanand , S. (Ed), 1974; "Test Procedures for Rocks." United States Department of the Interior, Bureau of Mines (USBM), IC 8628.

Lindholm, U.S. & Yeakley, L.M. 1968; "High Strain Rate Testing: Tension and Compression." Experimental Mechanics., Vol 8, pp1-9

Lipkin, J., Schuler, K. W. and Parry, T., 1980; "Dynamic torsion failure of limestone tubes, Mechanical properties at high rate of strain", (ed. Harding, J.) Conference Series No. 47, The Inst. of Physics, London, pp 187-197.

Lundberg, B. 1976; "Energy Absorption in Dynamic Rock Fragmentation." Int. J. of Rock Mech. Min. Sci. & Geomech. Abstr.. Vol. 1, No. 3, pp 187-197.

Mohanty, B. 1987; "Strength of rock under high strain rate loading conditions applicable to blasting. " Proc. of 2nd Sym. on Rock Fragmentation by Blasting, Keystone, U.S.A, pp 72-78.

Mohanty, B., 1982; "Characteristic crack patterns close to an exploding charge." Rock Breaking and Mechanical Excavation, Baumgartner, P. (Ed), 14 th Canadian Rock Mech. Symp., Canada. pp 32-36.

Mohanty, B., 1988; "Parameters affecting explosives energy release-A case for realistic rating of commercial explosives." Proc. 14 th Annual conference on Explosives and Blasting Tech.; Soc. of Expl. Egg., Anaheim, pp 304-317.

Momayazzadeh, M., 1993; "Stress memory measurement using the Kaiser Effect of acoustic emission." Ph.D. Thesis, McGill University, Montreal, Canada.

Olofsson, T., 1978; "Evaluation of fracture parameters and elastic properties of rock materials." Report 195E, Univ. of Lulea, Sweden.

Orowan, E., 1955; "Energy criteria of fracture." Welding Journal, Vol 34: pp 1575-1605.

Ouchterlony, F, 1988; co-ordinator "ISRM commission on testing methods." Int. J. of Rock Mech. and Min. Sci. & Geomech. Abstr., vol 25, no 2, pp71-96.

Ouchterlony, F, 1989; "On the background to the formulae and accuracy of rock fracture toughness measurements using ISRM standard core specimen," Int. J. of Rock Mech. and Min. Sci. & Geomech. Abstr., vol 26, no 1, pp 13-23.

Ouchterlony, F., 1974; "Fracture mechanics applied to rock blasting, advances in rock mech.", Proc. 3rd ISRM Congress, 11-B, Denver CO, 1377-1383.

Ouchterlony, F., 1986; "A core bend specimen with chevron edge notch for fracture toughness measurements, rock mechanics: key to energy production." Proc. 27th US Symp. On Rock Mech., H. L. Hartman, (Ed), SME Littleton Co., pp 177-184.

Prasad U., 1994; "Energy utilization in comminution and its application to rock blasting." M.Eng Thesis, McGill University, Montreal, Canada.

Price, , N. J., 1960; "The compressive strength of coal measure rocks," Colliery Engineering, Vol., 37, No. 437, pp 283-292.

Rinehart, J. S., 1965; "Dynamic fracture strengths of rocks." VII Sym. On Rock Mechanics vol I, the Pennsylvania University, University, Parks, Pennsylvania, pp. 205-208.

Rummel, F., and Muller, W., 1984; "Bruchmechanische Untersuchungen fur Salzgestein in der Schachtanlage Asse II." Ber. Zum GSF-Auftrag, Best. Nr. 31/139081/83, taken from Fracture Mechanics of Rock, Atkinson, B. K. (ed), Academic Press, 1989.

Sadri, Afsin., 1996; "Development of the miniature seismic reflection (MSR) system for nondestructive evaluation of concrete shaft and tunnel linings." Ph.D. Thesis, McGill University, Montreal, Canada.

Sanga, C. M., et al., 1974; "Microfracturing of a sandstone in uniaxial compression, " Int. J. of Rock Mech. and Min. Sci. & Geomech. Abstr., vol 11, pp 107-113.

Shockey, D.A. et al. 1974; "Fragmentation of rock under dynamic loads." Int. J. Rock Mech. min. Sci. & Geomech. Abstr. Vol 11, pp 303-317.

Sih, G. C., 1973; "Handbook of stress intensity factors," Inst. of Fracture and Solid Mechanics, Leihigh University, bethlehem, Pennsylvania.

Singh, R.N. and Sun, G.X., 1989; "Fracture mechanics applied to slope stability analysis, Int. Symp on Surface Mining - Future concepts," University of Nottingham, England.

Swanson. P. L., 1984; "Subcritical crack growth and other time-and environment-dependent behavior in crustal rocks ." J. Geophys. Res., Vol 89, pp 4137-4152.

Takeyama, Y. et.al. 1985; "Some experiments of determining flow stress curves of metals in some controlled courses of high strain rate with a soft testing machine." J. de Physique, C5, Vol 8, T46, pp645-653.

Taylor, L. M. et al., 1986; "Microcrack Induced damage accumulation in brittle rock under Dynamic loading," Computer methods in Applied mechanics and Engineering; vol. 55, pp. 301-320.

Whittaker, B., N., Singh, R. N., and Sun, G, (Eds), 1992; "Rock fracture mechanics-principles, design and applications." Elsevier.

Zhang, Z. X., et al., 1999; "Effects of loading rate on rock fracture." Int. J. of Rock Mech. and Min. Sci. & Geomech. Abstr., vol 36, no 5, pp 597-611.